ADAPTIVE AND DIVERSITY TECHNIQUES FOR WIRELESS DIGITAL COMMUNICATIONS OVER FADING CHANNELS

Thesis by

Mohamed-Slim Alouini

In Partial Fulfillment of the Requirements

for the Degree of

Doctor of Philosophy

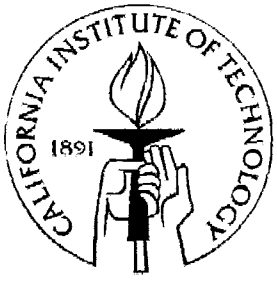

California Institute of Technology

Pasadena, California

1998

(Submitted May 29, 1998)

In memory of my father, Khemais Alouini,
and to my mother, Neziha Fourati.

Acknowledgements

Praise be to God, the most gracious and the most merciful. Without his blessing and guidance my accomplishments would never have been possible.

I would like to acknowledge many people who helped me during the course of this work. First, I would like to thank my thesis advisor, Professor Andrea Goldsmith, for giving me the opportunity to be a part of her research group and for providing me with the right balance of guidance and independence in my research. I am greatly indebted to her for her full support and constant encouragement and advice both in technical and non-technical matters. Her broad expertise and superb intuition have been a source of inspiration to me over the past three years. Her detailed comments and criticisms have greatly influenced my technical writing, and are reflected throughout the presentation of this dissertation.

I am also grateful to Dr. Marvin K. Simon of the Jet Propulsion Laboratory (JPL) for his excellent teaching. I know that I have learned from the very best in my field, and I hope that his clarity in presenting technical material has rubbed off on me. During my last year at Caltech I had the great fortune and honor to collaborate with him on problems of common interests, and many of the results presented in this thesis are the result of joint work.

I would also like to thank Dr. Dariush Divsalar of JPL for his encouragement and for his many illuminating and stimulating discussions. Dr. Divsalar always had time to answer my questions and my feedback to him can only be described as minimal when compared to what he had to offer to me in each discussion.

I am also grateful to Professors Robert J. McEliece and Michelle Effros for their time serving on my candidacy and defense examination committees, and for their various suggestions relating to my research.

I would like to thank Lilian Porter for her efficient and skillful assistance and help in my paper work during my stay at Caltech. I also would like to thank Robert Freeman for his availability and advice, and for keeping the computers up and running. In addition, I gratefully acknowledge the financial support of Caltech and National Semiconductors.

I am thankful to my former and current group-mates: Srinivas Aji, Jung-Fu Chen, Gavin Horn, Hui Jin, Lifang Li, Wei Lin, Kim Lumbard, Neelesh B. Mehta, Xiaoyi Tang, Meina Xu, and Zhong Yu for their friendship, help, and cheerfulness. I would also like to thank my good friends in the DSP group: Sony Akkarakaran, Murat Mese, Ahmet Kirac, and Jamal Tuqan for hosting me so many times in their lab. I also thank all my other numerous Caltech, USC and Georgia Tech alumni friends, too many to be listed here, who have made my stay in the L.A. area such an enjoyable experience.

Last, but certainly not the least, I would like to acknowledge the commitment, sacrifice and support of my parents, who have always motivated me. My mother has always believed in me and has supported every endeavor of mine. My father taught me what matters most in life: faith in God, honesty, and integrity. In reality this thesis is partly theirs too.

Abstract

Demand for mobile and personal communications is growing at a rapid pace, both in terms of the number of potential users and the introduction of new high-speed services. Meeting this demand is challenging since wireless communications are subject to three major constraints: a complex and harsh fading channel, a scarce usable radio spectrum, and limitations on the power and size of hand-held terminals. Therefore, effective spectral and power efficient fading mitigation techniques are required. In this thesis we discuss two particular techniques to overcome fading: diversity combining and adaptive transmission. We first present a new approach for the performance evaluation of digital communications over fading channels. This approach, which is based on alternate representations of classic functions arising in the error probability analysis such as the Gaussian Q-function and the Marcum Q-function, leads to a unified analytical framework to determine the exact error rate of digital communications with multichannel reception. The unified approach gives new analytical expressions for average bit error rate under very general channel conditions, in addition to simplifying previously-known results both analytically and computationally. We next present methods of adapting to random channel variations in order to increase the spectral efficiency of wireless systems. As a first step we determine the theoretical spectral efficiency limits of wireless communication systems subject to the underlying severe multipath fading. We then propose an adaptive M-QAM modulation technique and analyze its performance over Nakagami-m fading channels. We also propose an adaptive modulation technique which combines voice and data, and study its performance. Finally, we consider adaptive modulation in cellular systems, and compute the resulting area spectral efficiency, defined as the maximum bit/sec/Hz/Km^2, which can be supported in the system.

Contents

List of Figures

List of Tables

Chapter 1 Introduction

1.1 Motivation and Background

Unlike most current cellular telephone systems, future wireless systems will support not only voice communication but also other high-speed data and multimedia services including facsimile, file transfer, e-mail, and video teleconferencing. These services require high data rates with low delay and bit-error-rate (BER). It is difficult to support these requirements with wireless systems due to three major constraints in the system design. First of all, wireless systems operate over a complex and harsh time-varying radio channel which introduces severe multipath and shadow fading. In addition, wireless applications must share the limited available radio spectrum, and spectral efficiency is therefore of primary concern in the system design. Finally, the communication terminals must be small, low-power, and lightweight, which restricts their capabilities. Due to these major impairment and constraints, sophisticated spectral and power efficient fade mitigation techniques are required to improve radio link performance. In particular, diversity combining and adaptive transmission techniques have great potential to improve the performance of wireless systems such that they can support high-speed data and multimedia. In both techniques the improvement is achieved without an increase in the transmitted bandwidth and power but at the expense of a higher system complexity.

1.2 Thesis Objective

The objective of this thesis is two-fold. First it develops analytical methods and tools to assess the performance of digital communications over wireless fading channels, when diversity techniques are employed. Second it proposes and analyzes the performance of various adaptive modulations. For both topics emphasis is put on the development of "generic" analytical tools that can be used for a wide range of communication systems operating in various fading conditions typical of communication links of practical interest. As such the coverage is extremely broad in that coherent, differentially coherent, and noncoherent communication systems are all treated as well as a large variety of diversity and adaptive techniques. The final goal is to provide easy-to-compute analytical expressions that allow the researcher or system designer to perform comparison and tradeoff (performance versus complexity) studies among the various communication type and diversity/adaptive techniques combinations so as to determine the optimum choice in the face of his or her available constraints.

1.3 Thesis Outline

The thesis outline is as follows. We begin in Chapter 2 with a brief review of the principal characteristics and models of fading channels. The primary goal of this chapter is to introduce models, terminology and notations that will be used throughout the thesis. We first describe the main characteristics of fading channels. We then present a number of models for frequency-flat and frequency-selective fading channels and explain the relation between these models and the corresponding physical channels.

1.3.1 Diversity Techniques

The first part of the thesis studies the performance of nonadaptive digital communications (with and without diversity combining) over fading channels. To accomplish this task we develop a new approach to the performance evaluation of digital communications over fading channels with and without diversity. We also present a compendium of results that have not previously appeared in the literature. Our approach relies on alternate representations of classic functions arising in the error probability analysis of digital communication systems, and leads to average BER expressions which can be readily evaluated numerically. In many cases these expressions are obtained in closed-form while in other cases they involve a single integral with finite limits and an integrand composed of elementary or standard tabulated functions. These results reduce to well-known solutions, allow previously obtained results to be simplified both analytically and computationally, and provide new solutions to problems which heretofore resisted solution in a simple form. In particular a new generic form for the average error probability of binary signals over fading channels without diversity reception is given in Chapter 3. Chapter 4 presents a unified approach for the performance evaluation of coherent modulations with optimum diversity reception. Since optimality implies more hardware complexity and more sensitivity to channel estimation errors, Chapter 5 considers coherent modulations in conjunction with suboptimal diversity techniques which are less complex (hence more practical for actual implementation) and more robust to imperfect channel estimation. In many cases the phase of the received signal cannot be tracked accurately, and therefore coherent detection is not possible. Noncoherent and differentially coherent modulation does not require this coherent phase tracking, and in Chapter 6 we provide a unified approach for the performance of these modulation techniques with and without diversity reception. Since there are a number of real life scenarios in which the combined signals are independent of one another, Chapter 7 characterizes the impact of correlation on the outage probability and average error probability of various coherent, differentially coherent, and noncoherent diversity receivers.

1.3.2 Adaptive Techniques

Adaptive transmission schemes are currently receiving a great deal of attention as very promising techniques to achieve high spectral efficiency. The main objective of our work in this area is twofold. First, we seek to determine the theoretical spectral efficiency limits of wireless point-to-point and cellular communication systems which use adaptive modulation. Second, we attempt to design practical adaptive transmission schemes that approach these theoretical bounds. In particular, Chapter 8 provides closed-form expressions for the capacity of Rayleigh fading channels under various adaptive transmission and diversity combining techniques. Chapter 9 extends these results to Nakagami-m fading channels and then proposes adaptive multi-level quadrature amplitude modulation (M-QAM) to approach these rate limits. In Chapter 10 a new hybrid adaptive scheme which supports simultaneous voice and data transmission over fading channels is proposed and the performance of this scheme over Nakagami-m fading channels is evaluated. Cellular systems are subject not only to fading but also to co-channel interference. Chapter 11 introduces a general analytical framework quantifying the spectral efficiency limits of cellular systems in which the mobile adapts their rates relative to their fading and interference conditions. The thesis concludes in Chapter 12 with a summary and discussion of future research directions.

Chapter 2 Fading Channels Characterization and Modeling

2.1 Introduction

Radio wave propagation through wireless channels is a complicated phenomenon characterized by various effects such as multipath and shadowing. A precise mathematical description of this phenomenon is either unknown or too complex for tractable communications systems analyses. However, considerable efforts have been devoted to the statistical modeling and characterization of these different effects. The result is a range of relatively simple and accurate statistical models for fading channels which depend on the particular propagation environment and the underlying communication scenario.

The primary purpose of this chapter is to briefly review the principal characteristics and models for fading channels. A more detailed treatment of this subject can be found in standard textbooks such as [1, 2]. This chapter also introduces termininology and notation which will be used throughout the thesis. The chapter is organized as follows. The main characteristics of fading channels are presented in the next section. Models for frequency-flat fading channels, corresponding to narrowband transmission, are described in Section 2.3. Models for frequency-selective fading channels which characterize fading in wideband channels, are described in Section 2.4.

2.2 Main Characteristics of Fading Channels

2.2.1 Slow and Fast Fading

The distinction between slow and fast fading is important for the mathematical modeling of fading channels and for the performance evaluation of communication systems operating over these channels. This notion is related to the *coherence time* of the channel, defined as the inverse of the channel *Doppler spread*, which measures the period of time over which the fading process is correlated. The fading is said to be slow if the symbol time duration is smaller than the channel's coherence time, otherwise it is considered to be fast. In slow fading a particular fade level will affect many successive symbols, which leads to burst errors, whereas in fast fading the fading is independent from symbol to symbol.

In this thesis we focus on the performance evaluation of adaptive and diversity techniques. These

techniques are typically used in conjunction with slow fading. We therefore limit ourselves to this type of fading throughout the whole thesis.

2.2.2 Frequency-Flat and Frequency-Selective Fading

Frequency-selectivity is also an important characteristic of fading channels. If all the spectral components of the transmitted signal are affected in a similar manner, the fading is said to be frequency-nonselective or equivalently frequency-flat. This is the case for *narrow-band* systems in which the transmitted signal bandwidth is much smaller than the channel's *coherence bandwidth.* This bandwidth is defined as the inverse of the *maximum delay spread* τ_{max}, and measures the frequency range over which the fading process is correlated. On the other hand if the spectral components of the transmitted signal are affected by different amplitude gains and phase shifts, the fading is said to be frequency-selective. This applies to *wide-band* systems in which the transmitted bandwidth is bigger than the channel's *coherence bandwidth.*

2.2.3 Envelope and Phase Fluctuations

In fading both the envelope and the phase of the received signal fluctuate over time. However, for coherent modulation the fading effects on the phase can severely degrade performance. We assume in our analyses that these phase effects are perfectly corrected at the receiver. For noncoherent modulations phase information is not needed at the receiver and therefore the phase variation due to fading does not affect the performance of these modulations. Hence our performance analyses for both coherent and noncoherent modulation over fading channels requires only the fading envelope statistics. Since we assume slow fading the fading envelope random process can be represented by a random variable (RV) over any given symbol time.

2.3 Modeling of Flat Fading Channels

When fading affects narrow-band systems, the received carrier amplitude is modulated by the fading amplitude α, where α is an RV with mean square value $\Omega = \overline{\alpha^2}$ and probability density function (PDF) $p_\alpha(\alpha)$ which is dependent on the nature of the radio propagation environment. After passing through the fading channel, the signal is perturbed at the receiver by additive white Gaussian noise (AWGN) which is typically assumed to be statistically independent of the fading amplitude α, and which is characterized by a one-sided power spectral density N_0 (W/Hz). Equivalently, the received instantaneous signal power is modulated by α^2. Thus we define the instantaneous signal-to-noise power ratio (SNR) per symbol by $\gamma = \alpha^2 E_s/N_0$ and the average SNR per symbol by $\overline{\gamma} = \Omega E_s/N_0$, where E_s is the energy per symbol. Our performance evaluation of digital communications over

fading channels will generally be a function of the average SNR per symbol $\overline{\gamma}$. For slowly-varying channels the fading amplitude is constant over a symbol time and the PDF of γ is obtained by introducing a change of variables in the expression for the fading PDF $p_\alpha(\alpha)$ of α yielding

$$p_\gamma(\gamma) = \frac{p_\alpha\left(\sqrt{\frac{\Omega\,\gamma}{\overline{\gamma}}}\right)}{2\sqrt{\frac{\Omega\,\gamma}{\overline{\gamma}}}}. \tag{2.1}$$

The amount of fading (AF), or "fading figure," associated with the fading PDF is defined as

$$\mathrm{AF} = \frac{\mathrm{Var}[\alpha^2]}{(\mathrm{E}[\alpha^2])^2} = \frac{\mathrm{E}\left[(\alpha^2-\Omega)^2\right]}{\Omega^2} = \frac{\mathrm{E}[\gamma^2]-(\mathrm{E}[\gamma])^2}{(\mathrm{E}[\gamma])^2}, \tag{2.2}$$

with $\mathrm{E}[\cdot]$ denoting statistical average and $\mathrm{Var}[\cdot]$ denoting variance. This figure was introduced by Charash [3, (p. 29)], [4] as a unified measure of the severity of the fading, and is typically independent of the average fading power Ω.

We now present the different radio propagation effects involved in fading channels, their corresponding PDFs, AFs, and their relation to physical channels. Note that a more detailed treatment of this particular topic will be presented in [5, Chapter 2].

2.3.1 Multipath Fading

Multipath fading is due to the constructive and destructive combination of randomly delayed, reflected, scattered, and diffracted signal components. This type of fading is relatively fast and is therefore responsible for the short-term signal variations. Depending on the nature of the radio propagation environment, there are different models describing the statistical behavior of the multipath fading envelope.

Rayleigh

The Rayleigh distribution is frequently used to model multipath fading with no direct line-of-sight (LOS) path. In this case, the channel fading amplitude α is distributed according to

$$p_\alpha(\alpha;\Omega) = \frac{2\,\alpha}{\Omega}\exp\left(-\frac{\alpha^2}{\Omega}\right); \qquad \alpha \geq 0, \tag{2.3}$$

and hence the instantaneous SNR per symbol of the channel, γ, is distributed according to an exponential distribution given by

$$p_\gamma(\gamma;\overline{\gamma}) = \frac{1}{\overline{\gamma}}\exp\left(-\frac{\gamma}{\overline{\gamma}}\right); \qquad \gamma \geq 0. \tag{2.4}$$

The moments of this PDF are given by

$$\mathrm{E}(\gamma^k) = \Gamma(1+k)\ \overline{\gamma}^k, \tag{2.5}$$

where $\Gamma(.)$ is the gamma function. The Rayleigh distribution therefore has an AF equal to 1, and typically agrees very well with experimental data for mobile systems where no LOS path exists between the transmitter and receiver antennas [2]. It also applies to the propagation of reflected and refracted paths through the the troposphere [6] and ionosphere [7, 8], and to ship-to-ship [9, 10, 11] radio links.

Nakagami-q (Hoyt)

The Nakagami-q distribution, also referred to as the Hoyt distribution [12], is given in [13, Eqn. (52)] by

$$p_\alpha(\alpha;\Omega,q) = \frac{(1+q^2)\ \alpha}{q\ \Omega} \exp\left(-\frac{(1+q^2)^2\ \alpha^2}{4q^2\Omega}\right)\ I_0\left(\frac{(1-q^4)\ \alpha^2}{4\ q^2\ \Omega}\right); \qquad \alpha \geq 0, \tag{2.6}$$

where $I_0(.)$ is the zero-th order modified Bessel function of the first kind, and q is the Nakagami-q fading parameter which ranges from 0 to 1. Using (2.1), it can be shown that the SNR per symbol of the channel, γ, is distributed according to

$$p_q(\gamma;\overline{\gamma},q) = \frac{(1+q^2)}{2\ q\ \overline{\gamma}} \exp\left(-\frac{(1+q^2)^2\ \gamma}{4q^2\overline{\gamma}}\right)\ I_0\left(\frac{(1-q^4)\ \gamma}{4\ q^2\ \overline{\gamma}}\right); \qquad \gamma \geq 0. \tag{2.7}$$

It can be shown that the moments of this PDF are given by [13, Eqn. (52)]

$$\mathrm{E}(\gamma^k) = \Gamma(1+k)\ {}_2F_1\left(-\frac{k-1}{2}, -\frac{k}{2}; 1; \left(\frac{1-q^2}{1+q^2}\right)^2\right)\ \overline{\gamma}^k, \tag{2.8}$$

where ${}_2F_1(\cdot,\cdot;\cdot,\cdot)$ is the Gauss hypergeometric function, and the AF of the Nakagami-q distribution is therefore given by

$$\mathrm{AF}_q = \frac{2\ (1+q^4)}{(1+q^2)^2}; \qquad 0 \leq q \leq 1, \tag{2.9}$$

and hence ranges between 1 ($q = 1$) and 2 ($q = 0$). The Nakagami-q distribution spans the range from one-sided Gaussian fading ($q = 0$) to Rayleigh fading ($q = 1$). It is typically observed on satellite links subject to strong ionospheric scintillation [14, 15]. Note that one-sided Gaussian fading corresponds to the worst case fading or equivalently, the largest AF for all multipath distributions considered in our analyses.

Nakagami-n (Rice)

The Nakagami-n distribution is also known as the Rice distribution [16]. It is often used to model propagation paths consisting of one strong direct LOS component and many random weaker components. Here the channel fading amplitude follows the distribution [13, Eqn. (50)]

$$p_\alpha(\alpha;\Omega,n) = \frac{2\,(1+n^2)\,e^{-n^2}\,\alpha}{\Omega}\exp\left(-\frac{(1+n^2)\,\alpha^2}{\Omega}\right)\,I_0\left(2\,n\,\alpha\,\sqrt{\frac{1+n^2}{\Omega}}\right);\qquad \alpha\geq 0, \quad (2.10)$$

where n is the Nakagami-n fading parameter which ranges from 0 to ∞ and which is related to the Rician K factor by $K = n^2$. Applying (2.1) shows that the SNR per symbol of the channel, γ, is distributed according to a non-central chi-square distribution given by

$$p_n(\gamma;\overline{\gamma},n) = \frac{(1+n^2)\,e^{-n^2}}{\overline{\gamma}}\exp\left(-\frac{(1+n^2)\,\gamma}{\overline{\gamma}}\right)\,I_0\left(2\,n\,\sqrt{\frac{(1+n^2)\,\gamma}{\overline{\gamma}}}\right);\qquad \gamma\geq 0. \quad (2.11)$$

It can also be shown that the moments of this PDF are given by [13, Eqn. (50)]

$$\mathrm{E}(\gamma^k) = \frac{\Gamma(1+k)}{(1+n^2)^k}\,{}_1F_1(-k,1;-n^2)\,\overline{\gamma}^k, \quad (2.12)$$

where ${}_1F_1(\cdot,\cdot;\cdot)$ is the Kummer confluent hypergeometric function. The AF of the Nakagami-n distribution is given by

$$\mathrm{AF}_n = \frac{1+2\,n^2}{(1+n^2)^2};\qquad n\geq 0, \quad (2.13)$$

and hence ranges between 0 ($n=\infty$) and 1 ($n=0$). The Nakagami-n distribution spans the range from Rayleigh fading ($n=0$) to no fading (constant amplitude) ($n=\infty$). This type of fading is typically observed in the first resolvable LOS paths of microcellular urban and suburban land mobile [17], picocellular indoor [18], and factory [19] environments. It also applies to the dominant LOS path of satellite [20, 21] and ship-to-ship [9] radio links.

Nakagami-m

The Nakagami-m PDF is in essence a central chi-square distribution given by [13, Eqn. (11)]

$$p_\alpha(\alpha;\Omega,m) = \frac{2\,m^m\,\alpha^{2m-1}}{\Omega^m\,\Gamma(m)}\,\exp\left(-\frac{m\,\alpha^2}{\Omega}\right);\qquad \alpha\geq 0, \quad (2.14)$$

where m is the Nakagami-m fading parameter which ranges from 1/2 to ∞. Applying (2.1) shows that the SNR per symbol, γ, is distributed according to a gamma distribution given by

$$p_m(\gamma;\overline{\gamma},m) = \frac{m^m\,\gamma^{m-1}}{\overline{\gamma}^m\,\Gamma(m)}\,\exp\left(-\frac{m\,\gamma}{\overline{\gamma}}\right);\qquad \gamma\geq 0. \quad (2.15)$$

It can also be shown that the moments of this PDF are given by [13, Eqn. (65)]

$$\mathrm{E}[\gamma^k] = \frac{\Gamma(m-k)}{\Gamma(m)\ m^k}\ \overline{\gamma}^k \tag{2.16}$$

which yields an AF of

$$\mathrm{AF}_m = \frac{1}{m}; \qquad m \geq 1/2. \tag{2.17}$$

Hence, the Nakagami-m distribution spans via the m parameter the widest range of AF (from 0 to 2) among all the multipath distributions considered in this thesis. For instance, it includes the one-sided Gaussian distribution ($m = 1/2$) and the Rayleigh distribution ($m = 1$) as special cases. In the limit as $m \longrightarrow +\infty$, the Nakagami-$m$ fading channel converges to a nonfading AWGN channel. Furthermore, when $m < 1$, a one-to-one mapping between the m parameter and the q parameter allows the Nakagami-m distribution to closely approximate the Nakagami-q (Hoyt) distribution [13, Eqn. (59)]. Similarly, when $m > 1$, a one-to-one mapping between the m parameter and the n parameter (or equivalently the Rician K factor) allows the Nakagami-m distribution to closely approximate the Nakagami-n (Rice) distribution [13, (Eqn. 56)]. The Nakagami-m distribution often gives the best fit to land-mobile [22, 23, 24] and indoor-mobile [25] multipath propagation, as well as scintillating ionospheric radio links [8, 26, 27, 28, 29].

2.3.2 Log-normal Shadowing

In terrestrial and satellite land-mobile systems, the link quality is also affected by slow variation of the mean signal level due to the shadowing from terrain, buildings, and trees. Communication system performance will depend only on shadowing if the radio receiver is able to average out the fast multipath fading or if an efficient "micro"-diversity system is used to eliminate the effects of multipath. Based on empirical measurements, there is a general consensus that shadowing can be modeled by a log-normal distribution for various outdoor and indoor environments [30, 22, 31, 32, 33, 34], in which case the path SNR per symbol γ has a PDF given by the standard log-normal expression

$$p_\sigma(\gamma;\mu,\sigma) = \frac{\xi}{\sqrt{2\pi}\ \sigma\ \gamma}\ \exp\left[-\frac{(10\log_{10}\gamma - \mu)^2}{2\ \sigma^2}\right], \tag{2.18}$$

where $\xi = 10/\ln 10 = 4.3429$, and μ (dB) and σ (dB) are the mean and the standard deviation of $10\log_{10}\gamma$, respectively.

The moments of (2.18) are given by

$$\mathrm{E}[\gamma^k] = \exp\left(\frac{k}{\xi}\ \mu + \frac{1}{2}\left(\frac{k}{\xi}\right)^2\ \sigma^2\right) \tag{2.19}$$

yielding an AF of

$$\mathrm{AF}_{\sigma} = \exp\left(\frac{\sigma^2}{\xi^2}\right) - 1. \tag{2.20}$$

From (2.20) the AF associated with a lognormal PDF can be arbitrarily high. However, as noted by Charash [3, (p. 29)], in practical situations the standard deviation of shadow fading does not exceed 9 dB [2, p. 88]. Hence, the AF of lognormal shadowing is bounded by 73. This number exceeds the maximal AF exhibited by the various multipath PDFs studied in Section 2.3.1 by several order of magnitudes.

2.3.3 Composite Multipath/Shadowing

A composite multipath/shadowed fading environment consists of multipath fading superimposed on log-normal shadowing. In this environment the receiver does not average out the envelope fading due to multipath but rather reacts to the instantaneous composite multipath/shadowed signal [2, Sec. 2.4.2]. This is often the scenario in congested downtown areas with slow moving pedestrians and vehicles [22, 35, 36]. This type of composite fading is also observed in land-mobile satellite systems subject to vegetative and/or urban shadowing [37, 38, 39, 40, 41]. There are two approaches and various combinations suggested in the literature for obtaining the composite distribution. Here, as an example, we present the composite gamma/log-normal PDF introduced by Ho and Stüber [36]. This PDF arises in Nakagami-m shadowed environments and is obtained by averaging the gamma distributed signal power (or equivalently the SNR per symbol) (2.15) over the conditional density of the log-normally distributed mean signal power (or equivalently average the SNR per symbol) (2.18), giving the following channel PDF:

$$p_{m\sigma}(\gamma; m, \mu, \sigma) = \int_0^{\infty} \frac{m^m \, \gamma^{m-1}}{w^m \, \Gamma(m)} \exp\left[-\frac{m\,\gamma}{w}\right] \frac{\xi}{\sqrt{2\pi}\,\sigma\,w} \exp\left[-\frac{(10\log_{10} w - \mu)^2}{2\,\sigma^2}\right] dw. \tag{2.21}$$

For the special case where the multipath is Rayleigh distributed ($m = 1$), (2.21) reduces to a composite exponential/log-normal PDF which was initially proposed by Hansen and Meno [35].

The moments of a gamma/log-normal PDF are given by

$$\mathrm{E}[\gamma^k] = \frac{\Gamma(m+k)}{\Gamma(m)\, m^k} \exp\left(\frac{k}{\xi}\,\mu + \frac{1}{2}\left(\frac{k}{\xi}\right)^2 \sigma^2\right) \tag{2.22}$$

and the resulting AF is given by

$$\mathrm{AF}_{m\sigma} = \frac{1+m}{m} \exp\left(\frac{\sigma^2}{\xi^2}\right) - 1. \tag{2.23}$$

Note that when shadowing is absent ($\sigma = 0$), (2.23) reduces to (2.17), as expected. Similarly, as the fading is reduced ($m \to \infty$), (2.23) reduces to (2.20), as expected.

2.3.4 Combined (Time-Shared) Shadowed/Unshadowed

From their land-mobile satellite channel characterization experiments, Lutz *et al.* [40] and Barts and Stutzman [42] found that the overall fading process for land-mobile satellite systems is a convex combination of unshadowed multipath fading and a composite multipath/shadowed fading. Here, as an example, we present in more detail the Lutz *et al.* model [40]. When no shadowing is present, the fading follows a Rice (Nakagami-n) PDF. On the other hand when shadowing is present, it is assumed that no direct LOS path exists and the received signal power (or equivalently SNR per bit) is assumed to be an exponential/log-normal (Hansen-Meno) PDF [35]. The combination is characterized by the shadowing time-share factor which is denoted by A, $0 \leq A \leq 1$; hence, the resulting combined PDF is given by

$$p_{AK\sigma}(\gamma; A, \overline{\gamma}^u, K; \mu^s, \sigma) = (1 - A)\ p_n(\gamma; \overline{\gamma}^u, \sqrt{K}) + A\ p_{m\sigma}(\gamma; 1, \mu^s, \sigma), \tag{2.24}$$

where $\overline{\gamma}^u$ is the average SNR per symbol during the unshadowed fraction of time, and μ^s is the average of $10 \log_{10} \gamma$ during the shadowed fraction of time. The overall average SNR per symbol, $\overline{\gamma}$, is then given by

$$\overline{\gamma} = (1 - A)\ \overline{\gamma}^u + A\ 10^{\frac{\mu^s}{10} - \frac{\ln 10 \sigma^2}{200}}. \tag{2.25}$$

2.4 Modeling of Frequency-Selective Fading Channels

When wide-band signals propagate through a frequency-selective channel, their spectrum is affected by the channel transfer function, resulting in a time dispersion of the waveform. This type of fading can be modeled as a linear filter characterized by the following complex-valued lowpass equivalent impulse response

$$h(t) = \sum_{l=1}^{L} \alpha_l\ e^{-j\theta_l}\ \delta(t - \tau_l), \tag{2.26}$$

where $\delta(.)$ is the Dirac delta function, l is the channel index, and $\{\alpha_l\}_{l=1}^{L}$, $\{\theta_l\}_{l=1}^{L}$, and $\{\tau_l\}_{l=1}^{L}$ are the random channel amplitudes, phases, and delays, respectively.

In (2.26) L is the number of resolvable paths (the first path being the reference path whose delay $\tau_1 = 0$) and is related to the ratio of the maximum delay spread to the symbol time. Under the slow fading assumption, L is assumed to be constant over a certain period of time, and $\{\alpha_l\}_{l=1}^{L}$, $\{\theta_l\}_{l=1}^{L}$, and $\{\tau_l\}_{l=1}^{L}$ are all constant over a symbol interval. The different paths of a given impulse response are typically generated by different scatterers, and therefore they tend to exhibit negligible correlations [34, 43]. Therefore, it is reasonable to assume that the $\{\alpha_l\}_{l=1}^{L_p}$ are statistically independent RVs. In particular, the fading amplitude α_l of the lth resolved path is assumed to be a RV whose mean square value $\overline{\alpha_l^2}$ is denoted by Ω_l and whose PDF $p_{\alpha_l}(\alpha_l)$ can be any one of the PDFs

presented above.

The first arriving path in the impulse response typically exhibits a lower amount of fading than subsequent paths, since it may contain the LOS path [43, 17, 24]. Furthermore, since the specular power component typically decreases with respect to delay, the last arriving paths exhibit higher amounts of fading [43, 24].

The $\{\Omega_l\}_{l=1}^{L}$ are related to the channel's power delay profile (PDP) which is also referred to as the multipath intensity profile (MIP) and which is typically a decreasing function of the delay. The PDP model can assume various forms depending on whether the model is for indoor or outdoor environments and, for each environment, the general propagation conditions. For example PDPs for indoor partitioned office buildings, indoor factory buildings with heavy machinery, high density office buildings in urban areas, low density residential houses in suburban areas, open rural environment, hilly or mountainous regions, and maritime environment are described in [44]). For example, experimental measurements indicate that the mobile radio channel is well characterized by an exponentially decaying PDP for indoor office buildings [34] and congested urban areas [30, 45]:

$$\Omega_l = \Omega_1 \; e^{-\tau_l/\tau_{max}}; \qquad l = 1, 2, \cdots, L, \tag{2.27}$$

where Ω_1 is the average fading power corresponding to the first (reference) propagation path. In the literature the delays are often assumed to be equally spaced ($\tau_{l+1} - \tau_l$ is constant and equal to the symbol time T_s) [1, p. 730], [46] and, with this assumption, we get the equally spaced exponential profile given by

$$\Omega_l = \Omega_1 \; e^{-(l-1)\;\delta}; \qquad \delta \geq 0, \text{ and } l = 1, 2, \cdots, L, \tag{2.28}$$

where the parameter δ reflects the rate at which the average fading power decays. Other idealized PDP profiles reported or used in the literature include the constant (flat) [47], the flat exponential [48], the double-spike [47], the Gaussian [47], the power-function (polynomial) [49], and other more complicated composite profiles [50].

As in the flat fading case, after passing through the fading channel a wide-band signal is perturbed by AWGN with a one-sided power spectral density N_0 (W/Hz). The AWGN is assumed to be independent of the fading amplitudes $\{\alpha_l\}_{l=1}^{L}$. Hence the instantaneous SNR per symbol of the lth channel is given by $\gamma_l = \frac{\alpha_l^2 \, E_s}{N_0}$, and the average SNR per symbol of the lth channel is given by $\overline{\gamma}_l = \frac{\Omega_l E_s}{N_0}$.

2.5 Conclusion

In this chapter we presented a brief overview of fading channel characteristics. We then described various frequency-flat and frequency-selective fading channel models. With the above models in

hand, we are now in a position to analyze the performance of various communication systems operating over these channels.

Chapter 3 A Generic Form for the Average Error Probability of Binary Signals over Flat Fading Channels - Single Channel Reception

3.1 Introduction

Although specific results for the bit-error-rate of binary signals transmitted over a single additive white Gaussian noise (AWGN) channel exist for coherent, differentially coherent, and noncoherent modulations [51], an interesting unification of these results into a single bit-error-rate (BER) expression is possible as discussed by Wojnar [52]. In particular, Wojnar cites a result privately communicated to him by Linder (see footnote 2 of Wojnar paper [52]) which states that the BER of coherent, differentially coherent and noncoherent detection of binary signals transmitted over the AWGN channel is given by the generic expression

$$P_b(E) = \frac{\Gamma\left(b, a\frac{E_b}{N_0}\right)}{2\,\Gamma(b)}, \tag{3.1}$$

where $\Gamma(\cdot,\cdot)$ is the complementary incomplete gamma function [53, p. 949, Eqn. (8.350.2)] which is traditionally defined as

$$\Gamma(\alpha, x) = \int_x^\infty e^{-t}\, t^{\alpha-1}\, dt, \tag{3.2}$$

and $\Gamma(\cdot)$ is the gamma function [53, p. 942, Eqn. (8.310.1)]. In (3.1), E_b (J) represents the energy per bit, N_0 (W/Hz) is the AWGN power density, and a and b depend on the particular form of modulation and detection and are presented in Table 3.1. Hence, although the result in (3.1) does not provide any new results relative to those indicated in Table 3.1, it does offer a nice unification of several BER expressions into a single one which can easily be programmed using standard mathematical software packages such as Mathematica. Furthermore, when evaluating the average BER performance of these very same binary communication systems over a fading channel, an alternate representation of the complementary gamma function will also be helpful in unifying these results, as we will show next.

Table 3.1: The parameters a and b for various modulation/detection combinations.

(a,b)	1/2	1
1/2	orthogonal coherent BFSK	orthogonal noncoherent BFSK
1	antipodal coherent BPSK	antipodal differentially coherent BPSK (DPSK)
$0 \leq g \leq 1$	correlated coherent binary signaling	

3.2 Desired Representation of the Conditional BER

When flat fading is present, the received carrier amplitude is attenuated by the fading amplitude, α, which is a random variable (RV) with mean square value $\Omega = \overline{\alpha^2}$ and probability density function (PDF) dependent on the nature of the radio propagation environment. Equivalently, the received instantaneous signal power is attenuated by α^2 and thus it is appropriate to define the instantaneous signal-to-noise ratio (SNR) per bit by $\gamma = \alpha^2 E_b/N_0$ and the average SNR per bit by $\overline{\gamma} = \Omega E_b/N_0$. As such, for a fixed fade level α, the BER of any of the modulations considered in Table 1 is obtained by replacing E_b/N_0 by γ in (3.1). To evaluate the average BER one must then average (3.1) over the statistics of the fading. Since in the definition of (3.2) the argument x appears in the lower limit of the integral, it is analytically difficult to perform such averages. Rather it would be desirable to have (3.2) in an integral form with limits were independent of the argument x (preferably finite from a computational standpoint) and an integrand that is exponential in the argument x. We now develop such a desired form and deduce an alternate representation of the conditional BER (3.1).

Making the change of variable $t = \frac{x}{\sin^2\phi}$ in (3.2) and after some manipulations we arrive at the desired result

$$\Gamma(\alpha, x) = 2\, x^{\alpha} \int_0^{\pi/2} \frac{\cos\phi}{(\sin\phi)^{2\alpha+1}} \exp\left(-\frac{x}{\sin^2\phi}\right) d\phi. \tag{3.3}$$

Substituting (3.3) in (3.1) we get the alternate desired representation of the conditional BER as

$$P_b(\gamma) = \frac{(a\,\gamma)^b}{\Gamma(b)} \int_0^{\pi/2} \frac{\cos\phi}{(\sin\phi)^{2b+1}} \exp\left(-\frac{a\gamma}{\sin^2\phi}\right) d\phi. \tag{3.4}$$

3.3 Average BER over Fading Channels

Assuming that the fading is independent of the AWGN, the unconditional BER, $\overline{P}_b$, is obtained by averaging (3.4) over the underlying fading RV giving

$$\overline{P}_b = \int_0^{\infty} P_b(\gamma)\; p_\gamma(\gamma; \overline{\gamma}, i)\; d\gamma, \tag{3.5}$$

where i is the fading parameter associated with the fading PDF $p_\gamma(\gamma; \overline{\gamma}, i)$ and is denoted by r, q, n, and m, for the Rayleigh, Nakagami-q (Hoyt), Nakagami-n (Rice), and Nakagami-m PDFs,

respectively. Substituting (3.4) into (3.5), interchanging the order of integration, and grouping together like variables yields

$$\overline{P}_b = \frac{a^b}{\Gamma(b)} \int_0^{\pi/2} \frac{\cos\phi}{(\sin\phi)^{2b+1}} \mathcal{L}_i(\overline{\gamma}; a, b; \phi)\, d\phi, \tag{3.6}$$

where

$$\mathcal{L}_i(\overline{\gamma}; a, b; \phi) \triangleq \int_0^{\infty} \gamma^b\, p_\gamma(\gamma; \overline{\gamma}, i)\, \exp\left(-\frac{a\gamma}{\sin^2\phi}\right) d\gamma, \tag{3.7}$$

is in the form of a Laplace transform of the function $\gamma^b\, p_\gamma(\gamma; \overline{\gamma}, i)$. The form of the average BER in (3.6) is interesting in that the integrals $\mathcal{L}_i(\overline{\gamma}; a, b, \phi)$ can be obtained in closed form for the four PDFs under consideration, as we shall show now.

3.3.1 Rayleigh Fading

Recall from the previous chapter that the Rayleigh distribution is frequently used to model multipath fading with no direct line-of-sight (LOS) path. In this case the received SNR per bit is distributed according to an exponential distribution given by (2.4). Substituting (2.4) in (3.7) and making use of the Laplace transform [53, p. 1178, Eqn. (3)]

$$\int_0^{\infty} x^\nu e^{-sx}\, dx = \frac{\Gamma(\nu+1)}{s^{\nu+1}}; \qquad s > 0,\ \nu > -1, \tag{3.8}$$

we obtain

$$\mathcal{L}_r(\overline{\gamma}; a, b, \phi) = \frac{\Gamma(b+1)\,\overline{\gamma}^b}{\left(1 + \frac{a}{\overline{\gamma}\,\sin^2\phi}\right)^{b+1}}. \tag{3.9}$$

Substituting (3.9) in (3.6) and making the change of variable $t = \left(1 + \frac{a\overline{\gamma}}{\sin^2\phi}\right)^{-1}$, we arrive after some manipulations to the equivalent compact result

$$\overline{P}_b = \frac{b}{2}\, B_{(1+a\overline{\gamma})^{-1}}(1, b), \tag{3.10}$$

where $B_x(p, q)$ is the incomplete beta function [53, p. 960, Eqn. (8.391)].

3.3.2 Nakagami-q (Hoyt) Fading

When the channel follows a Nakagami-q distribution [13], also referred to as the Hoyt distribution [12], it can be shown that the SNR per bit is distributed according to (2.7). Substituting (2.7) in (3.7) and making use of the Laplace transform found in [54, p. 196, Eqn. (8)],

$$\int_0^{\infty} t^\mu\, I_0(at)\, e^{-pt}\, dt = \frac{\Gamma(\mu+1)}{s^{\mu+1}}\, P_\mu^0\left(\frac{p}{s}\right);\ \mu > -1, \tag{3.11}$$

where $s = \sqrt{p^2 - a^2}$ and $P_\mu^0(\cdot)$ is the associated Legendre function [53, p. 1013, Sect. (8.7)], then recognizing the relation [53, p. 1027, Eqn. (8.777.1)]

$$P_\mu^0(z) = P_\mu(z) = {}_2F_1\left(-\mu, \mu+1; 1; \frac{1-z}{2}\right) \tag{3.12}$$

between the associated Legendre function and the Gaussian hypergeometric function ${}_2F_1(\cdot,\cdot;\cdot;\cdot)$ [53, p. 1065, Eqn. (9.100)], we obtain

$$\begin{aligned}\mathcal{L}_q(\overline{\gamma}; a, b, \phi) &= \frac{1+q^2}{2\,q} \frac{\Gamma(b+1)\,\overline{\gamma}^b}{\left(\left(\frac{a\overline{\gamma}}{\sin^2\phi} + \frac{(1+q^2)^2}{4q^2}\right)^2 - \left(\frac{1-q^4}{4q^2}\right)^2\right)^{\frac{b+1}{2}}} \\ &\times {}_2F_1\left(-b, b+1; 1; \frac{1}{2} - \frac{1}{2}\frac{\frac{a\overline{\gamma}}{\sin^2\phi} + \frac{(1+q^2)^2}{4q^2}}{\sqrt{\left(\frac{a\overline{\gamma}}{\sin^2\phi} + \frac{(1+q^2)^2}{4q^2}\right)^2 - \left(\frac{1-q^4}{4q^2}\right)^2}}\right).\end{aligned} \tag{3.13}$$

3.3.3 Nakagami-n (Rice) Fading

Recall that the Nakagami-n distribution [13] is the same as the Rice distribution [16]. It is often used to model propagation paths consisting of one strong direct LOS component and many random weaker components. Here the SNR per bit follows the distribution given by (2.11). Substituting (2.11) in (3.7) and making use of the Laplace transform found in [54, p. 197, Eqn. (20)]

$$\int_0^\infty t^{\mu-1/2}\, I_0\left(2\sqrt{at}\right) = \frac{\Gamma(\mu+1/2)\; e^{a/(2p)}}{\sqrt{a}\; p^\mu}\; M_{-\mu,0}\left(\frac{a}{p}\right);\; \mu > -1/2, \tag{3.14}$$

where $M_{-\mu,0}(\cdot)$ is the Whittaker function [53, p. 1086, Sect. 9.22], then recognizing the relation [53, p. 1087, Eqn. (9.220.2)]

$$M_{\mu,0}(z) = \sqrt{z}\; e^{-z/2}\; {}_1F_1(-\mu+1/2, 1; z) \tag{3.15}$$

between the Whittaker function and the Kummer confluent hypergeometric function ${}_1F_1(\cdot,\cdot;\cdot)$ [53, p. 1084, Sect. 9.20], we obtain

$$\mathcal{L}_n(\overline{\gamma}; a, b, \phi) = \frac{(1+n^2)e^{-n^2}\;\Gamma(b+1)\;\overline{\gamma}^b}{\left(1+n^2+\frac{a\overline{\gamma}}{\sin^2\phi}\right)^{1+b}}\; {}_1F_1\left(1+b, 1; \frac{n^2(1+n^2)}{1-n^2+\frac{a\overline{\gamma}}{\sin^2\phi}}\right). \tag{3.16}$$

3.3.4 Nakagami-m Fading

When the channel follows a Nakagami-m distribution, the SNR per bit is distributed according to a gamma distribution given by (2.15). Substituting (2.15) in (3.7) and again making use of the

Laplace transform (3.8), we obtain

$$\mathcal{L}_m(\overline{\gamma}; a, b, \phi) = \frac{\Gamma(b+m)}{\Gamma(m)} \frac{\left(\frac{1}{m}\right)^b}{\left(1 + \frac{a\overline{\gamma}}{m \sin^2 \phi}\right)^{b+m}}. \tag{3.17}$$

Substituting (3.17) in (3.6) and making the change of variable $t = \left(1 + \frac{a\overline{\gamma}}{m \sin^2 \phi}\right)^{-1}$, we arrive after some manipulations at the equivalent compact result originally given in [52, Eqn. (17)] as

$$\overline{P}_b = \frac{1}{2} I_{(1+a\overline{\gamma}/m)^{-1}}(m, b), \tag{3.18}$$

where $I_x(p, q)$ is the incomplete beta function ratio [53, p. 960, Eqn. (8.392.2)].

3.4 Conclusion

We presented in this chapter a generic form for the average BER of coherent, differentially coherent, and noncoherent binary signals with single channel reception. This generic form relies on an alternate representation of the incomplete gamma function and for all the channel fading models under consideration leads to an expression of the average BER involving a single finite-range integral of tabulated functions which can easily be computed numerically.

Chapter 4 Performance of Coherent Modulations over Generalized Fading Channels - Optimum Multichannel Reception

4.1 Introduction

In this chapter we assume that the phase shift introduced by the channel is perfectly tracked by the receiver, and we consider the performance of coherent modulations techniques (with and without diversity) over fading channels. This particular topic has been addressed in many papers [55, 56, 57, 58, 59, 60, 61, 62, 9, 10, 11, 63]. With some special exceptions [59, 9, 10, 11] most of the models for these systems typically assume either single channel reception or multichannel reception over independent identically distributed (i.i.d.) paths. These idealizations are not always realistic since the average fading power [44, 45] and the severity of fading [24, 17, 43] may vary from one path to the other when RAKE reception is employed to improve performance over frequency-selective fading. In this chapter we consider a sufficiently general multipath channel model in which the paths are not necessarily identically-distributed nor even distributed according to the same family of distributions. We call these channels generalized fading channels and we describe them in more detail in Section 4.2.2. We derive expressions for the exact symbol-error-rate (SER) of linearly modulated signals over such channels. The results are applicable to systems that employ coherent demodulation and maximal-ratio combining (MRC) [64]. The proposed approach takes advantage of alternate integral representations [65, 66] of the probability of error of these signals over additive white Gaussian noise (AWGN) channels (i.e., the conditional SER), along with some known Laplace transforms and/or Gauss-Hermite quadrature integrals, to derive the SER expressions. These expressions involve a single finite-range integral whose integrand contains only elementary functions, and which can therefore be easily evaluated.

These alternate representations have recently been used by Simon and Divsalar [67] as well as by Hall and Wilson [68] to solve several other communication problems involving the averaging of the Gaussian tail probability function. In addition, Tellambura *et al.* [63] published a recent paper in which they used these representations to analyze the performance of M-ary phase shift keying (M-PSK) with diversity reception over i.i.d. land-mobile satellite channels. In this chapter, we unify and add to the above results by providing new generic expressions for the average SER performance of various coherent communication systems with MRC diversity reception over generalized

fading channels. We focus in this chapter on presenting the approach which enables us to unify the performance of these systems under a common framework. Further, since the number of different modulation and fading combinations discussed herein is quite large, numerical results for the error rates of these combinations and dependence on the various fading parameters are omitted here. Some of the referenced papers cover such numerical illustrations. A more comprehensive treatment which includes numerical results can be found in [5].

The remainder of this chapter is organized as follows. In the next section we describe the transmitted signals, introduce the generalized multipath channel model, and present the receiver structure. We derive the average bit-error-rate (BER) of binary signals over generalized fading channels in Section 4.3. The average SER of M-ary phase-shift-keying (M-PSK), M-ary amplitude modulation (M-AM), and square M-ary quadrature amplitude modulation (M-QAM) signals over generalized fading channels is derived in Sections 4.4, 4.5, and 4.6, respectively using an approach similar to that of Section 4.3. Last, we give a summary of our results and offer some concluding remarks in Section 4.7.

4.2 System and Channel Models

4.2.1 Transmitted Signals

With any memoryless linear modulation technique, the complex signal transmitted over the channel may be represented as

$$s(t) = \sum_{i=-\infty}^{\infty} S^{(i)}\, e^{-j2\pi f_c t}\, P_{T_s}(t - iT_s), \tag{4.1}$$

where the function $P_{T_s}(\cdot)$ is a pulse shaping waveform of duration T_s seconds, f_c is the carrier frequency, and $\{S^{(i)}\}_{i=-\infty}^{\infty}$ represents the sequence of symbols that results from mapping successive k-bit blocks into one of $M = 2^k$ possible waveforms. Each complex symbol $S^{(i)}$ takes on values whose energy is denoted by E_m ($m = 1, 2, \cdots, M$) and the average energy per k-bit symbol (averaged over the set of the M waveforms' energies) is denoted by E_s and is related to the average energy per bit, E_b, by $E_s = \log_2(M)\, E_b$.

4.2.2 Multilink Channel Model

We consider a multilink channel where the transmitted signal is received over L independent slowly-varying flat fading channels, as shown in Fig. 4.1. In Fig. 4.1, $\{r_l(t)\}_{l=1}^{L}$ is the set of received replicas of the transmitted signal $s(t)$ where l is the channel index, and $\{\alpha_l\}_{l=1}^{L}$, $\{\theta_l\}_{l=1}^{L}$, and $\{\tau_l\}_{l=1}^{L}$ are the random channel amplitudes, phases, and delays, respectively. We assume that the sets $\{\alpha_l\}_{l=1}^{L}$, $\{\theta_l\}_{l=1}^{L}$, and $\{\tau_l\}_{l=1}^{L}$ are mutually independent. The first channel is assumed to be the reference

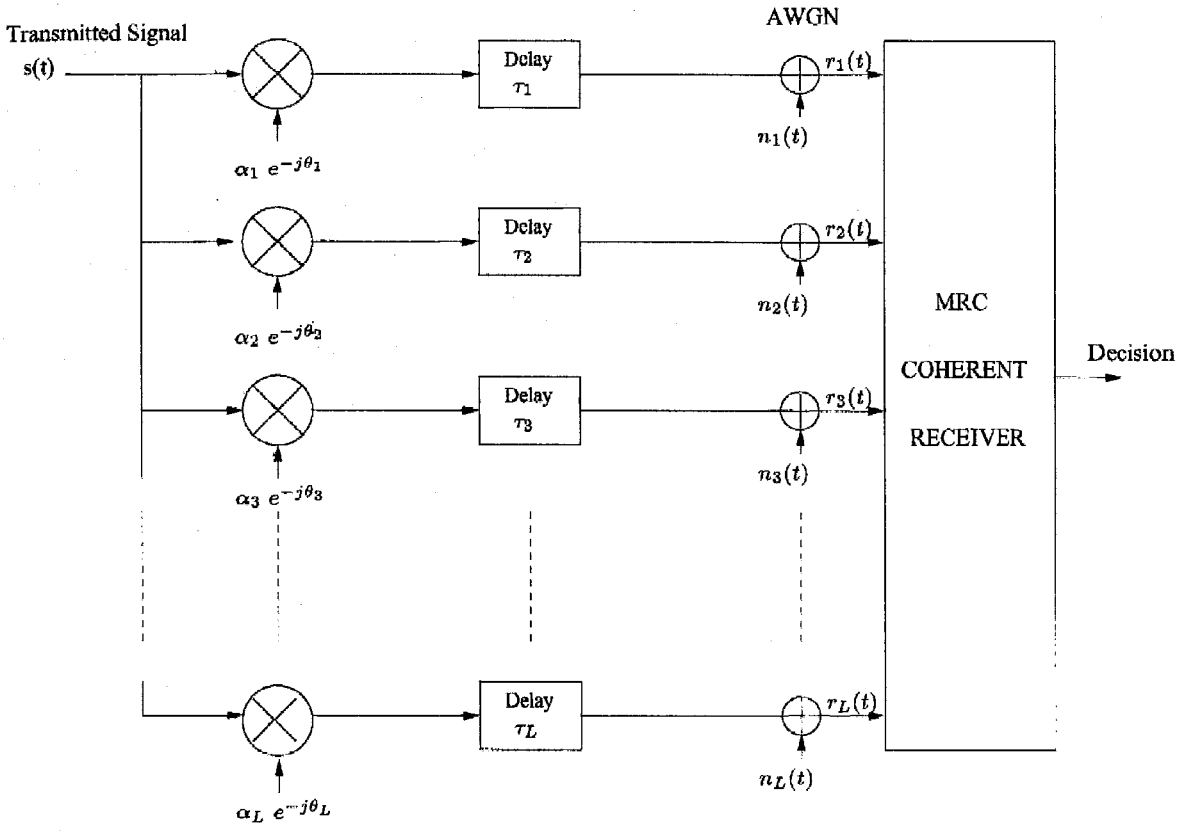

Figure 4.1: Multilink channel model.

channel with delay $\tau_1 = 0$ and, without loss of generality, we assume that $\tau_1 < \tau_2 < \cdots < \tau_L$. Because of the slow-fading assumption, we assume that the $\{\alpha_l\}_{l=1}^L$, $\{\theta_l\}_{l=1}^L$, and $\{\tau_l\}_{l=1}^L$ are all constant over a symbol interval.

The fading amplitudes $\{\alpha_l\}_{l=1}^L$ are assumed to be statistically independent random variables (RVs) whose mean square value $\overline{\alpha_l^2}$ is denoted by Ω_l and whose probability density function (PDF) is any of the different distributions described in Section 2.3. The multilink channel model used in our analyses is sufficiently general to include the case where the different channels are not necessarily identically distributed nor even distributed according to the same family of distributions. We call this type of multilink channel a generalized multilink fading channel.

After passing through the fading channel, each replica of the signal is perturbed by complex AWGN with a one-sided power spectral density which is denoted by $2N_l$ (W/Hz). The AWGN is assumed to be statistically independent from channel to channel and independent of the fading amplitudes $\{\alpha_l\}_{l=1}^L$. Hence, the instantaneous SNR per symbol of the lth channel is given by $\gamma_l = \frac{\alpha_l^2 E_s}{N_0}$, where E_s (J) is the energy per symbol, and $2N_0 = \sum_{l=1}^L 2N_l$ (W/Hz) is the total complex AWGN power spectral density.

4.2.3 MRC Receiver Model

We assume an L branch (finger) MRC receiver, as shown in Fig. 4.2. MRC is the optimal diversity scheme since it results in a maximum likelihood receiver [2, p. 244]. This receiver utilizes M correlators to detect the transmitted waveform (symbol) with the maximum a priori probability. Let us consider the mth waveform correlator. Each of the L received signals $r_l(t)$ is first delayed by $\tau_L - \tau_l$, coherently demodulated through multiplication by the unmodulated carrier $e^{j(2\pi f_c(t-\tau_L)+\theta_l)}$, then lowpass filtered to remove the second harmonics of the carrier. All these operations assume that the receiver is correctly time and phase synchronized at every branch (i.e., perfect carrier recovery, and perfect phase $\{\theta_l\}_{l=1}^{L}$ and time delay $\{\tau_l\}_{l=1}^{L}$ estimates). Using the MRC and assuming perfect knowledge of the fading amplitude on each branch, the L lowpass filter outputs $\{r_{m,l}\}_{l=1}^{L}$ are individually weighted by their respective fading amplitudes, and then combined by a linear combiner yielding

$$r_m = \sum_{l=1}^{L} \alpha_l \, r_{m,l}; \qquad m = 1, 2, \cdots, M. \tag{4.2}$$

The resulting signal is passed through a matched filter followed by a baud-rate sampler. The output of the sampler is then shifted by a bias term B_m given by [2, p. 244]

$$B_m = -\left(\sum_{l=1}^{L} \alpha_l^2\right) E_m; \qquad m = 1, 2, \cdots, M, \tag{4.3}$$

to form the decision variable $\mu(S_m)$[1]. Last of all the receiver selects the symbol corresponding to the maximum decision variable, as shown in Fig. 4.2.

The output of the MRC combiner reduces to the sum of a desired signal component and a Gaussian noise component. For equally-likely transmitted symbols, the total conditional SNR per symbol, γ_t, at the output of the MRC combiner is given by [2, p.246, Eqn. (5.98)]

$$\gamma_t = \sum_{l=1}^{L} \gamma_l. \tag{4.4}$$

4.3 Average Bit Error Rate of Binary Signals

4.3.1 Product Form Representation of the Conditional BER

The user's conditional BER in AWGN, $P_b(\gamma_t)$, is given by

$$P_b(\gamma_t) = Q\left(\sqrt{2\, g\, \gamma_t}\right), \tag{4.5}$$

[1]Note that if the waveforms have equal energy (as is the case for the M-PSK modulation scheme), the bias term can be ignored since it is the same for all the waveforms.

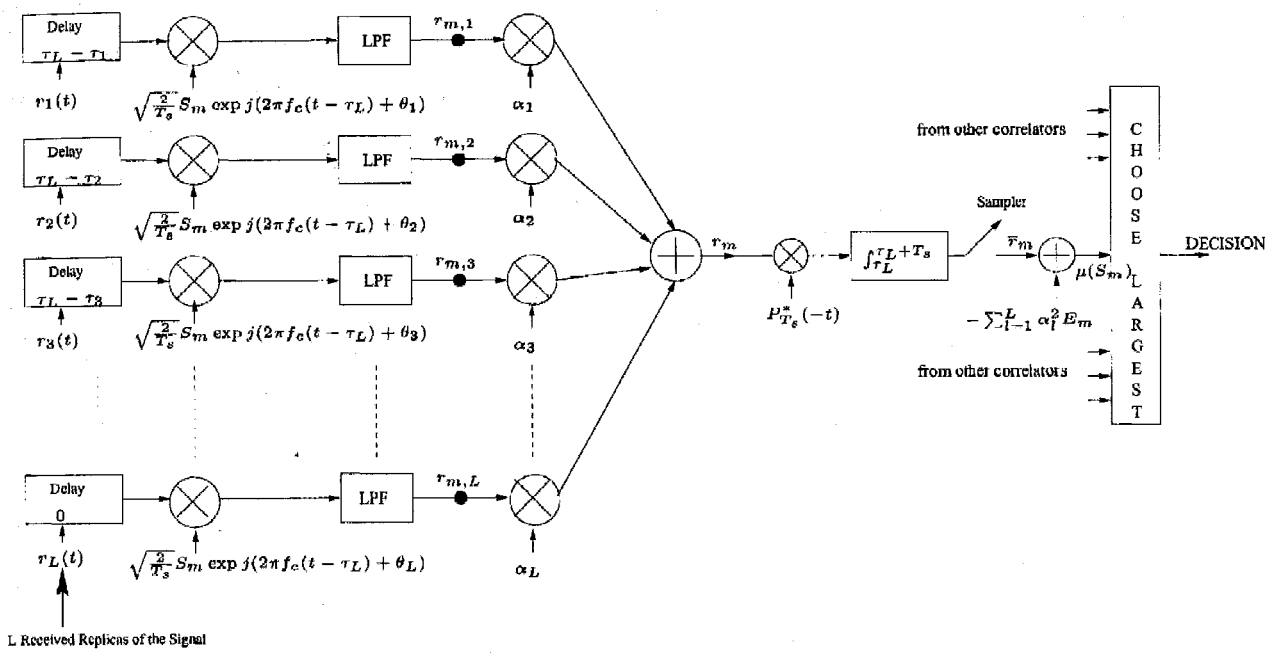

Figure 4.2: Maximal-ratio combining receiver block diagram (LPF: lowpass filter).

where $g = 1$ for coherent BPSK [51, Eqn. (4.55)], $g = 1/2$ for coherent orthogonal BFSK [51, Eqn. (4.59)], $g = \frac{1}{2} + \frac{1}{3\pi}$ for coherent BFSK with minimum correlation [51, Eqn. (4.63)], and $Q(.)$ is the Gaussian Q-function traditionally defined by

$$Q(x) = \frac{1}{\sqrt{2\pi}} \int_x^\infty e^{-t^2/2}\, dt. \tag{4.6}$$

Although (4.5) appears to be a very simple expression, it is often inconvenient when further analyses are required. In particular, our goal is to evaluate the performance of the system in terms of users' average BER, and for this purpose the conditional BER (4.5) has to be statistically averaged over the random parameters $\{\gamma_l\}_{l=1}^L$. This requires the integration of the Gaussian Q-function over these parameters, which is difficult since the argument of the function is in the *lower limit of the integral*. The classical approach to bypass this problem is to first find the PDF of γ_t and then average (4.5) over that PDF. In some cases of i.i.d. channels, the PDF of γ_t can be found which then often leads to simple closed-form expressions for the average BER. However, it is more difficult to find a simple expression for the PDF of γ_t when the channels have the same distribution (e.g., Nakagami-n (Rice)) but with different parameters (e.g., different average fading powers and/or different fading parameters). The most difficult case occurs when the PDFs of the different channels come from different families of distributions and in this case finding the PDF of γ_t appears intractable.

The key concept in our approach is to rely on an alternate representation of the Gaussian-Q

function. This representation allows us to obtain an elegant analytical expression for the average BER of the generalized multilink channel model which heretofore resisted a simple solution. The alternate representation was proposed by Craig who showed that the Gaussian Q-function could be represented in the following definite integral form [66, Eqn. (9)]:

$$Q(x) = \frac{1}{\pi}\int_0^{\pi/2} \exp\left(-\frac{x^2}{2\sin^2\phi}\right)\, d\phi; \qquad x \geq 0, \tag{4.7}$$

which can also be implied by the earlier work of Weinstein [69] and by Pawula *et al.* [65]. A simple derivation of this alternate representation of the Gaussian Q-function is given in Appendix A-1 of this chapter. This representation has the advantage of finite integration limits which are *independent of the argument* x, and also has an integrand which is *Gaussian in the argument* x. Using the alternate representation of the Gaussian-Q function (4.7) in (4.5), the conditional BER (4.5) may be rewritten in a more desirable product form given by

$$P_b(\gamma_t) = \frac{1}{\pi}\int_0^{\pi/2} \exp\left(-\frac{g\,\gamma_t}{\sin^2\phi}\right) d\phi = \frac{1}{\pi}\int_0^{\pi/2} \prod_{l=1}^{L} \exp\left(-\frac{g\,\gamma_l}{\sin^2\phi}\right) d\phi. \tag{4.8}$$

This form of the conditional BER is more desirable since we can first independently average over the individual statistical distributions of the γ_l's, and then perform the integral over ϕ, as described in more detail below.

4.3.2 Average BER with Single Channel Reception ($L = 1$)

Since the fading is assumed to be independent of the AWGN, the unconditional BER, $\overline{P}_b$, is obtained by averaging the single channel conditional BER, $P_b(\gamma)$, given by (4.8) for $L = 1$, over the underlying fading RV giving

$$\overline{P}_b = \int_0^{\infty} P_b(\gamma)\; p_\gamma(\gamma; \overline{\gamma}, i)\; d\gamma, \tag{4.9}$$

where i is the fading parameter(s) associated with the distribution $p_\gamma(\gamma; \overline{\gamma}, i)$ and is hence denoted by r, q, n, m, σ, $m\sigma$, and $AK\sigma$ for the Rayleigh, Nakagami-q (Hoyt), Nakagami-n (Rice), Nakagami-m, log-normal shadowing, composite multipath/shadowing, and combined (time-shared) shadowed/unshadowed PDFs, respectively. Substituting (4.8) for $L = 1$ into (4.9), then interchanging the order of integration, yields

$$\overline{P}_b = \frac{1}{\pi}\int_0^{\pi/2} \mathcal{I}_i(\overline{\gamma}; g; \phi)\; d\phi, \tag{4.10}$$

where

$$\mathcal{I}_i(\overline{\gamma}; g; \phi) \triangleq \int_0^{\infty} \exp\left(-\frac{g\,\gamma}{\sin^2\phi}\right)\; p_\gamma(\gamma; \overline{\gamma}, i)\; d\gamma \tag{4.11}$$

is in the form of a Laplace transform. The form of the average BER in (4.10) is interesting in that the integrals $\mathcal{I}_i(\overline{\gamma}; g; \phi)$ can either be obtained in closed-form with the help of classical Laplace transforms or can alternatively be efficiently computed by using Gauss-Hermite quadrature integration [70, p. 890, Eqn. (25.4.46)] for all previously mentioned fading channel models. We now evaluate these integrals for each of the fading models described in Section 2.3. In 4.3.3 we will use these integrals to obtain the average BER of binary signals with multichannel reception.

Multipath Fading

Rayleigh Substituting (2.4) into (4.11) then using the Laplace transform [53, Eqn. (1), p. 1178]

$$\int_0^\infty e^{-sx}\, dx = \frac{1}{s}; \qquad s > 0, \tag{4.12}$$

yields

$$\mathcal{I}_r(\overline{\gamma}; g; \phi) = \left(1 + \frac{g\,\overline{\gamma}}{\sin^2\phi}\right)^{-1}. \tag{4.13}$$

Substituting (4.13) in (4.10) then using [53, p. 185, Eqn. (2.562.1)], one can proceed further to obtain the well-known closed-form expression for the average BER over Rayleigh fading [1, Eqn. (7.3.7) and Eqn. (7.3.8)]

$$\overline{P}_b = \frac{1}{2}\left(1 - \sqrt{\frac{g\,\overline{\gamma}}{1 + g\,\overline{\gamma}}}\right). \tag{4.14}$$

Nakagami-q (Hoyt) Substituting (2.7) into (4.11) then using the Laplace transform [53, Eqn. (109), p. 1182]

$$\int_0^\infty I_0(ux)\, e^{-sx}\, dx = \left(s^2 - u^2\right)^{-1/2}; \qquad s > |u| \geq 0, \tag{4.15}$$

yields

$$\mathcal{I}_q(\overline{\gamma}; g; \phi) = \left(1 + \frac{2\,g\,\overline{\gamma}}{\sin^2\phi} + \frac{4\,q^2\,g^2\,\overline{\gamma}^2}{(1+q^2)^2\,\sin^4\phi}\right)^{-1/2}. \tag{4.16}$$

Nakagami-n (Rice) Substituting (2.11) into (4.11) then using the Laplace transform [70, Eqn. (29.3.81), p. 1026]

$$\int_0^\infty I_0(u\sqrt{x})\, e^{-sx}\, dx = \frac{e^{u^2/(4s)}}{s}; \qquad s > 0, \tag{4.17}$$

yields

$$\mathcal{I}_n(\overline{\gamma}; g; \phi) = \frac{(1+n^2)\,\sin^2\phi}{(1+n^2)\sin^2\phi + g\,\overline{\gamma}}\, \exp\left(-\frac{n^2\,g\,\overline{\gamma}}{(1+n^2)\sin^2\phi + g\,\overline{\gamma}}\right). \tag{4.18}$$

Nakagami-m Substituting (2.15) into (4.11) then using the Laplace transform [53, Eqn. (3), p. 1178]

$$\int_0^\infty x^\nu e^{-sx}\, dx = \frac{\Gamma(\nu+1)}{s^{\nu+1}}; \qquad s > 0,\ \nu > -1, \tag{4.19}$$

yields

$$\mathcal{I}_m(\overline{\gamma}; g; \phi) = \left(1 + \frac{g\ \overline{\gamma}}{m\ \sin^2 \phi}\right)^{-m}. \tag{4.20}$$

As a side result we show in Appendix B that by substituting (4.20) in (4.10) then using an equivalence with a known result, we obtain a closed-from expression for trigonometrics integrals which do not exist in classical tables of integrals such as [70, 53].

Log-normal Shadowing

If the channel statistics follow a log-normal distribution, it is straightforward to show that $\mathcal{I}_\sigma(\mu; g; \phi)$ can be accurately approximated by Gauss-Hermite integration yielding

$$\mathcal{I}_\sigma(\mu; g; \phi) \simeq \frac{1}{\sqrt{\pi}} \sum_{n=1}^{N_p} H_{x_n}\ \exp\left(-\frac{g\ 10^{(\sqrt{2}\ \sigma\ x_n + \mu)/10}}{\sin^2 \phi}\right), \tag{4.21}$$

where N_p is the order of the Hermite polynomial, $H_{N_p}(.)$. Setting N_p to 20 is typically sufficient for excellent accuracy. In (4.21) x_n are the zeros of the N_p-order Hermite polynomial, and H_{x_n} are the weight factors of the N_p-order Hermite polynomial and are given by

$$H_{x_n} = \frac{2^{N_p - 1}\ N_p!\ \sqrt{\pi}}{N_p^2\ H_{N_p-1}^2(x_n)}. \tag{4.22}$$

Both the zeros and the weights factors of the Hermite polynomial are tabulated in [70, Table (25.10), p. 924] for various polynomial orders N_p.

Composite Multipath/Shadowing

If the channel statistics follow a gamma/log-normal distribution, it is straightforward to show that $\mathcal{I}_{m\sigma}(\mu; g; \phi)$ can be accurately evaluated by using (4.19) followed by a Gauss-Hermite integration yielding

$$\mathcal{I}_{m\sigma}(\mu; g; \phi) \simeq \frac{1}{\sqrt{\pi}} \sum_{n=1}^{N_p} H_{x_n}\ \left(1 + \frac{g\ 10^{(\sqrt{2}\ \sigma\ x_n + \mu)/10}}{m\ \sin^2 \phi}\right)^{-m} \tag{4.23}$$

Combined (Time-Shared) Shadowed/Unshadowed

If the channel statistics follow a combined Lutz *et al.* distribution, it is straightforward to show that $\mathcal{I}_{AK\sigma}(\overline{\gamma}^u, \mu^s; g; \phi)$ can be broken into two terms, one which can be evaluated in closed-form and the other which can be accurately approximated by Gauss-Hermite integration yielding

$$\mathcal{I}_{AK\sigma}(\overline{\gamma}^u, \mu^s; g; \phi) \simeq (1 - A)\ \mathcal{I}_n(\overline{\gamma}^u; g; \phi) + A\ \mathcal{I}_{m\sigma}(\mu^s; g; \phi), \tag{4.24}$$

with $n = \sqrt{K}$ in $\mathcal{I}_n(\overline{\gamma}^u; g; \phi)$ and $m = 1$ in $\mathcal{I}_{m\sigma}(\mu^s; g; \phi)$.

4.3.3 Average BER with Multichannel Reception ($L > 1$)

To obtain the unconditional BER, $\overline{P}_b$, when multichannel reception is used, we must average the multichannel conditional BER, $P_b(\gamma_t)$, over the joint PDF of the instantaneous SNR sequence $\{\gamma_l\}_{l=1}^{L}$, namely $p_{\gamma_1,\gamma_2,\cdots,\gamma_L}(\gamma_1,\gamma_2,\cdots,\gamma_L)$. Since the RV's $\{\gamma_l\}_{l=1}^{L}$ are assumed to be statistically independent, then $p_{\gamma_1,\gamma_2,\cdots,\gamma_L}(\gamma_1,\gamma_2,\cdots,\gamma_L) = \prod_{l=1}^{L} p_{\gamma_l}(\gamma_l;\overline{\gamma}_l,i_l)$, and the averaging procedure results in

$$\overline{P}_b = \underbrace{\int_0^\infty \int_0^\infty \cdots \int_0^\infty}_{L-\text{fold}} P_b(\gamma_t) \prod_{l=1}^{L} p_{\gamma_l}(\gamma_l;\overline{\gamma}_l,i_l)\, d\gamma_1 d\gamma_2 \cdots d\gamma_L, \tag{4.25}$$

where i_l represents the fading parameter(s) associated with the lth channel. Note that if the traditional integral representation of the Gaussian Q-function (4.6) were to be used in the $P_b(\gamma_t)$ term, (4.25) would result in a $L+1$-fold integral with infinite limits (one of these integrals comes from the classical definition of the Gaussian Q-function (4.6) in $P_b(\{\gamma_l\}_{l=1}^{L})$), and a closed-form solution or an adequately efficient numerical integration method would not be available. Using the alternate product form representation of the conditional BER (4.8) in (4.25) yields

$$\overline{P}_b = \underbrace{\int_0^\infty \int_0^\infty \cdots \int_0^\infty}_{L-\text{fold}} \frac{1}{\pi} \int_0^{\pi/2} \prod_{l=1}^{L} \exp\left(-\frac{g\,\gamma_l}{\sin^2\phi}\right) p_{\gamma_l}(\gamma_l;\overline{\gamma}_l,i_l)\, d\phi\, d\gamma_1 d\gamma_2 \cdots d\gamma_L. \tag{4.26}$$

The integrand in (4.26) is absolutely integrable and hence the order of integration can be interchanged. Thus we have

$$\overline{P}_b = \frac{1}{\pi} \int_0^{\pi/2} \prod_{l=1}^{L} \mathcal{I}_{i_l}(\overline{\gamma}_l;g;\phi)\, d\phi, \tag{4.27}$$

where $\mathcal{I}_{i_l}(\overline{\gamma}_l;g;\phi)$ is given above for the various channel models associated with path l. Note that if the fading is identically distributed with the same fading parameter i and the same average SNR per bit $\overline{\gamma}$ for all L channels, then (4.27) reduces to

$$\overline{P}_b = \frac{1}{\pi} \int_0^{\pi/2} (\mathcal{I}_i(\overline{\gamma};g;\phi))^L\, d\phi. \tag{4.28}$$

Hence in all cases this approach reduces the $L+1$-fold integral with infinite limits of (4.25) to a single finite-range integral (4.27) whose integrand contains only elementary functions such as exponentials and trigonometrics, and which therefore can be easily evaluated numerically.

4.4 Average Symbol Error Rate of M-PSK Signals

4.4.1 Product Form Representation of the Conditional SER

The conditional SER for M-PSK, $P_s(\gamma_t)$, does not exist in closed-form. However, it can be shown that it is given exactly by the desirable integral expression [65, Eqn. (71)], [66, Eqn. (5)], [51, Eqn. (3.119)]

$$P_s(\gamma_t) = \frac{1}{\pi}\int_0^{\frac{(M-1)\pi}{M}} \exp\left(-\frac{g_{\text{psk}}\,\gamma_t}{\sin^2\phi}\right) d\phi = \frac{1}{\pi}\int_0^{\frac{(M-1)\pi}{M}} \prod_{l=1}^{L} \exp\left(-\frac{g_{\text{psk}}\,\gamma_l}{\sin^2\phi}\right) d\phi, \tag{4.29}$$

where $g_{\text{psk}} = \sin^2\left(\frac{\pi}{M}\right)$. .

4.4.2 Average SER of M-PSK

Following the same steps as in (4.25)-(4.27), it can be easily shown that the average SER of M-PSK, $\overline{P}_s$, over generalized fading channels is given by

$$\overline{P}_s = \frac{1}{\pi}\int_0^{\frac{(M-1)\pi}{M}} \prod_{l=1}^{L} \mathcal{I}_{i_l}\left(\overline{\gamma}_l; g_{\text{psk}}; \phi\right)\, d\phi. \tag{4.30}$$

Our result (4.30) generalizes the M-PSK average SER results of [55, Eqn. (22)] and [60, Eqn. (21)] for L independent identically distributed Rayleigh paths. It also gives an alternative approach for the performance evaluation of coherent M-PSK over frequency-selective channels characterized by a Rician dominant path with Rayleigh secondary paths [9, 11]. Furthermore, by setting L to 1, the result (4.30) can be used to evaluate the average SER performance of M-PSK with single channel reception. This leads, for example, to the following results:

- Rayleigh: Substituting (4.13) in (4.30) (with $L = 1$), then using [53, p. 185, Eqn. (2.562.1)] yields a closed-form expression [57, Eqn. (9)], [58, Eqn. (7)] for the SER of M-PSK over a Rayleigh channel which agrees with the results obtained using various other methods [55, Eqn. (22)] and [61, Eqn. (36)].

- Nakagami-n (Rice): Substituting (4.18) in (4.30), leads to an expression for the SER of M-PSK over a Nakagami-n (Rice) channel which is easily shown to agree with [61, Eqn. (35)].

- Nakagami-m Substituting (4.20) in (4.30) (with $L = 1$) gives the SER of M-PSK over a Nakagami-m channel as

$$\overline{P}_s = \frac{1}{\pi}\int_0^{\frac{(M-1)\pi}{M}} \left(1 + \frac{\overline{\gamma}\,\sin^2\left(\frac{\pi}{M}\right)}{m\,\sin^2\phi}\right)^{-m} d\phi. \tag{4.31}$$

Note that (4.31) yields the same numerical values as [56, Eqn. (17)] and [62, Eqn. (9)] and it is much easier to compute for any arbitrary value of m.

4.5 Average Symbol Error Rate of M-AM Signals

4.5.1 Product Form Representation of the Conditional SER

The conditional SER for M-AM, $P_s(\gamma_t)$, with signal points symmetrically located about the origin, is given by [51, p. 631]

$$P_s(\gamma_t) = \frac{2(M-1)}{M} Q\left(\sqrt{2\, g_{\text{am}}\, \gamma_t}\right), \tag{4.32}$$

where $g_{\text{am}} = \frac{3}{M^2-1}$. Using the alternate representation of the Gaussian Q-function (4.7) in (4.32) we obtain the conditional SER in the desired product form as

$$\overline{P}_s(\gamma_t) = \frac{2(M-1)}{M\,\pi} \int_0^{\pi/2} \exp\left(-\frac{g_{\text{am}}\,\gamma_t}{\sin^2\phi}\right) d\phi = \frac{2(M-1)}{M\,\pi} \int_0^{\pi/2} \prod_{l=1}^{L} \exp\left(-\frac{g_{\text{am}}\,\gamma_l}{\sin^2\phi}\right) d\phi. \tag{4.33}$$

4.5.2 Average SER of M-AM

Following the same steps as in (4.25)-(4.27), it is straightforward to show that the average SER of M-AM over generalized fading channels is given by

$$\overline{P}_s = \frac{2(M-1)}{M\,\pi} \int_0^{\pi/2} \prod_{l=1}^{L} \mathcal{I}_{i_l}(\bar{\gamma}_l; g_{\text{am}}; \phi)\; d\phi. \tag{4.34}$$

4.6 Average Symbol Error Rate of Square M-QAM Signals

4.6.1 Product Form Representation of the Conditional SER

Consider square M-QAM signals whose constellation size is given by $M = 2^k$ with k even. The conditional SER for square M-QAM is given by [51, Eqn. (10.32)]

$$P_s(\gamma_t) = 4\left(1 - \frac{1}{\sqrt{M}}\right) Q\left(\sqrt{2\, g_{\text{qam}}\, \gamma_t}\right) - 4\left(1 - \frac{1}{\sqrt{M}}\right)^2 Q^2\left(\sqrt{2\, g_{\text{qam}}\, \gamma_t}\right), \tag{4.35}$$

where $g_{\text{qam}} = \frac{3}{2(M-1)}$. Simon and Divsalar [67] generalized the alternate representation of the Gaussian Q-function to the two-dimensional case and showed in particular that [67, Eqn. (80)]

$$Q^2(x) = \frac{1}{\pi} \int_0^{\pi/4} \exp\left(-\frac{x^2}{2\,\sin^2\phi}\right) d\phi; \qquad x \geq 0. \tag{4.36}$$

A simple proof of this result is given in Appendix A-2. Using the Craig-Pawula representation of the Gaussian-Q function (4.7) as well as the Simon-Divsalar representation of the square of the

Gaussian-Q function (4.36), the conditional SER (4.35) may be rewritten in the more desirable product form given by

$$\begin{aligned} P_s(\gamma_t) &= \frac{4}{\pi}\left(1-\frac{1}{\sqrt{M}}\right)\int_0^{\pi/2}\exp\left(-\frac{g_{\text{qam}}\,\gamma_t}{\sin^2\phi}\right)d\phi - \frac{4}{\pi}\left(1-\frac{1}{\sqrt{M}}\right)^2\int_0^{\pi/4}\exp\left(-\frac{g_{\text{qam}}\,\gamma_t}{\sin^2\phi}\right)d\phi \\ &= \frac{4}{\pi}\left(1-\frac{1}{\sqrt{M}}\right)\int_0^{\pi/2}\prod_{l=1}^{L}\exp\left(-\frac{g_{\text{qam}}\,\gamma_l}{\sin^2\phi}\right)d\phi - \frac{4}{\pi}\left(1-\frac{1}{\sqrt{M}}\right)^2\int_0^{\pi/4}\prod_{l=1}^{L}\exp\left(-\frac{g_{\text{qam}}\,\gamma_l}{\sin^2\phi}\right)d\phi. \end{aligned}$$

4.6.2 Average SER of M-QAM

Following the same steps as in (4.25)-(4.27) yields the average SER of M-QAM over generalized fading channels as

$$\begin{aligned} \overline{P}_s &= \frac{4}{\pi}\left(1-\frac{1}{\sqrt{M}}\right)\int_0^{\pi/2}\prod_{l=1}^{L}\mathcal{I}_{i_l}\left(\overline{\gamma}_l; g_{\text{qam}}; \phi\right)\,d\phi \\ &- \frac{4}{\pi}\left(1-\frac{1}{\sqrt{M}}\right)^2\int_0^{\pi/4}\prod_{l=1}^{L}\mathcal{I}_{i_l}\left(\overline{\gamma}_l; g_{\text{qam}}, \phi\right)\,d\phi. \end{aligned} \tag{4.37}$$

Of particular interest is the average SER performance of M-QAM with single channel reception, which can be obtained by setting L to 1 in (4.37). For example, substituting (4.13) in (4.37) (with $L=1$), then using again [53, p. 185, Eqn. (2.562.1)] yields a new closed-form expression for the average SER of M-QAM over Rayleigh channels as

$$\begin{aligned} \overline{P}_s &= 2\left(1-\frac{1}{\sqrt{M}}\right)\left(1-\sqrt{\frac{g_{\text{qam}}\,\overline{\gamma}}{1+g_{\text{qam}}\,\overline{\gamma}}}\right) \\ &+ \left(1-\frac{1}{\sqrt{M}}\right)^2\left[\frac{4}{\pi}\sqrt{\frac{g_{\text{qam}}\,\overline{\gamma}}{1+g_{\text{qam}}\,\overline{\gamma}}}\,\arctan\left(\sqrt{\frac{1+g_{\text{qam}}\,\overline{\gamma}}{g_{\text{qam}}\,\overline{\gamma}}}\right)-1\right]. \end{aligned} \tag{4.38}$$

Note that (4.38) matches the result obtained by [61, Eqn. (44)] for the particular case where $M=16$. Note also that (4.38) can in fact be obtained alternatively by averaging (4.35) over the Rayleigh PDF (2.3) and by using a standard known integral involving the function $\text{erfc}^2(\cdot)$ [53, p. 941, Eqn. (8.258.2)]. In addition using [5, Eqns. (5A.4b) and (5A.21)] in (4.37) we obtain the performance of M-QAM over L i.i.d. Rayleigh fading channels as

$$\begin{aligned} \overline{P}_s = 4\left(1-\frac{1}{\sqrt{M}}\right)\left(\frac{1-\mu_c}{2}\right)^L\sum_{l=0}^{L-1}\binom{L-1+l}{l}\left(\frac{1+\mu_c}{2}\right)^L - 4\left(1-\frac{1}{\sqrt{M}}\right)^2 \\ \times\left(\frac{1}{4}-\frac{\mu_c}{\pi}\left(\left[\frac{\pi}{2}-\arctan\mu_c\right]\sum_{l=0}^{L-1}\frac{\binom{2l}{l}}{4(1+g_{\text{qam}}\overline{\gamma})^l}-\sin\left(\arctan\mu_c\right)\sum_{l=1}^{L-1}\sum_{i=1}^{l}\frac{T_{il}}{(1+g_{\text{qam}}\overline{\gamma})^l}\left[\cos\left(\arctan\mu_c\right)\right]^{2(l-i)+1}\right)\right), \end{aligned} \tag{4.39}$$

where

$$\mu_c = \sqrt{\frac{g_{\text{qam}}\overline{\gamma}}{1+g_{\text{qam}}\overline{\gamma}}}, \tag{4.40}$$

and

$$T_{il} = \frac{\binom{2l}{l}}{\binom{2(l-i)}{l-i}\, 4^i\, (2(l-i)+1)}. \tag{4.41}$$

Note that equation (4.39) is equivalent to the expression [71, Eqn. (12)] which involves a sum of Gauss hypergeometric functions. Furthermore, using a partial fraction expansion on the integrand of (4.37), we obtain with the help of [53, p. 185, Eqn. (2.562.1)] the average SER of M-QAM over L Rayleigh fading channels with different average power and with MRC reception as

$$\begin{aligned}\overline{P}_s &= 2\left(1-\frac{1}{\sqrt{M}}\right)\sum_{l=1}^{L}\rho_l\left(1-\sqrt{\frac{g_{\text{qam}}\,\overline{\gamma}_l}{1+g_{\text{qam}}\,\overline{\gamma}_l}}\right)\\ &\quad+\left(1-\frac{1}{\sqrt{M}}\right)^2\left[\frac{4}{\pi}\sum_{l=1}^{L}\rho_l\sqrt{\frac{g_{\text{qam}}\,\overline{\gamma}_l}{1+g_{\text{qam}}\,\overline{\gamma}_l}}\,\arctan\left(\sqrt{\frac{1+g_{\text{qam}}\,\overline{\gamma}_l}{g_{\text{qam}}\,\overline{\gamma}_l}}\right)-\sum_{l=1}^{L}\rho_l\right],\end{aligned}$$

where

$$\rho_l = \left(\prod_{\substack{k=1\\k\neq l}}^{L}\left(1-\frac{\overline{\gamma}_k}{\overline{\gamma}_l}\right)\right)^{-1}. \tag{4.42}$$

4.7 Conclusion

We have presented a unified analytical framework to determine the exact average SER of linearly modulated signals over generalized fading channels. The results are applicable to systems employing coherent demodulation with maximal-ratio combining multichannel reception. The multichannel model is sufficiently general to include paths which are not necessarily identically distributed nor even distributed according to the same family of distributions.

The unified framework is achieved by exploiting alternate integral representations of the conditional probability of error in which the conditional SNR is inside the integrand rather than in the limit of integration. This, combined with closed-form Laplace transforms and/or Gauss-Hermite quadrature integrations, leads to expressions of the average SER which involve a single finite-range integral whose integrand contains only elementary functions and which can therefore be easily computed numerically. In addition, we presented as special cases average SER expressions for single channel reception. These expressions reduce to well-known solutions, give alternate (often simpler) expressions for previous results, or provide new formulas which are either closed-form expressions or simple to evaluate numerically.

Appendix A

Derivations of the Alternate Representations of the Gaussian Q-function and its Square

A byproduct of Craig's work on the probability of error for two-dimensional signal constellations [66] was the alternate representation of the Gaussian Q-function given in (4.7). An extension of this representation for the square of the Gaussian Q-function (4.36) was obtained by Simon and Divsalar [67]. In this appendix we present another simple method of proving the alternate representations of the Gaussian Q-function and its square.

A-1 Proof of Eqn. (4.7)

The proposed proof is an extension of the classical method to evaluate the Laplace-Gauss integral [53, Eqn. (3.321.3)]:

$$J(a) \triangleq \int_0^\infty e^{-a^2 x^2}\, dx = \frac{\sqrt{\pi}}{2\,a}; \qquad a > 0. \tag{4.43}$$

Let us consider the double integral

$$\int_0^\infty \int_x^\infty e^{-\frac{u^2+v^2}{2}}\, du\, dv; \qquad x \geq 0. \tag{4.44}$$

Because of separability (4.44) can be rewritten as

$$\underbrace{\int_0^\infty e^{-u^2/2}\, du}_{J(1/\sqrt{2})} \underbrace{\int_x^\infty e^{-v^2/2}\, dv}_{\sqrt{2\pi}\; Q(x)} = \pi\; Q(x), \tag{4.45}$$

where we see that each integral in the LHS of (4.45) is a well-defined function. Further, transformation to polar coordinates $u = r\cos\phi$ and $v = r\sin\phi$ ($du\, dv = r dr\, d\phi$) may be carried out in (4.44) giving

$$\begin{aligned} \int_0^\infty \int_x^\infty e^{-\frac{u^2+v^2}{2}}\, du\, dv &= \int_0^{\pi/2} \int_{x/\sin\phi}^\infty e^{-r^2/2}\, r dr\, d\phi \\ &= \int_0^{\pi/2} \exp\left(-\frac{x^2}{2\,\sin^2\phi}\right) d\phi. \end{aligned} \tag{4.46}$$

Equating (4.45) and (4.46) we obtain an alternate proof of the desired result (4.7). Note that another purely algebraic proof of the result (4.7) was implied by Weinstein [69] and Pawula *et al.* [65] and is given in detail in [5, Appendix 4A].

A-2 Proof of Eqn. (4.36)

The proof presented in Appendix A-1 can be easily extended to arrive at the alternate representation of $Q^2(\cdot)$ given in (4.36). Let us now consider the following double integral

$$\int_x^\infty \int_x^\infty e^{-\frac{u^2+v^2}{2}}\, du\, dv; \qquad x \geq 0. \tag{4.47}$$

Again because of separability (4.47) can be rewritten as

$$\underbrace{\int_x^\infty e^{-u^2/2}\, du}_{\sqrt{2\pi}\ Q(x)} \underbrace{\int_x^\infty e^{-v^2/2}\, dv}_{\sqrt{2\pi}\ Q(x)} = 2\ \pi\ Q^2(x), \tag{4.48}$$

where each integral in the LHS of (4.48) is the Gaussian Q-function multiplied by $\sqrt{2\pi}$. The transformation to polar coordinates $u = r\cos\phi$ and $v = r\sin\phi$ ($du\ dv = r dr\ d\phi$) is carried out in (4.47) and by symmetry the rectangular region of integration is divided into two equal triangular parts giving

$$\begin{aligned} \int_x^\infty \int_x^\infty e^{-\frac{u^2+v^2}{2}}\, du\, dv &= 2 \int_0^{\pi/4} \int_{x/\sin\phi}^\infty e^{-r^2/2}\, r dr\, d\phi \\ &= 2 \int_0^{\pi/4} \exp\left(-\frac{x^2}{2\ \sin^2\phi}\right)\, d\phi. \end{aligned} \tag{4.49}$$

Equating (4.48) and (4.49) we obtain an alternate proof of the Simon-Divsalar result (4.36).

Appendix B

Closed-Form Expressions for $\int_0^{\pi/2} \left(\frac{\sin^2\phi}{\sin^2\phi+c}\right)^m\ d\phi$

The alternate representation of the Gaussian Q-function can also be used to find closed-form expressions for integrals not tabulated in classical table of integrals such as [70, 53]. As an example we evaluate in this appendix the integral $I_m(c)$ defined by

$$I_m(c) \triangleq \int_0^{\pi/2} \left(\frac{\sin^2\phi}{\sin^2\phi + c}\right)^m\ d\phi. \tag{4.50}$$

To do so consider first the integral $J_m(a,b)$ defined by

$$J_m(a,b) \triangleq \frac{a^m}{\Gamma(m)} \int_0^{+\infty} e^{-at}\, t^{m-1}\, Q(\sqrt{b\,t})\, dt, \qquad m \geq 0. \tag{4.51}$$

This integral (4.51) has a known closed-form expression. When m is a positive real number the integral $J_m(a,b)$ is given by [46, Eqn. (A8)]

$$J_m(a,b) \triangleq J_m(c) = \frac{\sqrt{c/\pi}}{2\,(1+c)^{m+1/2}} \frac{\Gamma(m+1/2)}{\Gamma(m+1)}\, {}_2F_1\left(1, m+1/2; m+1; \frac{1}{1-c}\right), \tag{4.52}$$

where $c = b/(2a)$ and ${}_2F_1(.,.;.;.)$ denotes the the *hypergeometric series* (known also as the *Gauss hypergeometric function*). When m is a positive integer, the integral $J_m(a,b)$ reduces to [1, Eqn. (7.4.15)], [46, Eqn. (A13)]

$$J_m(a,b) \triangleq J_m(c) = [P(c)]^m \sum_{k=0}^{m-1} \binom{m-1+k}{k} [1-P(c)]^k, \tag{4.53}$$

where

$$P(x) = \frac{1}{2}\left(1 - \sqrt{\frac{x}{1+x}}\right); \quad x \geq 0. \tag{4.54}$$

Using the alternate representation of the Gaussian Q-function (4.7) in (4.52), we obtain

$$J_m(a,b) = \frac{a^m}{\Gamma(m)} \int_0^\infty e^{-at} t^{m-1} \left(\frac{1}{\pi}\int_0^{\pi/2} \exp\left(-\frac{b\,t}{2\,\sin^2\phi}\right)\, d\phi\right)\, dt. \tag{4.55}$$

Interchanging the order of integration in (4.55), then using (4.19), gives

$$J_m(a,b) \triangleq J_m(c) = \frac{1}{\pi}\int_0^{\pi/2} \left(\frac{\sin^2\phi}{\sin^2\phi + c}\right)^m d\phi = \frac{1}{\pi}\, I_m(c), \tag{4.56}$$

which is the desired closed-form expression for $I_m(c)$. A similar equivalence can be made between a result derived by Chennakeshu and Anderson [60] and the integrals $\int_0^{(M-1)\,\pi/M} \left(\frac{\sin^2\phi}{\sin^2\phi+c}\right)^m d\phi$ and $\int_0^{\pi/M} \left(\frac{\sin^2\phi}{\sin^2\phi+c}\right)^m d\phi$. Full details on these equivalences can be found in [5, Appendix 5A]. The reason for mentioning these equivalences and the resulting closed-form expressions is that they can be used, for example, to simplify calculations involving the performance of BPSK and M-PSK with selection diversity over correlated Nakagami-m fading channels [72].

Chapter 5 Performance of Coherent Modulations over Nakagami-m fading channels - Suboptimum Multichannel Reception

5.1 Introduction

In the previous chapter we examined coherent modulations with maximal-ratio combining (MRC). As discussed in Chapter 4 MRC requires the individual signals from each path to be time-aligned, co-phased, optimally weighted by their own fading amplitude, and then summed. MRC provides the maximum performance improvement relative to all other combining techniques by maximizing the SNR of the combined signal. However MRC also has the highest complexity of all combining techniques since it requires knowledge of the fading amplitude in each signal branch. Alternative techniques such as equal gain combining (EGC) and selective combining (SC) are often used in practice because of their reduced complexity relative to the optimum MRC scheme [2, Section 5.5]. Therefore, in this chapter, we examine the performance of coherent modulation with these suboptimal combining techniques.

EGC equally weights each branch before combining, and therefore does not require estimation of the channel (path) fading amplitudes. While it is possible to use EGC with noncoherent and differentially coherent reception [1], our focus in this chapter shall be on coherent EGC reception [2]. In its conventional form, SC diversity only processes one of the diversity branches, specifically, the one determined by the receiver to have the highest signal-to-noise ratio (SNR). Recently Eng *et al.* [73] considered generalized SC diversity technique which in reality is a hybrid scheme involving first conventional SC followed by MRC [3]. The main motivation behind this suboptimal hybrid scheme is to approach the performance provided by MRC with a less complex receiver.

In this chapter we use the alternate representation of the Gaussian Q-function to analyze the performance of these two suboptimum schemes over Nakagami-m fading channels. The remainder of this chapter is organized as follows. The next section briefly outlines the system and channel

[1] Although MRC is also possible for these types of detection, it is impractical [2, p. 248] since this form of combining requires channel phase estimates to implement the complex path weights in the combiner. If these phase estimates are available then one should opt for a coherent system thereby achieving better performance.

[2] We emphasize that estimation of the channel carrier phase is still required in this case since the weights applied to each branch in the combiner are complex quantities whose phases are indeed equal to these carrier phase estimates.

[3] It is also possible to mate SC with other forms of diversity combining such as noncoherent EGC. Such a noncoherent SC/EGC hybrid scheme would be a suitable choice for differentially coherent and noncoherent systems where MRC is not appropriate because of the absence of the phase information for each branch [2].

models for these two schemes. A generic expression for the average error probability of EGC for ideal coherent detection of various modulations is developed in Section 5.3. The performance of hybrid SC-MRC is then addressed in Section 5.4. Based on two sets of numerical examples, a brief comparison is drawn between EGC and higher order SC in Section 5.5. A summary of our results as well as some concluding remarks are given in Section 5.6.

5.2 System and Channel Models

5.2.1 Transmitted Signals

We consider the same linearly modulated signals as the ones discussed in Section 4.2.1 of the previous chapter. However, we should point out that EGC is only appropriate for modulations with equal energy symbols such as binary phase-shift-keying (BPSK) and its M-ary version. Indeed for channels with unequal energy symbols such as M-ary amplitude modulation (M-AM) and quadrature amplitude modulation (QAM), estimation of the path amplitudes is also needed for automatic gain control (AGC) purposes and thus for these modulations MRC should be used [2]. On the other hand, any M-ary linearly modulated signal (M-PSK, M-ary amplitude modulation (M-AM), and M-ary quadrature amplitude modulation (M-QAM)) can be used in conjunction with hybrid SC-MRC, since the path weights are needed anyway for the MRC. Although we only consider the performance of hybrid SC-MRC with binary signals, performance results for M-ary signals can been derived in a manner similar to that presented in Section 5.4.

5.2.2 Multilink Channel Model

We consider a multilink channel similar to the one considered in Section 4.2.2 except that we only consider the Nakagami-m fading distribution for each link (i.e., the transmitted signal is received over L independent slowly varying Nakagami-m flat fading channels. Our EGC analyses are quite general and include the case where each path may have a different value of $m = m_l$ and a different average power $\Omega_l = \overline{\alpha_l^2}$. As such, the probability density function (PDF) of the lth path is given by (2.14)

$$p_{\alpha_l}(\alpha_l) = \frac{2\, m_l^{m_l}\, \alpha_l^{2m_l-1}}{\Omega_l^{m_l}\, \Gamma(m_l)} \exp\left(-\frac{m_l\, \alpha_l^2}{\Omega_l}\right); \qquad \alpha_l \geq 0. \tag{5.1}$$

The performance evaluation for hybrid SC-MRC is carried out for the special case where the L Nakagami-m fading channels are restricted to be identically distributed (i.e., all the paths are assumed to have the same fading parameter m and the same average fading power Ω).

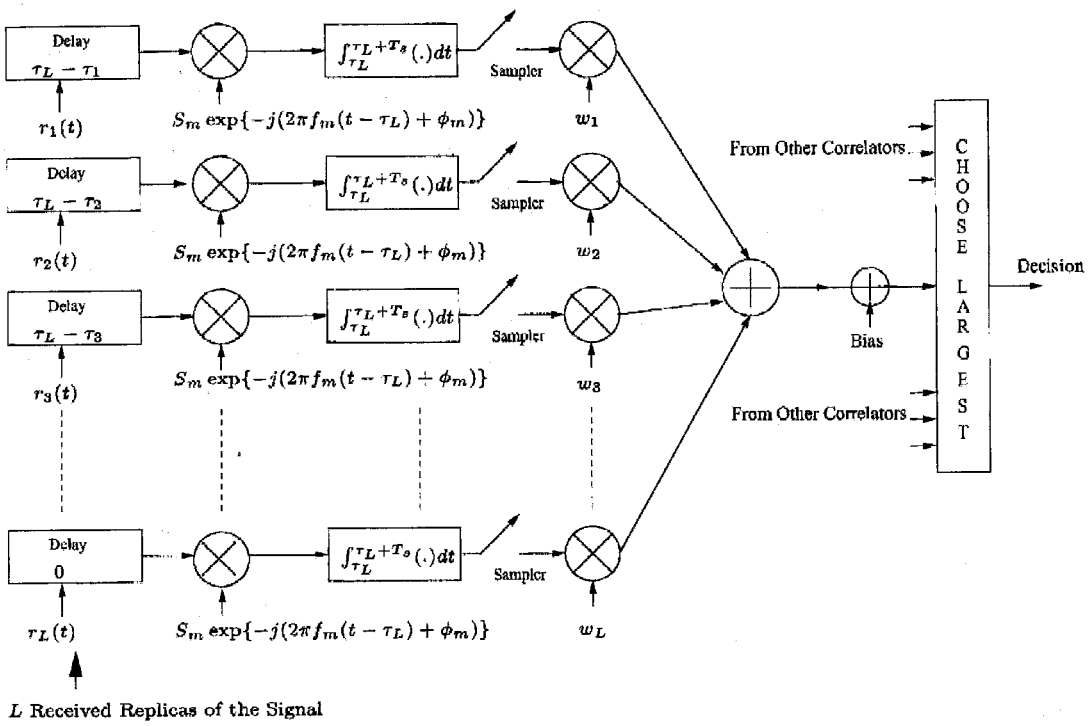

Figure 5.1: Suboptimum coherent diversity combiner receiver structure.

5.2.3 Receiver Model

We assume an L branch (finger) suboptimum receiver, as shown in Fig. 5.1. The EGC receiver processes L_c signals randomly chosen among the L received ones, equally weights them, then sums them to produce the decision statistic. In mathematical terms the weights w_l $(l = 1, \cdots, L_c)$ are set equal to 1 and the remaining weights w_l $(l = L_c + 1, \cdots, L)$ are set equal to 0. Note that irrespective of the diversity combining scheme, one reason for choosing a small value of L_c is to reduce the complexity of the receiver. For MRC, this results in a degradation in performance since the optimum value for L_c is L. For EGC, however, under certain circumstances, increasing L_c may induce a "combining loss." Indeed equal-weight combining of paths with very low average SNR degrades performance since these paths will contribute mostly to noise [1]. Thus, it is better not to include these paths in the combining process.

The hybrid SC-MRC chooses the L_c out of L received signals with the highest SNR, optimally weights them (as per the rules of MRC), and then sums them to produce the decision statistic. In mathematical terms let $\alpha_1, \alpha_2, \cdots, \alpha_{L_c}, \cdots \alpha_L$ denote the ordered (largest to smallest) set of fading amplitudes associated with the SC inputs. The higher order SC receiver sets the weights w_l equal to α_l for $(l = 1, \cdots, L_c)$ and w_l equal to 0 for $(l = L_c + 1, \cdots, L)$.

5.3 Equal Gain Combining Performance

In this section we derive the performance of coherent modulations with EGC over Nakagami-m fading channels. In [74] Beaulieu and Abu-Dayya employ an infinite series representation for the PDF of the sum of Nakagami-m RVs to analyze the performance of EGC. Another approach, for Rayleigh fading which leads to closed form solutions for particular cases is discussed in [75]. As we shall see, our approach lead to a final generic expression for the average error probability in the form of a single finite-range integral and an integrand composed of tabulated functions.

The remainder of this section is organized as follows. Section 5.3.1 gives the exact average bit error rate (BER) of binary signals with EGC reception over Nakagami-m fading channels. The results are extended to M-PSK signals in Section 5.3.2. Finally, a simple approximate approach for the performance evaluation for EGC reception of digital signals over i.i.d. Nakagami-m fading channels is presented in Section 5.3.3.

5.3.1 Binary Signals

We begin our discussion by considering the performance of an EGC receiver when BPSK or BFSK modulation is transmitted over a multilink channel with L paths. Conditioned on the total fading $\alpha_t = \sum_{l=1}^{L_c} \alpha_l$, the BER, $P_b(\alpha_t)$, of an EGC receiver is well known to be given by [2]

$$P_b(\alpha_t) = Q\left(\sqrt{\frac{2gE_b}{L_c\, N_0}\left(\left(\sum_{l=1}^{L_c}\alpha_l\right)^2\right)}\right), \tag{5.2}$$

where $Q(\cdot)$ is the Gaussian Q-function traditionally defined by (4.6)

$$Q(x) = \frac{1}{\sqrt{2\pi}}\int_x^\infty e^{-t^2/2}\, dt, \tag{5.3}$$

E_b/N_0 is the bit signal-to-noise ratio (SNR) on the AWGN channel, and g is the modulation parameter such that $g = 1$ for BPSK, $g = 1/2$ for orthogonal BFSK, and $g = \frac{1}{2} + \frac{1}{3\pi}$ for BFSK with minimum correlation [51]. The average BER is obtained by averaging (5.2) over the joint PDF of the channel fading amplitudes $P_{\alpha_1,\alpha_2,\cdots,\alpha_{L_c}}(\alpha_1,\alpha_2,\cdots,\alpha_{L_c})$, i.e.,

$$\overline{P}_b = \int_0^\infty \cdots \int_0^\infty Q\left(\sqrt{\frac{2gE_b}{L_c\, N_0}\left(\left(\sum_{l=1}^{L_c}\alpha_l\right)^2\right)}\right) P_{\alpha_1,\alpha_2,\cdots,\alpha_{L_c}}(\alpha_1,\alpha_2,\cdots,\alpha_{L_c})\, d\alpha_1\, d\alpha_2 \cdots d\alpha_{L_c}. \tag{5.4}$$

The L_c-fold integral in (5.4) can be collapsed to a single integral, namely,

$$\overline{P}_b = \int_0^\infty Q\left(\sqrt{\frac{2gE_b}{L_c\,N_0}\,\alpha_t^2}\right)\,p_{\alpha_t}(\alpha_t)\,d\alpha_t. \tag{5.5}$$

In general, there are two difficulties associated with analytically evaluating the average BER as expressed in (5.5). The first relates to the requirement of obtaining the PDF of the total fading RV α_t. When the fading amplitudes can be assumed independent (the case to be considered in this chapter), finding this PDF requires a convolution of the PDF's of the α_l's and can often be quite difficult to evaluate. The second difficulty has to do with the fact that the argument of the classical definition of the Gaussian Q-function in (5.3) appears in the lower limit of the integral which is undesirable when trying to perform the average over α_t.

To circumvent these difficulties, we now propose a new method of solution based the alternate representation of the Gaussian Q-function (4.7), namely,

$$Q(x) = \frac{1}{\pi}\int_0^{\pi/2} \exp\left(-\frac{x^2}{2\sin^2\phi}\right)\,d\phi; \qquad x \geq 0. \tag{5.6}$$

First using (5.6) in (5.4) gives

$$\overline{P}_b = \int_0^\infty \cdots \int_0^\infty \frac{1}{\pi}\int_0^{\pi/2} \exp\left(-\frac{gE_b\left(\sum_{l=1}^{L_c}\alpha_l\right)^2}{N_0 L\sin^2\phi}\right)\,p_{\alpha_1}(\alpha_1)\cdots p_{\alpha_{L_c}}(\alpha_{L_c})d\phi\,d\alpha_1\,d\alpha_2\cdots d\alpha_{L_c}. \tag{5.7}$$

Unfortunately, we cannot represent the exponential in (5.7) as a product of exponentials each involving only a single α_l because of the presence of the $\alpha_k\alpha_l$ crossproduct terms. Hence, we cannot partition the L-fold integral into a product of one-dimensional integrals as is possible for MRC (see Chapter 4) and thus we must abandon this approach. Instead, we use the alternate representation of the Gaussian Q-function in (5.5) which gives after switching the order of integration

$$\overline{P}_b = \frac{1}{\pi}\int_0^{\pi/2}\int_0^\infty \exp\left(-\frac{A^2}{2\sin^2\phi}\,\alpha_t^2\right)\,p_{\alpha_t}(\alpha_t)\,d\alpha_t\,d\phi, \tag{5.8}$$

where $A = \sqrt{\frac{2gE_b}{LN_0}}$. While this maneuver cures the second difficulty by getting the total fading RV α_t out of the lower limit of the integral and into the integrand, it appears that we are still faced with the problem of determining the PDF of α_t. To get around this difficulty, we next represent $p_{\alpha_t}(\alpha_t)$ in terms of its inverse Fourier transform, i.e., the characteristic function which, because of the independence assumption on the fading channel amplitudes, becomes

$$p_{\alpha_t}(\alpha_t) = \frac{1}{2\pi}\int_{-\infty}^{\infty}\Psi_{\alpha_t}(j\nu)\,e^{-j\nu\alpha_t}\,d\nu = \frac{1}{2\pi}\int_{-\infty}^{\infty}\left[\prod_{l=1}^{L_c}\Psi_{\alpha_l}(j\nu)\right]\,e^{-j\nu\alpha_t}\,d\nu \tag{5.9}$$

Substituting (5.9) into (5.8) gives

$$\overline{P}_b = \frac{1}{2\pi^2}\int_0^{\pi/2}\int_{-\infty}^{\infty}\left[\prod_{l=1}^{L_c}\Psi_{\alpha_l}(j\nu)\right]\underbrace{\int_0^{\infty}\exp\left(-\frac{A^2\alpha_t^2}{2\sin^2\phi}-j\nu\alpha_t\right)d\alpha_t}_{J(\nu,\phi)}\,d\nu\,d\phi. \tag{5.10}$$

The integral $J(\nu,\phi)$ can be obtained in terms of the complementary error function erfc$(\cdot)$ (with the help of [53, Eqn. ()]

$$J(\nu,\phi) = \sqrt{\frac{\pi}{2}}\,\frac{\sin\phi}{A}\,\exp\left(-\frac{\sin^2\phi}{2A^2}\,\nu^2\right)\,\left(1+\text{erfc}\left(j\frac{\sin\phi}{\sqrt{2}A}\nu\right)\right), \tag{5.11}$$

or alternatively by separatly evaluating its real and imaginary parts, namely, [53, Eqns. (3.896.4) and (3.896.3)]

$$\begin{aligned}\int_0^{\infty}\exp\left(-\frac{A^2}{2\sin^2\phi}\alpha_t^2\right)\cos(\nu\alpha_t)\,d\alpha_t &= \sqrt{\frac{\pi\sin^2\phi}{2A^2}}\,\exp\left(-\frac{\sin^2\phi}{2A^2}\nu^2\right)\\ \int_0^{\infty}\exp\left(-\frac{A^2}{2\sin^2\phi}\alpha_t^2\right)\sin(\nu\alpha_t)\,d\alpha_t &= \frac{\nu\sin^2\phi}{A^2}\,\exp\left(-\frac{\sin^2\phi}{2A^2}\nu^2\right)\,{}_1F_1\left(\frac{1}{2};\frac{3}{2};\frac{\sin^2\phi}{2A^2}\nu^2\right),\end{aligned} \tag{5.12}$$

where ${}_1F_1(\cdot;\cdot;\cdot)$ is the Kummer confluent hypergeometric function [70, p. 504, Eqn. (13.1.2)]. Thus, letting

$$\begin{aligned}X(\phi) &= \sqrt{\frac{\pi}{2}}\frac{\sin\phi}{A},\\ Y(\nu,\phi) &= \frac{\nu\,\sin^2\phi}{A^2}\,{}_1F_1\left(\frac{1}{2};\frac{3}{2};\frac{\sin^2\phi}{2A^2}\nu^2\right),\end{aligned} \tag{5.13}$$

we can write the integral $J(\nu,\phi)$ in the form

$$\begin{aligned}J(\nu,\phi) &= (X(\phi)+jY(\nu,\phi))\,\exp\left(-\frac{\sin^2\phi}{2A^2}\nu^2\right)\\ &= \sqrt{X^2(\phi)+Y^2(\nu,\phi)}\,\exp\left(j\arctan\left(\frac{Y(\nu,\phi)}{X(\phi)}\right)\right)\,\exp\left(-\frac{\sin^2\phi}{2A^2}\nu^2\right).\end{aligned} \tag{5.14}$$

In general, the characteristic function of a PDF will be a complex quantity and hence the product of characteristic functions in (5.10) will also be complex. However, since the average BER is real, it is sufficient to consider only the real part of the right-hand side of (5.10). Hence, we rewrite the equation (5.10) as

$$\overline{P}_b = \frac{1}{2\pi^2}\int_0^{\pi/2}\int_{-\infty}^{\infty}Re\left(\left[\prod_{l=1}^{L_c}\Psi_{\alpha_l}(j\nu)\right]J(\nu,\phi)\right)\,d\nu\,d\phi. \tag{5.15}$$

Expressing the characteristic function of each fading path PDF by

$$\begin{aligned}\Psi_{\alpha_l}(j\nu) &= U_l(\nu) + jV_l(\nu) \\ &= \sqrt{U_l^2(\nu) + V_l^2(\nu)}\ \exp\left(j \arctan\left(\frac{V_l(\nu)}{U_l(\nu)}\right)\right),\end{aligned} \tag{5.16}$$

then substituting (5.14) and (5.16) into (5.15) gives

$$\overline{P}_b = \frac{1}{2\pi^2}\int_0^{\pi/2}\int_{-\infty}^{\infty} f(\nu,\phi)\ \exp\left(-\frac{\sin^2\phi}{2A^2}\nu^2\right)\ d\nu\ d\phi, \tag{5.17}$$

where

$$\begin{aligned}f(\nu,\phi) &= R(\nu,\phi)\ \cos\Theta(\nu,\phi), \\ R(\nu,\phi) &= \sqrt{X^2(\phi)+Y^2(\nu,\phi)}\ \prod_{l=1}^{L_c}\sqrt{U_l^2(\nu)+V_l^2(\nu)}, \\ \Theta(\nu,\phi) &= \arctan\left(\frac{Y(\nu,\phi)}{X(\phi)}\right) + \sum_{l=1}^{L_c}\arctan\left(\frac{V_l(\nu)}{U_l(\nu)}\right).\end{aligned} \tag{5.18}$$

The characteristic function corresponding to the Nakagami-m fading PDF can be evaluated with the help of [53, Eqn. 3.462.1] in terms of the parabolic cylinder function $D_{-\nu}(\cdot)$ [53, Section 9.24-9.25]

$$\Psi_{\alpha_l}(jv) = \frac{1}{2^{m_l-1}}\ \frac{\Gamma(2m_l)}{\Gamma(m_l)}\ D_{-2m_l}\left(-jv\sqrt{\frac{\Omega_l}{2m_l}}\right)\ \exp\left(-\frac{\Omega_l}{8m_l}\ v^2\right), \tag{5.19}$$

or alternatively by separately evaluating its real and imaginary parts by using sine and cosine Fourier transforms found in [53] with the results (see Eqn. (5.16))

$$\begin{aligned}U_l(\nu) &= A_l(\nu)\ \exp\left(-\frac{\Omega_l}{4\ m_l}\ v^2\right), \\ V_l(\nu) &= B_l(\nu)\ \exp\left(-\frac{\Omega_l}{4\ m_l}\ v^2\right),\end{aligned} \tag{5.20}$$

where

$$\begin{aligned}A_l(\nu) &= {}_1F_1\left(\frac{1}{2}-m_l;\frac{1}{2};\frac{\nu^2\Omega_l}{4m_l}\right), \\ B_l(\nu) &= \frac{\Gamma\left(m_l+\frac{1}{2}\right)}{\Gamma(m_l)}\sqrt{\frac{\Omega_l}{m_l}}\ \nu\ {}_1F_1\left(1-m_l;\frac{3}{2};\frac{\nu^2\Omega_l}{4m_l}\right).\end{aligned} \tag{5.21}$$

Thus, the amplitude and phase functions defined in (5.18) become

$$R(\nu,\phi) = \sqrt{X^2(\phi)+Y^2(\nu,\phi)}\ \prod_{l=1}^{L_c}\sqrt{A_l^2(\nu)+B_l^2(\nu)}\ \exp\left(-\sum_{l=1}^{L_c}\ \frac{\Omega_l}{4\ m_l}\ v^2\right),$$

$$\Theta(\nu,\phi) \;=\; \arctan\left(\frac{Y(\nu,\phi)}{X(\phi)}\right) + \sum_{l=1}^{L_c} \arctan\left(\frac{B_l(\nu)}{A_l(\nu)}\right), \tag{5.22}$$

with $X(\phi)$ and $Y(\nu,\phi)$ as defined in (5.13) and $A_l(\nu)$ and $B_l(\nu)$ as defined in (5.21). It is convenient in this case to absorb the exponential factor in $R(\nu,\theta)$ into the exponential factor in the integrand of (5.17). Thus, we first write the average BER of (5.17) as

$$\overline{P}_b = \frac{1}{2\pi^2}\int_0^{\pi/2}\int_{-\infty}^{\infty} f_0(\nu,\phi)\ \exp\left(-\left(\frac{\sin^2\phi}{2A^2} + \sum_{l=1}^{L_c}\frac{\Omega_l}{4m_l}\right)\nu^2\right)\ d\nu\ d\phi, \tag{5.23}$$

where $f_0(\nu,\phi)$ is a normalized version of $f(\nu,\phi)$ defined by

$$f_0(\nu,\phi) = R_0(\nu,\phi)\ \cos\Theta(\nu,\phi), \tag{5.24}$$

with

$$R_0(\nu,\phi) = \sqrt{X^2(\phi)+Y^2(\nu,\phi)}\ \prod_{l=1}^{L_c}\sqrt{A_l^2(\nu)+B_l^2(\nu)} \tag{5.25}$$

and $\Theta(\nu,\phi)$ still as defined in (5.22). Finally, letting

$$\eta(\phi) = \frac{\sin^2\phi}{2A^2} + \sum_{l=1}^{L_c}\frac{\Omega_l}{4m_l}, \tag{5.26}$$

and making the change of variables $x = \sqrt{\eta(\phi)}\nu$, the doubly infinite integral is of the form

$$\int_{-\infty}^{\infty} f_0\left(\frac{x}{\sqrt{\eta(\phi)}},\phi\right)\ e^{-x^2}\ dx, \tag{5.27}$$

which can be readily evaluated by the Gauss-Hermite quadrature formula [70, p. 890, Eqn. (25.4.46)] yielding the desired final result in the form of a single finite range integral on ϕ, namely,

$$\overline{P}_b = \frac{1}{2\pi^2}\int_0^{\pi/2}\frac{1}{\sqrt{\eta(\phi)}}\sum_{n=1}^{N_p} H_{x_n}\ f_0\left(\frac{x_n}{\sqrt{\eta(\phi)}},\phi\right)\ d\phi, \tag{5.28}$$

where N_p is the order of the Hermite polynomial, $H_{N_p}(.)$. Setting N_p to 20 is typically sufficient for excellent accuracy. In (5.28) x_n are the zeros of the N_p-order Hermite polynomial, and H_{x_n} are the weight factors of the N_p-order Hermite polynomial and are given by (4.22)

$$H_{x_n} = \frac{2^{N_p-1}\ N_p!\ \sqrt{\pi}}{N_p^2\ H_{N_p-1}^2(x_n)}. \tag{5.29}$$

Both the zeros and the weights factors of the Hermite polynomial are tabulated in [70, Table (25.10), p. 924] for various polynomial orders N_p. Note that substituting (5.24), (5.25), and (5.26) in (5.28),

it can be shown that the average BER in (5.28) is a function of the different average SNR/bit/path $\gamma_l = \frac{\Omega_l E_b}{N_0}$.

5.3.2 Extension to M-PSK Modulation

The symbol error rate (SER) for M-PSK over an AWGN is given by the integral expression (4.29)

$$P_s = \frac{1}{\pi} \int_0^{\frac{(M-1)\pi}{M}} \exp\left(-\frac{g_{\text{psk}}\, E_s}{N_0 \sin^2 \phi} \right) d\phi, \tag{5.30}$$

where $g_{\text{psk}} = \sin^2\left(\frac{\pi}{M}\right)$ and E_s/N_0 is the received symbol SNR. For EGC reception in the presence of fading, the conditional SER is obtained from (5.28) by replacing E_s/N_0 by $\alpha_t E_s/N_0 = \left(\sum_{l=1}^{L_c} \alpha_l\right) E_s/N_0$ which represents the instantaneous SNR per symbol after combining. Following the same steps as in Section 5.3.1, it is straightforward to show that the average SER is given by an equation analogous to (5.28), namely,

$$\overline{P}_s = \frac{1}{2\pi^2} \int_0^{\frac{(M-1)\pi}{M}} \frac{1}{\sqrt{\eta_{\text{psk}}(\phi)}} \sum_{n=1}^{N_p} H_{x_n}\, f_0\left(\frac{x_n}{\sqrt{\eta_{\text{psk}}(\phi)}}, \phi \right) d\phi. \tag{5.31}$$

where

$$\begin{aligned} \eta_{\text{psk}}(\phi) &= \frac{\sin^2 \phi}{2A_{\text{psk}}^2} + \sum_{l=1}^{L_c} \frac{\Omega_l}{4m_l}, \\ A_{\text{psk}} &= \sqrt{\frac{2\, g_{\text{psk}}}{L} \frac{E_s}{N_0}} = \sqrt{\frac{2\, g_{\text{psk}}}{L_c} \frac{(\log_2 M) E_b}{N_0}}, \end{aligned} \tag{5.32}$$

and all other parameters and functions remain the same as for the binary signal case. It can also be shown that (5.31) is a function of the different average SNR/symbol/path $\gamma_l = \frac{\Omega_l E_s}{N_0}$.

5.3.3 An Approximate Approach for EGC of L Identically Distributed Nakagami-m Fading Paths

As previously mentioned, one of the difficulties in evaluating (5.5) is the requirement of obtaining the PDF of the total fading RV α_t. Even the use of the Craig representation of the Gaussian Q-function which leads to (5.8) does not alleviate this problem. Although there is no known closed-form exact expression for the PDF of the sum of L i.i.d. Nakagami-m RVs, Nakagami [13] showed after rather complex calculations that such a sum can be accurately approximated by another Nakagami-m distribution [13, p. 22] with a parameter ${}_0m$ and average power ${}_0\Omega$ given by

$${}_0m = mL$$

$$ {}_0\Omega \;=\; L\Omega\left(1+(L-1)\,\frac{\Gamma^2(m+1/2)}{m\,\Gamma^2(m)}\right) \simeq L^2\,\Omega\,\left(1-\frac{1}{5m}\right). \tag{5.33} $$

Specifically, modeling the PDF $p_{\alpha_t}(\alpha_t)$ by (5.1) with parameters ${}_0m$ and ${}_0\Omega$, the average BER for binary signals as given by (5.5) can be evaluated in closed form as

$$ \overline{P}_b = \frac{1}{2}\sqrt{\frac{g\overline{\gamma}_{\rm egc}/m}{\pi\,(1+g\overline{\gamma}_{\rm egc}/m)}}\,\frac{\Gamma\left(Lm+\frac{1}{2}\right)}{\Gamma\left(Lm+1\right)}\,\left(\frac{1}{1+g\overline{\gamma}_{\rm egc}/m}\right)^{Lm}\,{}_2F_1\left(1, Lm+\frac{1}{2}, Lm+1; \frac{1}{1+g\overline{\gamma}_{\rm egc}/m}\right), \tag{5.34} $$

where ${}_2F_1(\cdot,\cdot;\cdot;\cdot)$ is the Gauss hypergeometric function [70, p. 556, Eqn. (15.1.1)] and

$$ \overline{\gamma}_{\rm egc} = \frac{\overline{\gamma}}{L_c}\,\left(1+(L-1)\,\frac{\Gamma^2(m+1/2)}{m\,\Gamma^2(m)}\right) \simeq \overline{\gamma}\left(1-\frac{1}{5m}\right). \tag{5.35} $$

For the special case where m is integer, it can be shown (using [46, Appendix A]) that (5.35) simplifies to

$$ \overline{P}_b = \left[\frac{1}{2}\left(1-\sqrt{\frac{g\overline{\gamma}_{\rm egc}}{m+g\overline{\gamma}_{\rm egc}}}\right)\right]^{mL}\,\sum_{l=0}^{mL-1}\binom{mL-1+l}{l}\,\left[\frac{1}{2}\left(1-\sqrt{\frac{g\overline{\gamma}_{\rm egc}}{m+g\overline{\gamma}_{\rm egc}}}\right)\right]^{l}. \tag{5.36} $$

For M-PSK, the same approximate modeling of α_t can be used together with the conditional SER obtained from (5.30) to compute an approximate expression for average SER. Using results derived in [5, Appendix 5A] for the average SER of M-PSK over a single Nakagami-m channel, the appropriate approximate expression for the multichannel case being considered here becomes (for m integer)

$$ \begin{aligned} \overline{P}_s = \frac{M-1}{M} - \frac{1}{\pi}\sqrt{\frac{g_{\rm psk}\,\overline{\gamma}_{\rm egc}\,\log_2 M}{m+g_{\rm psk}\,\overline{\gamma}_{\rm egc}\,\log_2 M}}\,\Big[\Big(\frac{\pi}{2}+\arctan\alpha\Big)\,\sum_{l=0}^{mL-1}\binom{2l}{l}\,\left(\frac{m}{4(m+g_{\rm psk}\overline{\gamma}_{\rm egc}\log_2 M)}\right)^{l} \\ + \sin(\arctan\alpha)\,\sum_{l=1}^{mL-1}\,\sum_{i=1}^{l}\,T_{il}\,\left(\frac{m}{m+g_{\rm psk}\overline{\gamma}_{\rm egc}\log_2 M}\right)^{l}\,(\cos(\arctan\alpha))^{2(l-i)+1}\Big], \end{aligned} \tag{5.37} $$

where

$$ \alpha = \sqrt{\frac{g_{\rm psk}\overline{\gamma}_{\rm egc}\log_2 M}{m+g_{\rm psk}\overline{\gamma}_{\rm egc}\log_2 M}}\,\cot\frac{\pi}{M}, \tag{5.38} $$

and T_{il} is defined by

$$ T_{il} = \frac{\binom{2l}{l}}{\binom{2(l-i)}{(l-i)}\,4^i\,(2(l-i)+1)}. \tag{5.39} $$

For $M=2$, it can be shown that (5.37) reduces to (5.36).

5.4 Generalized Selective Combining

Consider a generalized selective combiner (as described in Section 5.2.3) in which the SC chooses the L_c largest signals from the L received ones, then optimally weights (as per the rules of MRC) and sums these signals to produce the decision statistic. We shall denote such a hybrid scheme as SC/MRC-L_c/L. In [73] Eng *et al.* presented a thorough comparison of the hybrid SC/MRC scheme with the SC and MRC schemes over Rayleigh fading channels with both i.i.d. distributions and with an exponentially decaying average fading power on the different paths. Eng *et al.* limited themselves to binary modulations and did not consider the performance of M-ary modulations in conjunction with this hybrid scheme. In addition the performance of the hybrid SC/MRC scheme over Nakagami-m fading by itself and in comparison with MRC, has not previously been reported in the literature. In this section, we examine these performance issues.

The remainder of this section is organized as follows. Section 5.4.1 gives the joint statistics of the generalized SC output.

5.4.1 Joint Statistics of the Generalized SC Output

In this section we consider a SC that chooses the L_c of its L input branches with the largest SNR. The branch SNRs are modeled as i.i.d. RVs. Let $\alpha_1, \alpha_2, \cdots, \alpha_L$ denote the ordered (largest to smallest) set of fading amplitudes associated with the SC inputs, each of which has average power Ω. We define the instantaneous SNR per bit for each channel $\gamma_l = \alpha_l^2 E_b/N_0, l = 1, 2, \cdots, L$ (E_b/N_0 is the bit energy-to-Gaussian noise spectral density ratio) and the corresponding average SNR per bit for each channel as $\overline{\gamma}_l = \overline{\alpha_l^2} E_b/N_0 = \Omega E_b/N_0$. The joint PDF of the L_c largest of the γ_l's is then given by [76, p. 185], [77, Eq. (9)]

$$p_{\gamma_1,\cdots,\gamma_{L_c}}(\gamma_1,\cdots,\gamma_{L_c}) = L_c! \binom{L}{L_c} [P_\gamma(\gamma_{L_c})]^{L-L_c} \prod_{l=1}^{L_c} p_\gamma(\gamma_l), \quad \gamma_1 \geq \cdots \geq \gamma_{L_c} \geq 0, \tag{5.40}$$

where $p_\gamma(\gamma)$ is the PDF of γ and $P_\gamma(\gamma) = \int_0^\gamma p_\gamma(y)dy$ is the corresponding cumulative distribution function (CDF). It is important to note that $\gamma_1, \gamma_2, \cdots, \gamma_{L_c}$ are not independent as can be seen from the form of (5.40).

Rayleigh Fading Channels

For Rayleigh fading channels $p_\gamma(\gamma)$ is given by (2.4):

$$p(\gamma;\overline{\gamma}) = \frac{1}{\overline{\gamma}} \exp\left(-\frac{\gamma}{\overline{\gamma}}\right); \quad \gamma \geq 0, \tag{5.41}$$

and the CDF $P_\gamma(\gamma) = \int_0^\gamma p_\gamma(y)dy$ can be evaluated as

$$P_\gamma(\gamma) = 1 - \exp\left(-\frac{\gamma_{L_c}}{\overline{\gamma}}\right), \quad \gamma \geq 0. \tag{5.42}$$

Substituting (5.41) and (5.42) in (5.40) yields the joint PDF given by

$$p_{\gamma_1,\cdots,\gamma_{L_c}}(\gamma_1,\cdots,\gamma_{L_c}) = \frac{L!}{(L-L_c)!\,\overline{\gamma}^{L_c}} \left(1 - \exp\left(-\frac{\gamma_{L_c}}{\overline{\gamma}}\right)\right)^{L-L_c} \prod_{l=1}^{L_c} \exp\left(-\frac{\gamma_l}{\overline{\gamma}}\right), \quad \gamma_1 \geq \cdots \geq \gamma_{L_c} \geq 0, \tag{5.43}$$

Nakagami-m Fading Channels

For Nakagami-m fading $p_\gamma(\gamma)$ is given by (2.15):

$$p_\gamma(\gamma) = \left(\frac{m}{\overline{\gamma}}\right)^m \frac{\gamma^{m-1}}{\Gamma(m)} \exp\left(-\frac{m\gamma}{\overline{\gamma}}\right), \quad \gamma \geq 0, \tag{5.44}$$

where $\Gamma(\cdot)$ denotes the gamma function [53, p. 942, Eqn. (8.310.1)] and the CDF $P_\gamma(\gamma) = \int_0^\gamma p_\gamma(y)dy$ can be evaluated as

$$P_\gamma(\gamma) = \frac{\gamma\left(m, \frac{m\gamma}{\overline{\gamma}}\right)}{\Gamma(m)}, \quad \gamma \geq 0, \tag{5.45}$$

with $\gamma(\cdot,\cdot)$ denoting the incomplete gamma function [53, p. 949, Eqn. (8.350.1)].

For the Nakagami-m fading we shall be interested in the special cases of $L_c = 2$ and $L = 3$ and 4 in which case (5.40) becomes

$$p_{\gamma_1,\gamma_2}(\gamma_1,\gamma_2) = 6\, p_\gamma(\gamma_1)\, p_\gamma(\gamma_2)\, \frac{\gamma\left(m, \frac{m\gamma_2}{\overline{\gamma}}\right)}{\Gamma(m)}, \quad \gamma_1 \geq \gamma_2 \ (L_c = 2, L = 3), \tag{5.46}$$

and

$$p_{\gamma_1,\gamma_2}(\gamma_1,\gamma_2) = 12\, p_\gamma(\gamma_1)\, p_\gamma(\gamma_2) \left[\frac{\gamma\left(m, \frac{m\gamma_2}{\overline{\gamma}}\right)}{\Gamma(m)}\right]^2, \quad \gamma_1 \geq \gamma_2 \ (L_c = 2, L = 4). \tag{5.47}$$

5.4.2 A Generic Approach for the Performance of SC/MRC over Rayleigh Fading Channels

Average BER of Binary Signals

Based on the alternate representation of the Gaussian Q-function [66, Eqn. (9)], the conditional BER (conditioned on the total combined SNR $\gamma_t = \sum_{l=1}^{L_c} \gamma_l$) of BPSK and BFSK can be written in

the integral form (4.8)

$$P_b(E,\gamma_t) = \frac{1}{\pi}\int_0^{\pi/2} \exp\left(-\frac{g\gamma_t}{\sin^2\phi}\right) d\phi = \frac{1}{\pi}\int_0^{\pi/2} \prod_{l=1}^{L_c} \exp\left(-\frac{g\,\gamma_l}{\sin^2\phi}\right) d\phi, \tag{5.48}$$

where $g = 1$ for BPSK, $g = 1/2$ for orthogonal BFSK, and $g = \frac{1}{2} + \frac{1}{3\pi}$ for BFSK with minimum correlation. The average BER, $P_b(E)$ is then obtained by averaging (5.48) over the joint PDF of the instantaneous SNR sequence $\{\gamma_l\}_{l=1}^{L_c}$ (5.43) yielding

$$\begin{aligned} P_b(E) &= \int_0^\infty \int_{\gamma_{L_c}}^\infty \cdots \int_{\gamma_2}^\infty P_b(E|\gamma_t)\; p_{\gamma_1,\cdots,\gamma_{L_c}}(\gamma_1,\cdots,\gamma_{L_c})\; d\gamma_1 \cdots d\gamma_{L_c-1} d\gamma_{L_c} \\ &= \frac{L!}{\pi(L-L_c)!\overline{\gamma}^{L_c}} \int_0^\infty \int_{\gamma_{L_c}}^\infty \cdots \int_{\gamma_2}^\infty \int_0^{\pi/2} \prod_{l=1}^{L_c} \exp\left[-\left(\frac{g}{\sin^2\phi}+\frac{1}{\overline{\gamma}}\right)\gamma_l\right] \\ &\quad \left[1-\exp\left(-\frac{\gamma_{L_c}}{\overline{\gamma}}\right)\right]^{L-L_c} d\phi d\gamma_1 \cdots d\gamma_{L_c-1} d\gamma_{L_c}. \end{aligned} \tag{5.49}$$

Although the integrand of (5.49) is in a desirable product form in the γ_l's, we cannot partition the L_c-fold integral into a product of one-dimensional integrals as is possible for MRC (see 4.27) because of the γ_l's in the lower limits of the semi-finite range (improper) integrals in (5.49). To get around this difficulty, we consider the following clever transformation used by Kong and Milstein in their derivation of the combined average SNR of GSC [78, Appendix]:

$$\begin{aligned} x_1 &= \gamma_1 - \gamma_2 \\ x_2 &= \gamma_2 - \gamma_3 \\ &\vdots \\ x_{L_c-1} &= \gamma_{L_c-1} - \gamma_{L_c} \\ x_{L_c} &= \gamma_{L_c}. \end{aligned} \tag{5.50}$$

Using (5.50) in (5.49) gives

$$\begin{aligned} P_b(E) &= \frac{L!}{\pi(L-L_c)!\overline{\gamma}^{L_c}} \int_0^\infty \int_0^\infty \cdots \int_0^\infty \int_0^{\pi/2} \prod_{l=1}^{L_c} \exp\left[-\left(\frac{g}{\sin^2\phi}+\frac{1}{\overline{\gamma}}\right) l x_l\right] \\ &\quad \left[1-\exp\left(-\frac{x_{L_c}}{\overline{\gamma}}\right)\right]^{L-L_c} d\phi dx_1 \cdots dx_{L_c-1} dx_{L_c} \end{aligned} \tag{5.51}$$

The transformation (5.50) has the advantage of transforming the lower limits of the improper integrals in (5.49) to 0 while conserving the desirable product form in the x_l's. Hence partitioning the L_c-fold integral into a product of one-dimensional integrals is now possible after switching the order

of integration on ϕ and on the x_l's. Applying this procedure and grouping like terms yields

$$P_b(E) = \frac{L!}{\pi(L-L_c)!\overline{\gamma}^{L_c}} \int_0^{\pi/2} \prod_{l=1}^{L_c} \mathcal{K}_l(\overline{\gamma}; g; \phi)\, d\phi, \tag{5.52}$$

where

$$\begin{aligned} \mathcal{K}_l(\overline{\gamma}; g; \phi) &= \int_0^{\infty} \exp\left[-\left(\frac{g}{\sin^2\phi}+\frac{1}{\overline{\gamma}}\right) l x_l\right] dx_l, \qquad l = 1, 2, \cdots L_c - 1 \\ &= \left[\left(\frac{g}{\sin^2\phi}+\frac{1}{\overline{\gamma}}\right) l\right]^{-1}, \qquad l = 1, 2, \cdots L_c - 1, \end{aligned} \tag{5.53}$$

and

$$\mathcal{K}_{L_c}(\overline{\gamma}; g; \phi) = \int_0^{\infty} \exp\left[-\left(\frac{g}{\sin^2\phi}+\frac{1}{\overline{\gamma}}\right) L_c x_{L_c}\right] \left[1-\exp\left(-\frac{x_{L_c}}{\overline{\gamma}}\right)\right]^{L-L_c} dx_{L_c}. \tag{5.54}$$

Using the binomial expansion

$$\left[1-\exp\left(-\frac{x_{L_c}}{\overline{\gamma}}\right)\right]^{L-L_c} = \sum_{l=0}^{L-L_c} (-1)^l \binom{L-L_c}{l} \exp\left(-\frac{l\, x_{L_c}}{\overline{\gamma}}\right) \tag{5.55}$$

in (5.54) $\mathcal{K}_{L_c}(\overline{\gamma}; g; \phi)$ can be expressed in closed-form as

$$\mathcal{K}_{L_c}(\overline{\gamma}; g; \phi) = \sum_{l=0}^{L-L_c} \frac{(-1)^l \binom{L-L_c}{l}}{\frac{g\, L_c}{\sin^2\phi} + \frac{L_c+l}{\overline{\gamma}}}. \tag{5.56}$$

Substituting (5.53) and (5.56) in (5.52) and after some manipulations the average BER can be expressed in terms of a single finite-range integral given by

$$P_b(E) = \frac{\binom{L}{L_c}}{\pi} \int_0^{\pi/2} \frac{\sum_{l=0}^{L-L_c} (-1)^l \binom{L-L_c}{l} \left(1 + \frac{l}{L_c} + \frac{g\overline{\gamma}}{\sin^2\phi}\right)^{-1}}{\left(1+\frac{g\overline{\gamma}}{\sin^2\phi}\right)^{L_c-1}} d\phi. \tag{5.57}$$

Switching the order of summation and integration, and defining the integral $I_n(\theta; c_1, c_2)$ as

$$I_n(\theta; c_1, c_2) = \frac{1}{\pi} \int_0^{\theta} \left(\frac{\sin^2\phi}{\sin^2\phi + c_1}\right)^n \left(\frac{\sin^2\phi}{\sin^2\phi + c_2}\right) d\phi, \tag{5.58}$$

where, in general c_1 and c_2 are two constants (independent of ϕ) that might be different, we can rewrite the average BER as

$$P_b(E) = \binom{L}{L_c} \sum_{l=0}^{L-L_c} \frac{(-1)^l \binom{L-L_c}{l}}{1+\frac{l}{L_c}} I_{L_c-1}\left(\frac{\pi}{2}; g\overline{\gamma}, \frac{g\overline{\gamma}}{1+\frac{l}{L_c}}\right). \tag{5.59}$$

Since the integrals $I_n(\theta; c_1, c_2)$ were found in closed-form by Pawula (for $c_1 = c_2$) and by Simon (for $c_1 \neq c_2$) (see Appendix A) (5.59) presents the final desired closed-form result. This result yields the same numerical results as [73, Eq. (9)] and [73, Eq. (12)], for the average BER of BPSK (g=1) with $L_c = 2$ and $L_c = 3$, respectively. Hence (5.59) (or equivalently (5.57)) is a generic expression valid for any $L_c \leq L$ without being "extremely unwieldy notationally" as would be the case if the approach adopted in [77], [73] was pursued further for $L_c > 3$.

Average SER of M-ary Signals

In Chapter 4 we showed that various M-ary modulations have a conditional SER which can put in the desired product form representation. Using the fact that these expressions have the same functional (product of exponentials) dependence on the γ_l's as does (5.48) we can easily extend the analysis developed in (5.4.2) to obtain the exact average SER of any two-dimensional constellation with GSC. We limit ourselves here to M-PSK, M-AM, and square M-QAM signals.

Average SER of M-PSK The conditional SER for M-PSK, $P_s(\gamma_t)$, was shown to be given exactly by the desirable product form expression (4.29), namely

$$P_s(\gamma_t) = \frac{1}{\pi}\int_0^{\frac{(M-1)\pi}{M}} \exp\left(-\frac{g_{\text{psk}}\,\gamma_t}{\sin^2\phi}\right) d\phi = \frac{1}{\pi}\int_0^{\frac{(M-1)\pi}{M}} \prod_{l=1}^{L_c} \exp\left(-\frac{g_{\text{psk}}\,\gamma_l}{\sin^2\phi}\right) d\phi, \tag{5.60}$$

where $g_{\text{psk}} = \sin^2\left(\frac{\pi}{M}\right)$. Hence, averaging (5.60) over (5.43) then following the same steps as in (5.49)-(5.59) we obtain by inspection the following expression for the average SER of M-PSK:

$$P_s(E) = \binom{L}{L_c} \sum_{l=0}^{L-L_c} \frac{(-1)^l \binom{L-L_c}{l}}{1-\frac{l}{L_c}}\, I_{L_c-1}\left(\frac{(M-1)\pi}{M}; g_{\text{psk}}\overline{\gamma}, \frac{g_{\text{psk}}\overline{\gamma}}{1+\frac{l}{L_c}}\right). \tag{5.61}$$

Our result (5.61) generalizes the M-PSK average SER results of Chennakeshu and Anderson [60] with MRC and conventional SC. For instance for the particular case of $L = L_c$ (i.e., MRC) it can be easily shown that (5.61) together with (5.80) agrees with [60, Eq. (21)]. Similarly, for the particular case of $L_c = 1$ (i.e., conventional SC) it can also be shown that (5.61) together with (5.82) reduces to [60, Eq. (26)].

Average SER of M-AM The conditional SER for M-AM, $P_s(\gamma_t)$, was shown to be given exactly by the desirable product form expression (4.33), namely

$$\overline{P}_s(\gamma_t) = \frac{2\,(M-1)}{M\,\pi}\int_0^{\pi/2} \exp\left(-\frac{g_{\text{am}}\,\gamma_t}{\sin^2\phi}\right) d\phi = \frac{2\,(M-1)}{M\,\pi}\int_0^{\pi/2} \prod_{l=1}^{L_c} \exp\left(-\frac{g_{\text{am}}\,\gamma_l}{\sin^2\phi}\right) d\phi. \tag{5.62}$$

where $g_{\text{am}} = \frac{3}{M^2-1}$. Hence, averaging (5.62) over (5.43) then following the same steps as in (5.49)-(5.59) we obtain by inspection the following expression for the average SER of M-AM:

$$P_s(E) = \frac{2(M-1)\binom{L}{L_c}}{M} \sum_{l=0}^{L-L_c} \frac{(-1)^l \binom{L-L_c}{l}}{1+\frac{l}{L_c}} I_{L_c-1}\left(\frac{\pi}{2}; g_{\text{am}}\overline{\gamma}, \frac{g_{\text{am}}\overline{\gamma}}{1+\frac{l}{L_c}}\right). \tag{5.63}$$

Average SER of Square M-QAM The conditional SER for square M-QAM, $P_s(\gamma_t)$, was shown to be given by the desirable product form expression (4.37), namely

$$\begin{aligned} P_s(E|\gamma_t) &= \frac{4}{\pi}\left(1-\frac{1}{\sqrt{M}}\right)\int_0^{\pi/2} \exp\left(-\frac{g_{\text{qam}}\,\gamma_t}{\sin^2\phi}\right) d\phi - \frac{4}{\pi}\left(1-\frac{1}{\sqrt{M}}\right)^2 \int_0^{\pi/4} \exp\left(-\frac{g_{\text{qam}}\,\gamma_t}{\sin^2\phi}\right) d\phi \\ &= \frac{4}{\pi}\left(1-\frac{1}{\sqrt{M}}\right)\int_0^{\pi/2} \prod_{l=1}^{L_c} \exp\left(-\frac{g_{\text{qam}}\,\gamma_l}{\sin^2\phi}\right) d\phi - \frac{4}{\pi}\left(1-\frac{1}{\sqrt{M}}\right)^2 \int_0^{\pi/4} \prod_{l=1}^{L_c} \exp\left(-\frac{g_{\text{qam}}\,\gamma_l}{\sin^2\phi}\right) d\phi. \end{aligned} \tag{5.64}$$

where $g_{\text{qam}} = \frac{3}{2(M-1)}$. Hence, averaging (5.64) over (5.43) then following the same steps as in (5.49)-(5.59) we obtain by inspection the following expression for the average SER of square M-QAM:

$$\begin{aligned} P_s(E) &= \binom{L}{L_c}\left[4\left(1-\frac{1}{\sqrt{M}}\right)\sum_{l=0}^{L-L_c} \frac{(-1)^l\binom{L-L_c}{l}}{1+\frac{l}{L_c}} I_{L_c-1}\left(\frac{\pi}{2}; g_{\text{qam}}\overline{\gamma}, \frac{g_{\text{qam}}\overline{\gamma}}{1+\frac{l}{L_c}}\right)\right. \\ &\quad \left. - 4\left(1-\frac{1}{\sqrt{M}}\right)^2 \sum_{l=0}^{L-L_c} \frac{(-1)^l\binom{L-L_c}{l}}{1+\frac{l}{L_c}} I_{L_c-1}\left(\frac{\pi}{4}; g_{\text{qam}}\overline{\gamma}, \frac{g_{\text{qam}}\overline{\gamma}}{1+\frac{l}{L_c}}\right)\right]. \end{aligned} \tag{5.65}$$

Our result (5.65) generalizes our square M-QAM SER result of Chapter 4 as well as those of Lu *al.* [71] with MRC and conventional SC. For instance for the particular case of $L = L_c$ (i.e., MRC) it can be easily shown that (5.65) together with (5.80) agrees with (4.39) or equivalently yields the same numerical results as [71, Eq. (12)]. Similarly, for the particular case of $L_c = 1$ (i.e., conventional SC) it can also be shown that (5.65) together with (5.82) reduces to [71, Eq. (23)].

5.4.3 Performance of SC/MRC over Nakagami-m Fading Channels

In this section we quantify the effect of the severity of the fading on the BER performance degradation arising from the use of SC/MRC instead of the optimal MRC scheme. The organization of this section is as follows. The performance of SC/MRC-2/3, SC/MRC-2/4, and MRC-L binary receivers is derived in Sections 5.4.3, 5.4.3, and 5.4.3 respectively. Numerical results and a discussion of these results are presented in Section 5.4.3.

Average Error Probability Performance of SC/MRC-2/3 Binary Receivers

For binary signals and a receiver that implements the hybrid SC/MRC scheme with $L_c = 2$ and $L = 3$ (i.e., MRC combining of the strongest two of the three received branches), the BER conditioned on the fading amplitudes is given by [51, p. 188]

$$P_b(\gamma_t) = Q\left(\sqrt{2\,g\,\gamma_t}\right), \tag{5.66}$$

where $Q(\cdot)$ is the Gaussian Q-function, $g = 1$ for coherent BPSK [51, Eqn. (4.55)], $g = 1/2$ for coherent orthogonal BFSK [51, Eqn. (4.49)], $g = \frac{1}{2} + \frac{1}{3\pi}$ for coherent BFSK with minimum correlation [51, Eqn. (4.63)], and $\gamma_t = \gamma_1 + \gamma_2$ denotes the total SNR. Traditionally, the average BER is computed by determining the PDF of γ_t and then averaging (5.66) over this PDF, i.e.,

$$\overline{P}_b = \int_0^\infty Q\left(\sqrt{2\,g\,\gamma_t}\right) p_{\gamma_t}(\gamma_t)\,d\gamma_t. \tag{5.67}$$

In fact, this was the procedure taken by Eng *et al.* [73] for the Rayleigh channel.

For the Nakagami-m channel, it is more expeditious to take a different approach based on the alternate reprcsentation of the Gaussian Q-function. To begin we first rewrite (5.67) as

$$\overline{P}_b = \int_0^\infty \int_0^{\gamma_1} Q\left(\sqrt{2\,g\,(\gamma_1+\gamma_2)}\right)\, p_{\gamma_1,\gamma_2}(\gamma_1,\gamma_2)\,d\gamma_2\,d\gamma_1, \tag{5.68}$$

which because of the dependence of γ_1 and γ_2 would require double integration using the joint PDF of (5.46). Now using the alternate representation of the Gaussian Q-function (4.7), namely,

$$Q(x) = \frac{1}{\pi}\int_0^{\pi/2} \exp\left(-\frac{x^2}{2\sin^2\phi}\right)\,d\phi; \qquad x \geq 0, \tag{5.69}$$

results in

$$\overline{P}_b = \frac{1}{\pi}\int_0^{\pi/2}\int_0^\infty\int_0^{\gamma_1} 6\,p_\gamma(\gamma_1)\,p_\gamma(\gamma_2)\,\frac{\gamma\left(m,\frac{m\gamma_2}{\overline{\gamma}}\right)}{\Gamma(m)}\,\exp\left(-\frac{g(\gamma_1+\gamma_2)}{\sin^2\phi}\right)\,d\gamma_2\,d\gamma_1\,d\phi. \tag{5.70}$$

At first glance, (5.70) appears formidable in that it involves evaluation of a triple integral. As we shall soon see, however, each of these integrals can be evaluated in closed form with the final result for $\overline{P}_b$ being expressible as a single infinite series of tabulated functions. To obtain this form, we proceed as in Appendix B with the result (see 5.94)

$$\begin{aligned}\overline{P}_b &= \frac{3}{(\Gamma(m))^3}\sqrt{\frac{g\overline{\gamma}/m}{\pi\,(1+g\overline{\gamma}/m)}}\sum_{n=0}^\infty \frac{(-1)^n\Gamma(3m+n+1/2)}{2^{3m+n}\,n!\,(m+n)(2m+n)(3m+n)}\left(\frac{1}{1+g\overline{\gamma}/m}\right)^{3m+n} \\ &\times\ {}_2F_1\left(1,3m+n;2m+n+1;\frac{1}{2}\right)\ {}_2F_1\left(1,3m+n+1/2;3m+n+1;\frac{1}{1+g\overline{\gamma}/m}\right)\end{aligned} \tag{5.71}$$

which is valid for any $m \geq 1/2$ (integer or noninteger). The Gaussian hypergeometric function ${}_2F_1(\cdot,\cdot;\cdot;\cdot)$ [70, p. 556, Eqn. (15.1.1)] is available in standard mathematical software packages such as Mathematica and thus (5.71) is readily evaluated. The specifics of this evaluation will be discussed in Section 5.4.3 on numerical results.

Average Error Probability Performance of SC/MRC-2/4 Binary Receivers

For the receiver in Section 5.4.3 with now $L_c = 2$ and $L = 4$ (i.e., MRC combining of the strongest two of the four received branches), the average BER is obtained by using the Gaussian Q-function representation of (5.69) and $p_{\gamma_1,\gamma_2}(\gamma_1,\gamma_2)$ of (5.47) in (5.68) resulting in

$$\overline{P}_b = \frac{1}{\pi}\int_0^{\pi/2}\int_0^{\infty}\int_0^{\gamma_1} 12\, p_\gamma(\gamma_1)\, p_\gamma(\gamma_2) \left[\frac{\gamma\left(m, \frac{m\gamma_2}{\overline{\gamma}}\right)}{\Gamma(m)}\right]^2 \exp\left(-\frac{g(\gamma_1+\gamma_2)}{\sin^2\phi}\right) d\gamma_2\, d\gamma_1\, d\phi. \quad (5.72)$$

As before, the triple integral in (5.72) can be evaluated in closed-form with the final result for $\overline{P}_b$ being expressible now as a double infinite series of the same tabulated functions as those in (5.71). To obtain this form, we proceed as in Appendix C with the result (see (5.101))

$$\overline{P}_b = \frac{6}{(\Gamma(m))^4}\sqrt{\frac{g\overline{\gamma}/m}{\pi\,(1+g\overline{\gamma}/m)}}\sum_{n=0}^{\infty}\sum_{l=0}^{\infty}\frac{(-1)^{n+l}\Gamma(4m+n+l+1/2)}{2^{4m+n+l}n!l!(m+n)(m+l)(3m+n+l)(4m+n+l)}\left(\frac{1}{1+g\overline{\gamma}/m}\right)^{4m+n+l}$$
$$\times\, {}_2F_1\left(1, 4m+n+l; 3m+n+l+1; \frac{1}{2}\right)\; {}_2F_1\left(1, 4m+n+l+1/2; 4m+n+l+1; \frac{1}{1+g\overline{\gamma}/m}\right). \quad (5.73)$$

Note that although (5.73) is a double infinite sum as opposed to the single infinite sum of (5.71), each term still only involves a product of two Gaussian hypergeometric functions.

In principle, the approach taken in Appendices B and C can be extended to evaluate the average BER of the hybrid SC/MRC scheme with $L_c = 2$ and arbitrary L. The result will be in the form of an $L-2$ order infinite sum whose individual terms involve a product of two Gaussian hypergeometric functions. The details of this extension are left to the interest of the reader since the conclusions that we wish to draw can be deduced from the two specific cases already considered.

We conclude this section by noting that the average symbol error rate of M-ary linearly modulated signals (M-PSK, M-ary amplitude modulation (M-AM), and M-ary quadrature amplitude modulation (M-QAM)) with hybrid SC/MRC can be derived in a manner similar to that presented in Appendices B and C. The approach taken to achieve these results would make use of the "desired" conditional symbol error rate formulas given in the previous chapter combined with new trigonometric integrals found by equivalence with results from [60] and shown in [5, Appendix 5A].

Average Error Probability Performance of SC and MRC Binary Receivers

In the section on numerical results, it will be of interest to compare the suboptimum (but simpler) hybrid SC/MRC scheme with conventional SC as well as with optimum MRC of L branches.

Selective Combining With conventional SC the receiver processes the branch with the largest SNR. The PDF of the SC output $p_{\gamma_{sc}}(\gamma_{sc})$ is then found by setting L_c to 1 in (5.40) yielding

$$p_{\gamma_{sc}}(\gamma_{sc}) = \left(\frac{m}{\overline{\gamma}}\right)^m \frac{L\ \gamma_{sc}^{m-1}}{(\Gamma(m))^L} \left[\gamma\left(m, \frac{m\gamma_{sc}}{\overline{\gamma}}\right)\right]^{L-1} \exp\left(-\frac{m\gamma_{sc}}{\overline{\gamma}}\right). \tag{5.74}$$

Substituting (5.74) in (5.67) yields

$$\overline{P}_b = \left(\frac{m}{\overline{\gamma}}\right)^m \frac{L}{(\Gamma(m))^L} \int_0^\infty \gamma_{sc}^{m-1}\, Q\left(\sqrt{2g\gamma_{sc}}\right) \left[\gamma\left(m, \frac{m\gamma_{sc}}{\overline{\gamma}}\right)\right]^{L-1} \exp\left(-\frac{m\gamma_{sc}}{\overline{\gamma}}\right) d\gamma_{sc}. \tag{5.75}$$

Since no closed-form solution is available for the intgral in (5.75) the average BER of SC is computed numerically.

Maximal-Ratio Combining For MRC diversity, the average BER is again given by (5.67) with $\gamma_t = \sum_{l=1}^{L_c} \gamma_l$, where now the γ_l's correspond to a randomly chosen (not ordered) subset of the L received branches including the possibility of all the branches, i.e., $L_c = L$. Since no attempt is made to choose those γ_l's having the largest values, the total fading, γ_t, now corresponds to the sum of L_c i.i.d. gamma RVs which has the PDF [79, Eqn. (7)]

$$p_{\gamma_t}(\gamma_t) = \left(\frac{m}{\overline{\gamma}}\right)^{L_c m} \frac{\gamma_t^{L_c m-1}}{\Gamma(L_c m)} \exp\left(-\frac{m\gamma_t}{\overline{\gamma}}\right), \quad \gamma_t \geq 0. \tag{5.76}$$

Substituting (5.76) in (5.67) and using a result obtained by Eng and Milstein [46, Appendix A, Eqn. (A8)] which is analogous to (5.93) of Appendix B, we obtain the desired result [79, Eqn. (15)].

$$\overline{P}_b = \frac{1}{2}\sqrt{\frac{g\overline{\gamma}/m}{\pi\,(1+g\overline{\gamma}/m)}}\, \frac{\Gamma\left(L_c m + \frac{1}{2}\right)}{\Gamma\left(L_c m + 1\right)} \left(\frac{1}{1+g\overline{\gamma}/m}\right)^{L_c m} {}_2F_1\left(1, L_c m + \frac{1}{2}, L_c m + 1; \frac{1}{1+g\overline{\gamma}/m}\right). \tag{5.77}$$

Numerical Results and Discussions

Illustrated in Figs. 5.2-5.5 are the average BER results ($\overline{P}_b$ vs. $g\overline{\gamma}$) for the hybrid SC/MRC-2/3 and SC/MRC-2/4 schemes as determined from (5.71) and (5.73), respectively, and for different values of m. Also shown for comparison are the MRC results obtained from (5.77) for values of L_c equal to 2, 3, and 4. The abscissa $g\overline{\gamma}$ represents the average SNR per bit adjusted by the modulation-dependent parameter g. For the purpose of this discussion we shall refer to $g\overline{\gamma}$ as simply SNR.

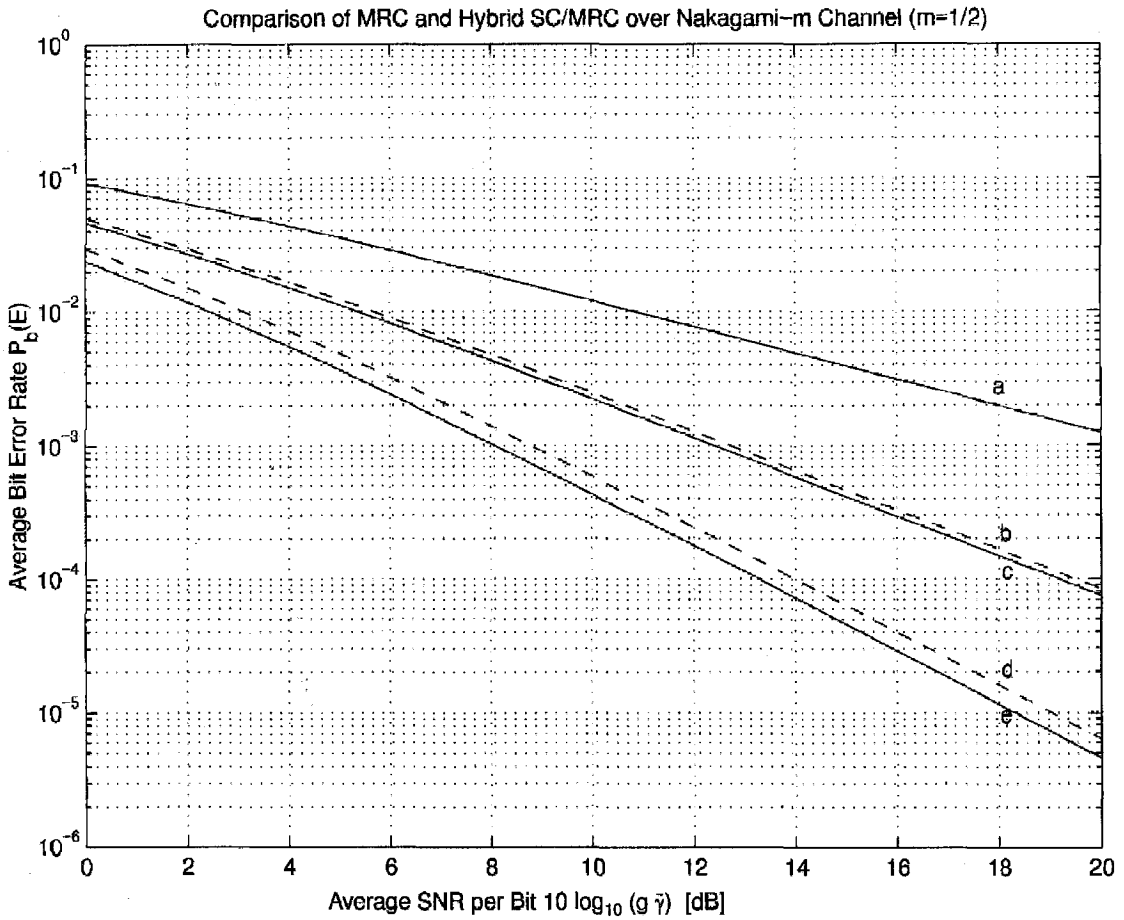

Figure 5.2: Comparison of MRC and hybrid SC/MRC over Nakagami-m channel ($m = 1/2$, Single-sided Gaussian fading) (g is the modulation-dependent parameter, (a) MRC-2, (b) SC/MRC-2/3, (c) MRC-3, (d) SC/MRC-2/4, and (e) MRC-4).

The case $m = 1/2$ corresponds to worst-case (single-sided Gaussian) fading. The results for $m = 1$ correspond to Rayleigh fading and agree with those reported in [73]. The cases $m = 2$ and $m = 4$ represent less severe fading conditions than either single-sided Gaussian or Rayleigh. The results corresponding to the evaluation of (5.71) and (5.73) were obtained by truncating the infinite series to 20 terms. Extending the infinite series beyond this number of terms produced no change in the first 8 decimal places of the numerical results.

A comparison of the MRC performance for $L_c = 2$ (the solid curves labeled "a") with that of the hybrid schemes (the dashed curves labeled "b" and "d") demonstrates the significant advantage of the latter gained by intelligent (i.e., choosing the largest) rather than random selection of which two branches to optimally combine as determined by the SC. The amount to be gained by this intelligent choice of the branches to be combined increases as the fading becomes more severe.

Comparison of the MRC results corresponding to (the solid curves labeled "c" and "e") with those for the hybrid schemes (the dashed curves labeled "b" and "d") demonstrates the advantage of

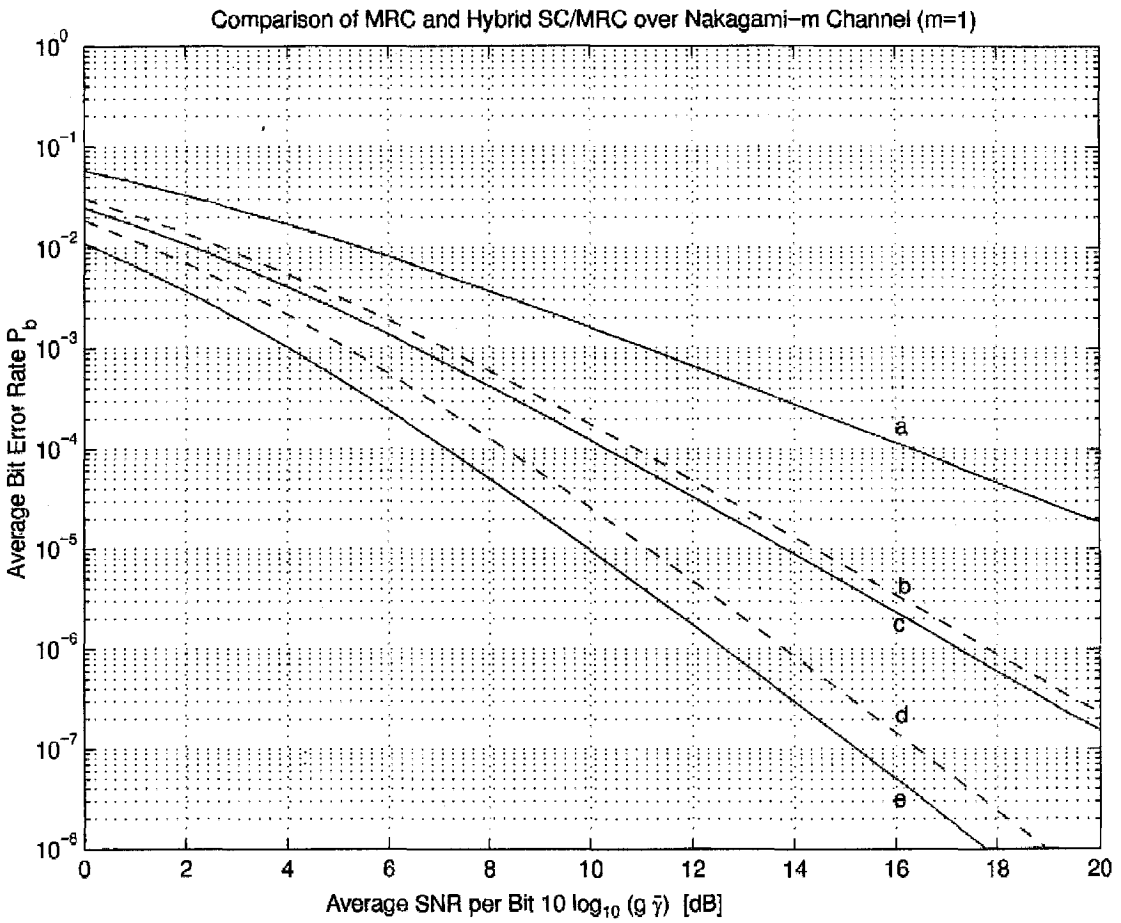

Figure 5.3: Comparison of MRC and hybrid SC/MRC over Nakagami-m channel ($m = 1$, Rayleigh fading) (g is the modulation-dependent parameter, (a) MRC-2, (b) SC/MRC-2/3, (c) MRC-3, (d) SC/MRC-2/4, and (e) MRC-4).

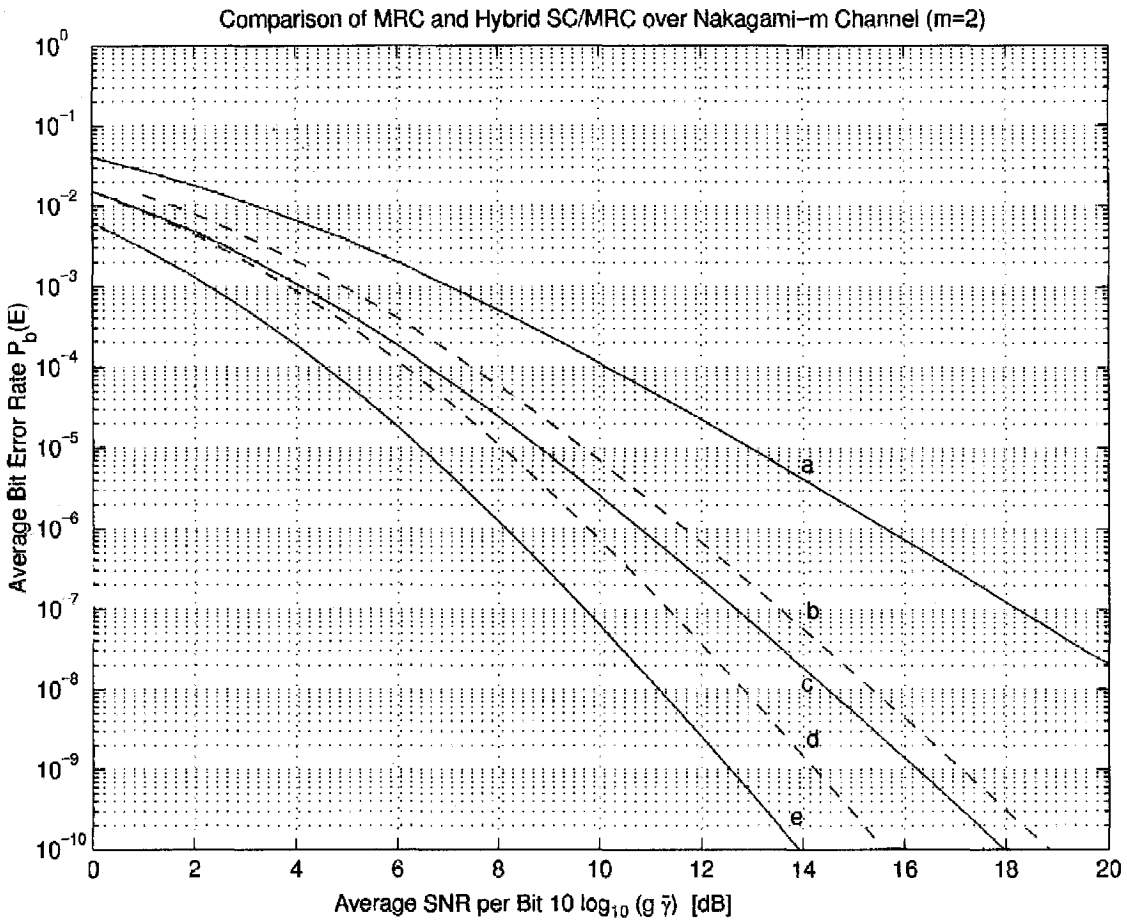

Figure 5.4: Comparison of MRC and hybrid SC/MRC over Nakagami-m channel ($m = 2$) (g is the modulation-dependent parameter, (a) MRC-2, (b) SC/MRC-2/3, (c) MRC-3, (d) SC/MRC-2/4, and (e) MRC-4).

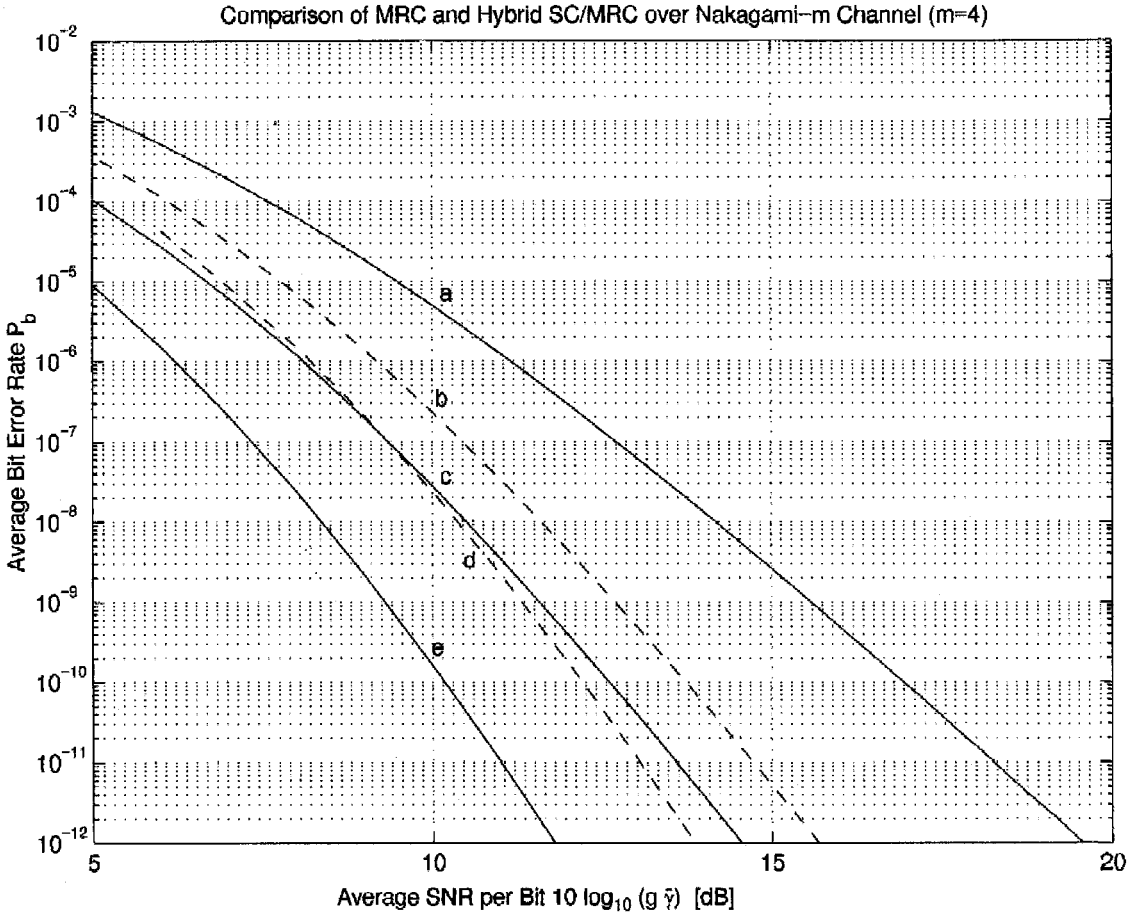

Figure 5.5: Comparison of MRC and hybrid SC/MRC over Nakagami-m channel ($m = 4$) (g is the modulation-dependent parameter, (a) MRC-2, (b) SC/MRC-2/3, (c) MRC-3, (d) SC/MRC-2/4, and (e) MRC-4).

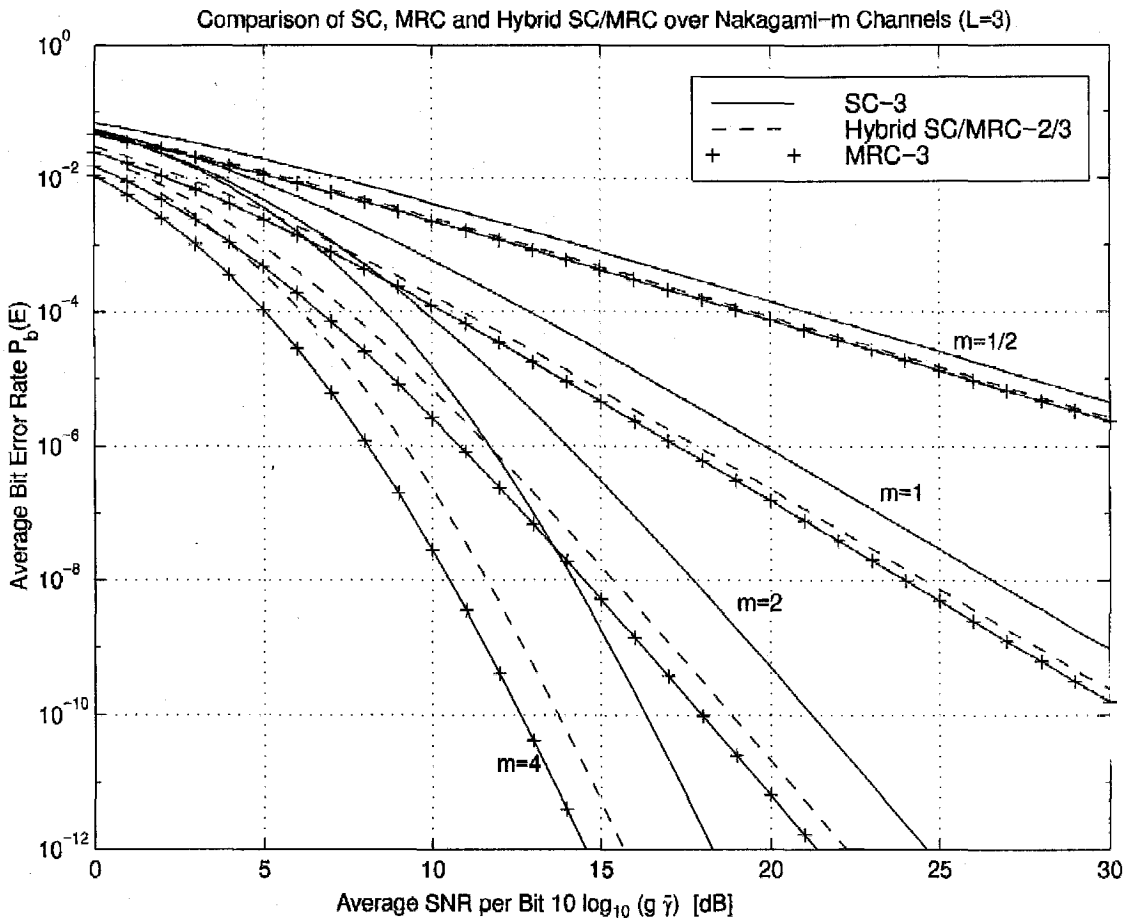

Figure 5.6: Comparison of SC-3, MRC-3, and hybrid SC/MRC-2/3 over Nakagami-m channel for a constant number of available branches L=3.

the former gained by optimally combining all received branches, i.e., making full use of the amount of diversity available. Three conclusions can be drawn from this comparison. First, the gain of the optimum (MRC-L) over the corresponding suboptimum (SC/MRC-L_c/L) scheme (i.e., curve "b" vs. "c" or "d" vs. "e") is constant *independent* of SNR. This result is obvious from the numerical results but certainly not obvious from the analytical expressions. Second, as one might expect, the amount of gain improves as L_c approaches L. Finally, from Figs. 5.6 and 5.7, we see that for a fixed number of available branches, the amount of gain varies inversely with the severity of the fading. That is, for the more severe fading cases, the suboptimum hybrid schemes are closer to the true optimum MRC scheme.

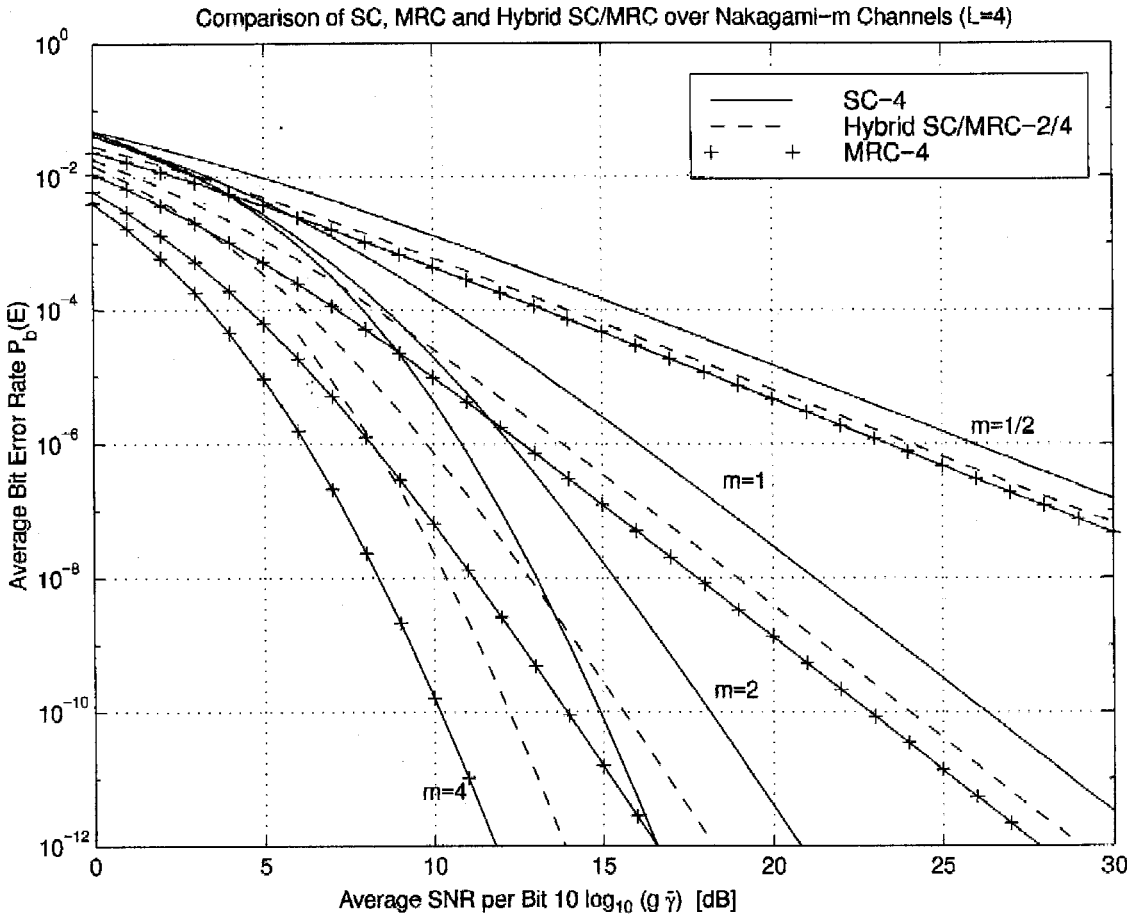

Figure 5.7: Comparison of SC-4, MRC-4, and hybrid SC/MRC-2/4 over Nakagami-m channel for a constant number of available branches L=4.

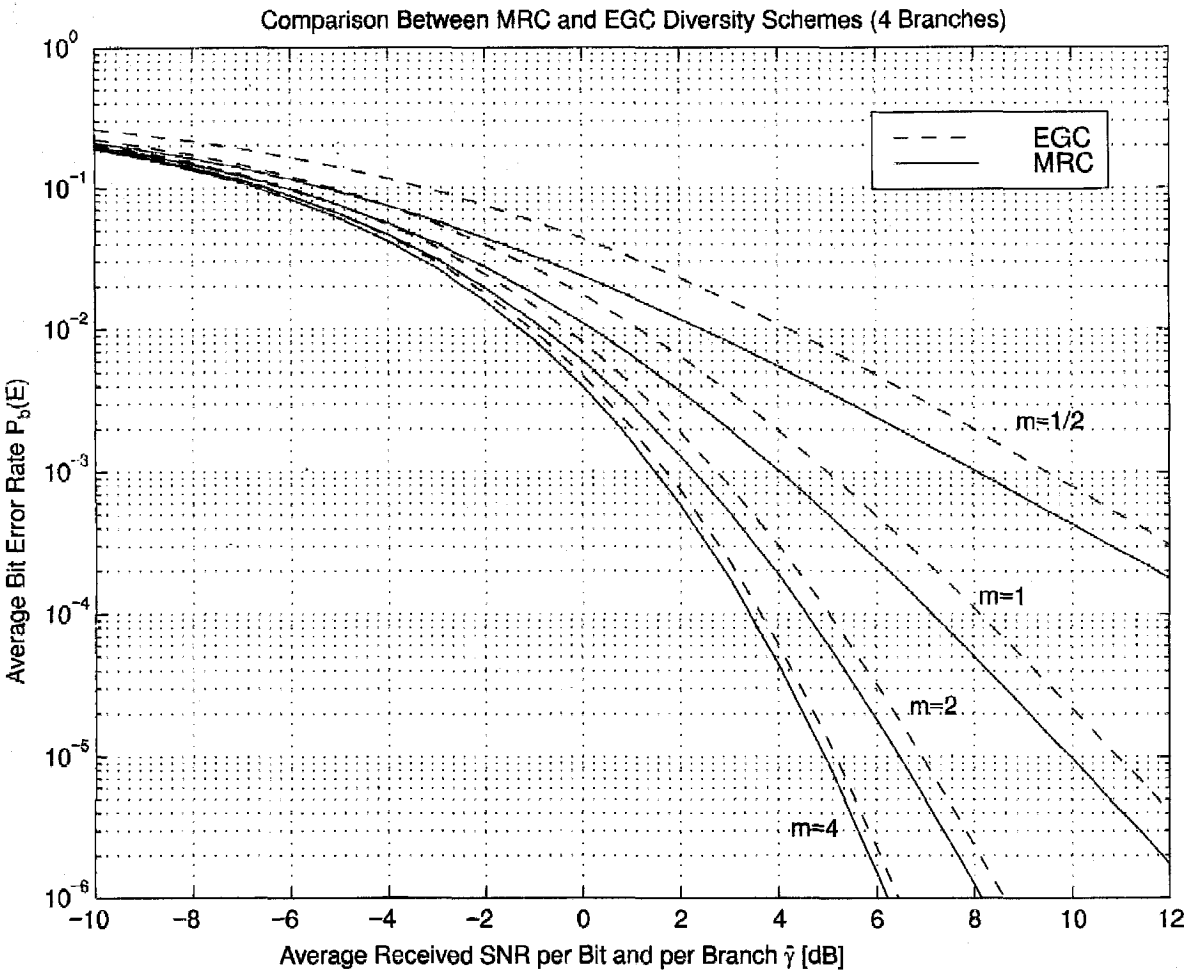

Figure 5.8: Comparison of MRC and EGC over Nakagami-m channel for various m parameters.

5.5 Comparison Between EGC and SC/MRC

In Figs. 5.8 and 5.9 we plot the average BER results ($\overline{P}_b$ vs. $g\overline{\gamma}$) for EGC and the hybrid SC/MRC-2/3, respectively, for different values of m. Also shown for comparison are the MRC results. The performance of EGC approaches the performance of MRC for channels with low amounts of fading (high m) whereas the performance of the hybrid SC/MRC scheme tends to MRC for fading channels with high amounts of fading. This behavior can be explained by the following argument. For channels with high amounts of fading EGC is combining very "noisy" branches and suffers therefore a serious penalty with respect to MRC. Since the hybrid SC/MRC ignores the branches with lowest SNR, this scheme has relatively good performance for this type of channels. On the other hand, for channels with low amounts of fading, EGC is taking full advantage of the combining of all the "good" branches whereas hybrid SC/MRC suffers a serious penalty since it is disregarding information carried in some of these branches.

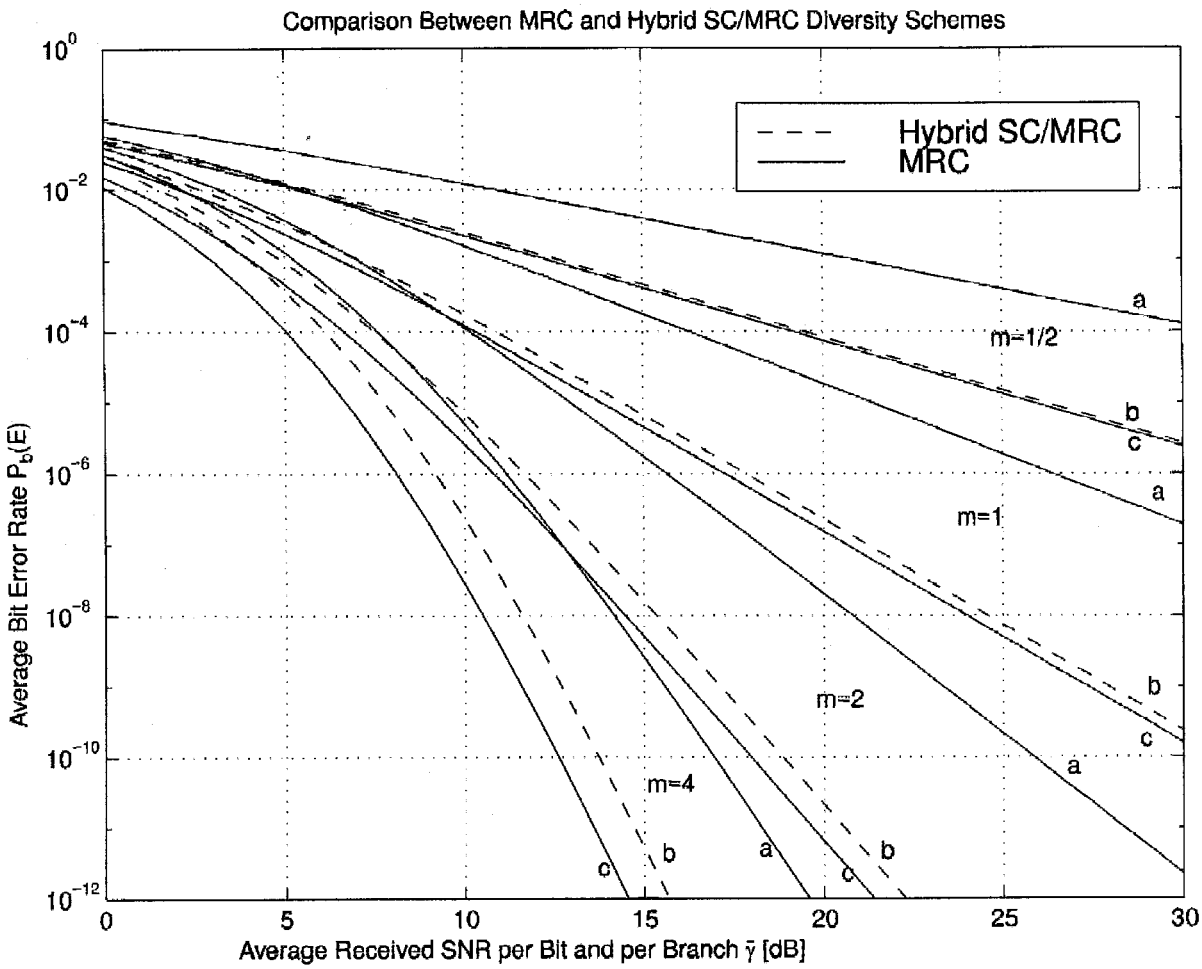

Figure 5.9: Comparison of MRC and hybrid SC/MRC-2/3 over Nakagami-m channel for various m parameters, ((a) MRC-2, (b) SC/MRC-2/3, (c) MRC-3).

5.6 Conclusion

We have presented a performance analysis of the EGC and the hybrid SC/MRC diversity schemes over Nakagami-m fading channels and compared this performance to that of optimal MRC. The analysis for EGC assumes that the fading amplitude statistics for each path are completely arbitrary. However, the analysis for hybrid SC/MRC was restricted to identically distributed Nakagami-m channels. The generic approach used to derive the performance of hybrid SC/MRC over identical Rayleigh fading channels can be extended to the case of non-identically distributed Rayleigh channels. Unfortunately, however it appears that the simplifications which lead to the performance results of the hybrid scheme are not possible for the case of non-identically distributed Nakagami-m channels.

Based on the numerical results of these diversity schemes, various conclusions can be drawn. First, the performance degradation arising from the use of these suboptimum schemes instead of MRC is independent of the average SNR regardless of the severity of the fading. Second, EGC has a higher rate of improvement than the hybrid SC/MRC scheme as the severity of fading decreases. As such, EGC approaches the performance of MRC for channels with a low amount of fading. Conversely, the hybrid SC/MRC scheme approaches the performance of MRC for channels with a high amount of fading.

Appendix A

Evaluation of the Integral $I_n(\theta; c_1, c_2)$

Define the integral

$$I_n(\theta; c_1, c_2) = \frac{1}{\pi}\int_0^{\theta}\left(\frac{\sin^2\phi}{\sin^2\phi + c_1}\right)^n\left(\frac{\sin^2\phi}{\sin^2\phi + c_2}\right)\,d\phi, \tag{5.78}$$

where, in general c_1 and c_2 are two constants (independent of ϕ) which might be different. For $c_1 = c_2 = c$ Simon deduced from the results of Chennakeshu and Anderson [60] a closed form expression for $I_n(\theta; c, c) \triangleq I_{n+1}(\theta; c)$ given by

$$I_{n+1}(\theta; c) = \frac{\theta}{\pi} - \frac{\beta}{\pi}\left[\left(\frac{\pi}{2} + \arctan\alpha\right)\sum_{k=0}^{n}\binom{2k}{k}\frac{1}{[4(1+c)]^k}\right. \tag{5.79}$$

$$\left. + \sin(\arctan\alpha)\sum_{k=1}^{n}\sum_{i=1}^{k}\frac{T_{ik}}{(1+c)^k}\left[\cos(\arctan\alpha)\right]^{2(k-i)+1}\right], \quad -\pi \le \theta \le \pi, \tag{5.80}$$

where $\beta = \sqrt{\frac{c}{1+c}}\,\mathrm{sgn}\theta$, $\alpha = -\beta\cot\alpha$, and

$$T_{ik} = \frac{\binom{2k}{k}}{\binom{2(k-i)}{k-i}\,4^i\,(2(k-i)+1)}. \tag{5.81}$$

For $n = 0$ (5.80) reduces to

$$I_1(\theta; c) = \frac{\theta}{\pi} - \frac{\beta}{\pi}\left(\frac{\pi}{2} + \arctan\alpha\right). \tag{5.82}$$

Another closed-form for the integral $I_{n+1}(\theta; c)$ has been derived by Pawula based on a clever change of variables due to Euler and Legendre [80, p. 316]. The final result can be found in [5, Appendix 5A] as

$$I_{n+1}(\theta; c) = \frac{\phi}{\pi} - \left(\frac{1 + \mathrm{sgn}(\theta - \pi)}{2} + \frac{T}{\pi}\right)\sqrt{\frac{c}{1+c}}\sum_{k=0}^{n}\binom{2k}{k}\frac{1}{[4(1+c)]^k}$$

$$- \frac{2}{\pi}\sqrt{\frac{c}{1+c}}\sum_{k=0}^{n}\sum_{j=0}^{k-1}\binom{2k}{j}\frac{(-1)^{j+k}}{[4(1+c)]^k}\frac{\sin[(2k-2j)T]}{2k-2j}, \quad 0 \le \theta \le 2\pi, \tag{5.83}$$

where T is defined by

$$T = \frac{1}{2}\arctan\left(\frac{N}{D}\right) + \frac{\pi}{2}\left[1 - \mathrm{sgn}N\left(\frac{1 + \mathrm{sgn}D}{2}\right)\right], \tag{5.84}$$

with $N = 2\sqrt{c(1+c)}\sin(2\theta)$ and $D = (1+2c)\cos(2\theta) - 1$. Using the approach used by Pawula to derive (5.83) Simon derived a closed-from expression for $I_n(\theta; c_1, c_2)$ when $c_1 \neq c_2$ given by

$$\begin{aligned} I_n(\theta; c_1, c_2) &= I_n(\theta; c_1) - \left(\frac{1+\text{sgn}(\theta-\pi)}{2} + \frac{T_2}{\pi}\right)\sqrt{\frac{c_2}{1+c_2}}\left(\frac{c_2}{c_2-c_1}\right)^n \\ &+ \left(\frac{1+\text{sgn}(\theta-\pi)}{2} + \frac{T_1}{\pi}\right)\sqrt{\frac{c_1}{1+c_1}}\sum_{k=0}^{n-1}\left(\frac{c_2}{c_2-c_1}\right)^{n-k}\binom{2k}{k}\frac{1}{[4(1+c_1)]^k} \\ &+ \frac{2}{\pi}\sqrt{\frac{c_1}{1+c_1}}\sum_{k=0}^{n-1}\sum_{j=0}^{k-1}\left(\frac{c_2}{c_2-c_1}\right)^{n-k}\binom{2k}{j}\frac{(-1)^{j+k}}{[4(1+c_1)]^k}\frac{\sin[(2k-2j)T_1]}{2k-2j}, \quad 0 \leq \theta \leq 2\pi, \end{aligned} \tag{5.85}$$

with T_1 and T_2 corresponding to T of (5.84) with c replaced by c_1 and c_2, respectively.

Appendix B

Evaluation of Eqn. (5.70) for the Average Bit Error Probability of SC/MRC-2/3

Define the integral

$$I(\gamma_1) = \int_0^{\gamma_1} p_\gamma(\gamma_2)\,\gamma\left(m, \frac{m\gamma_2}{\overline{\gamma}}\right)\,\exp\left(-\frac{g\gamma_2}{\sin^2\phi}\right)\,d\gamma_2. \tag{5.86}$$

Then, the average error probability given by (5.70) can be written as

$$\overline{P}_b = \frac{1}{\pi}\int_0^{\pi/2}\int_0^{\infty}\frac{6\,p_\gamma(\gamma_1)}{\Gamma(m)}\,\exp\left(-\frac{g\gamma_1}{\sin^2\phi}\right)\,I(\gamma_1)\,d\gamma_1\,d\phi. \tag{5.87}$$

To evaluate $I(\gamma_1)$ we first substitute (5.44) into (5.86) and then make use of the infinite series representation of the incomplete gamma function [53, p. 950, Eqn. (8.354.1)], namely,

$$\gamma\left(m, \frac{m\gamma_2}{\overline{\gamma}}\right) = \sum_{n=0}^{\infty}\frac{(-1)^n}{n!\,(m+n)}\,\left(\frac{m\gamma_2}{\overline{\gamma}}\right)^{m+n} \tag{5.88}$$

which results in

$$\begin{aligned} I(\gamma_1) &= \int_0^{\gamma_1}\left(\frac{m}{\overline{\gamma}}\right)^m\,\frac{\gamma_2^{m-1}}{\Gamma(m)}\,\gamma\left(m, \frac{m\gamma_2}{\overline{\gamma}}\right)\,\exp\left[-\left(\frac{m}{\overline{\gamma}} + \frac{g}{\sin^2\phi}\right)\,\gamma_2\right]\,d\gamma_2 \\ &= \left(\frac{m}{\overline{\gamma}}\right)^{2m}\frac{1}{\Gamma(m)}\sum_{n=0}^{\infty}\frac{(-1)^n}{n!\,(m+n)}\left(\frac{m}{\overline{\gamma}}\right)^n\int_0^{\gamma_1}\gamma_2^{2m+n-1}\,\exp\left[-\left(\frac{m}{\overline{\gamma}} + \frac{g}{\sin^2\phi}\right)\,\gamma_2\right]\,d\gamma_2. \end{aligned} \tag{5.89}$$

Next, the integral in (5.89) can be evaluated using [53, p. 364, Eqn. (3.381.1)] which gives

$$I(\gamma_1) = \left(\frac{m}{\overline{\gamma}}\right)^{2m} \frac{1}{\Gamma(m)} \sum_{n=0}^{\infty} \frac{(-1)^n}{n!\,(m+n)} \left(\frac{m}{\overline{\gamma}}\right)^n \left(\frac{m}{\overline{\gamma}} + \frac{g}{\sin^2\phi}\right)^{-2m-n} \gamma\left(2m+n, \left(\frac{m}{\overline{\gamma}} + \frac{g}{\sin^2\phi}\right)\gamma_1\right). \tag{5.90}$$

Substituting (5.90) in (5.87) and combining like terms gives for the integral on γ_1

$$\int_0^{\infty} \frac{6\, p_\gamma(\gamma_1)}{\Gamma(m)} \exp\left(-\frac{g\gamma_1}{\sin^2\phi}\right) I(\gamma_1)d\gamma_1 = \frac{6}{(\Gamma(m))^3} \left(\frac{m}{\overline{\gamma}}\right)^{3m} \sum_{n=0}^{\infty} \frac{(-1)^n}{n!\,(m+n)} \left(\frac{m}{\overline{\gamma}}\right)^n \left(\frac{m}{\overline{\gamma}} + \frac{g}{\sin^2\phi}\right)^{-2m-n}$$
$$\times \int_0^{\infty} \gamma_1^{m-1} \exp\left[-\left(\frac{m}{\overline{\gamma}} + \frac{g}{\sin^2\phi}\right)\gamma_1\right] \gamma\left(2m+n, \left(\frac{m}{\overline{\gamma}} + \frac{g}{\sin^2\phi}\right)\gamma_1\right) d\gamma_1. \tag{5.91}$$

The integral in (5.91) can be evaluated using [53, p. 690, Eq.(6.455.2)] with the result

$$\int_0^{\infty} \frac{6\, p_\gamma(\gamma_1)}{\Gamma(m)} \exp\left(-\frac{g\gamma_1}{\sin^2\phi}\right) I(\gamma_1)d\gamma_1 = \frac{6}{(\Gamma(m))^3} \sum_{n=0}^{\infty} \frac{(-1)^n}{n!\,(m+n)(2m+n)}$$
$$\times \frac{\Gamma(3m+n)}{2^{3m+n}}\, {}_2F_1(1, 3m+n; 2m+n+1; 1/2) \left(1 - \frac{g\,\overline{\gamma}}{m\,\sin^2\phi}\right)^{-3m-n}, \tag{5.92}$$

where ${}_2F_1(\cdot,\cdot;\cdot;\cdot)$ is the Gaussian hypergeometric function [70, p. 556, Eqn. (15.1.1)]. Finally, the integral on ϕ can be performed using a definite integral that can be derived from a result obtained by Eng and Milstein [46, Appendix A, Eqn. (A8)], namely, [81, Appendix A, Eqns. (63), (67)]

$$\frac{1}{\pi} \int_0^{\pi/2} \left(1 + \frac{c}{\sin^2\phi}\right)^{-m} d\phi = \frac{\sqrt{c/\pi}}{2\,(1+c)^{m+1/2}} \frac{\Gamma(m+1/2)}{\Gamma(m+1)}\, {}_2F_1\left(1, m+1/2; m+1; \frac{1}{1+c}\right). \tag{5.93}$$

Finally, substituting (5.92) in (5.87) and using (5.93), we obtain the desired result (5.71)

$$\overline{P}_b = \frac{3}{(\Gamma(m))^3} \sqrt{\frac{g\overline{\gamma}/m}{\pi\,(1+g\overline{\gamma}/m)}} \sum_{n=0}^{\infty} \frac{(-1)^n \Gamma(3m+n+1/2)}{2^{3m+n} n!(m+n)(2m+n)(3m+n)} \left(\frac{1}{1+g\overline{\gamma}/m}\right)^{3m+n}$$
$$\times \; {}_2F_1\left(1, 3m+n; 2m+n+1; 1/2\right)\, {}_2F_1\left(1, 3m+n+1/2; 3m+n+1; \frac{1}{1+g\overline{\gamma}/m}\right). \tag{5.94}$$

Appendix C

Evaluation of Eqn. (5.72) for the Average Bit Error Probability of SC/MRC-2/4

Define the integral

$$I(\gamma_1) = \int_0^{\gamma_1} p_\gamma(\gamma_2) \left[\gamma\left(m, \frac{m\gamma_2}{\overline{\gamma}}\right)\right]^2 \exp\left(-\frac{g\gamma_2}{\sin^2\phi}\right) d\gamma_2. \tag{5.95}$$

Then, the average error probability as given by (5.72) can be written as

$$\overline{P}_b = \frac{1}{\pi}\int_0^{\pi/2}\int_0^{\infty} \frac{12\, p_\gamma(\gamma_1)}{(\Gamma(m))^2} \exp\left(-\frac{g\gamma_1}{\sin^2\phi}\right) I(\gamma_1)\, d\gamma_1\, d\phi. \tag{5.96}$$

To evaluate $I(\gamma_1)$ we first substitute (5.44) into (5.95) and then twice make use of the infinite series representation of the incomplete gamma function of (5.88) which results in

$$\begin{aligned} I(\gamma_1) &= \left(\frac{m}{\overline{\gamma}}\right)^{3m} \frac{1}{\Gamma(m)} \sum_{n=0}^{\infty}\sum_{l=0}^{\infty} \frac{(-1)^{n+l}}{n!l!\,(m+n)(m+l)} \left(\frac{m}{\overline{\gamma}}\right)^{n+l} \\ &\times \int_0^{\gamma_1} \gamma_2^{3m+n+l-1} \exp\left[-\left(\frac{m}{\overline{\gamma}} + \frac{g}{\sin^2\phi}\right)\gamma_2\right] d\gamma_2. \end{aligned} \tag{5.97}$$

Once again the integral in (5.97) can be evaluated using [53, p. 364, Eqn. (3.381.1)] which gives

$$\begin{aligned} I(\gamma_1) &= \left(\frac{m}{\overline{\gamma}}\right)^{3m} \frac{1}{\Gamma(m)} \sum_{n=0}^{\infty}\sum_{l=0}^{\infty} \frac{(-1)^{n+l}}{n!l!\,(m+n)(m+l)} \left(\frac{m}{\overline{\gamma}}\right)^{n+l} \\ &\times \left(\frac{m}{\overline{\gamma}} + \frac{g}{\sin^2\phi}\right)^{-3m-n-l} \gamma\left(3m+n+l, \left(\frac{m}{\overline{\gamma}} + \frac{g}{\sin^2\phi}\right)\gamma_1\right). \end{aligned} \tag{5.98}$$

Substituting (5.98) in (5.96) and combining like terms gives for the integral on γ_1

$$\begin{aligned} &\int_0^{\infty} \frac{12\, p_\gamma(\gamma_1)}{(\Gamma(m))^2} \exp\left(-\frac{g\gamma_1}{\sin^2\phi}\right) I(\gamma_1) d\gamma_1 = \frac{12}{(\Gamma(m))^4} \left(\frac{m}{\overline{\gamma}}\right)^{4m} \sum_{n=0}^{\infty}\sum_{l=0}^{\infty} \frac{(-1)^{n+l}}{n!l!(m+n)(m+l)} \left(\frac{m}{\overline{\gamma}}\right)^{n+l} \\ &\times \left(\frac{m}{\overline{\gamma}} + \frac{g}{\sin^2\phi}\right)^{-3m-n-l} \int_0^{\infty} \gamma_1^{m-1} \exp\left[-\left(\frac{m}{\overline{\gamma}} + \frac{g}{\sin^2\phi}\right)\gamma_1\right] \gamma\left(3m+n+l, \left(\frac{m}{\overline{\gamma}} + \frac{g}{\sin^2\phi}\right)\gamma_1\right) d\gamma_1. \end{aligned} \tag{5.99}$$

Evaluating the integral in (5.99) using [53, p. 690, Eqn. (6.455.2)] results in

$$\begin{aligned} &\int_0^{\infty} \frac{12\, p_\gamma(\gamma_1)}{(\Gamma(m))^2} \exp\left(-\frac{g\gamma_1}{\sin^2\phi}\right) I(\gamma_1) d\gamma_1 = \frac{12}{(\Gamma(m))^4} \sum_{n=0}^{\infty}\sum_{l=0}^{\infty} \frac{(-1)^{n+l}}{n!l!(m+n)(m+l)(3m+n+l)} \\ &\times \frac{\Gamma(4m+n+l)}{2^{4m+n+l}}\, {}_2F_1\left(1, 4m+n+l, 3m+n+l+1; \frac{1}{2}\right) \left(1 + \frac{g\,\overline{\gamma}}{m\,\sin^2\phi}\right)^{-4m-n-l}. \end{aligned} \tag{5.100}$$

Finally, the integral on ϕ can be performed using the definite integral of (5.93) which leads to the final desired result for average BER (5.73), namely,

$$\overline{P}_b = \frac{6}{(\Gamma(m))^4}\sqrt{\frac{g\bar{\gamma}/m}{\pi\ (1+g\bar{\gamma}/m)}}\sum_{n=0}^{\infty}\sum_{l=0}^{\infty}\frac{(-1)^{n+l}\Gamma(4m+n+l+1/2)}{2^{4m+n+l}n!l!(m+n)(m+l)(3m+n+l)(4m+n+l)}\left(\frac{1}{1+g\bar{\gamma}/m}\right)^{4m+n+l}$$
$$\times\ {}_2F_1\left(1, 4m+n+l; 3m+n+l+1; \frac{1}{2}\right)\ {}_2F_1\left(1, 4m+n+l+1/2; 4m+n+l+1; \frac{1}{1+g\bar{\gamma}/m}\right). \tag{5.101}$$

Chapter 6 Performance of Noncoherent and Differentially Coherent Modulations over Generalized Fading Channels

6.1 Introduction

In many applications the phase of the received signal cannot be tracked accurately, and it is therefore not possible to perform coherent detection. In such scenarios communications systems must rely on noncoherent detection techniques such as envelope or square law detection of frequency-shift-keying (FSK) signals [51, Chapter 5] or on differentially coherent detection techniques such as differential phase-shift-keying (DPSK) [51, Chapter 7].

There are many papers dealing with the performance of noncoherent and differentially coherent communication and detection systems over additive white Gaussian noise (AWGN) as well as fading channels. For example, Proakis [82] developed a generic expression for evaluating the bit-error-rate (BER) for multichannel noncoherent and differentially coherent reception of binary signals over L independent AWGN channels. Further, in [1, Section 7.4, p. 725], Proakis provides closed-form expressions for the average BER of binary orthogonal square-law detected FSK and binary DPSK with multichannel reception over L independent identically distributed (i.i.d.) Rayleigh fading channels. In [83], Lindsey derived a general expression for the average BER of binary correlated FSK with multichannel communication over L independent Rician fading channels in which the strength of the scattered component is assumed to be constant for all the channels. In [4], Charash analyzed the average BER performance of binary orthogonal FSK with multichannel reception over L i.i.d. Nakagami-m fading channels. More recently, Weng and Leung [84] derived a closed form expression for the average BER of binary DPSK with multichannel reception over L i.i.d. Nakagami-m fading channels. Patenaude *et al.* [85] extended the results of Charash [4] and Weng and Leung [84] by providing a closed-form expression for the average BER performance of binary orthogonal square-law detected FSK and binary DPSK with multichannel reception over L independent but not necessarily identically distributed Nakagami-m fading channels. Their derivation is based on the characteristic function method and the resulting expression contains $L-1$ order derivatives, which can be found for small L but which become more complicated to find as L increases. In addition, because of its adoption in the most recent North American and Japanese digital cellular systems standards, differential quadrature PSK (DQPSK) has also received a lot of attention in the literature. For

instance, Tjhung *et al.* [86] and Tanda [87] analyzed the average BER performance of this particular scheme over Rician, and Nakagami-m fading channels, respectively. Further, Tellambura and Bhargava [88] presented an alternate unified BER analysis of DQPSK over Rician and Nakagami-m fading channels.

In this chapter we unify and add to the above results by providing new generalized expressions for the average BER performance of noncoherent and differentially coherent communication systems with single and multichannel reception over AWGN and fading channels. The multichannel reception results are applicable to independent channels which are not necessarily identically distributed nor even distributed according to the same family of distributions, and to systems that employ postdetection equal gain combining (EGC) [1, Section 4.4, p. 298], [2, Section 5.5.6, p. 253]. This unified framework relies on a new approach which does not attempt to compute or approximate the probability density function (PDF) of the signal-to-noise ratio (SNR) at the output of the combiner and then average the conditional BER over that PDF. It rather exploits an alternate form of the Marcum Q-function [89, Appendix C], [90] and the resulting alternate integral representation of the conditional BER as well as some known Laplace transforms and/or Gauss-Hermite quadrature integration to independently average over the PDF of each channel that fades. In all cases this approach leads to expressions of the average BER that involve a single finite-range integral whose integrand contains only elementary functions and which can therefore be easily computed numerically. Since all possible modulation and fading combinations are too numerous to evaluate, numerical results for the error rates as well as a study of their dependence on the various fading parameters are omitted in this thesis. These numerical results will be presented in the more comprehensive treatment in preparation [5] which will also cover communication systems with error correction coding and multiple symbol observation.

The remainder of this chapter is organized as follows. In the next section, the multichannel and the various fading models under consideration are described. Section 6.3 provides the performance of noncoherent and differentially coherent modulations with single channel reception. Section 6.4 presents a new product form representation of the BER for multichannel reception with noncoherent or differentially coherent detection, and this representation is used to derive the average BER with multichannel reception. Finally, a summary of all the results and some concluding remarks are offered in Section 6.5.

6.2 System and Channel Models

6.2.1 Transmitted Signals

Let

$$s(t) = \sum_{i=-\infty}^{\infty} Se^{j(2\pi f_i t + \phi_i)} \tag{6.1}$$

denote the generic complex baseband transmitted signal, where S is a constant amplitude related to the average signal power. For differentially coherent modulations, f_m is set equal to 0 and the information is conveyed via the phase $\phi_m = \pm(2m-1)\frac{\pi}{M}$ $(m = 1, 2, \cdots, M/2)$, where M is the size of the transmitted symbol set. The modulator *differentially phase encodes* the transmitted symbols. Hence if $\Delta\phi_i$ was the information to be communicated in the ith transmission interval, then the transmitter would first form $\phi_i = \phi_{i-1} + \Delta\phi_i$ modulo 2π and then modulate ϕ_i on the carrier. For noncoherent modulation, the information is transmitted via the frequency f_m. For instance, for binary FSK $\theta_m = 0$ and $f_m = \pm\Delta f$.

6.2.2 Multilink and Fading Channel Models

The transmitted signal is received over L independent channels, each of them being a slowly varying flat fading channel, as shown in Fig. 6.1. In Fig. 6.1, $\{r_l(t)\}_{l=1}^{L}$ is the set of received replicas of the signal where l is the channel index, and $\{\alpha_l\}_{l=1}^{L}$, $\{\theta_l\}_{l=1}^{L}$, and $\{\tau_l\}_{l=1}^{L}$ are the random channel amplitudes, phases, and delays, respectively. The first channel is assumed to be the reference channel whose delay $\tau_1 = 0$ and, without loss of generality we assume that $\tau_1 < \tau_2 < \cdots < \tau_L$. Because of the slow-fading assumption, we assume that the $\{\alpha_l\}_{l=1}^{L}$, $\{\theta_l\}_{l=1}^{L}$, and $\{\tau_l\}_{l=1}^{L}$ are all constant over a symbol interval.

The fading amplitude α_l on the lth channel, where l denotes the channel index $(l = 1, 2, \cdots, L)$, is assumed to be a random variable (RV) whose mean square value $\overline{\alpha_l^2}$ is denoted by Ω_l, and whose PDF is any of the family of distributions described in detail in Chapter 2.3. Furthermore, the fading amplitudes $\{\alpha_l\}_{l=1}^{L}$ are assumed to be statistically independent RVs. The multilink channel model under consideration in this chapter is a generalized fading channel in the sense that it is sufficiently general to include the case where the different channels are not necessarily identically distributed nor even distributed according to the same family of distributions. With such a general multilink channel model in hand, we are able to handle a large variety of diversity types such as antenna, frequency, site, or multipath diversity [2, p. 238].

After passing through the fading channel, each replica of the signal is perturbed by complex AWGN with a one-sided power spectral density which is denoted by $2N_l$ (W/Hz). The AWGN is assumed to be statistically independent from channel to channel and independent of the fading amplitudes $\{\alpha_l\}_{l=1}^{L}$. Hence the instantaneous SNR per bit of the lth channel is given by $\gamma_l = \frac{\alpha_l^2 E_b}{N_0}$,

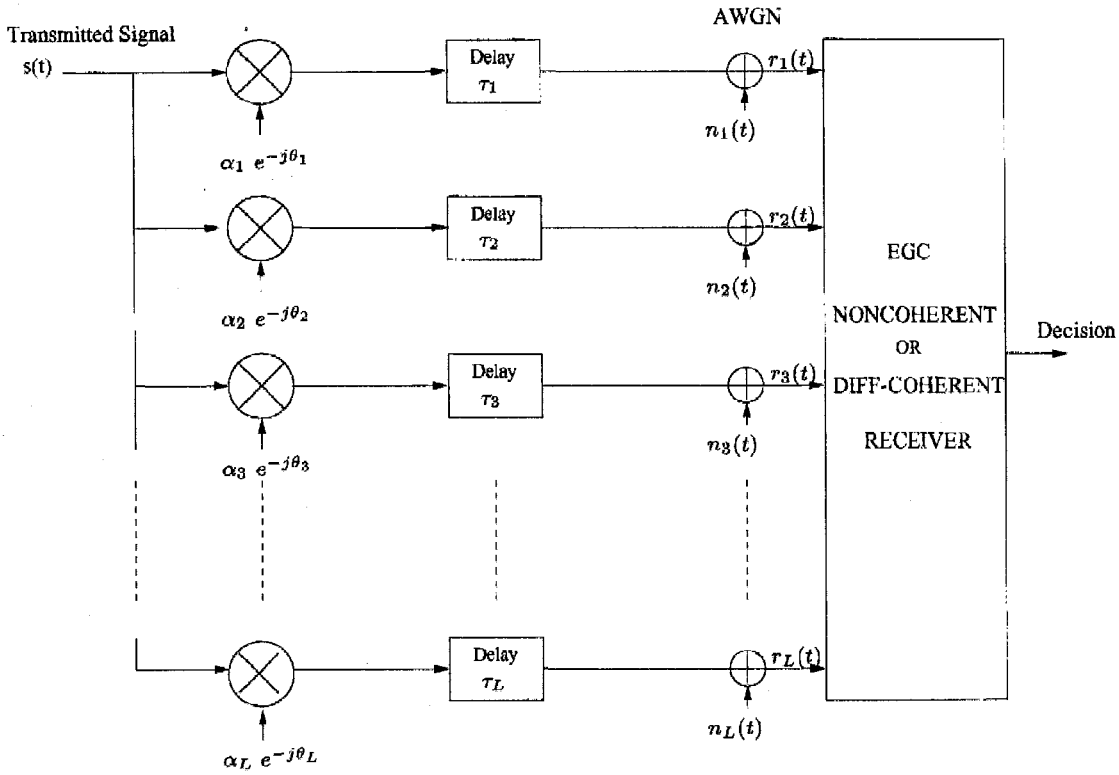

Figure 6.1: Multilink channel model.

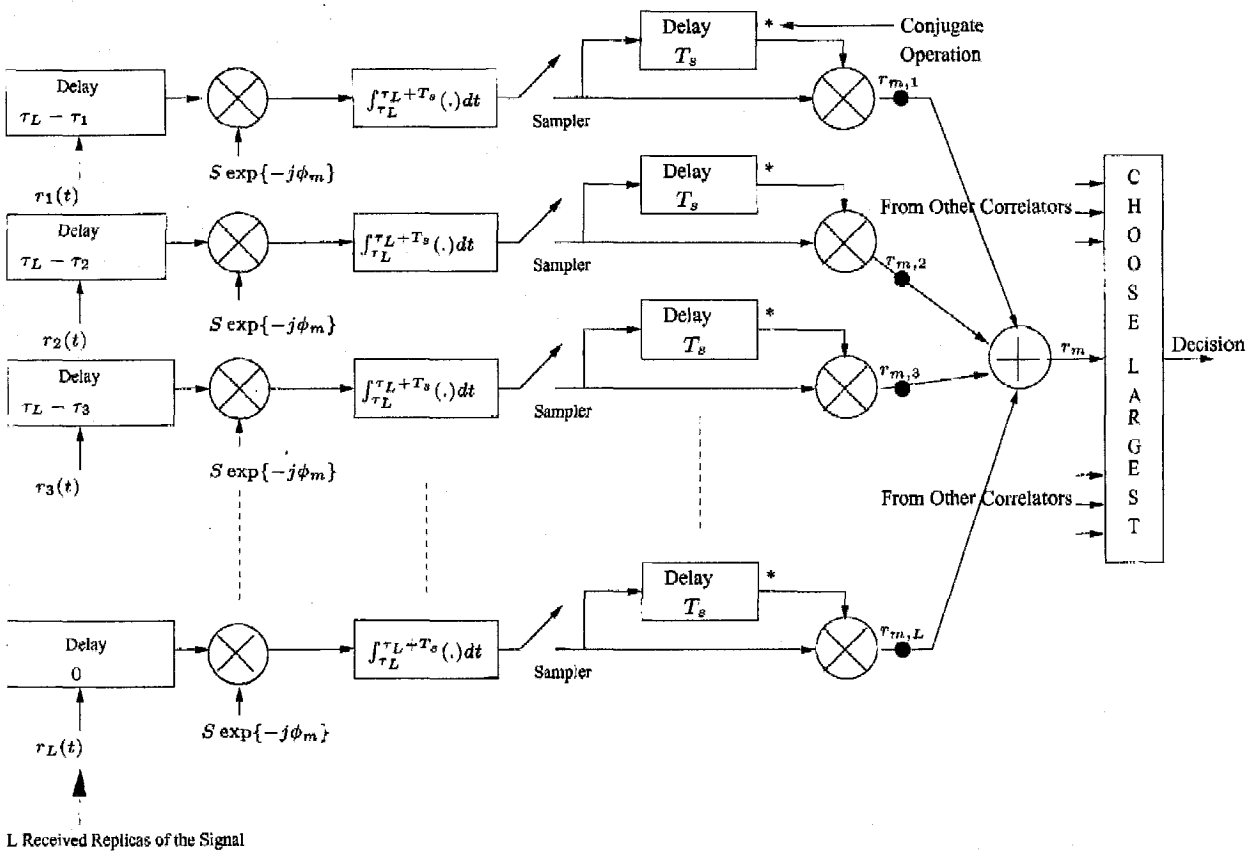

Figure 6.2: Differentially coherent postdetection equal-gain combining receiver structure.

where E_b (J) is the energy per bit, and $2N_0 = \sum_{l=1}^{L} 2N_l$ (W/Hz) is the total complex AWGN power spectral density.

6.2.3 Receiver Model

We consider L branch (finger) postdetection EGC receivers, as shown in Figs. 6.2 and 6.3 for differentially coherent and noncoherent detection, respectively. Both receivers utilize M correlators to detect the maximum a priori transmitted symbol. Without loss of generality let us consider the mth symbol correlator. Each of the L received signals $r_l(t)$ is first delayed by $\tau_L - \tau_l$ then appropriately demodulated (symbol correlation followed by integration and dump then baud-rate sampling). These operations assume that the receiver is correctly time synchronized at every branch (i.e., perfect time delay $\{\tau_l\}_{l=1}^{L}$ estimates).

For differentially coherent detection (see Fig. 6.2) the receiver takes, at every branch l, the difference of two adjacent transmitted phases to arrive at the decision $r_{m,l}$. For noncoherent detection (see Fig. 6.3) no attempt is made to estimate the phase and the receiver yields the decision $r_{m,l}$ based

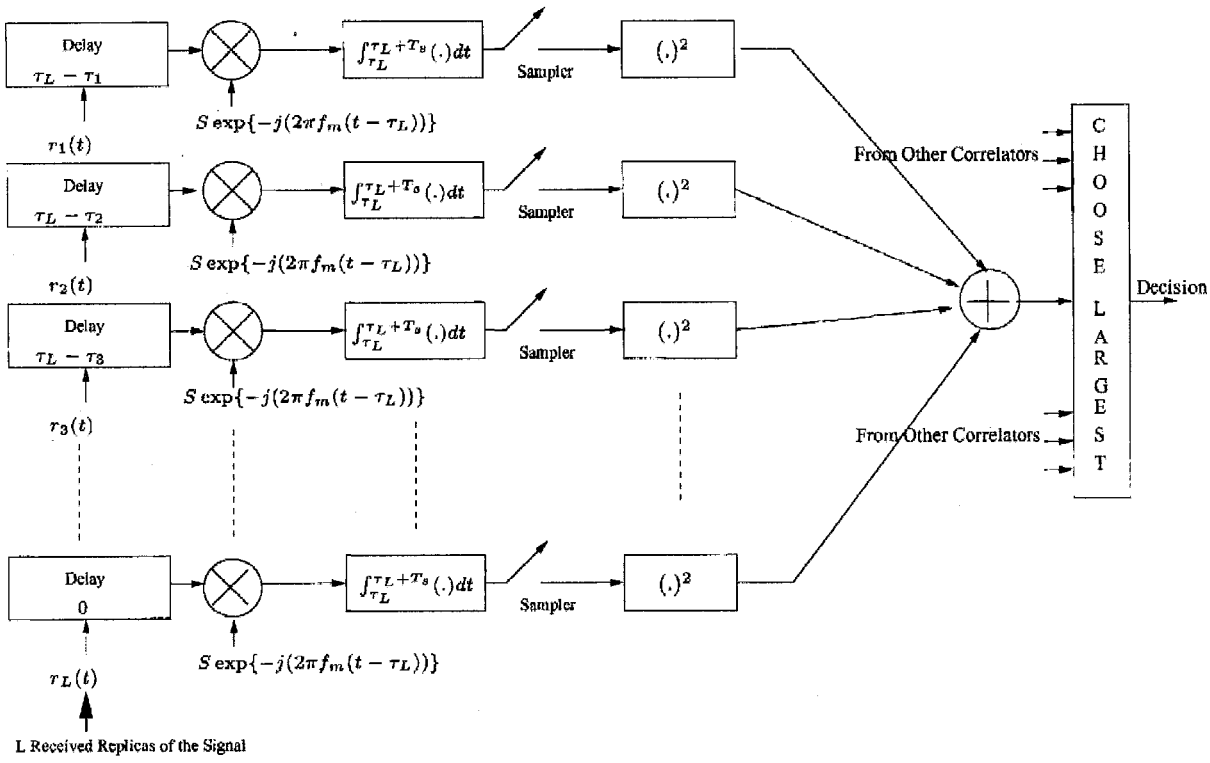

Figure 6.3: Noncoherent postdetection equal-gain combining receiver structure.

on the squared envelope (i.e., square-law detection). Using EGC the L decision outputs $\{r_{m,l}\}_{l=1}^{L}$ are summed to form the final decision variable r_m

$$r_m = \sum_{l=1}^{L} r_{m,l}; \qquad m = 1, 2, \cdots, M. \tag{6.2}$$

Last of all the receiver selects the symbol corresponding to the maximum decision variable, as shown in Figs. 6.2 and 6.3.

For equally-likely transmitted symbols, the total conditional SNR per bit, γ_t, at the output of the postdetection EGC combiner, is given by [1, p. 300, Eqn. (4.4.11)] and [1, p. 300, Eqn. (4.4.17)] as

$$\gamma_t = \sum_{l=1}^{L} \gamma_l. \tag{6.3}$$

6.3 BER with Single Channel Reception ($L = 1$)

6.3.1 Desired Representation of the Conditional BER

A generic expression for the BER of differentially coherent and noncoherent modulations, $P_b(\gamma; a, b, \eta)$, over AWGN is given by [1, Eqn. (4B.21)]

$$P_b(\gamma; a, b, \eta) = Q_1\left(a\sqrt{\gamma}, b\sqrt{\gamma}\right) - \frac{\eta}{1+\eta} \exp\left[-\frac{\left(a^2+b^2\right)\gamma}{2}\right] I_0\left(ab\gamma\right), \tag{6.4}$$

where γ is the SNR per bit, and $Q_1(\cdot,\cdot)$ is the first order Marcum Q-function traditionally defined by

$$Q_1(u, w) = \int_w^\infty x \exp\left[-\left(\frac{x^2+u^2}{2}\right)\right] I_0(ux)\, dx. \tag{6.5}$$

In (6.4) the parameters a and b are modulation-dependent and are defined in [1, Eqn. (4B.22)], and $\eta = v_2/v_1$, with the parameters v_1, v_2 defined in [1, Eqn. (4B.6)]. A number of special cases are of particular importance. For noncoherent detection of equal energy, equiprobable, correlated binary signals, $\eta = 1$ and

$$\begin{aligned} a &= \left(\frac{1-\sqrt{1-|\rho|^2}}{2}\right)^{1/2} \\ b &= \left(\frac{1+\sqrt{1-|\rho|^2}}{2}\right)^{1/2}, \end{aligned} \tag{6.6}$$

where $0 \le \rho \le 1$ is the complex-valued cross-correlation coefficient between the two signals, and in this case (6.4) reduces to [1, Eqn. (4.3.15)]. The special case $\rho = 0$ corresponds to orthogonal binary

FSK for which $a = 0$ and $b = 1$. Note that using the relation [91, Eqn. (9)]

$$Q_1(0, w) = e^{-w^2/2} \tag{6.7}$$

along with $I_0(0) = 1$, we see that (6.4) reduces in this particular case to the well-known expression reported by Proakis in [1, Eqn. (4.3.19)], namely,

$$P_b(\gamma; 0, 1, 1) = \frac{1}{2}\, e^{-\gamma/2}. \tag{6.8}$$

Furthermore, in the case of binary DPSK, $a = 0$, $b = \sqrt{2}$, and $\eta = 1$, whereupon using again (6.7) along with $I_0(0) = 1$, we see that (6.4) reduces to [1, Eqn. (4.2.117)]

$$P_b(\gamma; 0, \sqrt{2}, 1) = \frac{1}{2}\, e^{-\gamma}. \tag{6.9}$$

Finally $a = \sqrt{2 - \sqrt{2}}$, $b = \sqrt{2 + \sqrt{2}}$, and $\eta = 1$ correspond to DQPSK with Gray coding and in this case (6.4) reduces to [1, Eqn. (4.2.118)].

To evaluate the average BER one must average the BER expression (6.4) (considered to be the conditional BER) over the statistics of the fading. Since the second argument of the function (which is proportional to the square-root of the SNR) appears in the lower limit of the integral in the traditional definition of the Marcum Q-function (6.5), it is analytically difficult to perform such averages. We now introduce an alternate form of the Marcum Q-function which leads to a desirable representation of the conditional BER. We then show in the next section how this representation circumvents the difficulty of averaging over the fading distribution.

In virtually all applications of (6.4) to communication system performance analysis, the parameters a and b are typically independent of SNR and furthermore $b > a$. Let us introduce the parameter $\beta = \frac{a}{b}$ which depends on the particular application, e.g., noncoherent detection of nonorthogonal signals, differential detection of PSK signals, etc., but is independent of SNR. The alternate integral form of the Marcum Q-function was presented in [90]. The goal of this alternate representation was to have finite integration limits and an integrand with an exponential behavior in the argument w or u. In particular, it was shown in [89, Eqns. (C-26) and (C-27)] and in [90, Eqns. (8) and (11)] that the first order Marcum Q-function is given by

$$\begin{aligned} Q_1(u, w) &= \frac{1}{2\pi} \int_{-\pi}^{\pi} \frac{1 + \beta \sin\phi}{1 + 2\beta \sin\phi + \beta^2} \exp\left[-\frac{w^2}{2}\left(1 + 2\beta \sin\phi + \beta^2\right)\right] d\phi; \quad 0 \le \beta = \frac{u}{w} < 1, \\ Q_1(u, w) &= 1 + \frac{1}{2\pi} \int_{-\pi}^{\pi} \frac{\beta^2 + \beta \sin\phi}{1 + 2\beta \sin\phi + \beta^2} \exp\left[-\frac{u^2}{2}\left(1 + 2\beta \sin\phi + \beta^2\right)\right] d\phi; \quad 0 \le \beta = \frac{w}{u} < 1. \end{aligned} \tag{6.10}$$

Furthermore, using the integral representation of the 0th order modified Bessel function of the first kind [53], namely,

$$I_0(x) = \frac{1}{2\pi} \int_{-\pi}^{\pi} e^{-x \sin\phi}\, d\phi, \tag{6.11}$$

it is straightforward to show that

$$\exp\left(-\frac{u^2+w^2}{2}\right) I_0(uw) = \frac{1}{2\pi} \int_{-\pi}^{\pi} \exp\left[-\frac{w^2}{2}\left(1 + 2\beta \sin\phi + \beta^2\right)\right] d\phi; \quad \beta = \frac{u}{w}. \tag{6.12}$$

Substituting (6.10) and (6.12) in (6.4), the conditional BER (6.4) can be put in the desired representation given by

$$P_b(\gamma; a, b, \eta) = \frac{1}{2\pi(1+\eta)} \int_{-\pi}^{\pi} \frac{1 - \eta\beta^2 + \beta(1-\eta)\sin\phi}{1 + 2\beta\sin\phi + \beta^2} \exp\left[-\frac{b^2\gamma}{2}\left(1 + 2\beta\sin\phi + \beta^2\right)\right] d\phi; \quad 0 \le \beta = \frac{a}{b} < 1. \tag{6.13}$$

This form of the conditional BER (6.13) is more desirable since we can first integrate over a statistical distribution for γ and then perform the integral over ϕ, as described in more detail below. It should be noted that the specific form of the result in (6.13) with $\eta = 1$ can be obtained via the work of Pawula [92] who used certain relations between the Marcum Q-function and the Rice I_e-function, which is defined by

$$I_e(k, x) = \int_0^x I_0(kt)\, e^{-t}\, dt. \tag{6.14}$$

In particular, combining Eqns. (2a) and (2d) of Pawula [92] and making the substitutions $U = (b+a)/2$, $W = (b-a)/2$, and $V^2 = U^2 - W^2 = ab$ in these same equations, one arrives at the result

$$P_b(\gamma; a, b, 1) = \frac{1}{2\pi} \int_0^{\pi} \frac{1 - \beta^2}{1 - 2\beta\cos\phi + \beta^2} \exp\left[-\frac{b^2\gamma}{2}\left(1 + 2\beta\cos\phi + \beta^2\right)\right] d\phi; \quad 0 \le \beta = \frac{a}{b} < 1, \tag{6.15}$$

which in view of the symmetry properties of the trigonometric functions over the interval $[-\pi, 0]$ and $[0, \pi]$ can be shown to be identically equivalent to (6.13) with $\eta = 1$. Also as a check, again setting $\eta = 1$, $a = 0$ and $b = 1$ ($b = \sqrt{2}$) in (6.13), it is straightforward to see that (6.13) reduces to (6.8) ((6.9)) for orthogonal binary FSK (binary DPSK). Another special case of interest is DQPSK where $a = \sqrt{2 - \sqrt{2}}$ and $b = \sqrt{2 + \sqrt{2}}$. In this particular case making the change of variable $\phi' = \phi + \pi/2$ in (6.13) and using the symmetry properties of the cosine function over the interval $[-\pi, 0]$ and $[0, \pi]$, it can be shown that (6.13) reduces to the expression reported in [88, Eqn. (3)], namely,

$$P_b\left(\gamma; \sqrt{2-\sqrt{2}}, \sqrt{2+\sqrt{2}}, 1\right) = \frac{1}{2\pi} \int_0^{\pi} \frac{\exp\left(-(2 - \sqrt{2}\cos\phi)\gamma\right)}{\sqrt{2} - \cos\phi}\, d\phi. \tag{6.16}$$

6.3.2 Average BER

Recall that the conditional BER, conditioned on the SNR per bit γ, is given by (6.13). Since the fading is assumed to be independent of the AWGN, the unconditional BER, $\overline{P}_b(\overline{\gamma}, i; a, b, \eta)$, is obtained by averaging (6.13) over the underlying fading RV giving

$$\overline{P}_b(\overline{\gamma}, i; a, b, \eta) = \int_0^\infty P_b(\gamma; a, b, \eta)\, p_\gamma(\gamma; \overline{\gamma}, i)\, d\gamma, \tag{6.17}$$

where i is the fading parameter associated with the distribution $p_\gamma(\gamma; \overline{\gamma}, i)$, and is hence denoted by r, q, n, m, σ, $m\sigma$, and $AK\sigma$ for the Rayleigh, Nakagami-q (Hoyt), Nakagami-n (Rice), Nakagami-m, log-normal shadowing, composite multipath/shadowing, and combined (time-shared) shadowed/unshadowed PDFs, respectively. Substituting (6.13) into (6.17) then interchanging the order of integration yields

$$\overline{P}_b(\overline{\gamma}, i; a, b, \eta) = \frac{1}{2\pi(1+\eta)} \int_{-\pi}^{\pi} \frac{1 - \eta\beta^2 + \beta(1-\eta)\sin\phi}{1 + 2\beta\sin\phi + \beta^2}\, \mathcal{J}_i(\overline{\gamma}, i; a, b; \phi)\, d\phi; \quad 0 \le \beta = \frac{a}{b} < 1, \tag{6.18}$$

where

$$\mathcal{J}_i(\overline{\gamma}, i; a, b; \phi) \triangleq \int_0^\infty \exp\left[-\frac{b^2\gamma}{2}\left(1 + 2\beta\sin\phi + \beta^2\right)\right]\, p_\gamma(\gamma; \overline{\gamma}, i)\, d\gamma \tag{6.19}$$

is in the form of a Laplace transform. The form of the average BER in (6.18) is interesting in that the integrals $\mathcal{J}_i(\overline{\gamma}, i; a, b; \phi)$ can either be obtained in closed-form with the help of classical Laplace transforms or can alternatively be efficiently computed by using Gauss-Hermite quadrature integration [70, p. 890, Eqn. (25.4.46)] for all fading channel models described in Chapter 2. We now evaluate these integrals for each of the fading models described in Section 6.2.2. These integrals will also be useful to obtain the average BER with multichannel reception as described in Section 6.4.3.

Multipath Fading

Rayleigh Fading Substituting (2.4) into (6.19) then using the Laplace transform [53, Eqn. (1), p. 1178]

$$\int_0^\infty e^{-sx}\, dx = \frac{1}{s}; \qquad s > 0 \tag{6.20}$$

yields [1]

$$\mathcal{J}_r(\overline{\gamma}; a, b; \phi) = \left(1 + \frac{b^2\overline{\gamma}}{2}\left(1 + 2\beta\sin\phi + \beta^2\right)\right)^{-1}. \tag{6.21}$$

Inserting (6.21) in (6.18) we obtain the average BER performance over Rayleigh fading. For the special case of $\eta = 1$ one can proceed further to obtain a closed form expression for the average BER. Performing a partial fraction expansion on (6.18) with (6.21), then using the standard integral

[1] Note that for the Rayleigh fading case, the PDF has no dependency on the fading parameter, r. Hence, for simplicity of notations we omit it in the argument sequence of the function $\mathcal{J}_r(\cdot;\cdot,\cdot;\cdot)$.

identity [53, Eqn. (3.661.4), p. 425]

$$\int_{-\pi}^{\pi} \frac{1}{u - w\sin\phi}\, d\phi = 2\int_{0}^{\pi} \frac{1}{u + w\cos\phi}\, d\phi = \frac{2\pi}{\sqrt{u^2 - w^2}}; \qquad u \geq |w| \tag{6.22}$$

it can be shown that the average BER in Rayleigh fading is given by

$$\overline{P}_b(\overline{\gamma}, r; a, b, 1) = \frac{1}{2}\left[1 - \frac{(1-\beta^2)\, b^2\, \overline{\gamma}}{2\sqrt{1 + b^2\,\overline{\gamma}\,(1+\beta^2) + \left(\frac{b^2\,\overline{\gamma}}{2}\right)^2 (1-\beta^2)^2}}\right]; \quad 0 \leq \beta = \frac{a}{b} < 1. \tag{6.23}$$

Letting $a = 0$ and $b = 1$ in (6.23), it easy to see that $\overline{P}_b$ checks, as expected, with the expression reported by Proakis in [1, Eqn. (7.3.12), p. 718], namely,

$$\overline{P}_b(\overline{\gamma}, r; 0, 1, 1) = \frac{1}{2 + \overline{\gamma}}, \tag{6.24}$$

for orthogonal binary FSK. Similarly letting $a = 0$ and $b = \sqrt{2}$ in (6.23), it is easy to see that $\overline{P}_b$ checks, as expected, with the expression reported by Proakis in [1, Eqn. (7.3.10), p. 717], namely,

$$\overline{P}_b(\overline{\gamma}, r; 0, \sqrt{2}, 1) = \frac{1}{2(1 + \overline{\gamma})}, \tag{6.25}$$

for binary DPSK. Another special case of interest is that for $a = \sqrt{2 - \sqrt{2}}$ and $b = \sqrt{2 + \sqrt{2}}$. In this case, (6.23) reduces to

$$\overline{P}_b\left(\overline{\gamma}, r; \sqrt{2-\sqrt{2}}, \sqrt{2+\sqrt{2}}, 1\right) = \frac{1}{2}\left[1 - \frac{1}{\sqrt{\frac{(1+2\,\overline{\gamma})^2}{2\,\overline{\gamma}^2} - 1}}\right], \tag{6.26}$$

which is equivalent to the expression of $\overline{P}_b$ for DQPSK with Gray coding reported in [86, Eqn. (18)], [87, Eqn. (13)], namely,

$$\overline{P}_b\left(\overline{\gamma}, r; \sqrt{2-\sqrt{2}}, \sqrt{2+\sqrt{2}}, 1\right) = \frac{1}{2\sqrt{1 + 4\overline{\gamma} + 2\overline{\gamma}^2}} \frac{\sqrt{2}\,\overline{\gamma} + (\sqrt{2}-1)\left(1 + 2\overline{\gamma} - \sqrt{1 + 4\overline{\gamma} + 2\overline{\gamma}^2}\right)}{\sqrt{2}\,\overline{\gamma} - (\sqrt{2}-1)\left(1 + 2\overline{\gamma} - \sqrt{1 + 4\overline{\gamma} + 2\overline{\gamma}^2}\right)}, \tag{6.27}$$

or the one reported in [88, Eqn. (8)], namely,

$$\overline{P}_b\left(\overline{\gamma}, r; \sqrt{2-\sqrt{2}}, \sqrt{2+\sqrt{2}}, 1\right) = \frac{1}{2}\left(1 - \frac{\sqrt{2}\,\overline{\gamma}}{\sqrt{1 + 4\overline{\gamma} + 2\overline{\gamma}^2}}\right). \tag{6.28}$$

Nakagami-q (Hoyt) Fading Substituting (2.7) into (6.19) then using the Laplace transform [53, Eqn. (109), p. 1182]

$$\int_0^\infty I_0(ux)\, e^{-sx}\, dx = \left(s^2 - u^2\right)^{-1/2}; \qquad s > |u| \geq 0 \tag{6.29}$$

yields

$$\mathcal{J}_q(\overline{\gamma}, q; a, b; \phi) = \left(1 + b^2\, \overline{\gamma}\, \left(1 + 2\, \beta \sin\phi + \beta^2\right) + \frac{q^2\, b^4\, \overline{\gamma}^2}{(1+q^2)^2}\, (1 + 2\, \beta \sin\phi + \beta^2)^2\right)^{-1/2}. \tag{6.30}$$

For $q = 0$, (6.30) becomes

$$\mathcal{J}_q(\overline{\gamma}, 0; a, b; \phi) = \left(1 + b^2\, \overline{\gamma}\, \left(1 - 2\, \beta \sin\phi + \beta^2\right)\right)^{-1/2}, \tag{6.31}$$

which when inserted in (6.18) gives the BER performance over one-sided Gaussian fading. On the other hand, letting $q = 1$ in (6.30), it is easy to show that $\mathcal{J}_q(\overline{\gamma}, 1; a, b; \phi)$ reduces to $\mathcal{J}_r(\overline{\gamma}; a, b; \phi)$ as given by (6.21) and which corresponds to the Rayleigh fading case, as expected.

Letting $a = 0$ and $b = 1$ ($b = \sqrt{2}$) in (6.30) yields the average BER performance of orthogonal binary FSK (DPSK) over a Nakagami-q (Hoyt) fading channel as

$$\overline{P}_b(\overline{\gamma}, q; 0, \sqrt{2g}, 1) = \frac{1}{2}\, \left(1 + 2\, g\, \overline{\gamma} + \frac{4\, q^2\, g^2\, \overline{\gamma}^2}{(1+q^2)^2}\right)^{-1/2}, \tag{6.32}$$

where $g = 1/2$ for orthogonal binary FSK and $g = 1$ for DPSK.

Nakagami-n (Rice) Fading Substituting (2.11) into (6.19) then using the Laplace transform [70, Eqn. (29.3.81), p. 1026]

$$\int_0^\infty I_0(u\sqrt{x})\, e^{-sx}\, dx = \frac{e^{u^2/(4s)}}{s}; \qquad s > 0 \tag{6.33}$$

yields

$$\mathcal{J}_n(\overline{\gamma}, n; a, b; \phi) = \frac{2\, (1+n^2)}{2\, (1+n^2) + b^2\, \overline{\gamma}\, (1 + 2\, \beta \sin\phi + \beta^2)}\, \exp\left[-\frac{n^2\, b^2\, \overline{\gamma}\, (1 + 2\, \beta \sin\phi + \beta^2)}{2\, (1+n^2) + b^2\, \overline{\gamma}\, (1 + 2\, \beta \sin\phi + \beta^2)}\right]. \tag{6.34}$$

For $n = 0$, (6.34) reduces, as expected, to $\mathcal{J}_r(\overline{\gamma}; a, b; \phi)$ as given by (6.21), corresponding to the Rayleigh fading case. Furthermore, as $n \longrightarrow +\infty$,

$$\mathcal{J}_n(\overline{\gamma}, n; a, b; \phi) \longrightarrow \exp\left[-\frac{b^2\overline{\gamma}}{2}\left(1 + 2\beta \sin\phi + \beta^2\right)\right],$$

which when substituted in (6.18) yields, as expected, the BER performance over the nonfading (i.e., AWGN) channel as given by (6.13).

Letting $a = 0$ and $b = 1$ ($b = \sqrt{2}$) in (6.34) yields the average BER performance of orthogonal binary FSK (DPSK) over a Nakagami-n (Rice) fading channel as

$$\overline{P}_b(\overline{\gamma}, n; 0, \sqrt{2g}, 1) = \frac{1+n^2}{2(1+n^2+g\overline{\gamma})} \exp\left(-\frac{n^2\, g\, \overline{\gamma}}{1+n^2+g\overline{\gamma}}\right), \tag{6.35}$$

where $g = 1/2$ for orthogonal binary FSK and $g = 1$ for DPSK. Further setting $a = \sqrt{2-\sqrt{2}}$ and $b = \sqrt{2+\sqrt{2}}$, it can be easily shown that $\overline{P}_b(\overline{\gamma}, n; \sqrt{2-\sqrt{2}}, \sqrt{2+\sqrt{2}}, 1)$ is equivalent to the expression for DQPSK with Gray coding given in [88, Eqn. (6)], namely,

$$\overline{P}_b\left(\overline{\gamma}, n; \sqrt{2-\sqrt{2}}, \sqrt{2+\sqrt{2}}, 1\right) = \frac{(1+n^2)\, e^{-n^2}}{2\pi} \int_0^{\pi} \frac{\exp\left(\frac{n^2(1+n^2)}{1+n^2+2\overline{\gamma}-\sqrt{2}\overline{\gamma}\cos\phi}\right)}{(\sqrt{2}-\cos\phi)\,(1+n^2+2\overline{\gamma}-\sqrt{2}\overline{\gamma}\cos\phi)}\, d\phi. \tag{6.36}$$

Nakagami-m Fading Substituting (2.15) into (6.19) then using the Laplace transform [53, Eqn. (3), p. 1178]

$$\int_0^{\infty} x^{\nu} e^{-sx}\, dx = \frac{\Gamma(\nu+1)}{s^{\nu+1}}; \qquad s > 0,\ \nu > -1 \tag{6.37}$$

yields

$$\mathcal{J}_m(\overline{\gamma}, m; a, b; \phi) = \left[1 + \frac{b^2\, \overline{\gamma}}{2\, m}\, (1 - 2\,\beta \sin\phi + \beta^2)\right]^{-m}. \tag{6.38}$$

Note that for $m = 1/2$, $\mathcal{J}_m(\overline{\gamma}, 1/2; a, b; \phi) = \mathcal{J}_q(\overline{\gamma}, 0; a, b; \phi)$ which corresponds to the case of one-sided Gaussian fading. Further, for $m = 1$, $\mathcal{J}_m(\overline{\gamma}, 1/2; a, b; \phi) = \mathcal{J}_r(\overline{\gamma}; a, b; \phi)$ which corresponds to the Rayleigh fading case. Finally, as $m \to +\infty$, accounting for the identity

$$\lim_{m \to +\infty} \left(1 + \frac{h}{m}\right)^{-m} = e^{-h},$$

we see that

$$\mathcal{J}_m(\overline{\gamma}, m; a, b; \phi) \longrightarrow \exp\left[-\frac{b^2\overline{\gamma}}{2}\left(1 + 2\beta\sin\phi + \beta^2\right)\right],$$

which when substituted in (6.18) yields, as expected, the BER performance over the nonfading (i.e., AWGN) channel as given by (6.13).

For the special case of $\eta = 1$ and m restricted to positive integers values, one can proceed further to obtain a closed form expression for the average BER. Performing a partial fraction expansion on (6.18) with (6.38), then using the standard integral identity [53, Eqn. (3.661.4), p. 425]

$$\int_{-\pi}^{\pi} \frac{1}{(u - w\sin\phi)^{k+1}}\, d\phi = 2\int_0^{\pi} \frac{1}{(u + w\cos\phi)^{k+1}}\, d\phi = \frac{2\pi}{(u^2 - w^2)^{\frac{k+1}{2}}}\, \mathcal{P}_k\left(\frac{u}{\sqrt{u^2 - w^2}}\right); \qquad u \geq |w|, \tag{6.39}$$

where $\mathcal{P}_k(\cdot)$ is the Legendre polynomial of order k [53, Eqn. (8.911.1), p. 1044], it can be shown

that the average BER in Nakagami-m fading is given by

$$\overline{P}_b(\overline{\gamma}, m; a, b, 1) = \frac{1}{2}\left[1 + \sum_{k=1}^{m} \frac{(1-\beta^2)\, C_k}{\left[1 + \frac{b^2\overline{\gamma}}{m}(1+\beta^2) + \left(\frac{b^2\overline{\gamma}}{2m}\right)^2 (1-\beta^2)^2\right]^{k/2}} \mathcal{P}_{k-1}\left(\frac{1 + \frac{b^2\,\overline{\gamma}}{2\,m}\,(1+\beta^2)}{\left(1 + \frac{b^2\overline{\gamma}}{m}(1+\beta^2) + \left(\frac{b^2\overline{\gamma}}{2m}\right)^2 (1-\beta^2)^2\right)^{1/2}}\right)\right], \tag{6.40}$$

where

$$\begin{aligned} C_m &= -\frac{b^2\,\overline{\gamma}}{2\,m} \\ C_k &= \frac{1}{(m-k)!}\,\frac{d^{m-k}}{du^{m-k}}\left[\frac{1}{\left(1+\beta^2+\frac{2\,m}{b^2\,\overline{\gamma}}\,u\right)\,\left(1+\frac{b^2\,\overline{\gamma}}{2\,m}(1+\beta^2)+u\right)^m}\right]_{u=-1-\frac{b^2\,\overline{\gamma}}{2\,m}(1+\beta^2)}; k = 1, \cdots, m-1 \end{aligned} \tag{6.41}$$

Note that when $m = 1$, which corresponds to Rayleigh fading, (6.40) reduces to (6.23) since $\mathcal{P}_0(x) = 1$.

Letting $a = 0$ and $b = 1$ ($b = \sqrt{2}$) in (6.38), it is easy to see that $\overline{P}_b$ checks, as expected, with the expression attributed to Barrow [93] and reported in [52, Eqn. (11)] and in [94, Eqn. (B1)] for orthogonal binary FSK (binary DPSK), namely,

$$\overline{P}_b(\overline{\gamma}, m; 0, \sqrt{2g}, 1) = \frac{1}{2}\left(\frac{m}{m + g\overline{\gamma}}\right)^m, \tag{6.42}$$

$g = 1/2$ for orthogonal binary FSK and $g = 1$ for DPSK. The other special case of interest is that for $a = \sqrt{2-\sqrt{2}}$ and $b = \sqrt{2+\sqrt{2}}$. In this case, it can be easily shown that $\overline{P}_b(\overline{\gamma}, m; \sqrt{2-\sqrt{2}}, \sqrt{2+\sqrt{2}}, 1)$ is equivalent to the expression for DQPSK with Gray coding given in [88, Eqn. (7)], namely,

$$\overline{P}_b\left(\overline{\gamma}, m; \sqrt{2-\sqrt{2}}, \sqrt{2+\sqrt{2}}, 1\right) = \frac{1}{2\pi}\left(\frac{m}{m+2\overline{\gamma}}\right)^m \int_0^{\pi} \frac{1}{(\sqrt{2}-\cos\phi)\,\left(1-\frac{\sqrt{2}\overline{\gamma}}{m+2\overline{\gamma}}\cos\phi\right)^m}\, d\phi. \tag{6.43}$$

Log-normal Shadowing

If the channel statistics follow a log-normal distribution, it is straightforward to show that $\mathcal{J}_\sigma(\mu, \sigma; a, b; \phi)$, can be accurately approximated by Gauss-Hermite integration yielding

$$\mathcal{J}_\sigma(\mu, \sigma; a, b; \phi) \simeq \frac{1}{\sqrt{\pi}} \sum_{n=1}^{N_p} H_{x_n} \exp\left(-\frac{b^2\;\; 10^{(\sqrt{2}\;\sigma\;x_n+\mu)/10}}{1 + 2\beta\sin\phi + \beta^2}\right), \tag{6.44}$$

where N_p is the order of the Hermite polynomial, $H_{N_p}(.)$. Setting N_p to 20 is typically sufficient for excellent accuracy. In (6.44) x_n are the zeros of the N_p-order Hermite polynomial, and H_{x_n} are the

weight factors of the N_p-order Hermite polynomial and are given by

$$H_{x_n} = \frac{2^{N_p-1}\, N_p!\, \sqrt{\pi}}{N_p^2\, H_{N_p-1}^2(x_n)}. \tag{6.45}$$

Both the zeros and the weights factors of the Hermite polynomial are tabulated in [70, Table (25.10), p. 924] for various polynomial orders N_p.

Composite Multipath/Shadowing

If the channel statistics follow a gamma/log-normal distribution, it is straightforward to show that $\mathcal{J}_{m\sigma}(\mu, m\sigma; a, b; \phi)$ can be accurately evaluated by using (6.37) followed by a Gauss-Hermite integration yielding

$$\mathcal{J}_{m\sigma}(\mu, m\sigma; a, b; \phi) \simeq \frac{1}{\sqrt{\pi}} \sum_{n=1}^{N_p} H_{x_n} \left(1 + \frac{b^2\, 10^{(\sqrt{2}\,\sigma\, x_n + \mu)/10}}{m\,(1 + 2\beta \sin\phi + \beta^2)}\right)^{-m}. \tag{6.46}$$

Combined (Time-Shared) Shadowed/Unshadowed

If the channel statistics follow a combined Lutz *et al.* distribution, it is straightforward to show that $\mathcal{J}_{AK\sigma}(\overline{\gamma}^u, \mu^s, K, \sigma; a, b; \phi)$ can be broken into two terms, one which can be evaluated in closed-form and the other which can be accurately approximated by Gauss-Hermite integration yielding

$$\mathcal{J}_{AK\sigma}(\overline{\gamma}^u, \mu^s, K, \sigma; a, b; \phi) \simeq (1 - A)\, \mathcal{J}_n(\overline{\gamma}^u, \sqrt{K}; a, b; \phi) + A\, \mathcal{J}_{m\sigma}(\mu^s, m\sigma; a, b; \phi), \tag{6.47}$$

with $n = \sqrt{K}$ in $\mathcal{J}_n(\overline{\gamma}^u, n; a, b; \phi)$ and $m = 1$ in $\mathcal{J}_{m\sigma}(\mu^s, m\sigma; a, b; \phi)$.

6.4 BER with Multichannel Reception ($L > 1$)

6.4.1 Desired Product Form Representation of the Conditional BER (General Case)

Many problems dealing with the BER performance of multichannel reception of differentially coherent and noncoherent detection of PSK and FSK signals in AWGN channels have a decision variable which is a quadratic form in complex-valued Gaussian random variables. Almost three decades ago, Proakis [82] developed a general expression for evaluating the BER when the decision variable is in that particular form. Indeed the development and results originally obtained in [82] later appeared as Appendix 4B of [1] and have become a classic in the annals of communication system performance literature. The most general form of the BER expression, i.e., [1, Eqn. (4B.21)] obtained by Proakis was given in terms of the first order Marcum Q-function and modified Bessel functions of the first

kind. Although implied but not explicitly given in [82, 1], this general form can be rewritten in terms of the generalized Marcum Q-function, $Q_l(.,.)$, as:

$$\begin{aligned} P_b(L,\gamma_t;a,b,\eta) &= Q_1\left(a\sqrt{\gamma_t},b\sqrt{\gamma_t}\right) - \left[1-\frac{\sum_{l=0}^{L-1}\binom{2L-1}{l}\eta^l}{(1+\eta)^{2L-1}}\right]\exp\left[-\frac{\left(a^2+b^2\right)\gamma_t}{2}\right] I_0\left(ab\gamma_t\right) \\ &+ \frac{1}{(1+\eta)^{2L-1}}\left[\sum_{l=2}^{L}\binom{2L-1}{L-l}\eta^{L-l}\left[Q_l(a\sqrt{\gamma_t},b\sqrt{\gamma_t})-Q_1(a\sqrt{\gamma_t},b\sqrt{\gamma_t})\right]\right] \\ &- \frac{1}{(1+\eta)^{2L-1}}\left[\sum_{l=2}^{L}\binom{2L-1}{L-l}\eta^{L-1+l}\left[Q_l(b\sqrt{\gamma_t},a\sqrt{\gamma_t})-Q_1(b\sqrt{\gamma_t},a\sqrt{\gamma_t})\right]\right] \end{aligned} \tag{6.48}$$

where $\binom{2L-1}{L-l} = \frac{(2L-1)!}{(L-l)!\,(L+l-1)!}$ denotes the binomial coefficient, and where all the modulation-dependent parameters have already been defined previously. As a check for $L=1$, the latter two summations in (6.48) do not contribute and hence one immediately obtains the result (6.4), as expected. Note that although the form in (6.48) does not give the appearance of being much simpler than [1, Eqn. (4B.21)], we shall see shortly that it does have particular advantage for obtaining the average BER performance over generalized fading channels.

As in the single channel reception case the parameters a and b in (6.48) are typically independent of SNR and furthermore $b > a$. Let us introduce again the modulation dependent parameter $\beta = \frac{a}{b}$ which is independent of SNR. With this in mind, we now show how the alternate integral representation of the generalized Marcum Q-function yields a desired product form representation of the conditional BER. In particular, it was shown in [89] or equivalently in [90, Eqns. (7) and (10)] that

$$\begin{aligned} Q_l(u,w) &= \frac{1}{2\pi}\int_{-\pi}^{\pi}\frac{(-1)^{\frac{l-1}{2}}\,\beta^{-l+1}\left[\cos(l-1)\phi+\beta\sin l\phi\right]}{1+2\beta\sin\phi+\beta^2}\exp\left[-\frac{w^2}{2}\left(1+2\beta\sin\phi+\beta^2\right)\right]d\phi; \\ &\qquad 0^+ \le \beta = \frac{u}{w} < 1, \qquad l \text{ odd}, \\ Q_l(u,w) &= \frac{1}{2\pi}\int_{-\pi}^{\pi}\frac{(-1)^{\frac{l}{2}}\,\beta^{-l+1}\left[\sin(l-1)\phi-\beta\cos l\phi\right]}{1+2\beta\sin\phi+\beta^2}\exp\left[-\frac{w^2}{2}\left(1+2\beta\sin\phi+\beta^2\right)\right]d\phi; \\ &\qquad 0^+ \le \beta = \frac{u}{w} < 1, \qquad l \text{ even}, \\ Q_l(u,w) &= 1+\frac{1}{2\pi}\int_{-\pi}^{\pi}\frac{(-1)^{\frac{l-1}{2}}\,\beta^{l}\left[\sin l\phi+\beta\cos(l-1)\phi\right]}{1+2\beta\sin\phi+\beta^2}\exp\left[-\frac{u^2}{2}\left(1+2\beta\sin\phi+\beta^2\right)\right]d\phi; \\ &\qquad 0 \le \beta = \frac{w}{u} < 1, \qquad l \text{ odd}, \\ Q_l(u,w) &= 1-\frac{1}{2\pi}\int_{-\pi}^{\pi}\frac{(-1)^{\frac{l}{2}}\,\beta^{l}\left[\cos l\phi-\beta\sin(l-1)\phi\right]}{1+2\beta\sin\phi+\beta^2}\exp\left[-\frac{u^2}{2}\left(1+2\beta\sin\phi+\beta^2\right)\right]d\phi; \\ &\qquad 0 \le \beta = \frac{w}{u} < 1, \qquad l \text{ even}, \end{aligned} \tag{6.49}$$

with the special case of $l=1$ being given in (6.10). Now, using (6.10), (6.12), and (6.49) in (6.48), it can be shown after tedious manipulations that *the entire conditional BER expression (6.48) can*

be written as a single integral with an integrand that contains a single exponential factor in γ_t of the form $\exp\left[-\frac{b^2\gamma_t}{2}\left(1+2\beta\sin\phi+\beta^2\right)\right]$, namely,

$$P_b(L,\gamma_t;a,b,\eta)=\frac{\eta^L}{2\pi(1+\eta)^{2L-1}}\int_{-\pi}^{\pi}\frac{f(L;\beta,\eta;\phi)}{1+2\beta\sin\phi+\beta^2}\exp\left[-\frac{b^2\gamma_t}{2}\left(1+2\beta\sin\phi+\beta^2\right)\right]d\phi;\quad 0^+\le\beta=\frac{a}{b}<1, \tag{6.50}$$

where

$$f(L;\beta,\eta;\phi)=f_0(L;\beta,\eta;\phi)+f_1(L;\beta,\eta;\phi)+f_2(L;\beta,\eta;\phi),$$

with

$$\begin{aligned}
f_0(L;\beta,\eta;\phi)&=\left[-\frac{(1+\eta)^{2L-1}}{\eta^L}+\sum_{l=1}^{L}\binom{2L-1}{L-l}(\eta^{-l}+\eta^{l-1})\right]\beta(\beta+\sin\phi),\\
f_1(L;\beta,\eta;\phi)&=\sum_{\substack{l=1\\ l\text{ odd}}}^{L}\binom{2L-1}{L-l}(-1)^{\frac{l-1}{2}}\left[(\eta^{-l}\beta^{-l+1}-\eta^{l-1}\beta^{l+1})\cos((l-1)\phi)+(\eta^{-l}\beta^{-l+2}-\eta^{l-1}\beta^{l})\sin(l\phi)\right],\\
f_2(L;\beta,\eta;\phi)&=\sum_{\substack{l=2\\ l\text{ even}}}^{L}\binom{2L-1}{L-l}(-1)^{\frac{l}{2}}\left[(\eta^{-l}\beta^{-l+1}-\eta^{l-1}\beta^{l+1})\sin((l-1)\phi)-(\eta^{-l}\beta^{-l+2}-\eta^{l-1}\beta^{l})\cos(l\phi)\right].
\end{aligned} \tag{6.51}$$

As a check, for the special case of $L=1$, we obtain

$$\begin{aligned}
f_0(1;\beta,\eta;\phi)&=0,\\
f_1(1;\beta,\eta;\phi)&=\frac{1-\eta\beta^2+\beta(1-\eta)\sin\phi}{\eta},\\
f_2(1;\beta,\eta;\phi)&=0,
\end{aligned} \tag{6.52}$$

and hence (6.50) reduces to (6.13), as expected.

The form of the conditional BER in (6.50) has the advantage of being a single finite-range integral with limits independent of the conditional SNR and an integrand which can be written in a *product form*, such as

$$P_b(L,\gamma_t;a,b,\eta)=\frac{\eta^L}{2\pi(1+\eta)^{2L-1}}\int_{-\pi}^{\pi}\frac{f(L;\beta,\eta;\phi)}{1+2\beta\sin\phi+\beta^2}\prod_{l=1}^{L}\exp\left[-\frac{b^2\gamma_l}{2}\left(1+2\beta\sin\phi+\beta^2\right)\right]d\phi;\quad 0^+\le\beta=\frac{a}{b}<1. \tag{6.53}$$

Furthermore, the form of (6.53) is desirable since we can first independently average over the individual statistical distributions of the γ_l's, and then perform the integral over ϕ, as described in more detail below (Section 6.4.3). Before showing this, however, we first offer some simplifications of (6.48) and (6.50) for some special cases of interest.

6.4.2 Desired Product Form Representation of the Conditional BER (Special Case ($\eta = 1$))

For $\eta = 1$, and any $L \geq 1$, which corresponds to the case of multichannel detection of equal energy correlated binary signals, the conditional BER expression (6.48) becomes

$$\begin{aligned}
P_b(L,\gamma_t;a,b,1) &= Q_1\left(a\sqrt{\gamma_t}, b\sqrt{\gamma_t}\right) - \frac{1}{2}\exp\left[-\frac{\left(a^2+b^2\right)\gamma_t}{2}\right] I_0\left(ab\gamma_t\right) \\
&+ \frac{1}{2^{2L-1}}\left[\sum_{l=1}^{L}\binom{2L-1}{L-l}\right]\left[\left(Q_l\left(a\sqrt{\gamma_t}, b\sqrt{\gamma_t}\right) - Q_l\left(b\sqrt{\gamma_t}, a\sqrt{\gamma_t}\right)\right) - \left(Q_1\left(a\sqrt{\gamma_t}, b\sqrt{\gamma_t}\right) - Q_1\left(b\sqrt{\gamma_t}, a\sqrt{\gamma_t}\right)\right)\right] \\
&= Q_1\left(a\sqrt{\gamma_t}, b\sqrt{\gamma_t}\right) - \frac{1}{2}\exp\left(-\frac{\left(a^2+b^2\right)\gamma_t}{2}\right) I_0\left(ab\gamma_t\right) \\
&+ \frac{1}{2^{2L-1}}\sum_{l=1}^{L}\binom{2L-1}{L-l}\left[Q_l\left(a\sqrt{\gamma_t}, b\sqrt{\gamma_t}\right) - Q_l\left(b\sqrt{\gamma_t}, a\sqrt{\gamma_t}\right)\right] - \frac{1}{2}\left[Q_1\left(a\sqrt{\gamma_t}, b\sqrt{\gamma_t}\right) - Q_1\left(b\sqrt{\gamma_t}, a\sqrt{\gamma_t}\right)\right],
\end{aligned} \tag{6.5}$$

where we have added back the $l = 1$ term in the sums of (6.48) since they have zero value anyway. However, comparing Eqns. (40) and (42) of [95],

$$Q_1(u,w) - \frac{1}{2}\exp\left(-\frac{u^2+w^2}{2}\right) I_0\left(uw\right) = \frac{1}{2}\left[1 - Q_1\left(w,u\right) + Q_1\left(u,w\right)\right]. \tag{6.55}$$

Thus, combining (6.54) and (6.55) gives the simplified expression

$$P_b(L,\gamma_t;a,b,1) = \frac{1}{2} + \frac{1}{2^{2L-1}}\sum_{l=1}^{L}\binom{2L-1}{L-l}\left[Q_l\left(a\sqrt{\gamma_t}, b\sqrt{\gamma_t}\right) - Q_l\left(b\sqrt{\gamma_t}, a\sqrt{\gamma_t}\right)\right], \tag{6.56}$$

which appears not to be given in [82, 1]. Setting $a = 0$ and $b = 1$ ($b = \sqrt{2}$) in (6.56), then using the relations [91, Eqn. (9)]

$$\begin{aligned}
Q_l(0,w) &= e^{-w^2/2}\sum_{k=0}^{l-1}\frac{(w^2/2)^k}{k!}, \\
Q_l(u,0) &= 1,
\end{aligned}$$

along with the identity $\sum_{l=1}^{L}\binom{2L-1}{L-l} = 2^{2(L-1)}$, it can be shown that (6.56) reduces to the well-known expression reported by Proakis for multichannel binary orthogonal FSK (binary DPSK) given by [1, Eqn. (4.4.13), p. 301], namely,

$$P_b(L,\gamma_t;0,\sqrt{2g},1) = \frac{1}{2^{2L-1}}\, e^{-g\gamma_t}\sum_{l=0}^{L-1} c_l\,(g\gamma_t)^l, \tag{6.57}$$

where

$$c_l = \frac{1}{l!} \sum_{k=0}^{L-1-l} \binom{2L-1}{k},$$

$g = 1/2$ for orthogonal binary FSK, and $g = 1$ for binary DPSK. Note that an alternate (equivalent) form to (6.57), involving the confluent hypergeometric function, ${}_1F_1(\cdot;\cdot;\cdot)$, and given by Charash [4, Eqn. (32)] as

$$P_b(L, \gamma_t; 0, \sqrt{2g}, 1) = \frac{e^{-2g\gamma_t}}{2^L\,\Gamma(L)} \sum_{l=0}^{L-1} \frac{\Gamma(L+l)}{2^l\,\Gamma(l+1)}\, {}_1F_1(L+l; L; g\gamma_t), \tag{6.58}$$

has also been used in the literature for the BER of multichannel binary orthogonal FSK and binary DPSK [96, 97].

The conditional BER expression (6.54) for the special case of $\eta = 1$ and any $L \geq 1$ can also be put in the desired product form. Indeed it can be shown that in this particular case $f_0(L; \beta, 1; \phi) = 0$ and hence (6.50) reduces to

$$P_b(L, \gamma_t; a, b, 1) = \frac{1}{2^{2L}\pi} \int_{-\pi}^{\pi} \frac{f_1(L; \beta, 1; \phi) + f_2(L; \beta, 1; \phi)}{1 + 2\beta\sin\phi + \beta^2} \exp\left[-\frac{b^2\gamma_t}{2}\left(1 + 2\beta\sin\phi + \beta^2\right)\right] d\phi; \; 0^+ \leq \beta = \frac{a}{b} < 1, \tag{6.59}$$

where the functions $f_1(\cdot;\cdot,\cdot;\cdot)$ and $f_2(\cdot;\cdot,\cdot;\cdot)$ are now given by

$$f_1(L; \beta, 1; \phi) = \sum_{\substack{l=1 \\ l \text{ odd}}}^{L} \binom{2L-1}{L-l} (-1)^{\frac{l-1}{2}} \left[\left(\beta^{-l+1} - \beta^{l+1}\right) \cos((l-1)\phi) + \left(\beta^{-l+2} - \beta^{l}\right) \sin(l\phi)\right],$$

$$f_2(L; \beta, 1; \phi) = \sum_{\substack{l=2 \\ l \text{ even}}}^{L} \binom{2L-1}{L-l} (-1)^{\frac{l}{2}} \left[\left(\beta^{-l+1} - \beta^{l+1}\right) \sin((l-1)\phi) - \left(\beta^{-l+2} - \beta^{l}\right) \cos(l\phi)\right] \tag{6.60}$$

Again as a check for $L = 1$, we obtain

$$\begin{aligned} f_1(1; \beta, l; \phi) &= 1 - \beta^2, \\ f_2(1; \beta, l; \phi) &= 0, \end{aligned} \tag{6.61}$$

which, when substituted in (6.59), gives an expression for the BER which agrees with (6.13) for $\eta = 1$, as expected. Note also that as $\beta \to 0$ (6.59) assumes an indeterminate form and thus an analytical expression for the limit is more easily obtained from (6.57) with g replaced by $b^2/2$. We further point out that the limit of (6.59) as $\beta \to 0$ converges smoothly to the exact BER expression of (6.57). For example numerical evaluation of (6.59) setting $\beta = 10^{-3}$ ($a = 10^{-3}$, $b = 1$) gives an accuracy of 5 digits when compared with numerical evaluation of (6.57) for the same system parameters. The representation (6.59) is therefore useful even in this specific case. This is particularly true for the performance of binary orthogonal FSK and binary DPSK which cannot be obtained via the classical

representation of (6.57) in the most general fading case but which can be solved using the desirable conditional BER expression (6.59) as we will show next.

6.4.3 Average BER

To obtain the unconditional BER, $\overline{P}_b\left(L,\{\overline{\gamma}_l\}_{l=1}^L,\{i_l\}_{l=1}^L;a,b,\eta\right)$, we must average the conditional BER, $P_b(L,\gamma_t;a,b,\eta)$, over the joint PDF of the instantaneous SNR sequence $\{\gamma_l\}_{l=1}^L$, namely $p_{\gamma_1,\gamma_2,\cdots,\gamma_L}(\gamma_1,\gamma_2,\cdots,\gamma_L)$. Since the RV's $\{\gamma_l\}_{l=1}^L$ are assumed to be statistically independent, then $p_{\gamma_1,\gamma_2,\cdots,\gamma_L}(\gamma_1,\gamma_2,\cdots,\gamma_L)=\prod_{l=1}^L p_{\gamma_l}(\gamma_l;\overline{\gamma}_l,i_l)$, and the averaging procedure results in

$$\overline{P}_b\left(L,\{\overline{\gamma}_l\}_{l=1}^L,\{i_l\}_{l=1}^L;a,b,\eta\right)=\underbrace{\int_0^\infty\int_0^\infty\cdots\int_0^\infty}_{L-\text{fold}}P_b(L,\gamma_t;a,b,\eta)\left[\prod_{l=1}^L p_{\gamma_l}(\gamma_l;\overline{\gamma}_l,i_l)\right]d\gamma_1 d\gamma_2\cdots d\gamma_L. \tag{6.62}$$

If the classical representation of $P_b(L,\gamma_t;a,b,\eta)$, as given by [1, Eqn. (4B.21)] or equivalently (6.48), were to be used, (6.62) would result in an $L+1$-fold integral with infinite limits (one of these integrals comes from the classical definition of the generalized Marcum Q-function in $P_b(L,\gamma_t;a,b,\eta)$), and an adequately efficient numerical integration method would not be available.

Using the desired product form representation of $P_b(L,\gamma_t;a,b,\eta)$, namely (6.53) in (6.62) yields

$$\begin{aligned}\overline{P}_b\left(L,\{\overline{\gamma}_l\}_{l=1}^L,\{i_l\}_{l=1}^L;a,b,\eta\right) &= \frac{\eta^L}{2\pi\,(1+\eta)^{2L-1}}\underbrace{\int_0^\infty\int_0^\infty\cdots\int_0^\infty}_{L-\text{fold}}\int_{-\pi}^{\pi}\frac{f(L;\beta,\eta;\phi)}{1+2\beta\sin\phi+\beta^2}\\ &\times\left[\prod_{l=1}^L\exp\left[-\frac{b^2\,\gamma_l}{2}\left(1+2\beta\sin\phi+\beta^2\right)\right]\right]\left[\prod_{l=1}^L p_{\gamma_l}(\gamma_l;\overline{\gamma}_l,i_l)\right]d\phi\;d\gamma_1 d\gamma_2\cdots d\gamma_L.\end{aligned} \tag{6.63}$$

The integrand in (6.63) is absolutely integrable and the order of integration can therefore be interchanged. Thus grouping like terms we have

$$\begin{aligned}\overline{P}_b\left(L,\{\overline{\gamma}_l\}_{l=1}^L,\{i_l\}_{l=1}^L;a,b,\eta\right)&=\frac{\eta^L}{2\pi\,(1+\eta)^{2L-1}}\int_{-\pi}^{\pi}\frac{f(L;\beta,\eta;\phi)}{1+2\beta\sin\phi+\beta^2}\\ &\times\left[\prod_{l=1}^L\int_0^\infty\exp\left[-\frac{b^2\,\gamma_l}{2}\left(1+2\beta\sin\phi+\beta^2\right)\right]p_{\gamma_l}(\gamma_l;\overline{\gamma}_l,i_l)\,d\gamma_l\right]d\phi\\ &=\frac{\eta^L}{2\pi\,(1+\eta)^{2L-1}}\int_{-\pi}^{\pi}\frac{f(L;\beta,\eta;\phi)}{1+2\beta\sin\phi+\beta^2}\prod_{l=1}^L\mathcal{J}_{i_l}(\overline{\gamma}_l,i_l;a,b;\phi)\,d\phi,\end{aligned} \tag{6.64}$$

where $\mathcal{J}_{i_l}(\overline{\gamma}_l,i_l;a,b;\phi)$ is given above for the various channel models associated with path l. Note that if the fading is identically distributed with the same fading parameter i and the same average

SNR per bit $\overline{\gamma}$ for all L channels, then (6.64) reduces to

$$\overline{P}_b(L,\overline{\gamma},i;a,b,\eta) = \frac{\eta^L}{2\pi\ (1+\eta)^{2L-1}} \int_{-\pi}^{\pi} \frac{f(L;\beta,\eta;\phi)}{1+2\beta\sin\phi+\beta^2}\ [\mathcal{J}_i(\overline{\gamma},i;a,b;\phi)]^L\ d\phi. \tag{6.65}$$

Hence this approach reduces the $L+1$-fold integral with infinite limits of (6.62) to a single finite-range integral (6.64) whose integrand contains only elementary functions (i.e., no special functions) and which can therefore be easily evaluated numerically.

6.5 Conclusion

The myriad of results obtained by the cited authors for the error probability performance of non-coherent and differentially coherent modulations over generalized fading channels can now all be obtained as special cases of a unified approach to the problem. Aside from unifying the past results, the new approach also allows for a more general solution to the problem in that it includes many situations that in the past defied a simple solution. The best example of this occurs for multichannel reception where the fading on each channel need not be identically distributed nor even distributed according to the same family of distributions. It is now possible to obtain results for this case corresponding to a wide variety of modulation/fading channel combinations. Other situations of comparable complexity are also now solvable in simple and elegant forms.

Chapter 7 Performance of Multichannel Reception over Correlated Fading Channels

7.1 Introduction

In studying the performance of diversity systems, the usual assumption made is that the combined signals are independent of one another as discussed in previous chapters. As pointed out in [98, 56, 79, 99, 85] there are a number of real life scenarios in which this assumption is not valid because, for example, of insufficient antenna spacing in small-size mobile units equipped with space antenna diversity. As a result, the maximum theoretical diversity gain cannot be achieved and hence one must revamp their analysis to account for the effect of correlation between the combined signals. Hence, it is important to assess the effect of correlation on the outage probability and average error probability of diversity receivers, in particular, dual selective combining (SC), coherent maximal-ratio combining (MRC), and noncoherent equal-gain combining (EGC) receivers which are the specific cases to be considered in this chapter.

7.2 Selective Combining

Of the three types of linear diversity combining MRC, equal gain combining (EGC) and SC) normally employed in receivers of digital signals transmitted over multipath fading channels, SC is the least complicated of the three since it only processes one of the diversity branches. Specifically, the combiner chooses the branch with the highest signal-to-noise ratio (or equivalently with the strongest signal assuming equal noise power among the branches) [100, Sect. 10-4, p. 432]. Since the output of the SC combiner is equal to the signal on only one of the branches, the coherent sum of the individual branch signals is not required. Therefore, the SC scheme can be used in conjunction with differentially coherent and noncoherent modulation techniques since it does not require knowledge of the signal phases on each branch as would be needed to implement MRC or EGC in a coherent system.

Some special cases of the performance of various modulation schemes with dual SC over independent and correlated Rayleigh and Nakagami-m slow fading channels have been reported in the literature [101, 102, 103, 104]. For instance, [101] studied the performance of noncoherent binary frequency-shift-keying (BFSK) with dual SC over independent identically distributed Nakagami-m fading channels. Adachi *et al.* [102] analyzed the performance of differentially coherent quadriphase-

shift-keying (DQPSK) over correlated unequal average power Rayleigh fading channels. Okui [103] studied the probability of co-channel interference for selection diversity reception in the Nakagami-m fading channel, whereas Wan and Chen [104] presented simulation results for DQPSK with dual SC over correlated Rayleigh fading channels. Finally Fedele *et al.* [105] analyzed the performance of M-ary DPSK with dual SC over independent and correlated Nakagami-m fading channels.

To evaluate these performance measures it is necessary to obtain the cumulative distribution function (CDF) and the probability density function (PDF) of the SC output, i.e. $R_{sc} = \max(R_1, R_2)$, where R_1, R_2 are the signal envelopes that are input to the SC. The SC output CDF is used to evaluate outage probability while the SC output PDF is used to evaluate average error probability. One method of obtaining the CDF of the SC output is to evaluate the joint CDF of the SC inputs, namely, R_1 and R_2 and take the special case where both arguments of this function are equal. Having the SC output CDF one can then simply differentiate this result to obtain the SC output PDF. For a Rayleigh fading channel model, the envelopes are correlated Rayleigh random variables (RVs) and thus what is needed is the bivariate Rayleigh distribution. In a recent paper [106], Tan and Beaulieu presented an infinite series representation of the bivariate Rayleigh CDF in the form of an infinite series where each term of the series is the product of a pair of incomplete gamma functions. Using an alternate representation [89, Appendix C], [90] of the first-order Marcum Q-function, Simon was able to find an alternate expression for the bivariate Rayleigh CDF in the form of a single integral with finite limits and an integrand composed of elementary (exponential and trigonometric) functions [107]. As we will see, aside from its simplicity, this single integral form has the added advantage that it immediately gives the SC output CDF in the same simple form. Furthermore, differentiating with respect to the argument of the CDF gives the PDF of the SC output in a form that can be readily used to unify the evaluation of average error probability for coherent, differentially coherent, and noncoherent communication systems over correlated Rayleigh fading channels.

The organization of this Section is as follows. In the next section, we evaluate the CDF and PDF of the SC output for Rayleigh fading channels. Following this, we make use of the SC output CDFs to evaluate the outage probability for the cases of identical channels and nonidentical Rayleigh fading channels. In Section 7.2.3, we make use of the SC output PDF for Rayleigh fading to evaluate the average error probability for a large class of coherent, differentially coherent, and noncoherent modulation/detection combinations. In Section 7.2.4, we present various numerical examples to illustrate the effect of various parameters on the performance of the system.

7.2.1 CDF and PDF of SC Output

CDF

For the dual diversity case as considered in this section, the joint CDF of the SC inputs, namely, $F_{R_1,R_2}(r_1,\Omega_1;r_2,\Omega_2|\rho)$ was previously found by Simon in the form of a single integral [107, Eqs. (8),(9)], with an integrand dependent on the average powers Ω_1,Ω_2 associated with these inputs and the correlation coefficient ρ between the two signal envelopes defined by

$$\rho=\frac{\mathrm{cov}(R_1^2,R_2^2)}{\sqrt{\mathrm{var}(R_1^2)\mathrm{var}(R_2^2)}},\quad 0\le\rho<1. \tag{7.1}$$

Defining the instantaneous SNR per symbol for each channel $\gamma_i=r_i^2E_s/N_0$, i= 1,2 (E_s/N_0 is the symbol energy-to-Gaussian noise spectral density ratio) and the corresponding average SNR per symbol for each channel $\overline{\gamma}_i=\overline{r_i^2}E_s/N_0=\Omega_iE_s/N_0$, $i=1,2$, then the joint CDF of γ_1,γ_2 is equivalently given by [107, Eqs. (8),(9)]

$$\begin{aligned}F_{\gamma_1,\gamma_2}(\gamma_1,\overline{\gamma}_1;\gamma_2,\overline{\gamma}_2|\rho) &= 1-G\left(H\left(\gamma_1,\overline{\gamma}_1\right),H\left(\gamma_2,\overline{\gamma}_2\right)|\rho\right)+\frac{1}{2\pi}\int_{-\pi}^{\pi}\exp\left[-\frac{\frac{\gamma_1}{\overline{\gamma}_1}+\frac{\gamma_2}{\overline{\gamma}_2}+2\sqrt{\rho\frac{\gamma_1\gamma_2}{\overline{\gamma}_1\overline{\gamma}_2}}\sin\theta}{1-\rho}\right]\\ &\times\left[\frac{(1-\rho^2)\frac{\gamma_1\gamma_2}{\overline{\gamma}_1\overline{\gamma}_2}+\sqrt{\rho}(1-\rho)\sqrt{\frac{\gamma_1\gamma_2}{\overline{\gamma}_1\overline{\gamma}_2}}\left(\frac{\gamma_1}{\overline{\gamma}_1}+\frac{\gamma_2}{\overline{\gamma}_2}\right)\sin\theta}{\left(\rho\frac{\gamma_1}{\overline{\gamma}_1}+2\sqrt{\rho\frac{\gamma_1\gamma_2}{\overline{\gamma}_1\overline{\gamma}_2}}\sin\theta+\frac{\gamma_2}{\overline{\gamma}_2}\right)\left(\frac{\gamma_1}{\overline{\gamma}_1}+2\sqrt{\rho\frac{\gamma_1\gamma_2}{\overline{\gamma}_1\overline{\gamma}_2}}\sin\theta+\rho\frac{\gamma_2}{\overline{\gamma}_2}\right)}\right]d\theta,\end{aligned} \tag{7.2}$$

where

$$G\left(H(\gamma_1,\overline{\gamma}_1),H(\gamma_2,\overline{\gamma}_2)|\rho\right)=\begin{cases}H\left(\gamma_2,\overline{\gamma}_2\right), & 0\le\frac{\gamma_2}{\overline{\gamma}_2}<\rho\frac{\gamma_1}{\overline{\gamma}_1}\\ \frac{1}{2}H\left(\gamma_1,\overline{\gamma}_1\right)+H\left(\gamma_2,\overline{\gamma}_2\right), & \frac{\gamma_2}{\overline{\gamma}_2}=\rho\frac{\gamma_1}{\overline{\gamma}_1}\\ H\left(\gamma_1,\overline{\gamma}_1\right)+H\left(\gamma_2,\overline{\gamma}_2\right), & \rho\frac{\gamma_1}{\overline{\gamma}_1}<\frac{\gamma_2}{\overline{\gamma}_2}<\frac{1}{\rho}\frac{\gamma_1}{\overline{\gamma}_1}\\ \frac{1}{2}H\left(\gamma_2,\overline{\gamma}_2\right)+H\left(\gamma_1,\overline{\gamma}_1\right), & \frac{\gamma_2}{\overline{\gamma}_2}=\frac{1}{\rho}\frac{\gamma_1}{\overline{\gamma}_1}\\ H\left(\gamma_1,\overline{\gamma}_1\right), & \frac{1}{\rho}\frac{\gamma_1}{\overline{\gamma}_1}<\frac{\gamma_2}{\overline{\gamma}_2},\end{cases} \tag{7.3}$$

with $H(\gamma_i,\overline{\gamma}_i)=\exp(-\gamma_i/\overline{\gamma}_i)$, $i=1,2$. Defining the instantaneous SNR at the SC output by $\gamma=\gamma_{\mathrm{sc}}=\max(\gamma_1,\gamma_2)$, then the CDF of γ, namely $F_\gamma(\gamma)$, is immediately obtained by substituting $\gamma_1=\gamma_2=\gamma$ in (7.2) i.e.,[1]

$$F_\gamma(\gamma)=1-G\left(H(\gamma,\overline{\gamma}_1),H(\gamma,\overline{\gamma}_2)|\rho\right)+\frac{1}{2\pi}\int_{-\pi}^{\pi}\exp\left[-\gamma\ h_1(\theta|\rho)\right]\ h_2(\theta|\rho)\ d\theta, \tag{7.4}$$

where

$$h_1(\theta|\rho)=\frac{\overline{\gamma}_1+\overline{\gamma}_2+2\sqrt{\rho\overline{\gamma}_1\overline{\gamma}_2}\sin\theta}{(1-\rho)\overline{\gamma}_1\overline{\gamma}_2}, \tag{7.5}$$

[1]Note that when $\gamma_1=\gamma_2=\gamma$ as will be the case for the SC output PDF and CDF as well as outage and average error probability expressions derived from these, the five regions of validity for $G(\cdot,\cdot|\rho)$ of (7.3) are independent of γ and become: 1) $0\le\overline{\gamma}_1<\rho\overline{\gamma}_2$, 2) $\overline{\gamma}_1=\rho\overline{\gamma}_2$, 3) $\rho\overline{\gamma}_2<\overline{\gamma}_1<\overline{\gamma}_2/\rho$, 4) $\overline{\gamma}_1=\overline{\gamma}_2/\rho$, and 5) $\overline{\gamma}_2/\rho<\overline{\gamma}_1$.

and

$$h_2(\theta|\rho) = \frac{(1-\rho^2)\overline{\gamma}_1\overline{\gamma}_2 + \sqrt{\rho}(1-\rho)\sqrt{\overline{\gamma}_1\overline{\gamma}_2}(\overline{\gamma}_1+\overline{\gamma}_2)\sin\theta}{(\rho\overline{\gamma}_2 + 2\sqrt{\rho\overline{\gamma}_1\overline{\gamma}_2}\sin\theta + \overline{\gamma}_1)(\overline{\gamma}_2 + 2\sqrt{\rho\overline{\gamma}_1\overline{\gamma}_2}\sin\theta + \rho\overline{\gamma}_1)}. \tag{7.6}$$

Before continuing, we wish to mention that an expression of the CDF of the SC output in terms of first-order Marcum Q-functions is presented in [100, Eq. 10-10-4] for the general case of nonidentical channels ($\overline{\gamma}_1 \neq \overline{\gamma}_2$). For the particular case of identical channels ($\overline{\gamma}_1 = \overline{\gamma}_2$) the expression given in [100, Eq. 10-10-4] simplifies to a result still in terms of first-order Marcum Q-functions and which is given in [100, Eq. 10-10-7] and [108, Eq. 5.2-21].

PDF

To obtain the PDF of γ we differentiate (7.4) resulting in

$$\begin{aligned} p_\gamma(\gamma) &= -G'\left(H(\gamma_1,\overline{\gamma}_1), H(\gamma_2,\overline{\gamma}_2)|\rho\right) - \frac{1}{2\pi}\int_{-\pi}^{\pi} h_1(\theta|\rho)h_2(\theta|\rho)\exp\left[-\gamma\ h_1(\theta|\rho)\right]\ d\theta \\ &= G\left(-H'(\gamma_1,\overline{\gamma}_1), -H'(\gamma_2,\overline{\gamma}_2)|\rho\right) - \frac{1}{2\pi}\int_{-\pi}^{\pi} h_1(\theta|\rho)h_2(\theta|\rho)\exp\left[-\gamma\ h_1(\theta|\rho)\right]\ d\theta, \end{aligned} \tag{7.7}$$

where the prime denotes differentiation with respect to γ and thus $-H'(\gamma,\overline{\gamma}_i) = (1/\overline{\gamma}_i)\exp(-\gamma/\overline{\gamma}_i)$, $i = 1, 2$.

In the particular case of identical channels ($\overline{\gamma}_1 = \overline{\gamma}_2 = \overline{\gamma}$) Adachi *et al.* [102, Eq. 42] expressed this PDF in terms of the modified Bessel function $I_0(\cdot)$ and the Rice function $I_e(\cdot,\cdot)$ and then used an approximation of that PDF, namely [102, Eq. 44],

$$p_\gamma(\gamma) \approx \frac{2}{(1+\rho)\ \overline{\gamma}}\left[e^{-\frac{\gamma}{\overline{\gamma}}} - e^{-\frac{2\gamma}{(1-\rho)\overline{\gamma}}}\right] \tag{7.8}$$

in their average BER calculation of $\pi/4$-DQPSK. On the other hand our exact expression of the PDF (7.7) is expressed in terms of a single finite integral and an integrand with a dependence on γ which is entirely exponential and as such resembles the behavior of the instantaneous SNR per bit corresponding to a single Rayleigh RV, namely, $p_\gamma(\gamma) = 1/\overline{\gamma}\exp(-\gamma/\overline{\gamma})$. Because of this similarity, it is possible to draw an analogy with results previously obtained for the average error probability performance of single channel (no diversity) coherent, differentially coherent, and noncoherent detection of digital modulations transmitted over a Rayleigh fading channel (see Chapters 4 and 6), and to develop therefore *exact* simple average BER formulas for a wide range of modulation/detection schemes. However, because of the additional integration on θ required by the second term in (7.7), the functional form of the final results will be some what different, as we shall show in Section 7.2.3.

7.2.2 Outage Probability Performance

The outage probability, P_{out}, is defined as the probability that the SC output SNR $\gamma = \max(\gamma_1, \gamma_2)$ falls below a given threshold, say γ_{th}. Since this probability is simply the probability that neither γ_1 nor γ_2 exceeds the threshold, γ_{th}, then by inspection the outage probability is obtained by replacing γ with γ_{th} in the CDF expressions. Given below are the results for Rayleigh fading.

- Case 1: Identical Channels ($\overline{\gamma}_1 = \overline{\gamma}_2 = \overline{\gamma}$)

$$P_{\text{out}} = 1 - 2\exp\left(-\frac{\gamma_{\text{th}}}{\overline{\gamma}}\right) + \frac{1-\rho}{2\pi}\int_{-\pi}^{\pi} \frac{1}{1+\rho+2\sqrt{\rho}\sin\theta} \exp\left[-\frac{2\gamma_{\text{th}}}{\overline{\gamma}}\left(\frac{1+\sqrt{\rho}\sin\theta}{1-\rho}\right)\right] d\theta. \quad (7.9)$$

  Note that this result is equivalent to [100, Eq. (10-10-7)] which is expressed in terms of the Marcum Q-function. Note that even for this simpler case of identical channels, Tan and Beaulieu's result as given in [106, Eq. (4)] (or equivalently the result found in [109]) does not simplify considerably since it is still an infinite series of squares of integrals. Furthermore, in the limiting case of uncorrelated branches, i.e., $\rho = 0$, (7.9) reduces to $P_{\text{out}} = (1 - \exp(-\gamma_{\text{th}}/\overline{\gamma}))^2$, as expected.

- Case 2: Nonidentical Channels ($\overline{\gamma}_1 \neq \overline{\gamma}_2$)

$$\begin{aligned} P_{\text{out}} &= 1 - G\left(H(\gamma_{\text{th}}, \overline{\gamma}_1), H(\gamma_{\text{th}}, \overline{\gamma}_2)|\rho\right) \\ &+ \frac{1}{2\pi}\int_{-\pi}^{\pi} \exp\left(-\gamma_{\text{th}}\frac{\overline{\gamma}_1 + \overline{\gamma}_2 + 2\sqrt{\rho\overline{\gamma}_1\overline{\gamma}_2}\sin\theta}{\overline{\gamma}_1\overline{\gamma}_2(1-\rho)}\right) \\ &\times \frac{(1-\rho^2)\overline{\gamma}_1\overline{\gamma}_2 + \sqrt{\rho}(1-\rho)\sqrt{\overline{\gamma}_1\overline{\gamma}_2}(\overline{\gamma}_1 + \overline{\gamma}_2)\sin\theta}{(\rho\overline{\gamma}_2 + 2\sqrt{\rho\overline{\gamma}_1\overline{\gamma}_2}\sin\theta + \overline{\gamma}_1)(\overline{\gamma}_2 + 2\sqrt{\rho\overline{\gamma}_1\overline{\gamma}_2}\sin\theta + \rho\overline{\gamma}_1)} d\theta, \end{aligned} \quad (7.10)$$

  where $G\left(H(\gamma_{\text{th}}, \overline{\gamma}_1), H(\gamma_{\text{th}}, \overline{\gamma}_2)|\rho\right)$ is obtained from (7.3) by setting $\gamma_1 = \gamma_2 = \gamma_{\text{th}}$. Note that (7.10) is equivalent to [100, Eq.(10-10-3)] which is expressed in terms of the Marcum Q-function. Furthermore, in the limiting case of uncorrelated branches, i.e., $\rho = 0$, (7.10) together with (7.3) reduces to $P_{\text{out}} = (1 - \exp(-\gamma_{\text{th}}/\overline{\gamma}_1))(1 - \exp(-\gamma_{\text{th}}/\overline{\gamma}_2))$, as expected.

7.2.3 Average Error Probability Performance

To assess the average error probability performance of a SC diversity receiver in the presence of fading we must first provide an expression for the conditional (on γ) error probability and then average this expression over the PDFs of γ as given in Section 7.2.1, i.e.,

$$P(E) = \int_0^{\infty} P(E|\gamma)\, p_{\gamma}(\gamma) d\gamma. \quad (7.11)$$

We now present the specific results for various classes of modulation/detection schemes.

Differentially Coherent and Noncoherent Detection

Binary Differential Phase-Shift-Keying (BDPSK) and Noncoherent Binary Orthogonal Frequency-Shift-Keying (BFSK) The conditional bit error rate (BER) for BDPSK and noncoherent BFSK is given by [1, Eqs.(4.3.19),(4.4.15)]

$$P_b(E|\gamma) = \frac{1}{2}\exp(-g\gamma) \tag{7.12}$$

where g now denotes a modulation constant, i.e., $g = 1$ for BDPSK and $g = 1/2$ for BFSK. Substituting (7.7) and also (7.12) into (7.11), we obtain the following expression for the average BER:

$$P_b(E) = \frac{1}{2}\left[G((1+g\overline{\gamma}_1)^{-1},(1+g\overline{\gamma}_2)^{-1}|\rho) - \frac{1}{2\pi}\int_{-\pi}^{\pi}\frac{h_1(\theta|\rho)h_2(\theta|\rho)}{g+h_1(\theta|\rho)}d\theta\right]. \tag{7.13}$$

The integral term in (7.13) can be evaluated in closed form by first expanding the integrand into a partial fraction expansion then making use of a well-known definite integral. In particular, identifying $h_1(\theta|\rho)$ and $h_2(\theta|\rho)$ from (7.5) and (7.6), respectively, it is straightforward to show that

$$\begin{aligned}\frac{h_1(\theta|\rho)h_2(\theta|\rho)}{g+h_1(\theta|\rho)} &= \frac{\overline{\gamma}_1+\overline{\gamma}_2+2\sqrt{\rho\overline{\gamma}_1\overline{\gamma}_2}\sin\theta}{g(1-\rho)\overline{\gamma}_1\overline{\gamma}_2+\overline{\gamma}_1+\overline{\gamma}_2+2\sqrt{\rho\overline{\gamma}_1\overline{\gamma}_2}\sin\theta} \\ &\times \frac{(1-\rho^2)\overline{\gamma}_1\overline{\gamma}_2+\sqrt{\rho}(1-\rho)\sqrt{\overline{\gamma}_1\overline{\gamma}_2}(\overline{\gamma}_1+\overline{\gamma}_2)\sin\theta}{(\rho\overline{\gamma}_2+2\sqrt{\rho\overline{\gamma}_1\overline{\gamma}_2}\sin\theta+\overline{\gamma}_1)(\overline{\gamma}_2+2\sqrt{\rho\overline{\gamma}_1\overline{\gamma}_2}\sin\theta+\rho\overline{\gamma}_1)},\end{aligned} \tag{7.14}$$

which is in the form

$$\frac{h_1(\theta|\rho)h_2(\theta|\rho)}{g-h_1(\theta|\rho)} = \frac{\overline{\gamma}_1+\overline{\gamma}_2}{\overline{\gamma}_1+\overline{\gamma}_2+g\overline{\gamma}_1\overline{\gamma}_2}, \quad \rho = 0. \tag{7.15}$$

$$\begin{aligned}\frac{h_1(\theta|\rho)h_2(\theta|\rho)}{g+h_1(\theta|\rho)} &= \frac{A+B\sin\theta+C\sin^2\theta}{(a_1+b\sin\theta)(a_2+b\sin\theta)(a_3+b\sin\theta)} \\ &= \frac{c_1}{a_1+b\sin\theta}+\frac{c_2}{a_2+b\sin\theta}+\frac{c_3}{a_3+b\sin\theta}, \quad \rho \neq 0.\end{aligned} \tag{7.16}$$

with

$$\begin{aligned}a_1 &= g(1-\rho)\overline{\gamma}_1\overline{\gamma}_2+\overline{\gamma}_1+\overline{\gamma}_2 \\ a_2 &= \rho\overline{\gamma}_2+\overline{\gamma}_1 \\ a_3 &= \rho\overline{\gamma}_1+\overline{\gamma}_2 \\ b &= 2\sqrt{\rho\overline{\gamma}_1\overline{\gamma}_2} \\ A &= (1-\rho^2)\overline{\gamma}_1\overline{\gamma}_2(\overline{\gamma}_1+\overline{\gamma}_2) \\ B &= 2\sqrt{\rho}(1-\rho^2)(\overline{\gamma}_1\overline{\gamma}_2)^{\frac{3}{2}}+\sqrt{\rho}(1-\rho)\sqrt{\overline{\gamma}_1\overline{\gamma}_2}(\overline{\gamma}_1+\overline{\gamma}_2)^2 \\ C &= 2\rho(1-\rho)\overline{\gamma}_1\overline{\gamma}_2(\overline{\gamma}_1+\overline{\gamma}_2).\end{aligned} \tag{7.17}$$

The coefficients of the partial fraction expansion are readily determined as

$$\begin{aligned} c_1 &= \frac{b^2A - a_1bB + a_1^2C}{(a_1-a_2)(a_1-a_3)b^2} \\ c_2 &= -\frac{b^2A - a_2bB + a_2^2C}{(a_1-a_2)(a_2-a_3)b^2} \\ c_3 &= \frac{b^2A - a_3bB + a_3^2C}{(a_1-a_3)(a_2-a_3)b^2}. \end{aligned} \tag{7.18}$$

Finally, substituting (7.15) and (7.16) into (7.13) and making use of the definite integral [53, p. 425, Eq. (3.661.4)],

$$\frac{1}{2\pi}\int_{-\pi}^{\pi}\frac{1}{a+b\sin\theta}d\theta = \frac{1}{\sqrt{a^2-b^2}}, \quad a \geq b, \tag{7.19}$$

we get the desired closed form result[2]

$$P_b(E) = \frac{1}{2}\sum_{i=1}^{3}\beta_i\frac{1}{1+g\overline{\gamma}_i}, \quad (\overline{\gamma}_3 \triangleq \frac{\overline{\gamma}_1\overline{\gamma}_2}{\overline{\gamma}_1+\overline{\gamma}_2}, \beta_1=\beta_2=1, \beta_3=-1), \quad \rho = 0, \tag{7.20}$$

$$P_b(E) = \frac{1}{2}\left[G((1+g\overline{\gamma}_1)^{-1},(1+g\overline{\gamma}_2)^{-1}|\rho) - \sum_{i=1}^{3}\frac{c_i}{\sqrt{a_i{}^2-b^2}}\right], \quad \rho \neq 0. \tag{7.21}$$

Note that for the special case of $\overline{\gamma}_1 = \overline{\gamma}_2$ and $g = 1$ (BDPSK), (7.20) is in agreement with [2, p. 242, Eq. (5.88)].

Quaternary Differential Phase-Shift-Keying (DQPSK) with Gray Coding and Noncoherent Binary Correlated Frequency-Shift-Keying (BFSK) The conditional BER for DQPSK with Gray coding and noncoherent correlated BFSK is given by (see Chapter (6))

$$P_b(E|\gamma) = \frac{1}{4\pi}\int_{-\pi}^{\pi}\left[\frac{1-\zeta^2}{1+2\zeta\sin\theta+\zeta^2}\right]\exp\left(-\frac{b'^2\gamma}{2}\left[1+2\zeta\sin\theta+\zeta^2\right]\right)d\theta, \quad 0 \leq \zeta = \frac{a'}{b'} < 1, \tag{7.22}$$

where a', b' are modulation constants, i.e., for DQPSK with Gray coding

$$a' = \sqrt{2-\sqrt{2}}, \quad b' = \sqrt{2+\sqrt{2}} \tag{7.23}$$

and for correlated BFSK with complex correlation coefficient λ, $(0 \leq |\lambda| \leq 1)$

$$a' = \sqrt{\frac{1-\sqrt{1-|\lambda|^2}}{2}}, \quad b' = \sqrt{\frac{1+\sqrt{1-|\lambda|^2}}{2}} \tag{7.24}$$

Note that (7.22) has the same functional (exponential) dependence on γ as does (7.12). Hence, substituting (7.22) into (7.11), we obtain by inspection the following expression for the average

[2]Note from (7.17) that it can easily be shown that $a_i \geq b$ for $i = 1, 2, 3$. Hence, (7.19) applies.

BER:

$$\begin{aligned} P_b(E) &= \frac{1}{4\pi}\int_{-\pi}^{\pi}\left[\frac{1-\zeta^2}{1+2\zeta\sin\theta+\zeta^2}\right]\left[\sum_{i=1}^{3}\beta_i\frac{1}{1+g(\theta)\overline{\gamma}_i}\right]d\theta \\ &= \frac{1}{2}\left[1-\sum_{i=1}^{3}\beta_i\frac{1-\zeta^2}{2\zeta^2}\sqrt{\frac{(\overline{\gamma}_i b'^2\zeta^2)^2}{(1+\frac{\overline{\gamma}_i b'^2}{2}(1-\zeta^2))^2+2\overline{\gamma}_i b'^2\zeta^2}}\right], \quad \rho=0. \end{aligned} \tag{7.25}$$

$$P_b(E)=\frac{1}{4\pi}\int_{-\pi}^{\pi}\left[\frac{1-\zeta^2}{1+2\zeta\sin\theta+\zeta^2}\right]\left[G((1+g(\theta)\overline{\gamma}_1)^{-1},(1+g(\theta)\overline{\gamma}_2)^{-1}|\rho)-\sum_{i=1}^{3}\frac{c_i(\theta)}{\sqrt{a_i{}^2(\theta)-b^2}}\right]d\theta, \quad \rho\neq 0 \tag{7.26}$$

where $g(\theta)=(b'^2/2)\left[1+2\zeta\sin\theta+\zeta^2\right]$, $a_2(\theta)=a_2$, $a_3(\theta)=a_3$ and $a_1(\theta)$, $c_1(\theta)$, $c_2(\theta)$, and $c_3(\theta)$ are obtained by substituting $g(\theta)$ for g in (7.17) and (7.18), respectively, and the same substitution is made in $G((1+g\overline{\gamma}_1)^{-1},(1+g\overline{\gamma}_2)^{-1}|\rho)$.

Multiple Differential Phase-Shift-Keying (M-DPSK) The conditional symbol error rate (SER) for M-DPSK is easily derived from the SER for an additive white Gaussian noise (AWGN) channel [65, Eq. (44)], [51, Eq. (7.7)] and is given by the integral expression

$$P_s(E|\gamma)=\frac{\sqrt{g_{\rm psk}}}{2\pi}\int_{-\pi/2}^{\pi/2}\frac{\exp\left(-\gamma\left[1-\sqrt{1-g_{\rm psk}}\cos\theta\right]\right)}{1-\sqrt{1-g_{\rm psk}}\cos\theta}d\theta \tag{7.27}$$

where $g_{\rm psk}=\sin^2(\pi/M)$. Again noting that (7.27) has the same exponential dependence on γ as does (7.12) and (7.22), then substituting (7.27) into (7.11), we obtain by inspection the following expression for the average SER, for $\rho=0$,

$$\begin{aligned} P_s(E) &= \frac{\sqrt{g_{\rm psk}}}{2\pi}\int_{-\pi/2}^{\pi/2}\frac{1}{g(\theta)}\left[\sum_{i=1}^{3}\beta_i\frac{1}{1+g(\theta)\overline{\gamma}_i}\right]d\theta \\ &= \frac{2}{\pi}\left[\arctan\left(\frac{\sqrt{g_{\rm psk}}}{1-\sqrt{1-g_{\rm psk}}}\right)-\sum_{i=1}^{3}\beta_i\frac{\overline{\gamma}_i\sqrt{g_{\rm psk}}}{\sqrt{1+2\overline{\gamma}_i+\overline{\gamma}_i{}^2 g_{\rm psk}}}\arctan\left(\frac{\sqrt{1+2\overline{\gamma}_i+\overline{\gamma}_i{}^2 g_{\rm psk}}}{1+\overline{\gamma}_i\left[1-\sqrt{1-g_{\rm psk}}\right]}\right)\right], \end{aligned} \tag{7.28}$$

and for $\rho\neq 0$

$$P_s(E)=\frac{\sqrt{g_{\rm psk}}}{2\pi}\int_{-\pi/2}^{\pi/2}\frac{1}{g(\theta)}\left[G((1+g(\theta)\overline{\gamma}_1)^{-1},(1+g(\theta)\overline{\gamma}_2)^{-1}|\rho)-\sum_{i=1}^{3}\frac{c_i(\theta)}{\sqrt{a_i{}^2(\theta)-b^2}}\right]d\theta, \tag{7.29}$$

where now $g(\theta)=1-\sqrt{1-g_{\rm psk}}\cos\theta$, $a_2(\theta)=a_2$, $a_3(\theta)=a_3$ and $a_1(\theta)$, $c_1(\theta)$, $c_2(\theta)$, and $c_3(\theta)$ are obtained by substituting $g(\theta)$ for g in (7.17) and (7.18), respectively, and the same substitution is made in $G((1+g\overline{\gamma}_1)^{-1},(1+g\overline{\gamma}_2)^{-1}|\rho)$. If Gray coding is assumed, then for large average SNR, where it can be assumed that the only significant symbol errors that occur are adjacent symbol errors, then

the average BER is approximated by [51, Eq. (4.135)]

$$P_b(E) \cong \frac{P_s(E)}{\log_2 M}. \tag{7.30}$$

Coherent Detection

Binary Phase-Shift-Keying (BPSK) and Binary Frequency-Shift-Keying (BFSK) Based on an alternate representation of the Gaussian Q-function [66], the conditional BER of BPSK and BFSK can be written in the integral form (see Chapter 4)

$$P_b(E|\gamma) = \frac{1}{\pi}\int_0^{\pi/2} \exp\left(-\frac{g\gamma}{\sin^2\theta}\right) d\theta \tag{7.31}$$

where $g = 1$ for BPSK, $g = 1/2$ for orthogonal BFSK, and $g = \frac{1}{2} + \frac{1}{3\pi}$ for BFSK with minimum correlation. Recognizing the analogy between (7.31) and (7.27) in so far as its functional dependence on γ, we can immediately write the average BER as

$$P_b(E) = \frac{1}{\pi}\int_0^{\pi/2} \left[\sum_{i=1}^{3} \beta_i \frac{1}{1+g(\theta)\overline{\gamma}_i}\right] d\theta = \frac{1}{2}\left[1 - \sum_{i=1}^{3}\beta_i \sqrt{\frac{g\overline{\gamma}_i}{1+g\overline{\gamma}_i}}\right], \quad \rho = 0 \tag{7.32}$$

$$P_b(E) = \frac{1}{\pi}\int_0^{\pi/2} \left[G((1+g(\theta)\overline{\gamma}_1)^{-1}, (1+g(\theta)\overline{\gamma}_2)^{-1}|\rho) - \sum_{i=1}^{3}\frac{c_i(\theta)}{\sqrt{a_i{}^2(\theta) - b^2}}\right] d\theta, \rho \neq 0 \tag{7.33}$$

where now $g(\theta) = g/\sin^2\theta$, $a_2(\theta) = a_2$, $a_3(\theta) = a_3$ and $a_1(\theta)$, $c_1(\theta)$, $c_2(\theta)$, and $c_3(\theta)$ are obtained by substituting $g(\theta)$ for g in (7.17) and (7.18), respectively, and the same substitution is made in $G((1+g\overline{\gamma}_1)^{-1}, (1+g\overline{\gamma}_2)^{-1}|\rho)$.

For identical channels ($\overline{\gamma}_1 = \overline{\gamma}_2 = \overline{\gamma}$) using the Adachi *et al.* approximate expression of the PDF (7.8) it can be shown that the average BER of BPSK can be written in closed form as

$$P_b(E) = \frac{1}{(1+\rho)}\left[\frac{1+\rho}{2} - \sqrt{\frac{g\,\overline{\gamma}}{1+g\,\overline{\gamma}}} + \frac{1-\rho}{2}\sqrt{\frac{(1-\rho)\,g\,\overline{\gamma}}{2+(1-\rho)\,g\,\overline{\gamma}}}\right]. \tag{7.34}$$

Since it would be useful to know the relative accuracy improvements of the exact expressions (7.32) and (7.33) over the approximation (7.34) we plot all of them in Fig. 7.2. Note that the approximation tightly upper-bounds the exact BER expression and the bound gets tighter as the average SNR increases and as the correlation coefficient decreases.

Multiple Phase-Shift-Keying (M-PSK) The generalization of (7.31) to M-ary signaling is straightforward in view of the form of the symbol error rate for M-PSK on the AWGN [65, Eq. (71)], [66, Eq. (5)], [51, Eq.(3.119)] which on the fading channel becomes the conditional SER (see

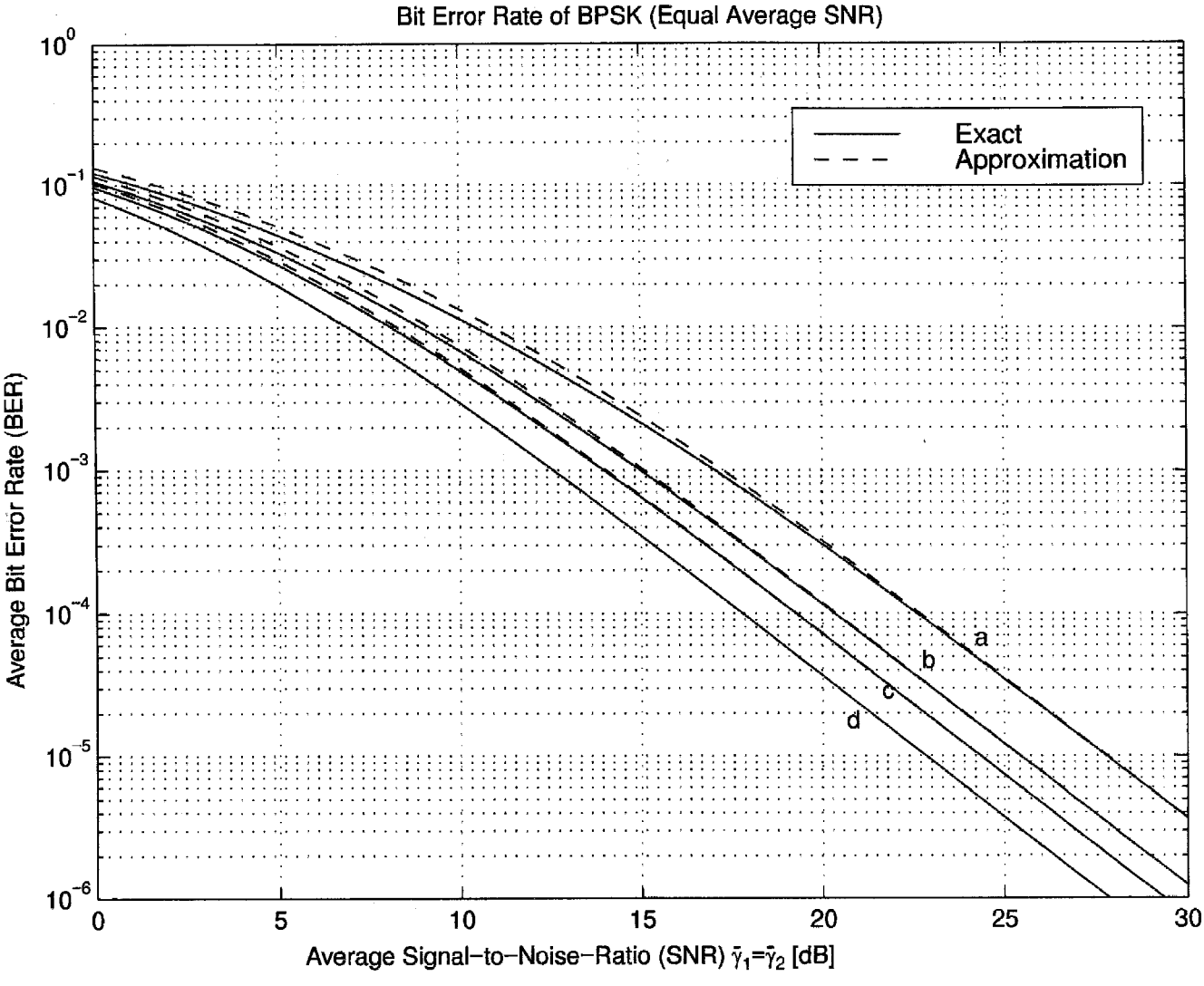

Figure 7.1:

Figure 7.2: Exact and approximate average BER of BPSK versus average SNR of the first branch for equal average branch SNRs ($\overline{\gamma}_1 = \overline{\gamma}_2$) and for various values of the correlation coefficient ((a) $\rho = 0.9$, (b) $\rho = 0.7$, (c) $\rho = 0.5$, (d) $\rho = 0$).

Chapter 4)

$$P_s(E|\gamma) = \frac{1}{\pi}\int_0^{(M-1)\pi/M} \exp\left(-\frac{g_{\text{psk}}\gamma}{\sin^2\theta}\right) d\theta. \tag{7.35}$$

Thus, by inspection we immediately obtain

$$\begin{aligned} P_s(E) &= \frac{1}{\pi}\int_0^{\frac{(M-1)\pi}{M}} \left[\sum_{i=1}^{3}\beta_i \frac{1}{1+g(\theta)\overline{\gamma}_i}\right] d\theta \\ &= \left(\frac{M-1}{M}\right) - \sum_{i=1}^{3}\beta_i\sqrt{\frac{g_{\text{psk}}\overline{\gamma}_i}{1+g_{\text{psk}}\overline{\gamma}_i}}\left[1+\frac{1}{\pi}\arctan\left(\sqrt{\frac{1+g_{\text{psk}}\overline{\gamma}_i}{g_{\text{psk}}\overline{\gamma}_i}}\tan\left(\frac{(M-1)\pi}{M}\right)\right)\right], \quad \rho = 0 \end{aligned} \tag{7.36}$$

$$P_s(E) = \frac{1}{\pi}\int_0^{(M-1)\pi/M}\left[G((1+g(\theta)\overline{\gamma}_1)^{-1},(1+g(\theta)\overline{\gamma}_2)^{-1}|\rho) - \sum_{i=1}^{3}\frac{c_i(\theta)}{\sqrt{a_i^2(\theta)-b^2}}\right] d\theta, \quad \rho \neq 0, \tag{7.37}$$

where now $g(\theta) = g_{\text{psk}}/\sin^2\theta$, $a_2(\theta) = a_2$, $a_3(\theta) = a_3$ and $a_1(\theta)$, $c_1(\theta)$, $c_2(\theta)$, and $c_3(\theta)$ are obtained by substituting $g(\theta)$ for g in (7.17) and (7.18), respectively, and the same substitution is made in $G((1+g\overline{\gamma}_1)^{-1},(1+g\overline{\gamma}_2)^{-1}|\rho)$. Note that (7.36) is valid for $M > 2$ (for $M = 2$ use (7.32)) where the arctangent function is defined with respect to the standard principal value as available, for example, in the Mathematica routine for that function. Again for large average SNR the average BER can be obtained by applying the approximate relation in (7.30) to (7.36) or (7.37).

M-ary Amplitude Modulation (M-AM) and Quadrature Amplitude Modulation (M-QAM) Without belaboring the details, it is a simple matter to extend the previous analyses to M-AM and M-QAM. For M-AM, again using the alternate form of the Gaussian Q-function enables one to arrive at an expression for the conditional SER in a form analogous to (7.31), namely (see Chapter 4),

$$P_s(E|\gamma) = \frac{2(M-1)}{M\pi}\int_0^{\pi/2}\exp\left(-\frac{g_{\text{am}}\gamma}{\sin^2\theta}\right) d\theta, \tag{7.38}$$

where $g_{\text{am}} = 3/(M^2-1)$. Hence, the average SER is given by

$$P_s(E) = \frac{2(M-1)}{M\pi}\int_0^{\pi/2}\left[\sum_{i=1}^{3}\beta_i\frac{1}{1+g(\theta)\overline{\gamma}_i}\right] d\theta = \left(\frac{M-1}{M}\right)\left[1-\sum_{i=1}^{3}\beta_i\sqrt{\frac{g_{\text{am}}\overline{\gamma}_i}{1+g_{\text{am}}\overline{\gamma}_i}}\right], \quad \rho = 0 \tag{7.39}$$

$$P_s(E) = \frac{2(M-1)}{M\pi}\int_0^{\pi/2}\left[G((1+g(\theta)\overline{\gamma}_1)^{-1},(1+g(\theta)\overline{\gamma}_2)^{-1}|\rho) - \sum_{i=1}^{3}\frac{c_i(\theta)}{\sqrt{a_i^2(\theta)-b^2}}\right] d\theta, \quad \rho \neq 0 \tag{7.40}$$

where now $g(\theta) = g_{\text{am}}/\sin^2\theta$, $a_2(\theta) = a_2$, $a_3(\theta) = a_3$ and $a_1(\theta)$, $c_1(\theta)$, $c_2(\theta)$, and $c_3(\theta)$ are obtained by substituting $g(\theta)$ for g in (7.17) and (7.18), respectively, and the same substitution is made in $G((1+g\overline{\gamma}_1)^{-1},(1+g\overline{\gamma}_2)^{-1}|\rho)$. Also for $M = 2$, (7.39) and (7.40) reduce to (7.32) and (7.33), as expected.

For square M-QAM, the expression for the SER on the AWGN involves both the Gaussian Q-function and the square of this function. Using an alternate representation for the square of the Gaussian Q-function [67, Eq. (80)], the conditional SER for the fading channel is given by (see Chapter 4)

$$P_s(E|\gamma) = \frac{4}{\pi}\left(1-\frac{1}{\sqrt{M}}\right)\int_0^{\pi/2}\exp\left(-\frac{g_{\text{qam}}\gamma}{\sin^2\theta}\right)d\theta - \frac{4}{\pi}\left(1-\frac{1}{\sqrt{M}}\right)^2\int_0^{\pi/4}\exp\left(-\frac{g_{\text{qam}}\gamma}{\sin^2\theta}\right)d\theta, \tag{7.41}$$

where $g_{\text{qam}} = 3/[2(M-1)]$. Hence, by inspection, the average SER is given by

$$\begin{aligned} P_s(E) &= \frac{4}{\pi}\left(1-\frac{1}{\sqrt{M}}\right)\int_0^{\pi/2}\left[\sum_{i=1}^{3}\beta_i\frac{1}{1+g(\theta)\overline{\gamma}_i}\right]d\theta - \frac{4}{\pi}\left(1-\frac{1}{\sqrt{M}}\right)^2\int_0^{\pi/4}\left[\sum_{i=1}^{3}\beta_i\frac{1}{1+g(\theta)\overline{\gamma}_i}\right]d\theta \\ &= 2\left(1-\frac{1}{\sqrt{M}}\right)\left[1-\sum_{i=1}^{3}\beta_i\sqrt{\frac{g_{\text{qam}}\overline{\gamma}_i}{1+g_{\text{qam}}\overline{\gamma}_i}}\right] \\ &- \left(1-\frac{1}{\sqrt{M}}\right)^2\left[1-\frac{4}{\pi}\sum_{i=1}^{3}\beta_i\sqrt{\frac{g_{\text{qam}}\overline{\gamma}_i}{1+g_{\text{qam}}\overline{\gamma}_i}}\arctan\left(\sqrt{\frac{1+g_{\text{qam}}\overline{\gamma}_i}{g_{\text{qam}}\overline{\gamma}_i}}\right)\right], \quad \rho = 0 \end{aligned} \tag{7.42}$$

$$\begin{aligned} P_s(E) &= \frac{4}{\pi}\left(1-\frac{1}{\sqrt{M}}\right)\int_0^{\pi/2}\left[G((1+g(\theta)\overline{\gamma}_1)^{-1},(1+g(\theta)\overline{\gamma}_2)^{-1}|\rho) - \sum_{i=1}^{3}\frac{c_i(\theta)}{\sqrt{a_i^2(\theta)-b^2}}\right]d\theta \\ &- \frac{4}{\pi}\left(1-\frac{1}{\sqrt{M}}\right)^2\int_0^{\pi/4}\left[G((1+g(\theta)\overline{\gamma}_1)^{-1},(1+g(\theta)\overline{\gamma}_2)^{-1}|\rho) - \sum_{i=1}^{3}\frac{c_i(\theta)}{\sqrt{a_i^2(\theta)-b^2}}\right]d\theta, \quad \rho \neq 0, \end{aligned} \tag{7.43}$$

where now $g(\theta) = g_{\text{qam}}/\sin^2\theta$, $a_2(\theta) = a_2$, $a_3(\theta) = a_3$ and $a_1(\theta)$, $c_1(\theta)$, $c_2(\theta)$, and $c_3(\theta)$ are obtained by substituting $g(\theta)$ for g in (7.17) and (7.18), respectively, and the same substitution is made in $G((1+g\overline{\gamma}_1)^{-1},(1+g\overline{\gamma}_2)^{-1}|\rho)$.

7.2.4 Numerical Examples

Figures 7.3 and 7.4 plot the outage probability, P_{out}, versus the normalized threshold SNR for various values of the correlation coefficient ρ for equal average branch SNRs and unequal average branch SNRs, respectively. Figures 7.5 and 7.6 plot the average BER of BDPSK versus the average SNR of the first branch for various values for various values of the correlation coefficient ρ for equal average branch SNRs and unequal average branch SNRs, respectively. Figures 7.7 and 7.8 plot the average BER of BPSK versus the average SNR of the first branch for various values of the correlation coefficient ρ for equal average branch SNRs and unequal average branch SNRs, respectively. Note in all figures that the diversity gain decreases with the increase of the correlation coefficient, as expected. Comparing the equal average branch SNR figures (Figs. 7.3, 7.5, 7.7) with the unequal

average branch ones (Figs. 7.4, 7.6, 7.8), observe that: (1) unbalance in the average branch SNRs always leads to lower overall system performance, and (2) the effect of correlation is more important for equal average branch SNRs.

7.3 Maximal-Ratio and Equal-Gain Combining

In this section we assess the effect of correlation on the average error probability of coherent MRC and noncoherent EGC receivers. There is a large number of papers dealing with this topic and along these lines several correlation models have been proposed [98, 13, 99], and using these models several authors [98, 56, 79, 99, 85] have analyzed special cases of the performance of various systems corresponding to specific detection, modulation, and diversity combining schemes. For instance, Pierce and Stein [98] considered the performance of binary coherent and noncoherent systems over correlated identically distributed Rayleigh fading channels. In particular they obtained the average bit error rate (BER) of coherent binary phase-shift-keying (BPSK) when used in conjunction with maximal-ratio combining (MRC) [64], [2, Section 5.5.3, p. 24], and of noncoherent frequency-shift-keying (BFSK) when used with postdetection equal-gain (square law) combining (EGC) [1, Section 4.4, p. 298], [2, Section 5.5.6, p. 253]. Miyagaki *al.* [56] analyzed the outage probability and the average symbol error rate (SER) performance of M-ary phase-shift-keying (M-PSK) for various dual-branch diversity receivers over correlated identically distributed Nakagami-m fading channels [13]. Al-Hussaini and Al-Bassiouni [79] obtained a closed form expression for the average BER of noncoherent BFSK with dual-branch MRC reception over correlated non identically distributed Nakagami-m fading channels. More recently Aalo [99] analyzed the outage probability and the average BER of various coherent, differentially coherent, and noncoherent binary modulations with multichannel MRC reception over identically distributed Nakagami-m fading channels with two correlation models, namely the constant (equal) correlation model and the exponential correlation model. Finally, Patcnaude *et al.* [85] extended the results of Al-Hussaini and Al-Bassiouni [79] and of [99] by providing closed form expressions for the average BER of orthogonal noncoherent BFSK with postdetection EGC reception over two correlated nonidentical and also L equicorrelated identically distributed Nakagami-m channels.

In this section we obtain general results for the exact average BER or SER of M-ary coherent, differentially-coherent, and noncoherent modulations over equicorrelated and exponentially correlated slowly varying Nakagami-m fading channels. Aside from allowing for many detection, modulation, and diversity combining cases not previously treated, these general results provide often simpler forms for the average BER or SER expressions corresponding to the special cases treated by the cited authors. In particular, each average BER or SER expression is obtained in the form of a single integral with finite limits and an integrand composed of elementary functions.

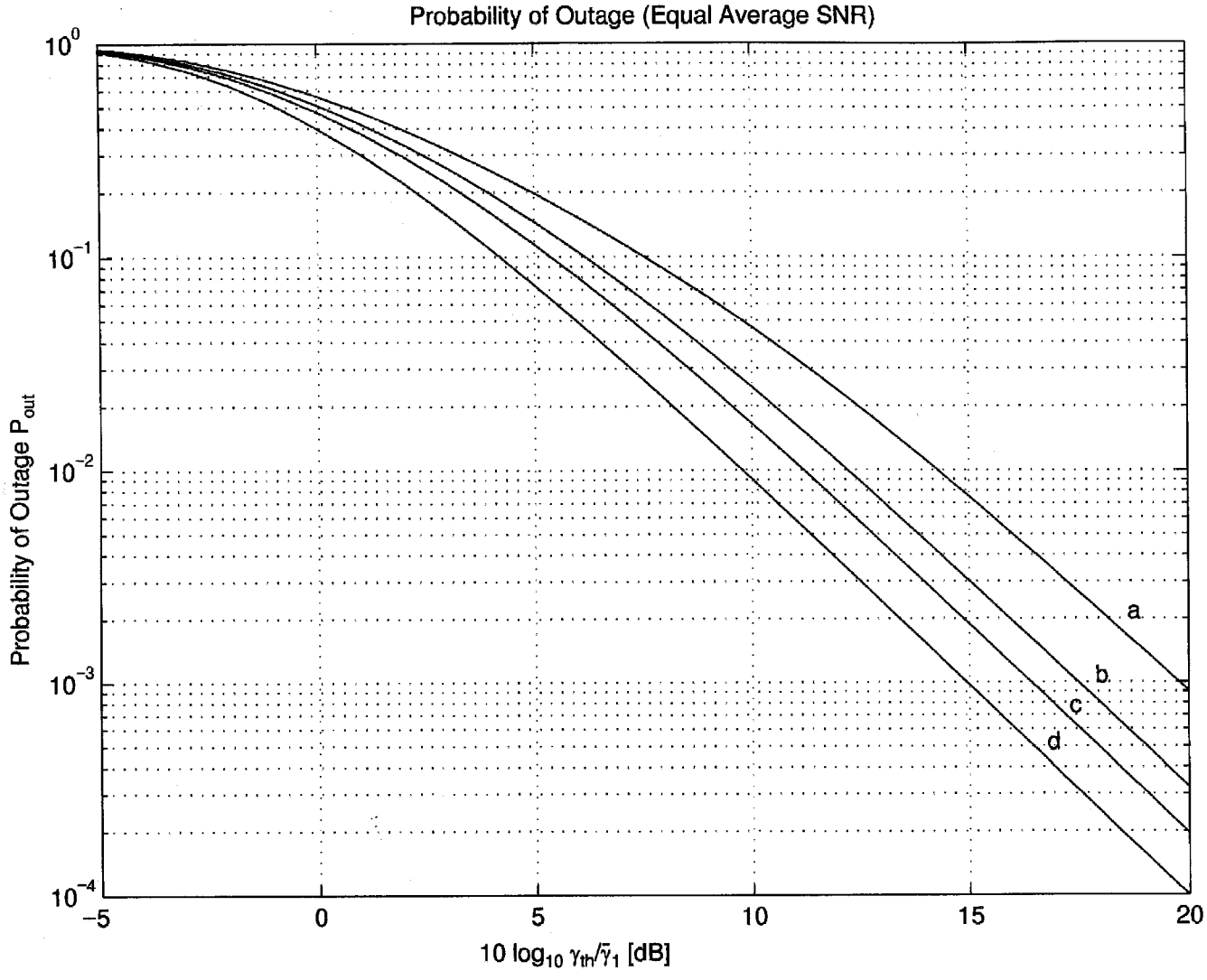

Figure 7.3: Outage probability versus normalized threshold SNR for equal average branch SNRs ($\overline{\gamma}_1 = \overline{\gamma}_2$) and for various values of the correlation coefficient ((a) $\rho = 0.9$, (b) $\rho = 0.7$, (c) $\rho = 0.5$, (d) $\rho = 0$) .

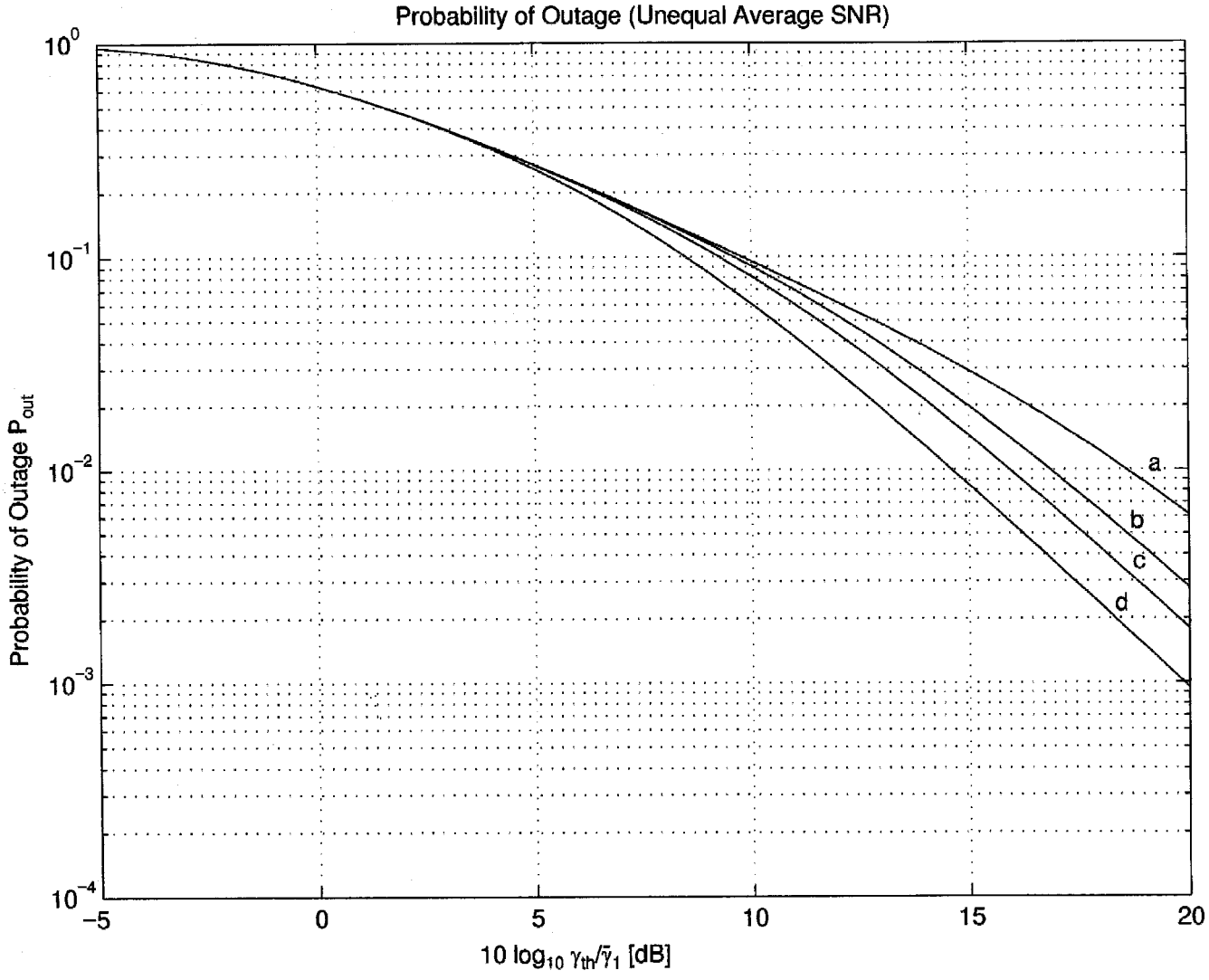

Figure 7.4: Outage probability versus normalized threshold SNR for unequal average branch SNRs ($\overline{\gamma}_1 = 10\,\overline{\gamma}_2$) and for various values of the correlation coefficient ((a) $\rho = 0.9$, (b) $\rho = 0.7$, (c) $\rho = 0.5$, (d) $\rho = 0$).

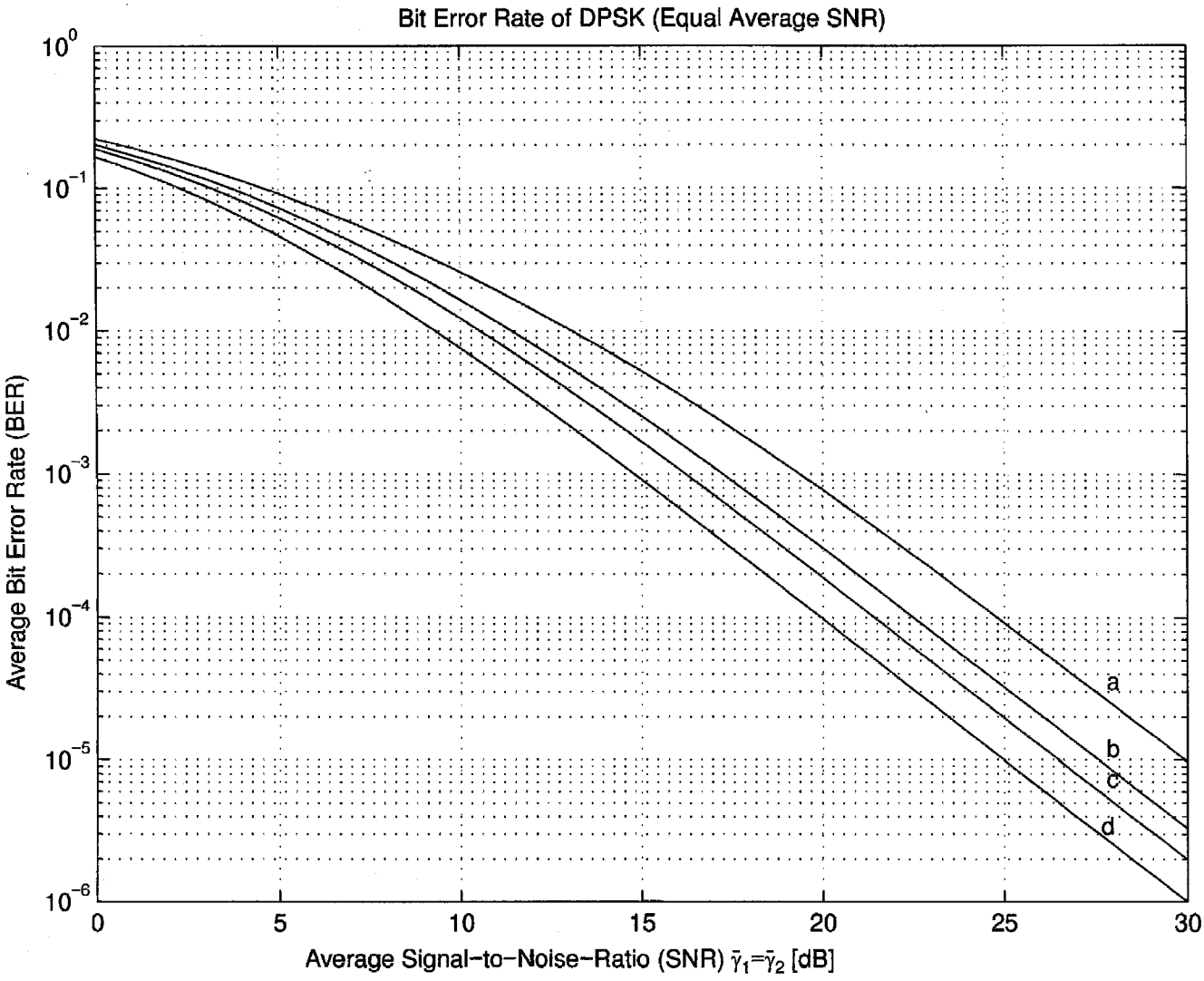

Figure 7.5: Average BER of BDPSK versus average SNR of the first branch for equal average branch SNRs ($\overline{\gamma}_1 = \overline{\gamma}_2$) and for various values of the correlation coefficient ((a) $\rho = 0.9$, (b) $\rho = 0.7$, (c) $\rho = 0.5$, (d) $\rho = 0$).

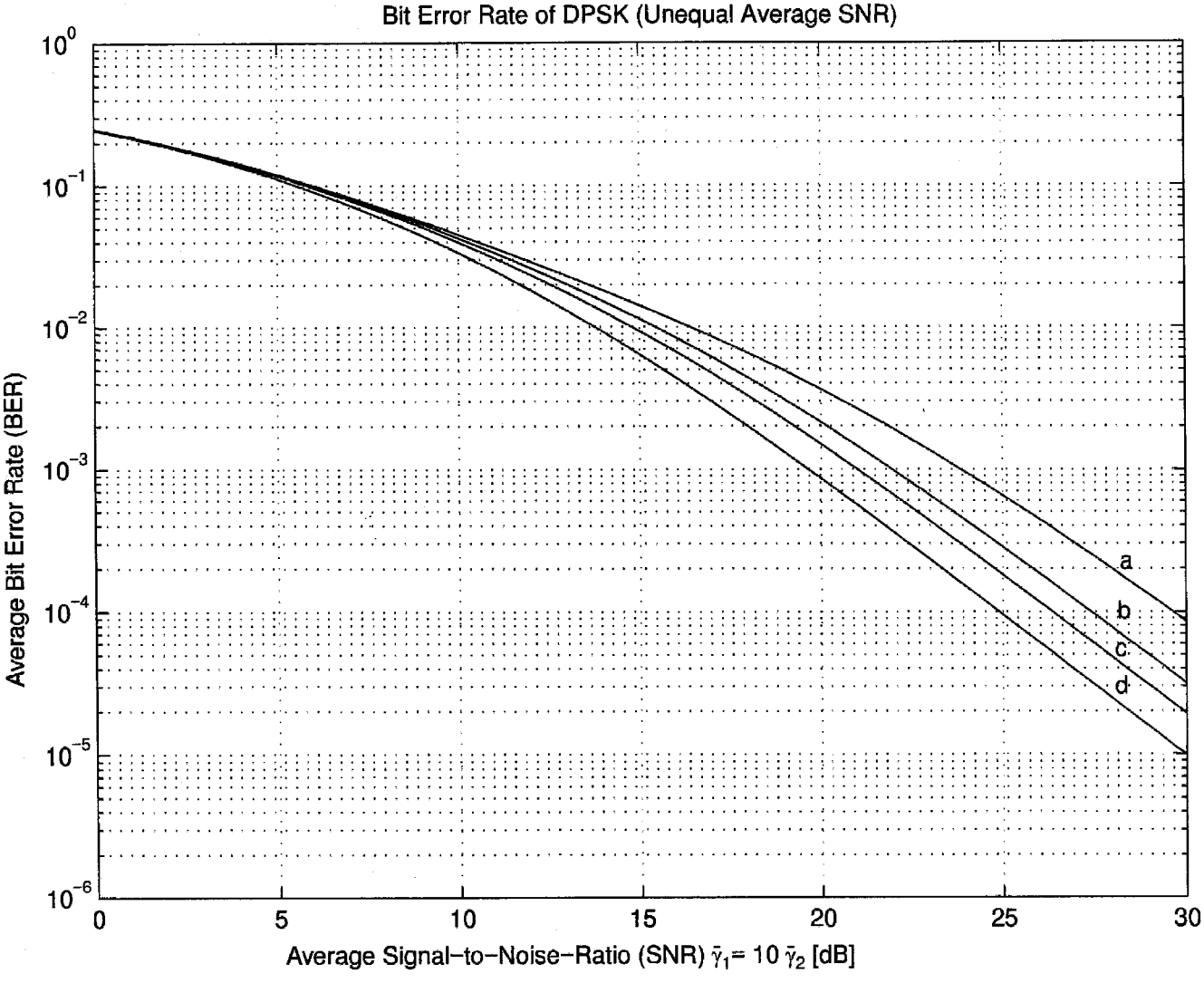

Figure 7.6: Average BER of BDPSK versus average SNR of the first branch for unequal average branch SNRs ($\overline{\gamma}_1 = 10\ \overline{\gamma}_2$) and for various values of the correlation coefficient ((a) $\rho = 0.9$, (b) $\rho = 0.7$, (c) $\rho = 0.5$, (d) $\rho = 0$).

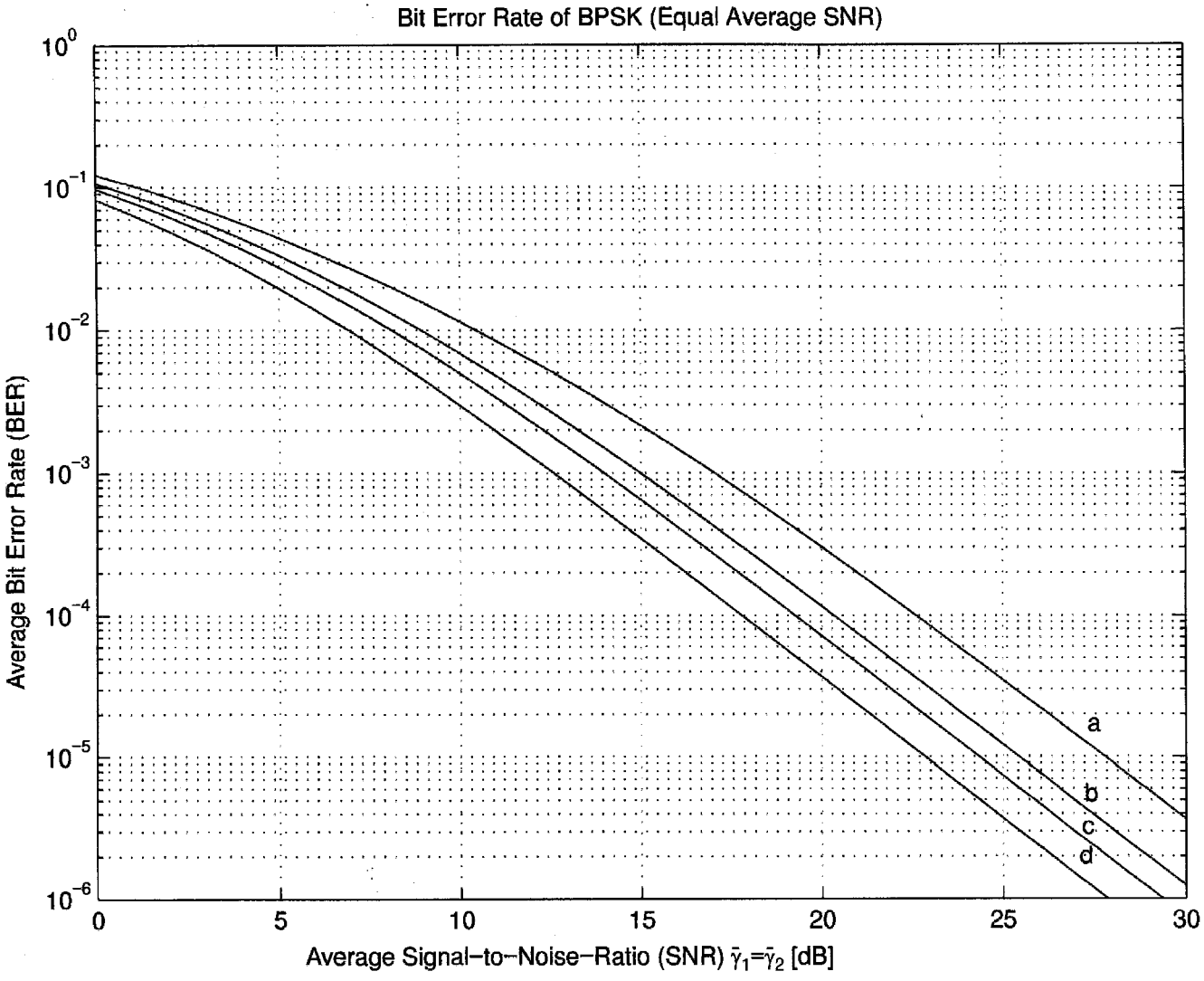

Figure 7.7: Average BER of BPSK versus average SNR of the first branch for equal average branch SNRs ($\overline{\gamma}_1 = \overline{\gamma}_2$) and for various values of the correlation coefficient ((a) $\rho = 0.9$, (b) $\rho = 0.7$, (c) $\rho = 0.5$, (d) $\rho = 0$).

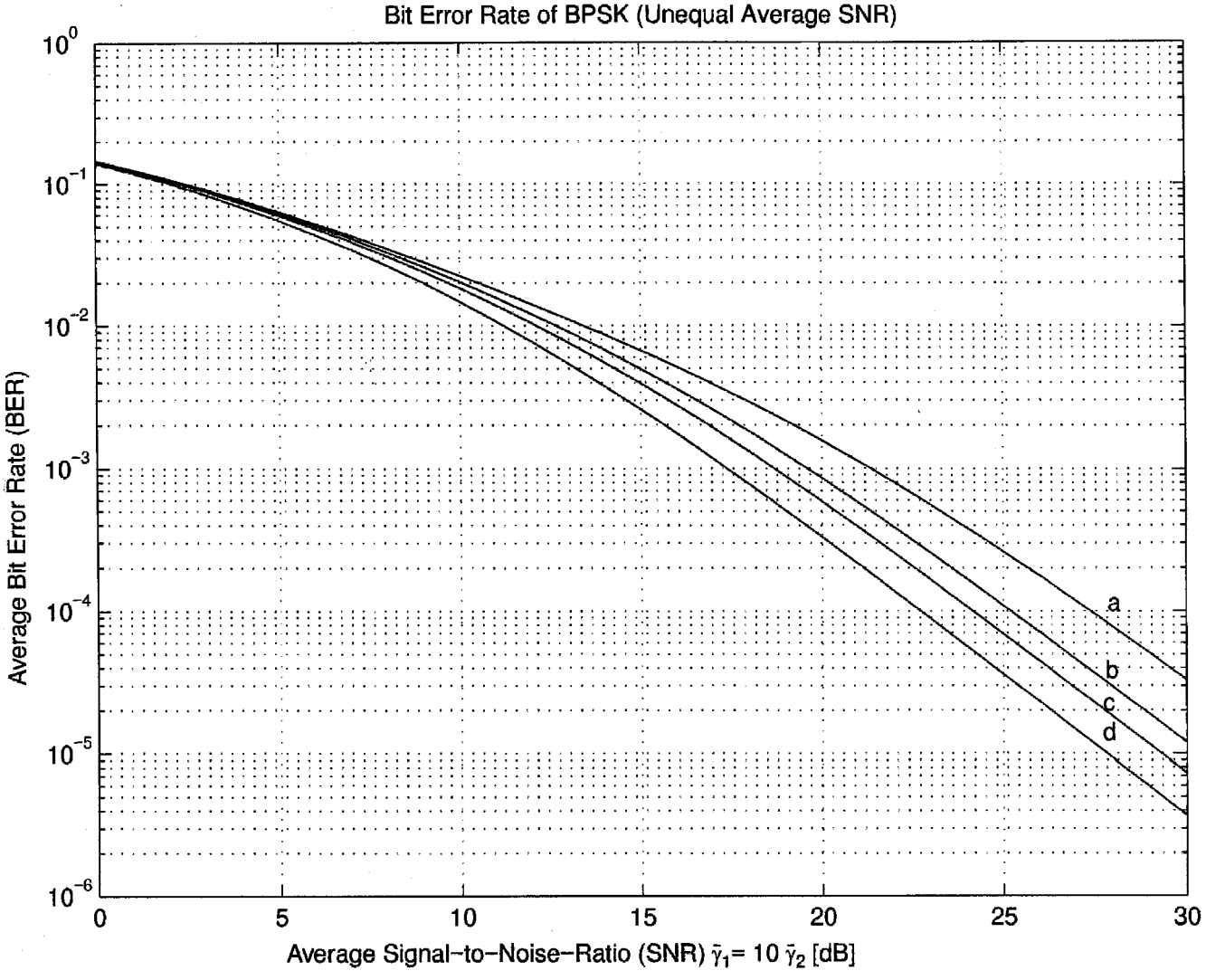

Figure 7.8: Average BER of BPSK versus average SNR of the first branch for unequal average branch SNRs ($\overline{\gamma}_1 = 10\ \overline{\gamma}_2$) and for various values of the correlation coefficient ((a) $\rho = 0.9$, (b) $\rho = 0.7$, (c) $\rho = 0.5$, (d) $\rho = 0$).

The remainder of this paper is organized as follows. In the next section, the various channel correlation models under consideration are described. Section 7.3.2 provides in a generic fashion the performance of coherent modulations with MRC reception. Section 7.3.3 extends these performance results to differentially coherent and noncoherent modulations with postdetection EGC reception. Some numerical examples illustrating the effect of various system performance on the performance of binary modulations are presented in Section 7.3.4.

7.3.1 Channel Correlation Models

In this section we present the three channel correlation models (models A, B, and C) of interest in this paper. Since both of the diversity schemes (MRC and postdetection EGC) under consideration are known to have conditional error rates which are function of the sum of the combined individual signals' signal-to-noise ratio (SNR) per symbol, $\gamma_l = r_l^2 E_s/N_0$ $(l = 1, 2, \cdots, L)$, where l is the branch index, L is the number of combined branches, r_l is the lth branch fading amplitude, and E_s/N_0 is the symbol energy-to-Gaussian noise spectral density ratio, we present for every model the probability function density (PDF) for the combined SNR per symbol, $\gamma_t = \sum_{l=1}^{L} \gamma_l$. Furthermore since our generic approach to evaluate the average error rate performance relies on the knowledge of the moment generating function (MGF) of the combined SNR PDF we derive this quantity for the three channel models under consideration. In what follows, $p_i(\gamma_t)$ denotes the PDF of the combined SNR per symbol, with the index i identifying the model type and is hence equal to a, b, or c. In addition, the MGF of $p_i(\gamma_t)$ is denoted by $\mathcal{M}_i(s)$ and is defined by

$$\mathcal{M}_i(s) \triangleq E_{\gamma_t}\left[e^{-s\gamma_t}\right] = \int_0^\infty p_i(\gamma_t)\, e^{-s\gamma_t}\, d\gamma_t. \tag{7.44}$$

Model A: Two Correlated Branches with Nonidentical Fading

Model A was proposed by Nakagami [13, Section 6.4] and corresponds to the scenarios of dual diversity reception over correlated Nakagami-m channels which are not necessarily identically distributed.

PDF In this case the PDF of the combined signal envelope, $p_a(r_t)$, is given by [13, Eq. (142), p.34]

$$p_a(r_t) = \frac{2r_t\sqrt{\pi}}{\Gamma(m)(\sigma_1\sigma_2(1-\rho))^m}\left(\frac{r_t^2}{2\beta}\right)^{m-\frac{1}{2}} I_{m-\frac{1}{2}}(\beta r_t^2)\, e^{-\alpha r_t^2};\quad r_t \geq 0, \tag{7.45}$$

where $I_\nu(\cdot)$ denotes the νth-order modified Bessel function [70, Section10.2, p. 443],

$$\rho = \frac{\mathrm{cov}(r_1^2, r_2^2)}{\sqrt{\mathrm{var}(r_1^2)\mathrm{var}(r_2^2)}},\quad 0 \leq \rho < 1. \tag{7.46}$$

is the envelope correlation coefficient between the two signals [3], and the parameters σ_l (l=1, 2), α, and β are defined as follows:

$$\sigma_l = \frac{\Omega_l}{m}, \quad (l = 1, 2), \tag{7.47}$$

$$\alpha = \frac{(\sigma_1 + \sigma_2)}{2\sigma_1\sigma_2(1-\rho)}, \tag{7.48}$$

$$\beta^2 = \frac{(\sigma_1 - \sigma_2)^2 + 4\sigma_1\sigma_2\rho}{4\sigma_1^2\sigma_2^2(1-\rho)^2}. \tag{7.49}$$

By using a standard transformation of random variables, it can be shown that the PDF of the combined SNR per symbol, $p_a(\gamma_t)$, is given by

$$p_a(\gamma_t) = \frac{\sqrt{\pi}}{\Gamma(m)}\left[\frac{m^2}{\overline{\gamma}_1\overline{\gamma}_2(1-\rho)}\right]^m \left(\frac{\gamma_t}{2\beta'}\right)^{m-\frac{1}{2}} I_{m-\frac{1}{2}}(\beta'\gamma_t)\, e^{-\alpha'\gamma_t}; \quad \gamma_t \geq 0, \tag{7.50}$$

where the parameters α' and β' are normalized version of the parameters α and β, and are given by

$$\alpha' \triangleq \frac{\alpha}{E_s/N_0} = \frac{m(\overline{\gamma}_1 + \overline{\gamma}_2)}{2\overline{\gamma}_1\overline{\gamma}_2(1-\rho)}, \tag{7.51}$$

$$\beta' \triangleq \frac{\beta}{E_s/N_0} = \frac{m\left((\overline{\gamma}_1 + \overline{\gamma}_2)^2 - 4\overline{\gamma}_1\overline{\gamma}_2(1-\rho)\right)^{1/2}}{2\overline{\gamma}_1\overline{\gamma}_2(1-\rho)}. \tag{7.52}$$

For the cases of identical channels ($\overline{\gamma}_1 = \overline{\gamma}_2 = \overline{\gamma}$), (7.50) reduces to

$$p_a(\gamma_t) = \frac{\pi}{\Gamma(m)\sqrt{1-\rho}}\left(\frac{m}{\overline{\gamma}}\right)^{m+\frac{1}{2}}\left(\frac{\gamma_t}{2\sqrt{\rho}}\right)^{m-\frac{1}{2}} \exp\left[-\frac{m\gamma_t}{(1-\rho)\overline{\gamma}}\right] I_{m-\frac{1}{2}}\left(\frac{m\sqrt{\rho}\gamma_t}{\overline{\gamma}(1-\rho)}\right); \ \gamma_t \geq 0, \tag{7.53}$$

For the Rayleigh fading case ($m = 1$) using the identity [70, Eq. (10.2.13), p.443]

$$\sqrt{\frac{\pi}{2z}} I_{\frac{1}{2}}(z) = \frac{\sinh z}{z}, \tag{7.54}$$

where $\sinh(\cdot)$ denotes the sin hyperbolic function [70, Section 4.5, p.83], it can be shown that (7.50) reduces to

$$p_a(\gamma_t) = \frac{\exp\left[-\frac{\overline{\gamma}_1+\overline{\gamma}_2-\sqrt{(\overline{\gamma}_1+\overline{\gamma}_2)^2-4\overline{\gamma}_1\overline{\gamma}_2(1-\rho)}}{2\overline{\gamma}_1\overline{\gamma}_2(1-\rho)}\gamma_t\right] - \exp\left[-\frac{\overline{\gamma}_1+\overline{\gamma}_2+\sqrt{(\overline{\gamma}_1+\overline{\gamma}_2)^2-4\overline{\gamma}_1\overline{\gamma}_2(1-\rho)}}{2\overline{\gamma}_1\overline{\gamma}_2(1-\rho)}\gamma_t\right]}{\sqrt{(\overline{\gamma}_1+\overline{\gamma}_2)^2 - 4\overline{\gamma}_1\overline{\gamma}_2(1-\rho)}}; \gamma_t \geq 0, \tag{7.55}$$

[3] We use the envelope correlation coefficient throughout this paper as a measure of the degree of correlation between the fading signals since, as pointed it out in [98, 99], experimental data on the correlation between fading signals are typically given in terms of this figure because of its relative ease of measurement.

which itself reduces to the well-known expression for the case of identical Rayleigh channels originally derived in [110] and which can also be found in [98, Eq. (40)], [108, Eq. ()]

$$p_a(\gamma_t) = \frac{1}{2\sqrt{\rho\overline{\gamma}}}\left[\exp\left[-\frac{\gamma_t}{(1+\sqrt{\rho})\overline{\gamma}}\right] - \exp\left[-\frac{\gamma_t}{(1-\sqrt{\rho})\overline{\gamma}}\right]\right]; \quad \gamma_t \geq 0. \tag{7.56}$$

MGF Substituting (7.50) in (7.44) then using the Laplace transform [53, p. 1182, Eq. (110)], it can be shown after some manipulations that the MGF of $p_a(\gamma_t)$ is given by

$$\mathcal{M}_a(s;\overline{\gamma}_1,\overline{\gamma}_2;m;\rho) \triangleq \mathcal{M}_a(s) = \left(1 + \frac{(\overline{\gamma}_1+\overline{\gamma}_2)}{m}\, s + \frac{(1-\rho)\overline{\gamma}_1\overline{\gamma}_2}{m^2}\, s^2\right)^{-m}; \quad s \geq 0. \tag{7.57}$$

Model B: L Identically Distributed Branches with Constant Correlation

Model B was proposed by Aalo [99, Section II-A] for identically distributed Nakagami-m channels (i. e., all channels are assumed to have the same average SNR per symbol $\overline{\gamma}$ and the same fading parameter m). This model assumes that the envelope correlation coefficient ρ is the same between all the channel pairs (l,k) $(l = 1,2,\cdots,L)$ and $(k = 1,2,\cdots,L)$, i.e.

$$\rho = \rho_{lk} = \frac{\mathrm{cov}(r_l^2, r_k^2)}{\sqrt{\mathrm{var}(r_l^2)\mathrm{var}(r_k^2)}}, \quad l \neq k, \quad 0 \leq \rho < 1, \tag{7.58}$$

and may therefore correspond to the scenario of multichannel reception from closely placed diversity antennas.

PDF Based on the work of Gurland [111], Aalo showed the the PDF of γ_t is given in this case by [99, Eq. (18)][4]

$$p_b(\gamma_t) = \frac{\left(\frac{m\gamma_t}{\overline{\gamma}}\right)^{Lm-1} \exp\left(-\frac{m\gamma_t}{(1-\sqrt{\rho})\overline{\gamma}}\right)\ {}_1F_1\left(m, Lm; \frac{Lm\sqrt{\rho}\gamma_t}{(1-\sqrt{\rho})(1-\sqrt{\rho}+L\sqrt{\rho})\overline{\gamma}}\right)}{\left(\frac{\overline{\gamma}}{m}\right)\ (1-\sqrt{\rho})^{m(L-1)}\ (1-\sqrt{\rho}+L\sqrt{\rho})^{m}\ \Gamma(Lm)}; \quad \gamma_t \geq 0, \tag{7.59}$$

where ${}_1F_1(\cdot,\cdot;\cdot)$ is the confluent hypergeometric function [70, Chapter 13, p. 503]. For $L = 2$ using [70, Eq. (13.6.3), p. 509], namely

$${}_1F_1(m, 2m; 2z) = \Gamma\left(m + \frac{1}{2}\right)\left(\frac{z}{2}\right)^{-m+\frac{1}{2}} I_{m-\frac{1}{2}}(z)\ e^z, \tag{7.60}$$

[4]It should be noted at this point that in [99, Eq. (18)] the symbol ρ is used to denote the correlation coefficient of the underlying Gaussian processes that produce the fading on the channels. This correlation coefficient is equal to the square root of the power correlation coefficient. Based on the work of [112, p. 62] it is shown in [98, Appendix V] that for all practical purposes the power correlation coefficient can be assumed to be equal to the envelope correlation coefficient which is denoted by ρ throughout this paper so as to follow what seems to be the more conventional usage of this symbol.

as well as the identities [70, Eq. (6.1.12) and Eq. (6.1.8), p. 255] yielding

$$\Gamma\left(m+\frac{1}{2}\right)=\frac{1\cdot 3\cdot 5\cdot 7\cdots(2m-1)}{2^m}\sqrt{\pi} \tag{7.61}$$

then it can be shown after some manipulations that (7.59) reduces to (7.53) of Model A, as expected.

MGF Substituting (7.59) in (7.44) then using the Laplace transform [53, Eq. (4), p. 864],

$$\int_0^\infty x^{b-1}\,{}_1F_1(a;c;kx)\,e^{-sx}\,dx=\frac{\Gamma(b)}{s^b}\,{}_2F_1\left(a,b;c;\frac{k}{s}\right),\qquad |s|>|k|, b>0, s>0, s>k, \tag{7.62}$$

together with the identity [70, Eq. (15.1.8), p. 556], [99, Eq. (A-5)]

$${}_2F_1(a,b;b;z)=(1-z)^{-a}, \tag{7.63}$$

it can be shown that

$$\mathcal{M}_b(s;\overline{\gamma};m;\rho;L)\triangleq\mathcal{M}_b(s)=\left(1+\frac{\overline{\gamma}(1-\sqrt{\rho}-L\sqrt{\rho})}{m}\,s\right)^{-m}\left(1+\frac{\overline{\gamma}(1-\sqrt{\rho})}{m}\,s\right)^{-m(L-1)};\quad s\geq 0. \tag{7.64}$$

For $L=2$, as a check, it can be easily shown that (7.64) agrees with (7.57) for $\overline{\gamma}_1=\overline{\gamma}_2$

Model C: L Identically Distributed Branches with Exponential Correlation

Model C was also proposed by Aalo [99, Section II-B] for identically distributed Nakagami-m channels (i. e., all channels are assumed to have the same average SNR per symbol $\overline{\gamma}$ and the same fading parameter m). This model assumes an exponential envelope correlation coefficient ρ_{lk} between any channel pairs (l,k) $(l=1,2,\cdots,L)$ and $(k=1,2,\cdots,L)$ as given by

$$\rho_{lk}=\frac{\mathrm{cov}(r_l^2,r_k^2)}{\sqrt{\mathrm{var}(r_l^2)\mathrm{var}(r_k^2)}}=\rho^{|l-k|}, 0\leq\rho\leq 1, \tag{7.65}$$

and may therefore correspond to the scenario of multichannel reception from equispaced diversity antennas in which the correlation between the pairs of combined signals decays as the spacing between the antennas increases.

PDF Based on the work of Kotz and Adams [113], Aalo showed the the PDF of γ_t can be very well approximated by a gamma distribution given by [99, Eq. (19)][5]

$$p_c(\gamma_t) = \frac{\gamma_t^{\frac{mL^2}{r_\rho}-1} \exp\left(-\frac{mL\gamma_t}{r_\rho \overline{\gamma}}\right)}{\Gamma\left(\frac{mL^2}{r_\rho}\right)\left(\frac{r_\rho \overline{\gamma}}{mL}\right)^{\frac{mL^2}{r_\rho}}}; \quad \gamma_t \geq 0, \tag{7.66}$$

where[6]

$$r_\rho = L + \frac{2\sqrt{\rho}}{1-\sqrt{\rho}}\left(L - \frac{1-\rho^{L/2}}{1-\sqrt{\rho}}\right). \tag{7.67}$$

MGF Substituting (7.66) in (7.44) then using the Laplace transform [53, Eq. (3.381.4)], namely

$$\int_0^\infty x^{\nu-1}\, e^{-sx}\, dx = \frac{\Gamma(\nu)}{s^\nu}, \tag{7.68}$$

it can be shown that

$$\mathcal{M}_c(s;\overline{\gamma};m;\rho;L) \triangleq \mathcal{M}_c(s) = \left(1 + \frac{r_\rho \overline{\gamma}}{mL}\, s\right)^{-\frac{mL^2}{r_\rho}}; \quad s \geq 0. \tag{7.69}$$

7.3.2 Coherent Multichannel Reception

To assess the average error probability performance of a diversity receiver in the presence of slow fading we must first provide an expression for the conditional (on γ_t) error probability and then average this expression over the PDFs of γ_t as given in Section 2, i.e.,

$$P_i(E) = \int_0^\infty P(E|\gamma_t)\, p_i(\gamma_t)\, d\gamma_t. \tag{7.70}$$

We now present specific results for different coherent modulations with MRC reception.

Binary Phase-Shift-Keying (BPSK) and Binary Frequency-Shift-Keying (BFSK)

Based on an alternate representation of the Gaussian Q-function [66], the conditional BER of BPSK and BFSK can be written in the integral form (see Chapter 4)

$$P_b(E|\gamma_t) = \frac{1}{\pi}\int_0^{\pi/2} \exp\left(-\frac{g\gamma_t}{\sin^2\phi}\right) d\phi, \tag{7.71}$$

where $g = 1$ for BPSK, $g = 1/2$ for orthogonal BFSK, and $g = \frac{1}{2} + \frac{1}{3\pi}$ for BFSK with minimum correlation. The average BER, $P_b(E)$ is then obtained by averaging (7.71) over (7.50), (7.59), or

[5] Based on the work of Kotz and Adams [113], Aalo [99] points out that the approximation (7.66) is valid for high values of L but is still accurate for values of L as small as 5.

[6] We remind the reader that contrary to its usage in [99] the coefficient ρ denotes in this paper the envelope correlation coefficient.

(7.66) yielding after interchanging the order integration the desired generic result

$$P_{b_i}(E) = \frac{1}{\pi}\int_0^{\pi/2} \mathcal{M}_i\left(\frac{g}{\sin^2\phi}\right)\, d\phi. \tag{7.72}$$

For model B, (7.72) with (7.64) should be contrasted with the previous available equivalent result [99, Eq. (32)] which required the evaluation of the Appell's hypergeometric function, $F_2(\cdot;\cdot,\cdot;\cdot,\cdot;\cdot,\cdot)$, which is typically not available in standard mathematical software libraries such us Mathematica, Matlab, and Maple, and which is defined either in term of an infinite range integral of a special function [99, Eq. (A-12)] or alternatively as a double infinite sum [99, Eq. (A-13)]. For model C, (7.72) along with (7.69) is equivalent to [99, Eq. (40)] which is expressed in terms of the hypergeometric function ${}_2F_1(\cdot,\cdot,\cdot;\cdot)$ [70, Chapter 15, p.555].

Multiple Phase-Shift-Keying (M-PSK)

The generalization of (7.71) to M-ary signaling is straightforward in view of the form of the symbol error rate for M-PSK on the AWGN [65, Eq. (71)], which on the fading channel becomes the conditional SER (see Chapter 4)

$$P_s(E|\gamma_t) = \frac{1}{\pi}\int_0^{(M-1)\pi/M} \exp\left(-\frac{g_{\text{psk}}\gamma_t}{\sin^2\phi}\right) d\phi, \tag{7.73}$$

where $g_{\text{psk}} = \sin^2\left(\frac{\pi}{M}\right)$ Thus, by inspection we immediately obtain

$$P_{s_i}(E) = \frac{1}{\pi}\int_0^{(M-1)\pi/M} \mathcal{M}_i\left(\frac{g_{\text{psk}}}{\sin^2\phi}\right)\, d\phi. \tag{7.74}$$

It should be noted that for model A (7.74) together with (7.57) is an *exact* expression equivalent to [56, Eq. (54)] with the advantage of being expressed in terms of a single finite-range integral (contrary to [56, Eq. (54)]) and whose integrand is much simpler than [56, Eq. (54)], and hence easier to compute for any arbitrary value of the fading parameter m.

M-ary Amplitude Modulation (M-AM)

Without belaboring the details, it is a simple matter to extend the previous analyzes to M-AM with signal points symmetrically located about the origin. Again using the alternate form of the Gaussian Q-function enables one to arrive at an expression for the conditional SER in a form analogous to (7.71), namely (see Chapter 4),

$$P_s(E|\gamma_t) = \frac{2(M-1)}{M\pi}\int_0^{\pi/2} \exp\left(-\frac{g_{\text{am}}\gamma_t}{\sin^2\phi}\right) d\phi, \tag{7.75}$$

where $g_{\text{am}} = 3/(M^2 - 1)$. Hence, the average SER is given by

$$P_{s_i} = \frac{2(M-1)}{\pi M} \int_0^{\pi/2} \mathcal{M}_i \left(\frac{g_{\text{am}}}{\sin^2 \phi} \right) d\phi. \tag{7.76}$$

M-ary Quadrature Amplitude Modulation (M-QAM)

Consider square M-QAM signals whose constellation size is given by $M = 2^k$ with k even. For these type of constellations, the expression for the SER on the AWGN involves both the Gaussian Q-function and the square of this function. Using an alternate representation for the square of the Gaussian Q-function [67, Eq. (80)], the conditional SER for the fading channel is given by (see Chapter 4)

$$P_s(E|\gamma t) = \frac{4}{\pi} \left(1 - \frac{1}{\sqrt{M}} \right) \int_0^{\pi/2} \exp \left(-\frac{g_{\text{qam}} \gamma_t}{\sin^2 \phi} \right) d\phi - \frac{4}{\pi} \left(1 - \frac{1}{\sqrt{M}} \right)^2 \int_0^{\pi/4} \exp \left(-\frac{g_{\text{qam}} \gamma_t}{\sin^2 \phi} \right) d\phi, \tag{7.77}$$

where $g_{\text{qam}} = 3/[2(M-1)]$. Hence, by inspection, the average SER is given by

$$P_{s_i}(E) = \frac{4}{\pi} \left(1 - \frac{1}{\sqrt{M}} \right) \int_0^{\pi/2} \mathcal{M}_i \left(\frac{g_{\text{qam}}}{\sin^2 \phi} \right) d\phi - \frac{4}{\pi} \left(1 - \frac{1}{\sqrt{M}} \right)^2 \int_0^{\pi/4} \mathcal{M}_i \left(\frac{g_{\text{qam}}}{\sin^2 \phi} \right) d\phi. \tag{7.78}$$

7.3.3 Differentially Coherent and Noncoherent Multichannel Reception

For differentially coherent and noncoherent detection, MRC is not practical since it requires channel phase estimates for its implementation. As pointed out by Stüber [2, p. 255], if in fact it were possible to estimate the channel phases on each channel, then the reasons for employing differentially coherent and noncoherent detection would become mute and instead one should resort to coherent detection since it results in superior performance. In view of this observation, post-detection EGC [1, Section 4.4, p. 298], [2, Section 5.5.6, p. 253] is the more common form of diversity combining for these type of receivers [85]. We present in this section a generic result for the average BER for differentially coherent and noncoherent multichannel receivers when used in conjunction with post-detection EGC over correlated Nakagami-m fading channels.

Conditional BER

Using an alternate integral representation of the generalized Marcum Q-function [89, Appendix C], [90], it was shown in Chapter 6 that the conditional BER of a wide class of differentially coherent and noncoherent modulations can be written in the desired form consisting of a single integral with finite limits and an integrand which is composed of elementary functions and where the total instantaneous SNR per bit γ_t (over which we must average) appears only in the argument of the

exponential term, namely,

$$P_b(E|\gamma_t)=\frac{b^2\eta^L}{2\pi(1+\eta)^{2L-1}}\int_{-\pi}^{\pi}\frac{f\left(L;\frac{a}{b},\eta;\phi\right)}{(a^2+b^2+2ab\sin\phi)}\exp\left[-(a^2+b^2+2ab\sin\phi)\frac{\gamma_t}{2}\right]\,d\phi, 0^+\le a<b, \tag{7.79}$$

where

$$f(L;\beta,\eta;\phi)=f_0(L;\beta,\eta;\phi)+f_1(L;\beta,\eta;\phi),$$

with

$$f_0(L;\beta,\eta;\phi)=\left[-\frac{(1+\eta)^{2L-1}}{\eta^L}+\sum_{l=1}^{L}\binom{2L-1}{L-l}(\eta^{-l}+\eta^{l-1})\right]\,\beta(\beta+\sin\phi),$$

$$f_1(L;\beta,\eta;\phi)=\sum_{l=1}^{L}\binom{2L-1}{L-l}\left[(\eta^{-l}\beta^{-l+1}-\eta^{l-1}\beta^{l+1})\cos((l-1)(\phi+\pi/2))-(\eta^{-l}\beta^{-l+2}-\eta^{l-1}\beta^{l})\cos(l(\phi+\pi/2))\right]. \tag{7.80}$$

In (7.79) the parameters a and b are modulation-dependent and are defined in [1, Eq. (4B.22)], and $\eta = v_2/v_1$, with the parameters v_1, v_2 defined in Recall that a number of special cases are of particular importance. For noncoherent detection of equal energy, equiprobable, correlated binary signals, $\eta = 1$ and

$$\begin{aligned} a &= \left(\frac{1-\sqrt{1-|\lambda|^2}}{2}\right)^{1/2} \\ b &= \left(\frac{1+\sqrt{1-|\lambda|^2}}{2}\right)^{1/2}, \end{aligned} \tag{7.81}$$

where λ $(0 \le |\lambda| \le 1)$ is the complex-valued cross-correlation coefficient between the two signals. The special case $\lambda = 0$ corresponds to orthogonal noncoherent BFSK for which $a = 0$ and $b = 1$. Furthermore, in the case of binary differential phase-shift-keying (BDPSK), $a = 0$, $b = \sqrt{2}$, and $\eta = 1$. Finally $a = \sqrt{2-\sqrt{2}}$, $b = \sqrt{2+\sqrt{2}}$, and $\eta = 1$ correspond to quaternary differential phase-shift-keying (DQPSK) with Gray coding. It should be noted that as $a \to 0$ (7.79) assumes an indeterminate form but the limit converges smoothly to the exact conditional BER expression.

Average BER

To evaluate the average BER one must average the conditional BER expression (7.79) over one of the fading PDFs under consideration as given by (7.50), (7.59), or (7.66). Recognizing the analogy between (7.79) and (7.71) in so far as its functional dependence on γ_t, we can immediately write the

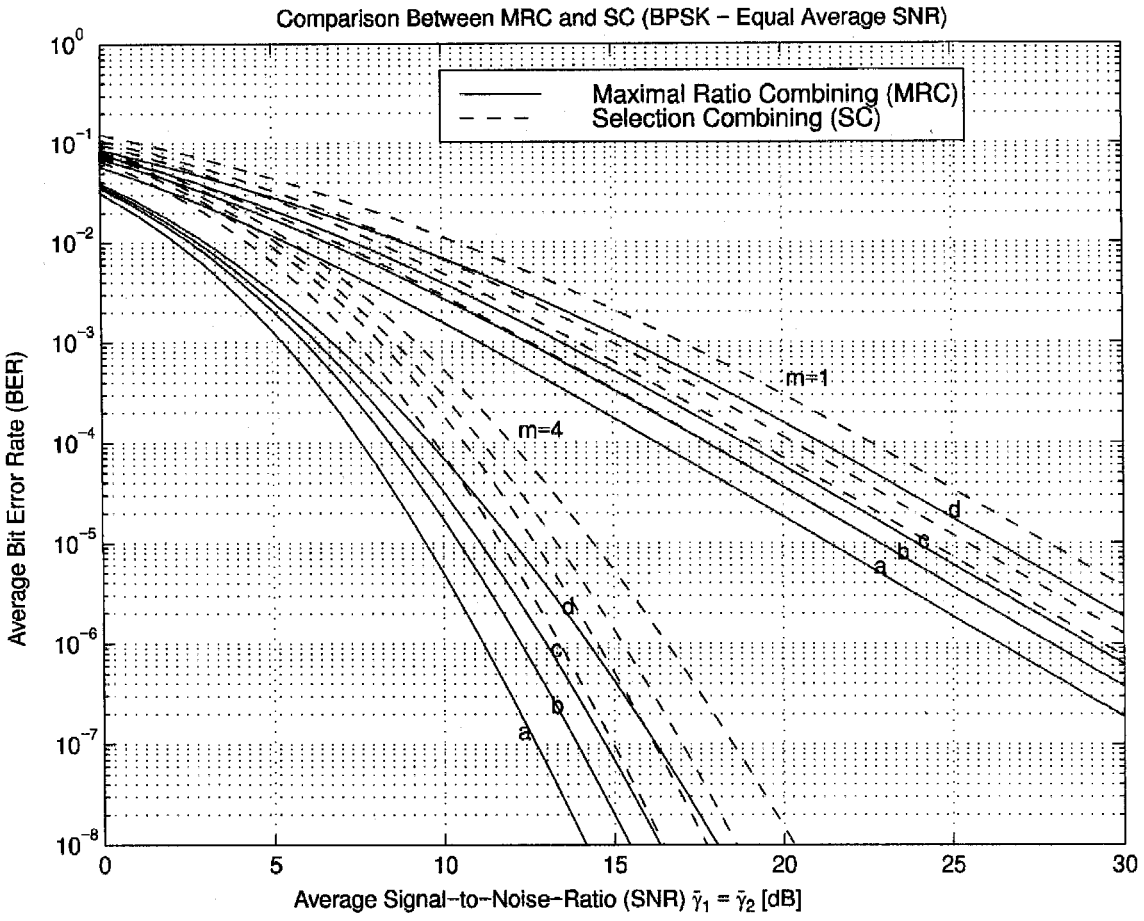

Figure 7.9: Average BER of BPSK versus average SNR of the first branch for equal average branch SNRs ($\overline{\gamma}_1 = \overline{\gamma}_2$) and for various values of the correlation coefficient ((a) $\rho = 0$, (b) $\rho = 0.5$, (c) $\rho = 0.7$, (d) $\rho = 0.9$).

average BER as

$$P_{b_i}(E) = \frac{b^2\eta^L}{2\pi(1+\eta)^{2L-1}} \int_{-\pi}^{\pi} \frac{f\left(L; \frac{a}{b}, \eta; \phi\right)}{(a^2+b^2+2ab\sin\phi)} \mathcal{M}_i\left(\frac{a^2+b^2+2ab\sin\phi}{2}\right) d\phi. \tag{7.82}$$

Letting $a \to 0$ and $b = 1$ ($b = \sqrt{2}$) in (7.82) yields the average BER performance of orthogonal BFSK (BDPSK), and in this particular case (7.82) is equivalent to the closed-forms [85, Eq. (21)] and [85, Eq. (16)], for models A and B, respectively.

7.3.4 Numerical Examples

As examples Figs. 7.9 and 7.10 compare the performance of dual branch maximal ratio combining and selection combining diversity over correlated Nakagami-m fading channels, for equal and unequal average SNR, respectively.

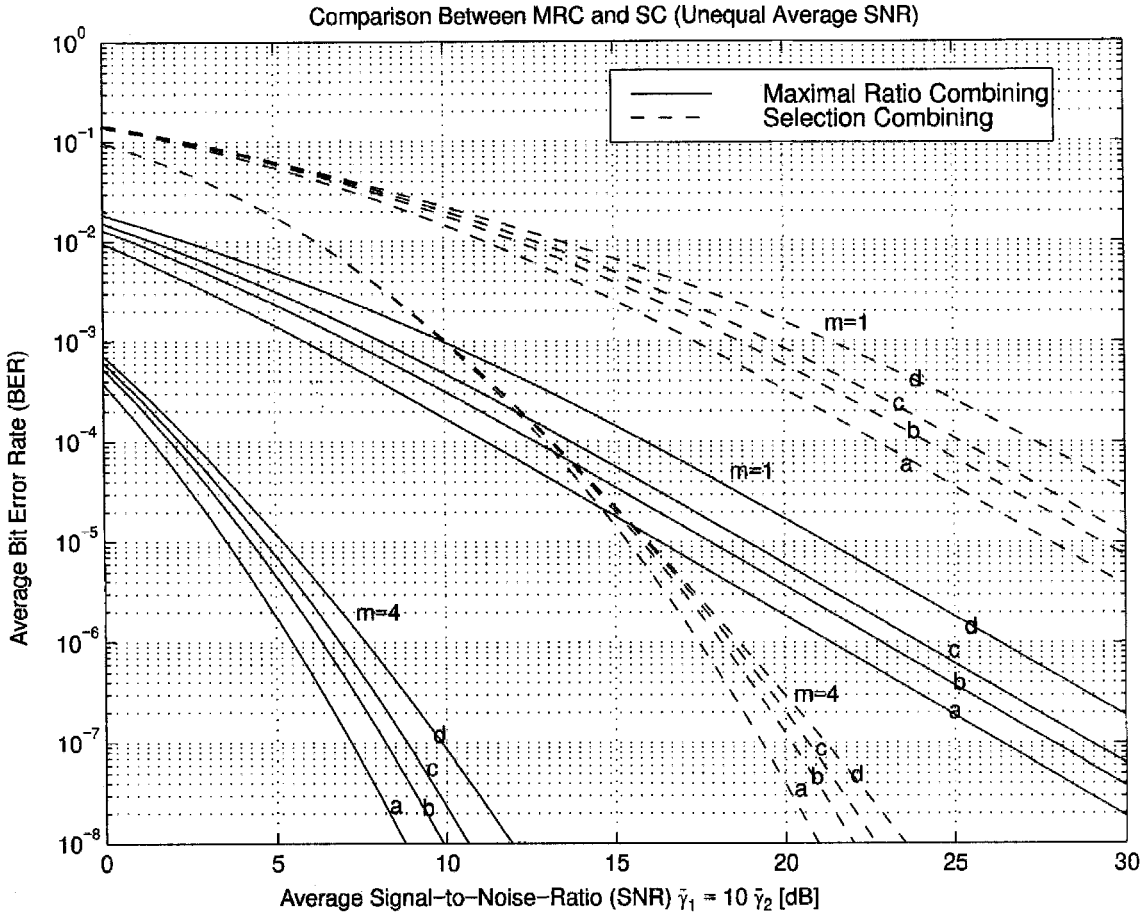

Figure 7.10: Average BER of BPSK versus average SNR of the first branch for unequal average branch SNRs ($\overline{\gamma}_1 = 10\ \overline{\gamma}_2$) and for various values of the correlation coefficient ((a) $\rho = 0$, (b) $\rho = 0.5$, (c) $\rho = 0.7$, (d) $\rho = 0.9$).

7.4 Conclusion

We studied the effect of correlation on the performance of SC and MRC diversity receivers. For SC it was shown that using a simple finite integral representations for the CDF and PDF of the output of a dual diversity selective combiner, it is possible to express the outage probability and error probability performances of this system in the presence of slow correlated Rayleigh fading either in closed form or in terms of a single integral with finite limits and an integrand composed of elementary (exponential and trigonometric) functions. Having expressions in this form readily allows numerical evaluation for specific cases of interest. These expressions and numerical results have been extended by Simon to correlated Nakagami-m channels and can be found in [72].

For coherent MRC and noncoherent EGC receivers we obtained generic easy-to-compute expressions for the average error rate of multichannel reception of digital signals over equicorrelated and exponentially correlated slowly varying Nakagami-m fading channels. The results are applicable to coherent detection with maximal-ratio combining as well as to differentially coherent and noncoherent detection with post-detection equal-gain (square law) combining. Aside from extending previous analyses of diversity reception over correlated Nakagami-m fading channels to include the performance of M-ary modulations, these results provide equivalent forms for known expressions corresponding to the performance of binary modulations. Because of their simple forms, these results offer a useful analytical tool for the accurate performance evaluation of various systems of practical interest.

Chapter 8 Capacity of Rayleigh Fading Channels

8.1 Introduction

The radio spectrum available for wireless services is extremely scarce, while demand for these service is growing at a rapid pace [114]. Spectral efficiency is therefore of primary concern in the design of future wireless data communications systems. High overall spectral efficiency of a wireless cellular system may be achieved at several levels of the system design [2]:

- at the radio coverage planning level by minimizing cell area and the co-channel reuse distance.
- at the network/system level by using sophisticated channel allocation schemes that maximize the overall carried traffic.
- at the communication link level through a skillful combination of bandwidth efficient coding and modulation techniques.

In this chapter we focus on the link spectral efficiency, defined as the average transmitted data rate per unit bandwidth for a specified average transmit power and bit-error-rate (BER). Over the last three decades researchers have looked at various ways to improve the link spectral efficiency of wireless systems. In what follows, we first briefly summarize the major steps and progress achieved in that arena. We then present the objectives and outline of this chapter.

8.1.1 Spectral Efficiency over Fading Channels

Multilevel modulation schemes, such as M-QAM, increase link spectral efficiency by sending multiple bits per symbol [115]. Unfortunately, mobile radio links are subject to severe multipath fading due to the combination of randomly-delayed, reflected, scattered, and diffracted signal components [108]. Fading leads to serious degradation in the link carrier-to-noise ratio (CNR), resulting in either a higher BER or a higher required transmit power for a given multilevel modulation technique. Thus, fading compensation is typically required to improve link performance. One compensation technique, proposed by Sampei and Sunaga [116], uses pilot symbol assisted modulation (PSAM). This technique inserts a training sequence into the stream of M-QAM data symbols to extract the channel-induced attenuation and phase shift, which are then used for symbol detection. Space diversity, which combines signals received over several antenna branches, as discussed in previous chapters, is another powerful technique to combat fading [64]. Diversity can often be combined with other fading compensation methods to mitigate most of the fading degradation. For example, joint

use of PSAM and maximal-ratio combining (MRC) antenna diversity was proposed in [117], and field trials with this technique demonstrated considerable performance improvement over M-QAM without compensation [118, 119].

Other fading compensation techniques include an increased link budget margin or interleaving with channel coding [2]. However, these techniques are designed relative to the worst-case channel conditions, resulting in poor utilization of the full channel capacity a good percentage of the time (under negligible or shallow fading conditions). Adapting certain parameters of the transmitted signal to the channel fading leads to better utilization of the channel capacity. The concept of adaptive transmission, which requires accurate channel estimation at the receiver and a reliable feedback path between that estimator and the transmitter, was first proposed around the late sixties [120, 121, 122]. Interest in these techniques was short-lived, perhaps due to hardware constraints, lack of good channel estimation techniques, and/or systems focusing on point-to-point radio links without transmitter feedback. The fact that these issues are less constraining in current land mobile radio systems, coupled with the need for spectrally-efficient communication, has revived interest in adaptive modulation methods. The main idea behind these schemes is real-time balancing of the link budget through adaptive variation of the transmitted power level [120], symbol rate [121], constellation size [123, 124, 125], coding rate/scheme [126], or any combination of these parameters [122, 127, 128, 129, 130, 131, 132]. Thus, without sacrificing BER these schemes provide a much higher average spectral efficiency by taking advantage of the "time-varying" nature of the wireless channel: transmitting at high speeds under favorable channel conditions and responding to channel degradation through a smooth reduction of their data throughput. The performance of these schemes is further improved by combining them with space diversity [133]. The disadvantage of these adaptive techniques is that they require an accurate channel estimate at the transmitter, additional hardware complexity to implement adaptive transmission, and buffering/delay of the input data since the transmission rate varies with channel conditions.

8.1.2 Objective and Outline

The aim of this chapter is to investigate the theoretical spectral efficiency limits of adaptive modulation in Rayleigh fading channels. This fading channel model applies to land mobile radio channels without a line-of-sight path between the transmitter and receiver antennas, as well as to ionospheric [7] and tropospheric scatter [6] channels.

The Shannon capacity of a channel defines its theoretical upper bound for the maximum rate of data transmission at an arbitrarily small BER, without any delay or complexity constraints. Therefore, the Shannon capacity represents an optimistic bound for practical communication schemes, and also serves as a bench-mark against which to compare the spectral efficiency of all practical adaptive transmission schemes [132]. In [134] the capacity of a single-user flat-fading channel with

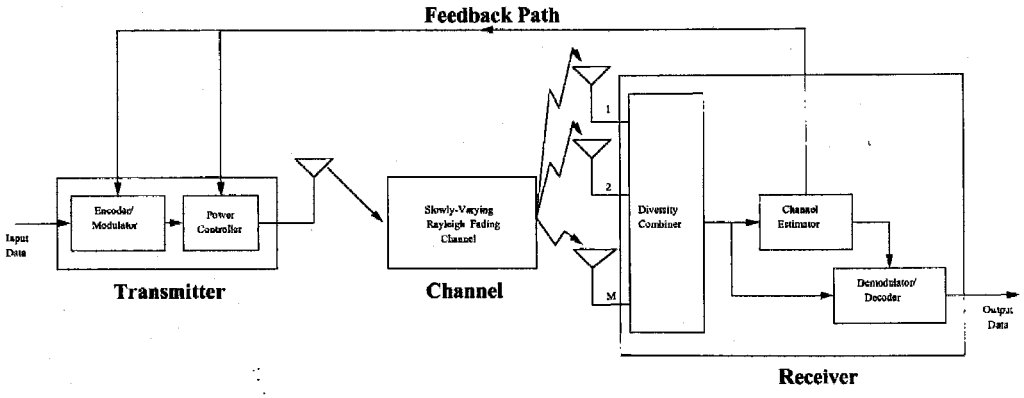

Figure 8.1: Transmission system block diagram.

channel measurement information at the transmitter and receiver was derived for various adaptive transmission policies. In this chapter, we apply the general theory developed in [134] to obtain closed-form expressions for the capacity of Rayleigh fading channels under different adaptive transmission and diversity-combining techniques. In particular, we consider three adaptation policies: optimal simultaneous power and rate adaptation, constant power with optimal rate adaptation, and channel inversion with fixed rate. We investigate the relative impact of MRC and selective combining (SC) diversity schemes in conjunction with each of these adaptive transmission schemes. Note that an analytical evaluation of the capacity in a Rayleigh fading environment with the constant power policy was carried out in [135, 136, 137]. We extend this analysis to derive closed-from expressions for capacity with MRC and SC, and compare it to the capacity of the other adaptive methods.

The remainder of this chapter is organized as follows. In Section 8.2 we outline the channel and communication system model. We derive the capacity of a Rayleigh fading channel (with and without diversity) for the optimal adaptation policy, constant power policy, and channel inversion policy in Sections 8.3, 8.4, and 8.5, respectively. In Section 8.6, we present some numerical examples comparing (i) the Rayleigh channel capacity with the capacity of an additive white Gaussian noise (AWGN) channel, and (ii) the Rayleigh channel capacity for the various adaptation policies and diversity-combining techniques under consideration. We review our main results and offer some concluding remarks in Section 8.7.

8.2 Channel and System Model

In this section, we describe the channel and communication system model. A block diagram of the transmission system is shown in Fig. 8.1.

We assume that the channel changes at a rate much slower than the data rate, so the channel remains constant over hundreds of symbols. We call this a slowly-varying channel. We assume a Rayleigh fading channel so that the probability distribution function (PDF) of CNR, γ, is given by

an exponential distribution (2.4)

$$p_\gamma(\gamma) = \frac{e^{-\gamma/\overline{\gamma}}}{\overline{\gamma}}, \qquad \gamma \geq 0, \tag{8.1}$$

where $\overline{\gamma}$ is the average received CNR.

We consider both MRC and SC diversity combining of the received signal. MRC diversity combining requires that the individual signals from each branch be weighted by their signal voltage to noise power ratios, then summed coherently [108, p. 316]. In our MRC analyses we assume perfect knowledge of the branch amplitudes and phases, which we call *perfect combining*. MRC with perfect combining is the optimal diversity scheme [108, p. 316], and therefore provides the maximum capacity improvement relative to all combining techniques. The disadvantage of MRC is that it requires knowledge of the branch parameters and independent processing of each branch. Let $\overline{\gamma}_k$ denote the average CNR on the kth branch. For independent branch signals and equal average branch CNR $\overline{\gamma}$:

$$\overline{\gamma}_k = \overline{\gamma} \quad \text{for all} \quad k \in \{1, 2, 3, .., M\}, \tag{8.2}$$

the PDF of the received CNR at the output of a perfect M-branch MRC combiner is a chi-square distribution with $2M$ degrees of freedom [108, (5.2-14), p. 319] given by

$$p_\gamma^{\text{mrc}}(\gamma) = \frac{\gamma^{M-1}\, e^{-\gamma/\overline{\gamma}}}{(M-1)!\, \overline{\gamma}^M}, \qquad \gamma \geq 0. \tag{8.3}$$

SC diversity only processes one of the diversity branches. Specifically, the combiner chooses the branch with the highest CNR [108, p. 313]. Thus, this diversity-combining technique is simpler than MRC, but also yields suboptimal performance. Since the output of the SC combiner is equal to the signal on one of the branches, the coherent sum of the individual branch signals is not required[1]. Assuming independent branch signals and equal average branch CNR (8.2), the PDF of the received CNR at the output of an M-branch SC combiner is given by [108, (5.2-7), p. 316]

$$p_\gamma^{\text{sc}}(\gamma) = \frac{M}{\overline{\gamma}}\, (1 - e^{-\gamma/\overline{\gamma}})^{M-1}\, e^{-\gamma/\overline{\gamma}}, \qquad \gamma \geq 0. \tag{8.4}$$

Note that using the binomial expansion, we can rewrite (8.4) as

$$p_\gamma^{\text{sc}}(\gamma) = \frac{M}{\overline{\gamma}} \sum_{k=0}^{M-1} (-1)^k \binom{M-1}{k} e^{-(1+k)\gamma/\overline{\gamma}}, \tag{8.5}$$

[1]The SC scheme can therefore be used in conjunction with differential modulation techniques, in contrast to MRC, which is restricted by design to coherent modulations.

where $\binom{M-1}{k}$ denotes the binomial coefficient given by

$$\binom{M-1}{k} = \frac{(M-1)!}{(M-k-1)!\,k!}. \tag{8.6}$$

We assume throughout our analyses that the variation in the combiner output CNR γ is tracked perfectly by the receiver. We also assume that the variation in γ is sent back to the transmitter via an error-free feedback path. The time delay in this feedback path is assumed to be negligible compared to the rate of the channel variation. All these assumptions, which are reasonable for high-speed data transmission over a slowly-fading channel, allow the transmitter to adapt its power and/or rate relative to the actual channel state.

8.3 Optimal Simultaneous Power and Rate Adaptation

Given an average transmit power constraint, the channel capacity of a fading channel with received CNR distribution $p_\gamma(\gamma)$ and optimal power and rate adaptation ($< C >_{\text{opra}}$ [Bit/Sec]) is given in [134] as

$$< C >_{\text{opra}} = B \int_{\gamma_o}^{+\infty} \log_2\left(\frac{\gamma}{\gamma_o}\right)\, p_\gamma(\gamma)\, d\gamma, \tag{8.7}$$

where B [Hz] is the channel bandwidth and γ_o is the optimal cutoff CNR level below which data transmission is suspended. This optimal cutoff must satisfy the equation

$$\int_{\gamma_o}^{+\infty} \left(\frac{1}{\gamma_o} - \frac{1}{\gamma}\right)\, p_\gamma(\gamma)\, d\gamma \;= 1. \tag{8.8}$$

To achieve the capacity (8.7), the channel fade level must be tracked at both the receiver and transmitter, and the transmitter has to adapt its power and rate accordingly, allocating high power levels and rates for good channel conditions (γ large), and lower power levels and rates for unfavorable channel conditions (γ small). Since no data is sent when $\gamma < \gamma_o$, the optimal policy suffers a probability of outage P_{out}, equal to the probability of no transmission, given by

$$P_{\text{out}} = P[\gamma \le \gamma_o] = \int_0^{\gamma_o} p_\gamma(\gamma)\, d\gamma = 1 - \int_{\gamma_o}^{+\infty} p_\gamma(\gamma)\, d\gamma. \tag{8.9}$$

We now obtain closed-form expressions for the optimal cutoff CNR γ_o, capacity $< C >_{\text{opra}}$, and outage probability P_{out} of this optimal adaptation technique with and without diversity combining. No numerical integrations are required, though numerical root finding is needed to find γ_o.

8.3.1 No Diversity

Substituting (8.1) in (8.8) we find that γ_o must satisfy

$$E_0\left(\frac{\gamma_o}{\bar{\gamma}}\right) - E_1\left(\frac{\gamma_o}{\bar{\gamma}}\right) = \bar{\gamma}, \tag{8.10}$$

where $E_n(x)$ is the exponential integral of order n defined by

$$E_n(x) = \int_1^{+\infty} t^{-n}\, e^{-\,xt}\, dt; \qquad x \geq 0. \tag{8.11}$$

In particular, $E_0(x) = e^{-x}/x$, so (8.10) reduces to

$$\frac{e^{-\gamma_o/\bar{\gamma}}}{\gamma_o/\bar{\gamma}} - E_1\left(\frac{\gamma_o}{\bar{\gamma}}\right) = \bar{\gamma}. \tag{8.12}$$

Let $x = \gamma_o/\bar{\gamma}$ and define

$$f(x) = \frac{e^{-x}}{x} - E_1(x) - \bar{\gamma}. \tag{8.13}$$

Note that $\frac{df(x)}{dx} = \frac{-e^{-x}}{x^2} < 0$ for all $x \geq 0$. Moreover, from (8.13), $\lim_{x\to 0+} f(x) = +\infty$ and $\lim_{x\to+\infty} f(x) = -\bar{\gamma} < 0$. Thus we conclude that there is a unique x_o for which $f(x_o) = 0$ or, equivalently, there is a unique γ_o which satisfies (8.12). An asymptotic expansion of (8.12) shows that as $\bar{\gamma} \to +\infty$, $\gamma_o \to 1$. Our numerical results show that γ_o increases as $\bar{\gamma}$ increases, so γ_o always lies in the interval [0,1].

Substituting (8.1) in (8.7), and defining the integral $\mathcal{J}_n(\mu)$ as

$$\mathcal{J}_n(\mu) = \int_1^{+\infty} t^{n-1}\, \ln t\, e^{-\mu\, t}\, dt; \qquad \mu > 0;\ n = 1, 2, ..., \tag{8.14}$$

we can rewrite the channel capacity $<C>_{\text{opra}}$ as

$$<C>_{\text{opra}} = B\, \log_2(e)\, \frac{\gamma_o}{\bar{\gamma}}\, \mathcal{J}_1\left(\frac{\gamma_o}{\bar{\gamma}}\right). \tag{8.15}$$

The evaluation of $\mathcal{J}_1(\mu)$ is derived in Appendix A and given in (8.71). Using that result we obtain the capacity per unit bandwidth $<C>_{\text{opra}}/B$ [Bits/Sec/Hz] as

$$\frac{<C>_{\text{opra}}}{B} = \log_2(e)\, E_1\left(\frac{\gamma_o}{\bar{\gamma}}\right). \tag{8.16}$$

Using (8.12) in (8.16), the optimal capacity per unit bandwidth reduces to the simple expression

$$\frac{<C>_{\text{opra}}}{B} = \log_2(e)\, \left(\frac{e^{-\gamma_o/\bar{\gamma}}}{\gamma_o/\bar{\gamma}} - \bar{\gamma}\right). \tag{8.17}$$

Using (8.1) in the probability of outage equation (8.9) yields

$$P_{\text{out}} = 1 - e^{-\gamma_o/\overline{\gamma}}. \tag{8.18}$$

8.3.2 Maximal-Ratio Combining

Inserting the CNR distribution (8.3) in (8.8), we see that with MRC combining γ_o must satisfy

$$\frac{\Gamma\left(M, \frac{\gamma_o}{\overline{\gamma}}\right)}{\frac{\gamma_o}{\overline{\gamma}}} - \Gamma\left(M-1, \frac{\gamma_o}{\overline{\gamma}}\right) = (M-1)!\,\overline{\gamma}, \tag{8.19}$$

where $\Gamma(.,.)$ is the complementary incomplete gamma function defined in (8.65). Let $x = \gamma_o/\overline{\gamma}$ and define

$$f_{\text{mrc}}(x) = \frac{\Gamma(M,x)}{x} - \Gamma(M-1,x) - (M-1)!\,\overline{\gamma}. \tag{8.20}$$

Note that $\frac{df_{\text{mrc}}(x)}{dx} = \frac{-\Gamma(M,x)}{x^2} < 0$ for all $x \geq 0$ and $M \geq 2$. Since $\lim_{x\to 0^+} f_{\text{mrc}}(x) = +\infty$ and $\lim_{x\to+\infty} f_{\text{mrc}}(x) = -(M-1)!\,\overline{\gamma} < 0$ we conclude that there is a unique x_o such that $f_{\text{mrc}}(x_o) = 0$ or, equivalently, there is a unique γ_o which satisfies (8.19). An asymptotic expansion on (8.19) shows that $\gamma_o \to 1$ as $\overline{\gamma} \to +\infty$, so $\gamma_o \in [0,1]$. Comparing this with the results in Section 8.3.1, we see that as the average received CNR grows to infinity, the optimal cutoff value is the same for both diversity methods.

Substituting (8.3) in (8.7) we obtain the channel capacity with MRC diversity, $< C >^{\text{mrc}}_{\text{opra}}$ [Bits/Sec], in terms of the integral $\mathcal{J}_M(.)$ as

$$<C>^{\text{mrc}}_{\text{opra}} = \frac{B\,\log_2(e)}{(M-1)!}\left(\frac{\gamma_o}{\overline{\gamma}}\right)^M \mathcal{J}_M\left(\frac{\gamma_o}{\overline{\gamma}}\right). \tag{8.21}$$

The evaluation of $\mathcal{J}_n(\mu)$ is derived in Appendix A and given in (8.70). Using this result we obtain the capacity per unit bandwidth $<C>^{\text{mrc}}_{\text{opra}}/B$ [Bits/Sec/Hz] as

$$\frac{<C>^{\text{mrc}}_{\text{opra}}}{B} = \log_2(e)\left(E_1(\gamma_o/\overline{\gamma}) + \sum_{k=1}^{M-1}\frac{\mathcal{P}_k(\gamma_o/\overline{\gamma})}{k}\right), \tag{8.22}$$

where $\mathcal{P}_k(.)$ denotes the Poisson distribution defined in (8.67). The corresponding probability of outage $P^{\text{mrc}}_{\text{out}}$ is obtained by substituting (8.3) into (8.9), and using [53, (8.381.3), p. 364] and (8.66):

$$P^{\text{mrc}}_{\text{out}} = 1 - \mathcal{P}_M(\gamma_o/\overline{\gamma}). \tag{8.23}$$

8.3.3 Selective Combining

Substituting the CNR distribution (8.5) into (8.8) we find that γ_o must satisfy

$$\sum_{k=0}^{M-1}(-1)^k \binom{M-1}{k} \left(\frac{e^{-(1+k)\gamma_o/\overline{\gamma}}}{(1+k)\gamma_o/\overline{\gamma}} - E_1((1+k)\gamma_o/\overline{\gamma})\right) = \overline{\gamma}/M. \tag{8.24}$$

Let $x = \gamma_o/\overline{\gamma}$ and define

$$f_{\rm sc}(x) = \sum_{k=0}^{M-1}(-1)^k \binom{M-1}{k} \left(\frac{e^{-(1+k)x}}{(1+k)x} - E_1((1+k)x)\right) - \overline{\gamma}/M. \tag{8.25}$$

Note that $\frac{df_{\rm sc}(x)}{dx} = -\sum_{k=0}^{M-1} a_k(x)$, where $a_k(x) = (-1)^k \binom{M-1}{k} \frac{e^{-(1+k)x}}{(1+k)^2\, x^2}$. Since $a_0(x) = e^{-x}/x^2 > 0$ and, for all $k \leq M$, $|a_{k+1}(x)| < |a_k(x)|$ we have $\frac{df_{\rm sc}(x)}{dx} < 0$ for all $x \geq 0$. Moreover, from (8.25), $\lim_{x\to 0+} f_{\rm sc}(x) = +\infty$ and $\lim_{x\to+\infty} f_{\rm sc}(x) = -\overline{\gamma}/M < 0$. Thus we conclude that there is a unique x_o for which $f_{\rm sc}(x_o) = 0$ or, equivalently, there is a unique γ_o which satisfies (8.24). An asymptotic expansion of (8.24) shows that as $\overline{\gamma} \to +\infty$, $\gamma_o \to 1$. Therefore, as in the no diversity and MRC diversity cases, γ_o always lies in the interval [0,1].

Inserting (8.5) into (8.7), we can express the channel capacity with SC diversity, $< C >^{\rm sc}_{\rm opra}$ [Bits/Sec], in terms of the integral $\mathcal{J}_1(.)$ as

$$< C >^{\rm sc}_{\rm opra} = B\ M\ \log_2(e)\ \frac{\gamma_o}{\overline{\gamma}} \sum_{k=0}^{M-1}(-1)^k \binom{M-1}{k} \mathcal{J}_1\left(\frac{(1+k)\ \gamma_o}{\overline{\gamma}}\right). \tag{8.26}$$

Using (8.71) from Appendix A, we obtain the capacity per unit bandwidth, $< C >^{\rm sc}_{\rm opra}/B$ [Bits/Sec/Hz], as

$$\frac{< C >^{\rm sc}_{\rm opra}}{B} = M\ \log_2(e) \sum_{k=0}^{M-1}(-1)^k \binom{M-1}{k} \frac{E_1((1+k)\ \gamma_o/\overline{\gamma})}{1+k}. \tag{8.27}$$

The corresponding probability of outage $P^{\rm sc}_{\rm out}$ is obtained by substituting (8.5) into (8.9):

$$P^{\rm sc}_{\rm out} = 1 - M \sum_{k=0}^{M-1}(-1)^k \binom{M-1}{k} \frac{e^{-(1+k)\gamma_o/\overline{\gamma}}}{1+k}. \tag{8.28}$$

We see from (8.28) that as $\overline{\gamma}$ tends to infinity (and γ_o tends to 1), $P^{\rm sc}_{\rm out}$ tends to zero, as expected. Similarly, we can also see from (8.28) that as γ_o tends to zero (i.e., total channel inversion), $P^{\rm sc}_{\rm out}$ tends to zero.

8.4 Optimal Rate Adaptation with Constant Transmit Power

With optimal rate adaptation to channel fading and a constant transmit power, the channel capacity $<C>_{\text{ora}}$ [Bits/Sec] becomes [134, 138],

$$<C>_{\text{ora}} = B \int_0^{+\infty} \log_2(1+\gamma)\, p_\gamma(\gamma)\, d\gamma. \tag{8.29}$$

$< C >_{\text{ora}}$ was previously introduced by Lee [135] as the average channel capacity of a flat-fading channel, since it is obtained by averaging the capacity of an AWGN channel

$$C_{\text{awgn}} = B\ \log_2(1+\gamma), \tag{8.30}$$

over the distribution of the received CNR γ. In fact, (8.29) represents the capacity of the fading channel without transmitter feedback (i.e., with the channel fade level known at the receiver only) [136, 139, 140], under some mild regularity conditions on the fading process. In the following analysis, we first obtain the channel capacity without diversity (correcting some minor errors in [135]), and then derive analytical expressions as well as simple accurate asymptotic approximations of the capacity improvement with both MRC and SC diversity.

8.4.1 No Diversity

Substituting (8.1) into (8.29), the channel capacity $<C>_{\text{ora}}$ of a Rayleigh fading channel is obtained as

$$<C>_{\text{ora}} = \int_0^{+\infty} B\ \log_2(1+\gamma)\ \frac{e^{-\gamma/\overline{\gamma}}}{\overline{\gamma}}\ d\gamma. \tag{8.31}$$

Defining the integral $\mathcal{I}_n(\mu)$ as:

$$\mathcal{I}_n(\mu) = \int_0^{+\infty} t^{n-1}\ \ln(1+t)\ e^{-\mu\, t}\ dt; \qquad \mu > 0;\ n = 1, 2, ..., \tag{8.32}$$

we can rewrite $<C>_{\text{ora}}$ as

$$<C>_{\text{ora}} = B\ \log_2(e)\ \frac{\mathcal{I}_1(1/\overline{\gamma})}{\overline{\gamma}}. \tag{8.33}$$

Using the result of (8.80) from Appendix B, we can write $<C>_{\text{ora}}\ /B$ [Bits/Sec/Hz] as

$$\frac{<C>_{\text{ora}}}{B} = \log_2(e)\ e^{1/\overline{\gamma}}\ E_1(1/\overline{\gamma}). \tag{8.34}$$

Note that the exponential-integral function of first order, $E_1(.)$, is related to the exponential-integral function, $E_i(.)$, used in [135] by $E_1(x) = -E_i(-x)$.

Using the first series expansion for $E_1(.)$ [135, (6)], and substituting it into (8.34), yields

$$\frac{<C>_{\text{ora}}}{B} = \log_2(e)\ e^{1/\overline{\gamma}} \left(-E + \ln \overline{\gamma} - \sum_{k=1}^{+\infty} \frac{(-1/\overline{\gamma})^k}{k \cdot k!} \right), \tag{8.35}$$

where E is the Euler constant ($E = 0.577215665$). Therefore, for $\overline{\gamma} >> 1$, we get the following approximation for (8.34):

$$\frac{<C>_{\text{ora}}}{B} \simeq \log_2(e)\ e^{1/\overline{\gamma}} \left(-E + \ln \overline{\gamma} + \frac{1}{\overline{\gamma}} \right). \tag{8.36}$$

Using the second series expansion for $E_1(.)$ given by [135, (7)] and substituting it in (8.34) yields

$$<C>_{\text{ora}} = \ B\ \log_2(e)\ \sum_{k=1}^{n} (-1)^{(k+1)}\ (k-1)!\ \overline{\gamma}^k + R_n, \tag{8.37}$$

where R_n is a remainder term. Taking the limit as the channel bandwidth approaches infinity yields

$$\lim_{B \to +\infty} <C>_{\text{ora}} = \ \log_2(e)\ \frac{<S>}{N_o}, \tag{8.38}$$

where $< S >$ [W] is the average carrier power and N_o [W/Hz] is the noise density power per unit bandwidth[2].

8.4.2 Maximal-Ratio Combining

Substituting (8.3) into (8.29), we obtain the channel capacity $< C >_{\text{ora}}^{\text{mrc}}$ [Bits/Sec] with MRC in terms of the integral $\mathcal{I}_M(.)$ as

$$<C>_{\text{ora}}^{\text{mrc}} = B\ \log_2(e)\ \frac{\mathcal{I}_M(1/\overline{\gamma})}{(M-1)!\ \overline{\gamma}^M}. \tag{8.39}$$

Using (8.78) from Appendix B, we can rewrite $<C>_{\text{ora}}^{\text{mrc}}/B$ [Bits/Sec/Hz] as

$$\frac{<C>_{\text{ora}}^{\text{mrc}}}{B} = \log_2(e)\ e^{1/\overline{\gamma}} \sum_{k=0}^{M-1} \frac{\Gamma(-k, 1/\overline{\gamma})}{\overline{\gamma}^k}, \tag{8.40}$$

where $\Gamma(.,.)$ is the complementary incomplete gamma function defined in (8.65). Note that by using [53, (8.359.1), p. 951], the capacity with the MRC diversity scheme (8.40) with a single branch ($M = 1$) reduces to (8.34), as expected. Note also that by using [53, (8.352.3), p. 950] and

[2] In [135], the average CNR $\overline{\gamma}$ is denoted by Γ. Note the typo error in [135, (4)] (γ instead of Γ in the denominator), and the resulting sign difference in the argument of the exponential term $e^{1/\overline{\gamma}}$ between our result (8.34) and [135, (5)], and between (8.36) and [135, (9)]. There is also a sign difference between (8.37) and [135, (10)]. However, the limit (8.38) matches the limiting expression [135, (11)], so the sign error in [135, (10)] was corrected in the limit.

[53, (8.359.1), p. 951], one may express (8.40) in terms of the Poisson distribution as [137, (7)]:

$$\frac{<C>_{\text{ora}}^{\text{mrc}}}{B} = \log_2(e) \left(\mathcal{P}_M(-1/\overline{\gamma})\ E_1(1/\overline{\gamma}) + \sum_{k=1}^{M-1} \frac{\mathcal{P}_k(1/\overline{\gamma})\ \mathcal{P}_{M-k}(-1/\overline{\gamma})}{k} \right). \tag{8.41}$$

Moreover, using the first series expansion for $E_1(.)$ [135, (6)] in (8.41) we obtain an asymptotic approximation ($\overline{\gamma} >> 1$) for $<C>_{\text{ora}}^{\text{mrc}}/B$ as

$$\frac{<C>_{\text{ora}}^{\text{mrc}}}{B} \simeq \log_2(e) \left(\mathcal{P}_M(-1/\overline{\gamma}) \left(-E + \ln \overline{\gamma} + \frac{1}{\overline{\gamma}} \right) + \sum_{k=1}^{M-1} \frac{\mathcal{P}_k(1/\overline{\gamma})\ \mathcal{P}_{M-k}(-1/\overline{\gamma})}{k} \right). \tag{8.42}$$

Fig. 8.5 compares plots of (8.40) with its asymptotic approximation (8.42) and the results are discussed in Section 8.6.1.

8.4.3 Selective Combining

Substituting (8.5) into (8.29), we obtain the channel capacity $<C>_{\text{ora}}^{\text{sc}}$ [Bits/Sec] with SC in terms of the integral $\mathcal{I}_1(.)$ as

$$<C>_{\text{ora}}^{\text{sc}} = \frac{B\ M}{\overline{\gamma}}\ \log_2(e) \sum_{k=0}^{M-1} (-1)^k \binom{M-1}{k} \mathcal{I}_1\left(\frac{1+k}{\overline{\gamma}} \right). \tag{8.43}$$

Then, using (8.80) from Appendix B, we can write $<C>_{\text{ora}}^{\text{sc}}/B$ [Bits/Sec/Hz] as

$$\frac{<C>_{\text{ora}}^{\text{sc}}}{B} = M\ \log_2(e) \sum_{k=0}^{M-1} (-1)^k \binom{M-1}{k} e^{(k+1)/\overline{\gamma}}\ \frac{E_1\left((1+k)/\overline{\gamma}\right)}{1+k}. \tag{8.44}$$

We again note that for a single branch ($M = 1$), (8.44) reduces to (8.34) as expected.

Using the first series expansion for $E_1(.)$ [135, (6)] and substituting it into (8.44) yields a simple asymptotic approximation ($\overline{\gamma} >> 1$) for $<C>_{\text{ora}}^{\text{sc}}/B$ given by

$$\frac{<C>_{\text{ora}}^{\text{sc}}}{B} \simeq M\ \log_2(e) \sum_{k=0}^{M-1} \frac{(-1)^{k+1}}{1+k} \binom{M-1}{k} e^{(1+k)/\overline{\gamma}} \left[E + \ln\left(\frac{1+k}{\overline{\gamma}} \right) - \left(\frac{1+k}{\overline{\gamma}} \right) \right]. \tag{8.45}$$

Fig. 8.6 compares plots of (8.44) with its asymptotic approximation (8.45) and the results are discussed in Section 8.6.1.

8.5 Channel Inversion with Fixed Rate

The channel capacity when the transmitter adapts its power to maintain a constant CNR at the receiver (i.e., inverts the channel fading) was also investigated in [134]. This technique uses fixed-rate

modulation and a fixed code design, since the channel after channel inversion appears as a time-invariant AWGN channel. As a result, channel inversion with fixed rate is the least complex technique to implement, assuming good channel estimates are available at the transmitter and receiver. The channel capacity with this technique ($<C>_{\text{cifr}}$ [Bits/Sec]) is derived from the capacity of an AWGN channel and is given in [134] as

$$<C>_{\text{cifr}} = B \log_2 \left(1 + \frac{1}{\int_0^{+\infty} p_\gamma(\gamma)/\gamma \, d\gamma}\right). \tag{8.46}$$

Channel inversion with fixed rate suffers a large capacity penalty relative to the other techniques, since a large amount of the transmitted power is required to compensate for the deep channel fades. A better approach is to use a modified inversion policy which inverts the channel fading only above a fixed cutoff fade depth γ_o. The capacity with this truncated channel inversion and fixed rate policy ($<C>_{\text{tifr}}$ [Bits/Sec]) was derived in [134] to be

$$<C>_{\text{tifr}} = B \log_2 \left(1 + \frac{1}{\int_{\gamma_o}^{+\infty} p_\gamma(\gamma)/\gamma \, d\gamma}\right) (1 - P_{\text{out}}), \tag{8.47}$$

where P_{out} is given by (8.9). The cutoff level γ_o can be selected to achieve a specified outage probability or, alternatively, to maximize (8.47). The choice of γ_o is examined in more detail in the following subsections.

We now derive closed-form expressions for the capacity under channel inversion with the different diversity combining techniques.

8.5.1 No Diversity

By substituting the CNR distribution (8.1) in (8.46), we find that the capacity of a Rayleigh fading channel with total channel inversion, $<C>_{\text{cifr}}$, is zero. However, with truncated channel inversion the capacity per unit bandwidth $<C>_{\text{tifr}}/B$ [Bits/Sec/Hz] can be expressed in terms of $\overline{\gamma}$ and γ_o as

$$\frac{<C>_{\text{tifr}}}{B} = \log_2 \left(1 + \frac{\overline{\gamma}}{E_1(\gamma_o/\overline{\gamma})}\right) e^{-\gamma_o/\overline{\gamma}}. \tag{8.48}$$

Fig. 8.2 shows the dependence of $<C>_{\text{tifr}}/B$ on γ_o for different $\overline{\gamma}$ values. All these curves show that capacity is maximized for an optimal cutoff CNR γ_o^* which increases as a function of $\overline{\gamma}$. Recall that we proved the existence of a unique optimal cutoff CNR for the optimal adaptation policy in Section 8.3.1. However, for optimal adaptation the optimal cutoff CNR γ_o was always bounded between [0,1] (i.e., smaller than 0 dB), whereas for this policy γ_o^* is bigger than 0 dB when $\overline{\gamma} > 5$ dB. This means that, for a fixed $\overline{\gamma}$, truncated channel inversion has both a smaller capacity (see Fig. 8.9) and a higher probability of outage (see Fig. 8.10) than the optimal policy of Section 8.3.

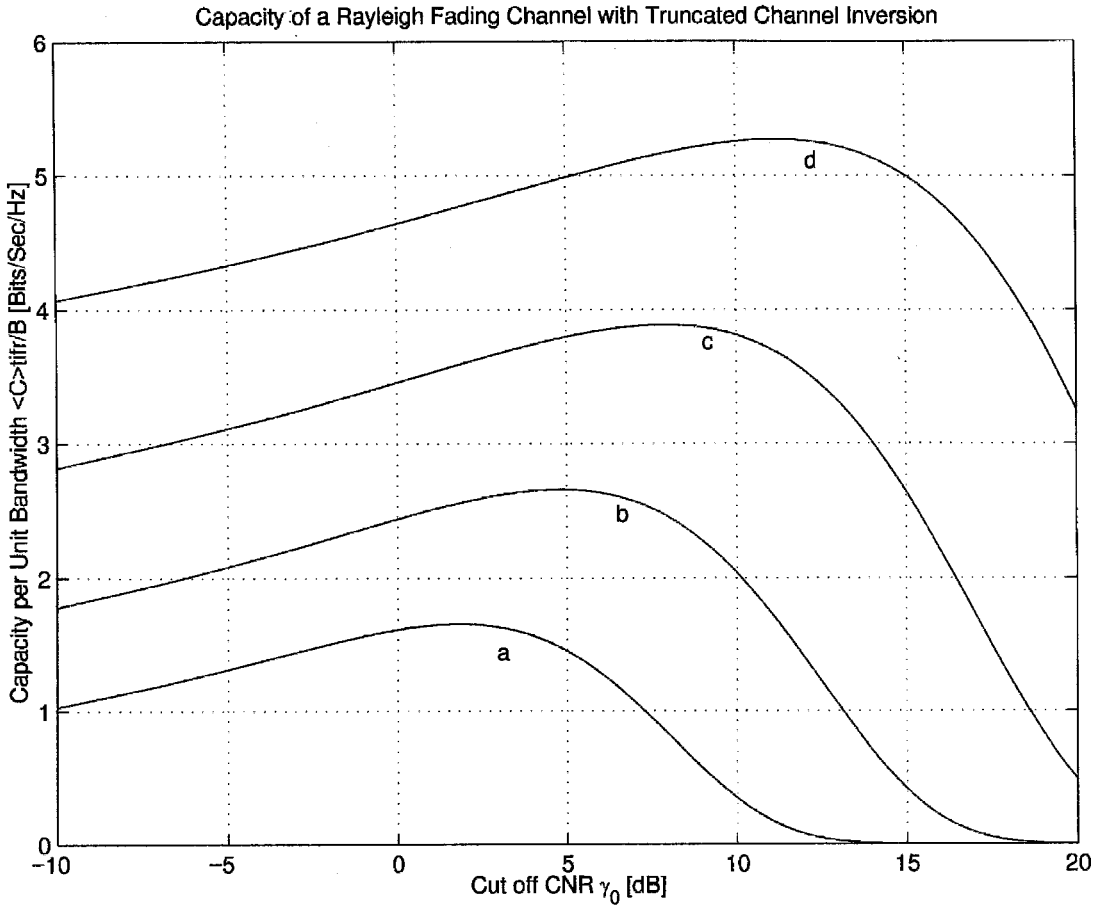

Figure 8.2: Channel capacity per unit bandwidth for a Raleigh fading channel versus cut off CNR γ_o with truncated channel inversion and $\overline{\gamma}$ = (a) 5 dB, (b) 10 dB, (c) 15 dB, and (d) 20 dB.

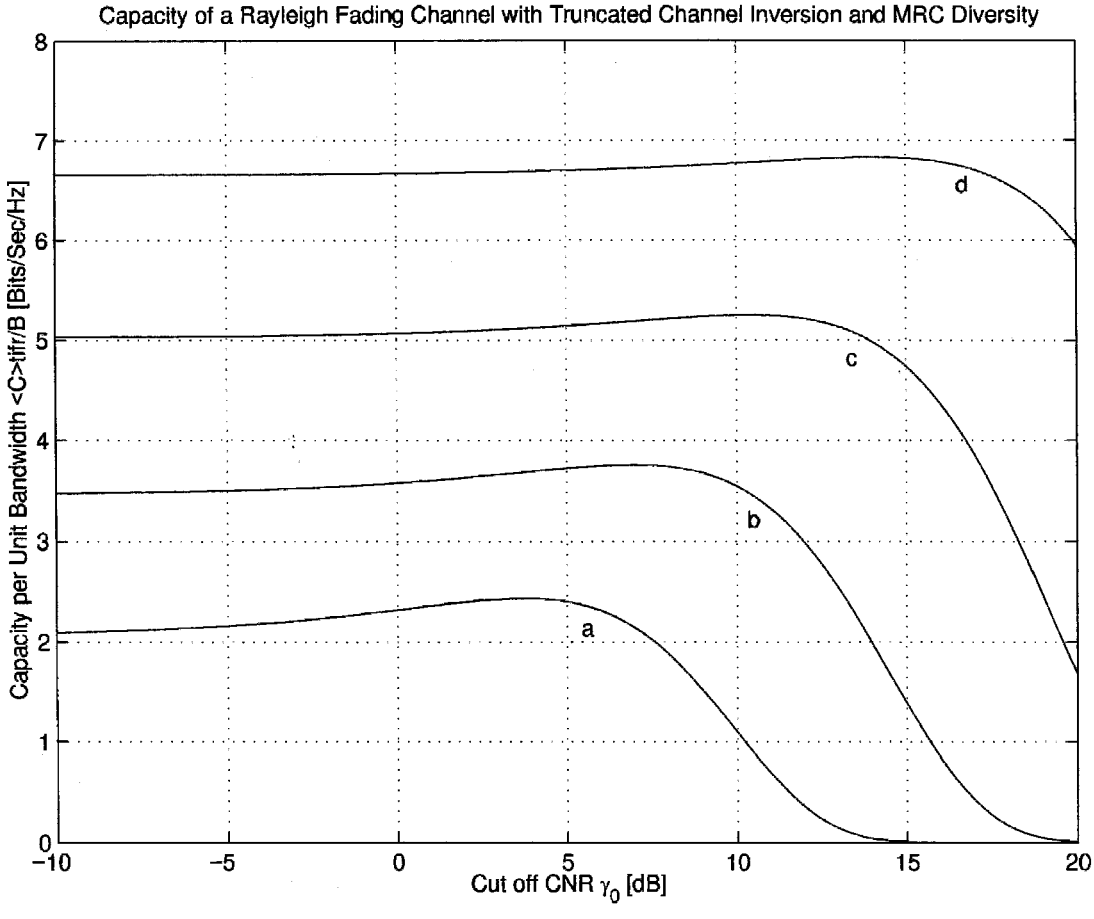

Figure 8.3: Channel capacity per unit bandwidth for a Raleigh fading channel versus cut off CNR γ_o with truncated channel inversion, MRC diversity ($M = 2$), and $\overline{\gamma}$ = (a) 5 dB, (b) 10 dB, (c) 15 dB, and (d) 20 dB.

8.5.2 Maximal-Ratio Combining

We obtain the capacity per unit bandwidth for total channel inversion with MRC diversity combining, $<C>_{\text{cifr}}^{\text{mrc}}$, by substituting (8.3) into (8.46) and using [53, (3.381.4), p. 364]:

$$\frac{<C>_{\text{cifr}}^{\text{mrc}}}{B} = \log_2(1 + (M-1)\,\overline{\gamma}). \tag{8.49}$$

Note that the capacity of this policy for a Rayleigh fading channel with an M-branch perfect MRC combiner (8.49) is the same as the capacity of a set of $M-1$ parallel, independent AWGN channels [141, (15)].

Truncated channel inversion improves the capacity (8.49) at the expense of outage probability $P_{\text{out}}^{\text{mrc}}$. The capacity of truncated channel inversion with MRC combining, $<C>_{\text{tifr}}^{\text{mrc}}$, is obtained by inserting (8.3) in (8.47) and using [53, (3.381.3), p. 364]:

$$\frac{<C>_{\text{tifr}}^{\text{mrc}}}{B} = \log_2\left(1 + \frac{(M-1)!\,\overline{\gamma}}{\Gamma(M-1, \gamma_o/\overline{\gamma})}\right) \frac{\Gamma(M, \gamma_o/\overline{\gamma})}{(M-1)!}. \tag{8.50}$$

Using property (8.66) of the complementary incomplete gamma function, we can rewrite (8.50) as the simple expression

$$\frac{<C>_{\text{tifr}}^{\text{mrc}}}{B} = \log_2\left(1 + \frac{(M-1)\,\overline{\gamma}}{\mathcal{P}_{M-1}(\gamma_o/\overline{\gamma})}\right) \mathcal{P}_M(\gamma_o/\overline{\gamma}), \qquad M \geq 2. \tag{8.51}$$

Fig. 8.3 shows the dependence of $<C>_{\text{tifr}}^{\text{mrc}}/B$ on γ_o at different $\overline{\gamma}$ values for 2-branch MRC diversity. Comparing Fig. 8.2 and Fig. 8.3 we see that, for a fixed $\overline{\gamma}$, the maximizing cutoff CNR γ_o^* increases when MRC diversity is used. In addition, the relative flatness of the curves in Fig. 8.3 for $\gamma_o < \gamma_o^*$ indicates that the capacity improvement provided by truncated channel inversion ($\gamma_o = \gamma_o^*$) compared to total channel inversion ($\gamma_o = 0$) is relatively small, and this little improvement comes at the expense of a higher probability of outage (see Fig. 8.12). This suggests that, as long as diversity is used, total channel inversion is a better alternative than truncated channel inversion.

8.5.3 Selective Combining

We obtain the the capacity per unit bandwidth of a Rayleigh fading channel with total channel inversion and SC diversity, $<C>_{\text{cifr}}^{\text{sc}}$, by substituting (8.5) in (8.46),

$$\frac{<C>_{\text{cifr}}^{\text{sc}}}{B} = \log_2\left(1 + \frac{\overline{\gamma}}{M\ \lim_{u\to 0^+} \sum_{k=0}^{M-1}(-1)^k \binom{M-1}{k} E_1\left((1+k)\,u/\overline{\gamma}\right)}\right). \tag{8.52}$$

When truncated channel inversion is used in combination with SC, the capacity per unit bandwidth becomes

$$\frac{<C>_{\text{tifr}}^{\text{sc}}}{B} = \log_2\left(1 + \frac{\overline{\gamma}}{M\ \sum_{k=0}^{M-1}(-1)^k\ \binom{M-1}{k}\ E_1\left((1+k)\ \gamma_o/\overline{\gamma}\right)}\right)\ (1 - P_{\text{out}}^{\text{sc}}). \tag{8.53}$$

Recall that $P_{\text{out}}^{\text{sc}}$ tends to zero as γ_o tends to 0 (i.e., total channel inversion). Hence, as expected, we see that (8.53) reduces to (8.52) when γ_o tends to zero.

8.6 Numerical Results and Comparisons

In this section, we start by comparing the capacity of an AWGN channel (C_{awgn}) with the capacity of a Rayleigh channel with optimal rate adaptation, $<C>_{\text{ora}}$, constant transmit power, and various diversity-combining techniques. We then compare the Rayleigh channel capacities for the various adaptation policies and diversity-combining techniques.

8.6.1 Comparison with AWGN Channel Capacity

In Fig. 8.4, channel capacity without diversity, $<C>_{\text{ora}}$, given by (8.34), as well as its asymptotic approximation (8.36), are plotted against $\overline{\gamma}$. This figure also displays the capacity per unit bandwidth of an AWGN channel, C_{awgn} (8.30). With these results we find, for example, that

- For $\overline{\gamma} = 10$ dB, $<C>_{\text{ora}} \simeq 2.91\ B$, whereas $C_{\text{awgn}} \simeq 3.46\ B$.
- For $\overline{\gamma} = 25$ dB, $<C>_{\text{ora}} \simeq 7.50\ B$, whereas $C_{\text{awgn}} \simeq 8.31\ B$.

Therefore, the channel capacity of a Rayleigh fading channel is reduced by 15.9% for $\overline{\gamma} = 10$ dB and by 9.75% for $\overline{\gamma} = 25$ dB[3]. Note in Fig. 8.4 that the asymptotic approximation (8.36) closely matches the exact average capacity (8.34) when $\overline{\gamma} > 5$ dB.

Fig. 8.5 shows plots of $<C>_{\text{ora}}^{\text{mrc}}/B$ (8.40) as well as its asymptotic approximation (8.42) as functions of the average CNR *per branch*, $\overline{\gamma}$, for various values of M. We use the CNR per branch for this comparison so that we can later compare the improvements provided by MRC and SC diversity schemes on a fair basis, as we will explain in more detail below. Note the large diversity gain obtained by two-branch combining: the capacity with two branches in fading exceeds that of a single branch AWGN channel. Fig. 8.5 also displays the capacity per unit bandwidth of an array of M independent AWGN channels with optimal combining (MRC) [141, (15)]:

$$\frac{C_{\text{awgn}}^{\text{mrc}}}{B} = \log_2(1 + M\ \gamma). \tag{8.54}$$

[3]These results correct the 32% and 11% values reported in [135]. Moreover, from Fig. 8.4, note that a smaller value of $\overline{\gamma}$ results in a smaller difference between C_{awgn} and $<C>_{\text{ora}}$, contrary to what was concluded in [135].

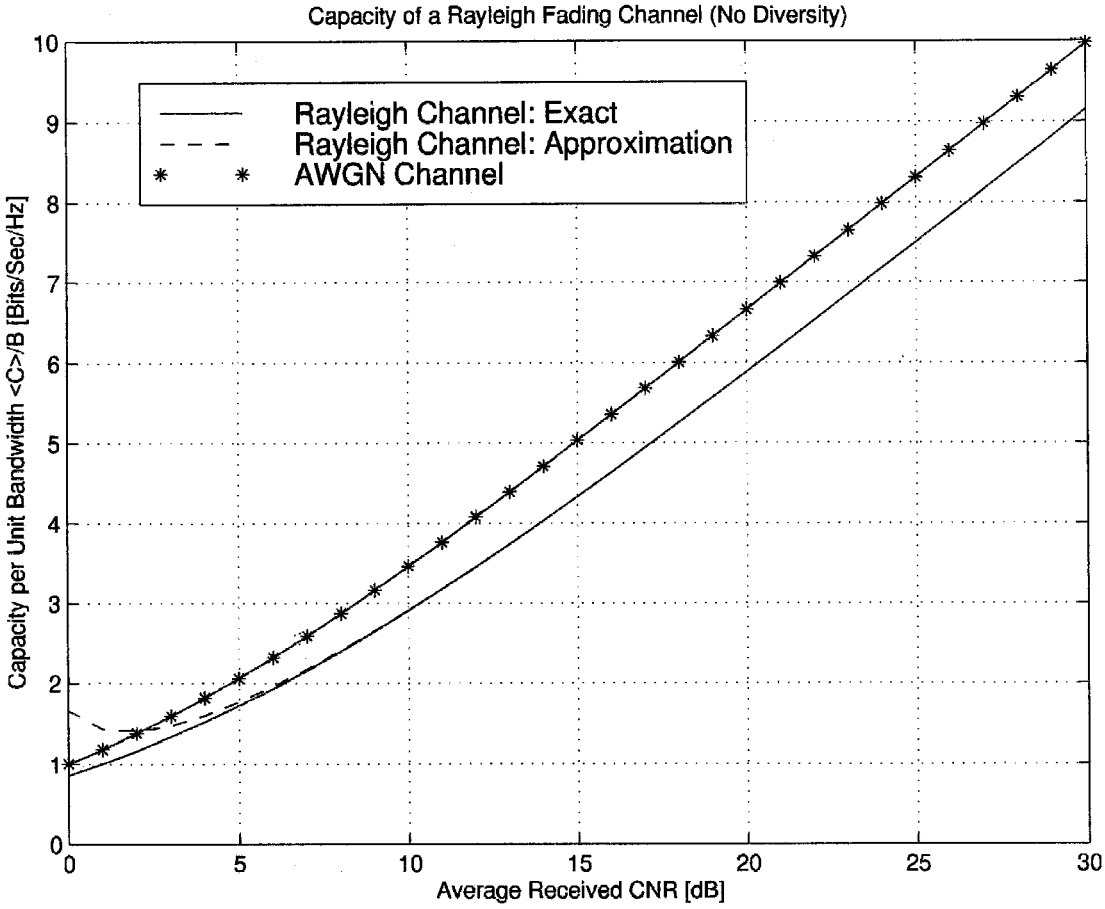

Figure 8.4: Average channel capacity per unit bandwidth for a Raleigh fading and an AWGN channel versus average carrier-to-noise ratio $\overline{\gamma}$ (with no diversity).

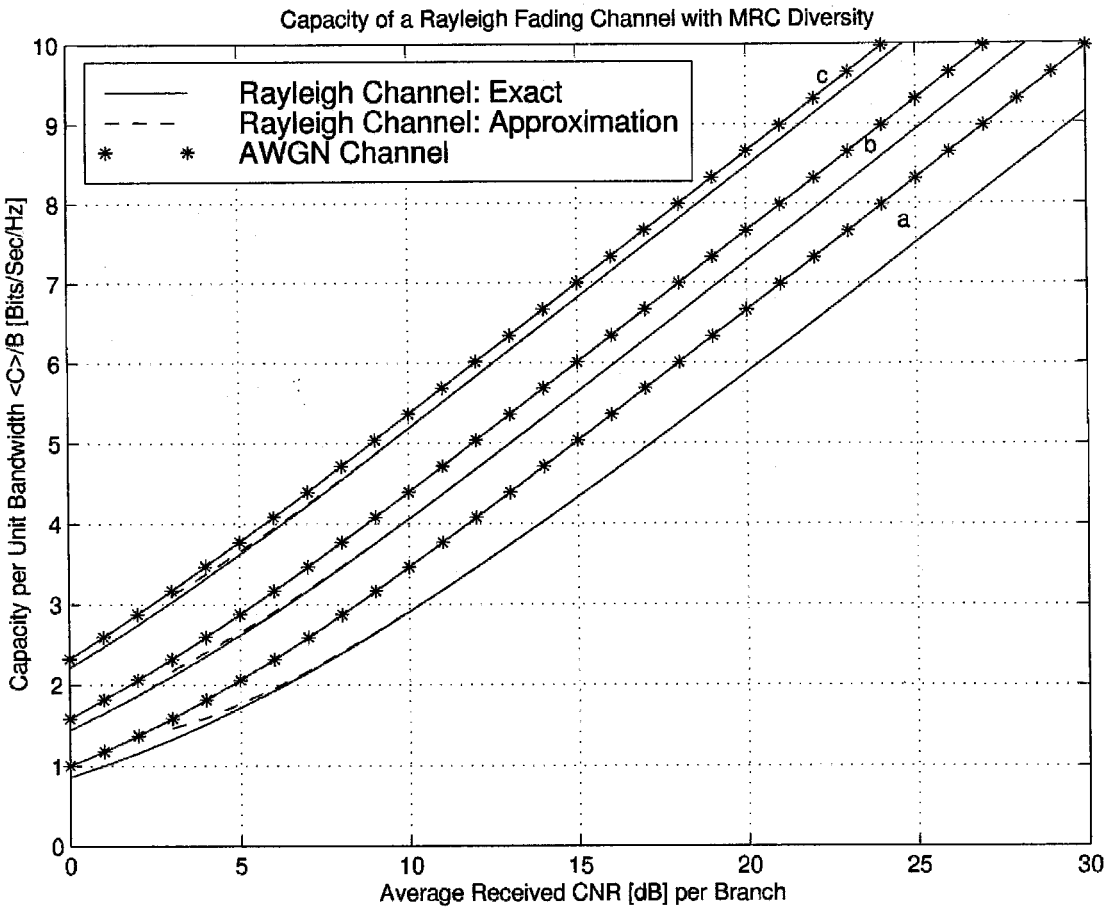

Figure 8.5: Average channel capacity per unit bandwidth for a Raleigh fading channel with maximal-ratio combining diversity versus average CNR per branch $\overline{\gamma}$ ((a) $M = 1$, (b) $M = 2$, and (c) $M = 4$).

Note that the capacity of an array of M independent Rayleigh channels with MRC combining approaches the capacity of an array of M independent AWGN channels as M tends to infinity. Note also the diminishing capacity returns that are obtained as the number of branch increases. This diminishing returns characteristic is also exhibited when the performance evaluation is based on outage probabilities [108]. Finally, note again that the asymptotic approximation (8.42) closely matches the exact average capacity (8.40) when $\overline{\gamma} > 5$ dB.

Fig. 8.6 shows plots of $< C >_{\text{ora}}^{\text{sc}} / B$ (8.44) as well as its asymptotic approximation (8.45) as function of the average CNR per branch $\overline{\gamma}$ for various values of M. Comparing Fig. 8.5 and Fig. 8.6 we see that, as expected, the SC scheme provides less diversity gain and a lower rate of improvement than the MRC scheme. However, the greatest improvement is still obtained in going from a single-branch to two-branch combining, which again yields a higher capacity than that of a single branch AWGN channel. Fig. 8.6 also displays the capacity per unit bandwidth of an array of

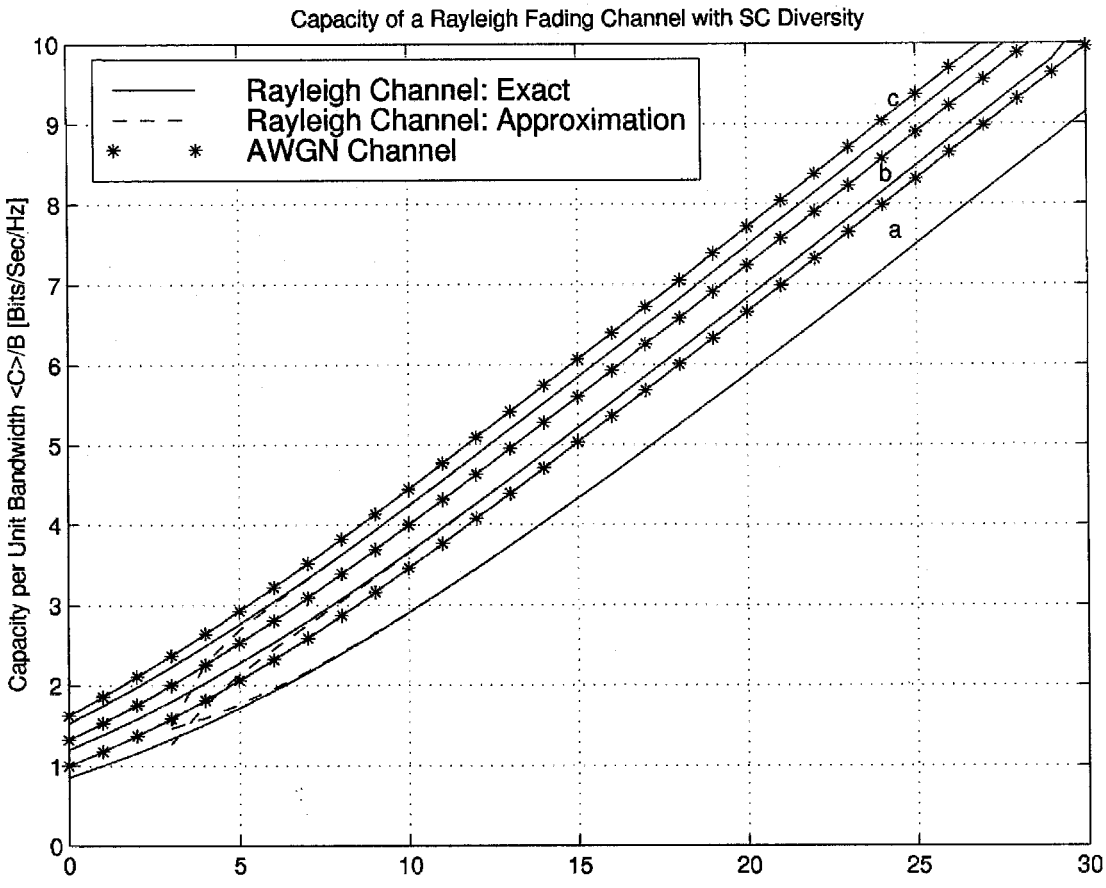

Figure 8.6: Average channel capacity per unit bandwidth for Raleigh fading channels with selective-combining diversity versus the average CNR per branch $\overline{\gamma}$ ((a) $M = 1$, (b) $M = 2$, and (c) $M = 4$).

M independent AWGN channels with selective-combining:

$$\frac{C_{\text{awgn}}^{\text{sc}}}{B} = \log_2(1 + \sum_{n=1}^{M} \frac{1}{n} \gamma). \tag{8.55}$$

We again note that the capacity of an array of M independent Rayleigh channels approaches the capacity of an array of M independent AWGN channels as M tends to infinity. Finally, for all M the asymptotic approximation (8.45) closely matches the exact average capacity (8.44) when $\overline{\gamma} > 5$ dB.

For the M-branch MRC diversity scheme, the average combined CNR $<\gamma>_{\text{mrc}}$ is related to the average CNR per branch $\overline{\gamma}$ by [108, (5.2-16), p. 319] $<\gamma>_{\text{mrc}} = M\,\overline{\gamma}$. We can therefore also express $<C>_{\text{ora}}^{\text{mrc}}/B$ in terms of $<\gamma>_{\text{mrc}}$ as

$$\frac{<C>_{\text{ora}}^{\text{mrc}}}{B} = \log_2(e)\ \exp\left(\frac{M}{<\gamma>_{\text{mrc}}}\right) \sum_{k=0}^{M-1} \left(\frac{M}{<\gamma>_{\text{mrc}}}\right)^k \Gamma\left(-k,\ \frac{M}{<\gamma>_{\text{mrc}}}\right). \tag{8.56}$$

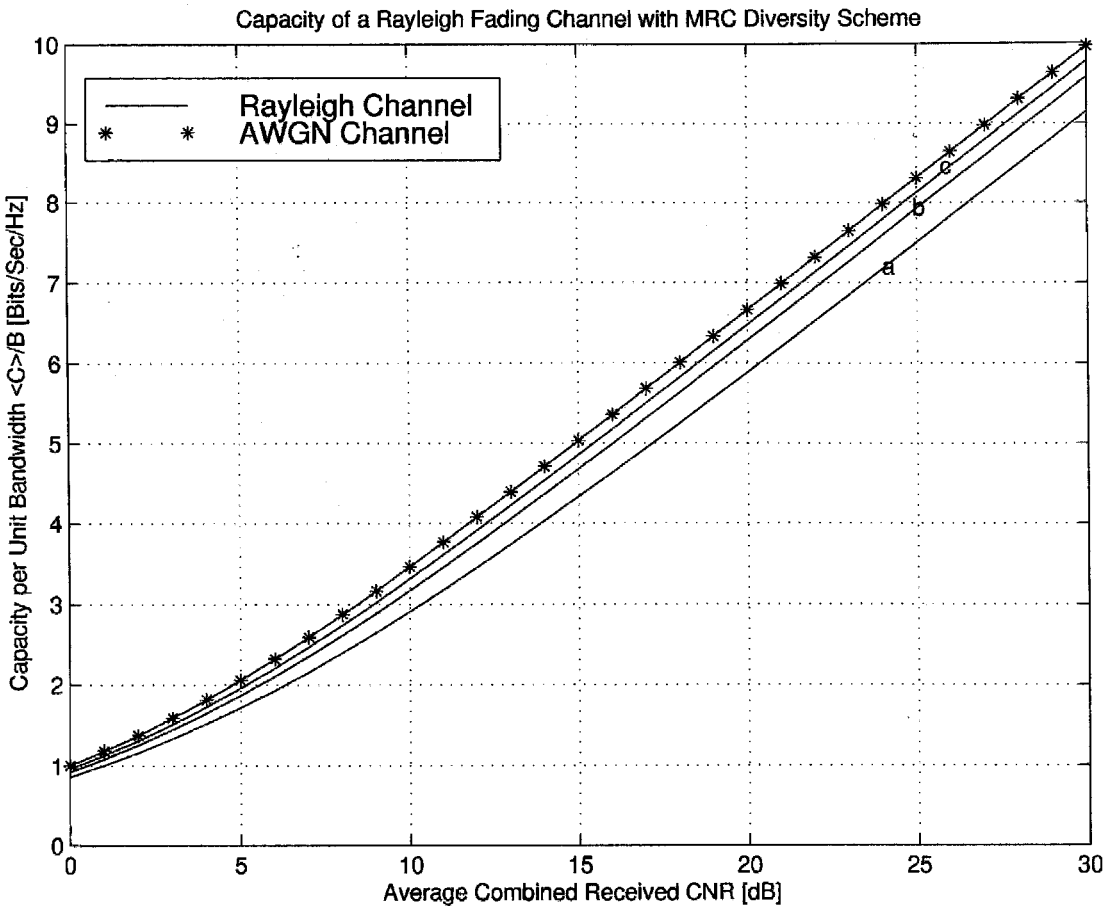

Figure 8.7: Average channel capacity per unit bandwidth for a Raleigh fading channel with maximal-ratio combining diversity versus average combined CNR $<\gamma>_{\text{mrc}}$ ((a) $M = 1$, (b) $M = 2$, and (c) $M = 4$).

Fig. 8.7 shows plots of $<C>_{\text{ora}}^{\text{mrc}}/B$ versus the average combined CNR $<\gamma>_{\text{mrc}}$ for various values of M. These plots show the same numerical results as [135, Fig. 2] for $M \geq 2$, and [137, Fig. 1] for $M \geq 1$. These results show that, when expressed in terms of the average combined CNR, the capacity of a Rayleigh channel can never "beat" the capacity of a single branch AWGN channel, but it comes close to the AWGN channel capacity as the number of diversity branches M approaches infinity.

For the M-branch SC diversity scheme, the average combined CNR $<\gamma>_{\text{sc}}$ is related to the average CNR of a single branch $\overline{\gamma}$ by [108, (5.2-8), p. 316] $<\gamma>_{\text{sc}} = \overline{\gamma} \sum_{n=1}^{M} \frac{1}{n}$. We can therefore also express $<C>_{\text{ora}}^{\text{sc}}/B$ in terms of $<\gamma>_{\text{sc}}$ as

$$\frac{<C>_{\text{ora}}^{\text{sc}}}{B} = M \log_2(e) \sum_{k=0}^{M-1} \frac{(-1)^k}{1+k} \binom{M-1}{k} \exp\left(\frac{(1+k)\sum_{n=1}^{M}\frac{1}{n}}{<\gamma>_{\text{sc}}}\right) E_1\left(\frac{(1+k)\sum_{n=1}^{M}\frac{1}{n}}{<\gamma>_{\text{sc}}}\right). \tag{8.57}$$

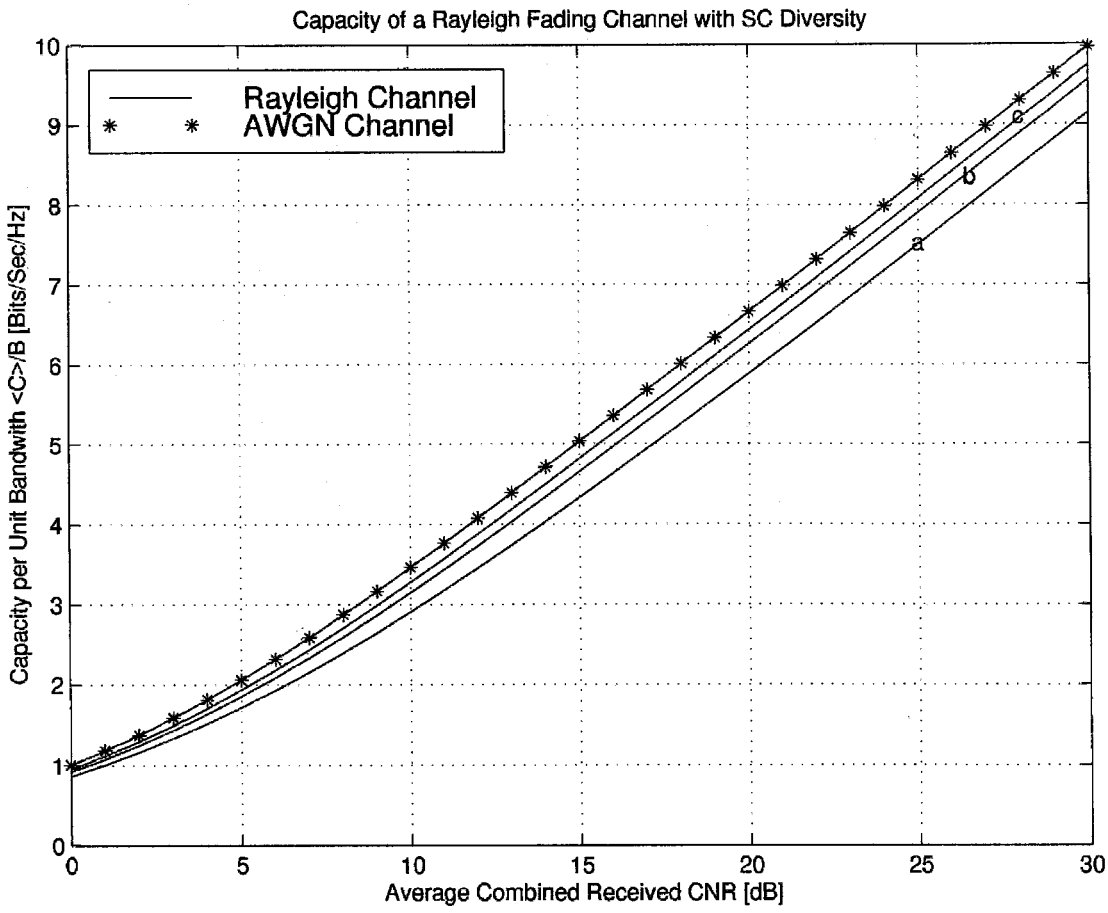

Figure 8.8: Average channel capacity per unit bandwidth for Raleigh fading channels with selective-combining diversity versus the average combined CNR $<\gamma>_{\text{sc}}$ ((a) $M = 1$, (b) $M = 2$, and (c) $M = 4$).

Fig. 8.8 shows plots of $<C>^{\text{sc}}_{\text{ora}}/B$ versus the average combined CNR $<\gamma>_{\text{sc}}$ for various values of M. In fact, Fig. 8.7 and Fig. 8.8 are very similar, since $<C>^{\text{sc}}_{\text{ora}}$ approaches the capacity of the single branch AWGN channel C as the number of diversity branches M increases. However, a close look at the numerical results shows that for a fixed M, $<C>^{\text{mrc}}_{\text{ora}}$ is always slightly bigger than $<C>^{\text{sc}}_{\text{ora}}$ for an equal average CNR at the output of the combiner (i.e., for $<\gamma>_{\text{mrc}}=<\gamma>_{\text{sc}}$). Note that this slim difference is due to the fact that the average CNR per branch for SC ($\overline{\gamma}=<\gamma>_{\text{sc}}/\sum_{n=1}^{M}\frac{1}{n}$) is bigger than the average CNR per branch for MRC ($\overline{\gamma}=<\gamma>_{\text{mrc}}/M$) for an equal average combined CNR. That is why, as mentioned above, we believe that a fair comparison between the MRC and SC diversity schemes should be based on the average CNR per branch (Fig. 8.5 and Fig. 8.6). However, when looked at individually, Figs. 8.7-8.8 are also of interest since they show that the capacity of a single branch AWGN channel with CNR $\overline{\gamma}$ (≥ 0) is always bigger than the capacity of a fading channel with the same average received CNR $\overline{\gamma}$ at the output of the diversity combiner, regardless of the adaptation and diversity-combining strategy in the latter case.

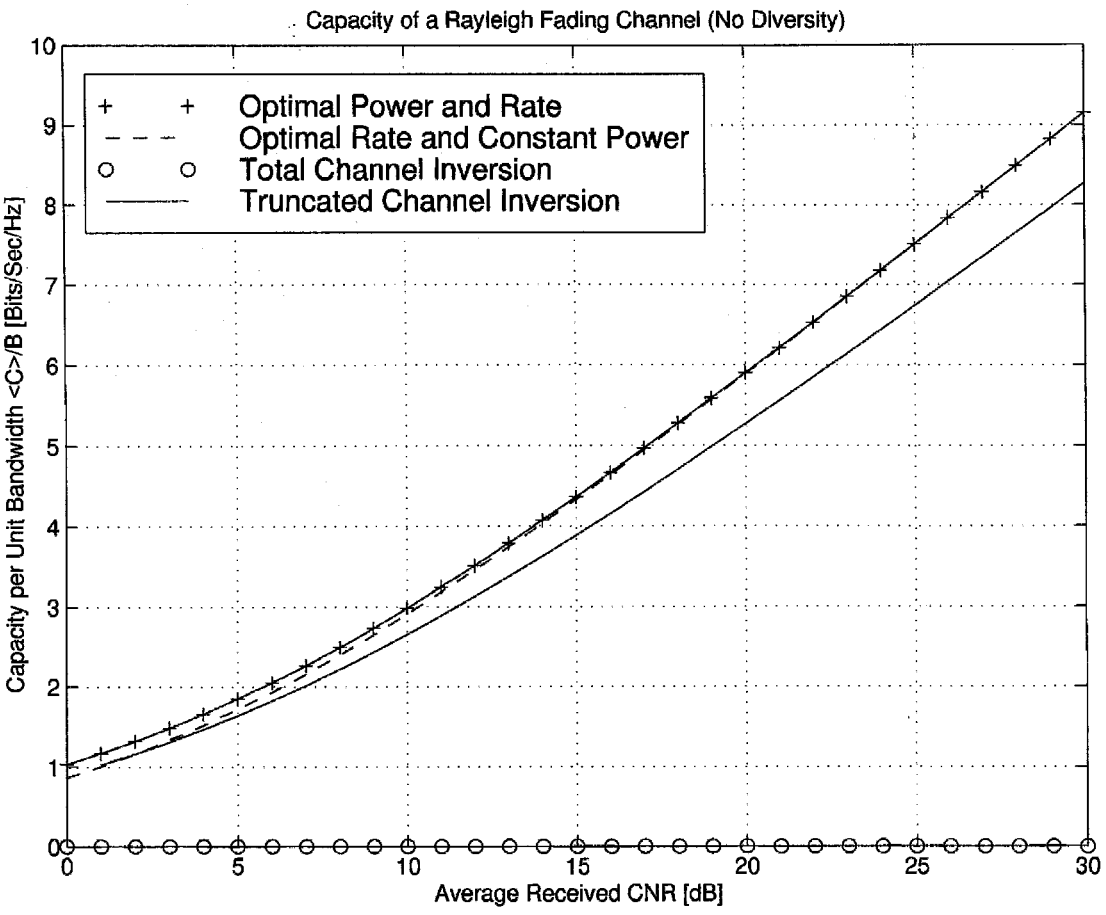

Figure 8.9: Channel capacity per unit bandwidth for a Raleigh fading channel versus average carrier-to-noise ratio $\overline{\gamma}$ for different adaptation policies when $M = 1$.

8.6.2 Comparison of the Different Policies

Fig. 8.9 shows the calculated channel capacity per unit bandwidth as a function of $\overline{\gamma}$ for the different adaptation policies without diversity-combining. These curves confirm the previous numerical results reported in [134] using the closed-form expressions (8.17), (8.34), and (8.48) instead of numerical integration. From this figure we see that the optimal power and rate adaptation (8.17) yields a small increase in capacity over just rate adaptation (8.34), and this small increase in capacity diminishes as $\overline{\gamma}$ increases. The corresponding outage probability (8.18) for the optimal adaptation and truncated channel inversion (with optimal cutoff γ_o^*) are shown in Fig. 8.10.

Fig. 8.11 shows the channel capacity per unit bandwidth as a function of $\overline{\gamma}$ for the different policies with MRC diversity. As the number of combining branches increases, the capacity difference between optimal power and rate adaptation versus optimal rate adaptation alone becomes negligible for all values of $\overline{\gamma}$. For any M, fixed rate transmission with total channel inversion suffers the largest capacity penalty relative to the other policies. However, as M increases, the fading is progressively

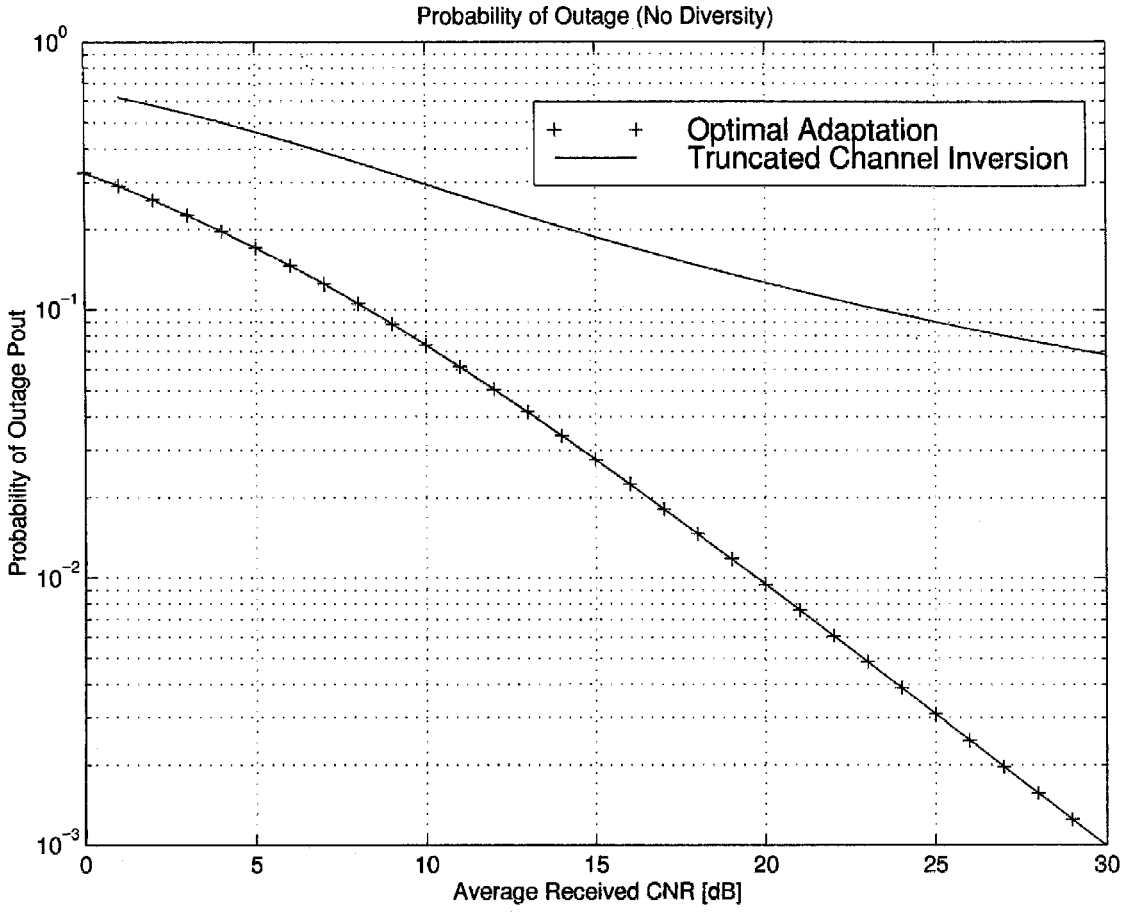

Figure 8.10: Outage probability of the optimal adaptation and truncated channel inversion.

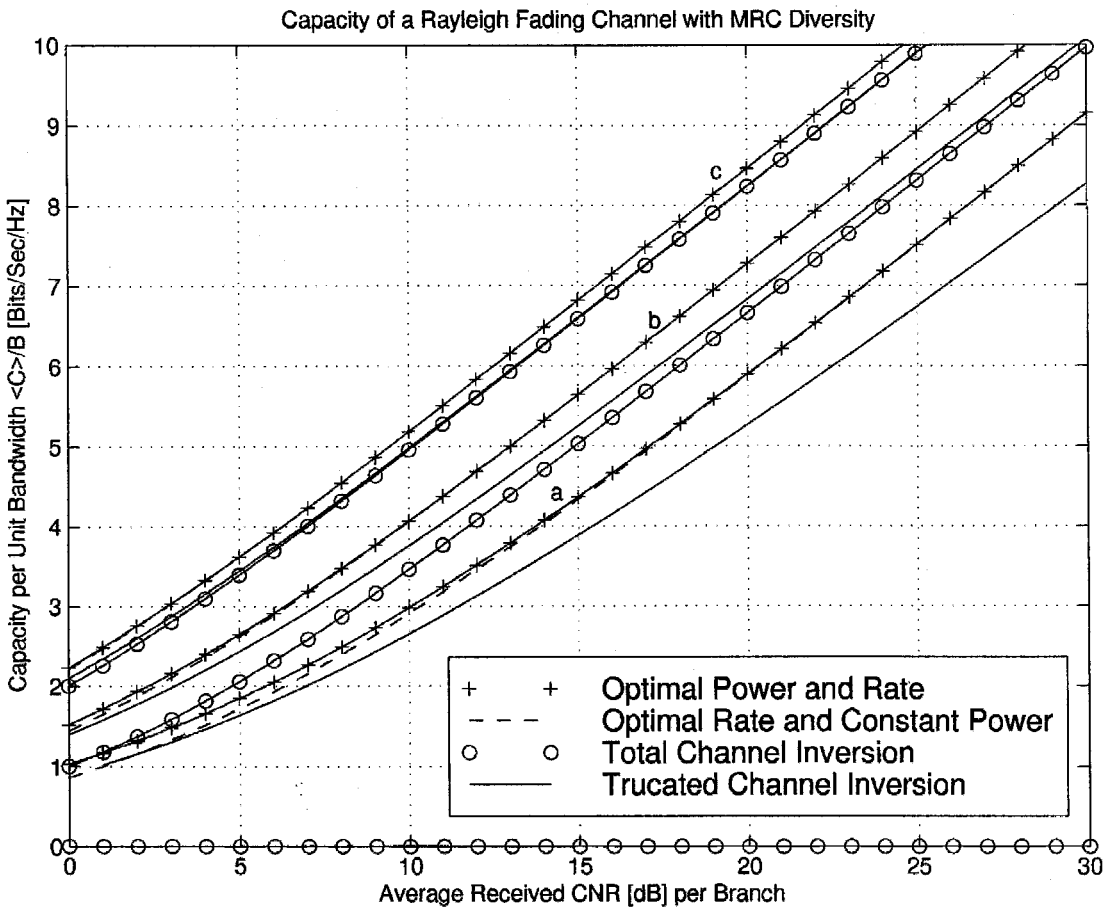

Figure 8.11: Channel capacity per unit bandwidth for a Raleigh fading channel versus average carrier-to-noise ratio $\overline{\gamma}$ for different adaptation policies with MRC diversity ((a) $M = 1$, (b) $M = 2$, and (c) $M = 4$).

reduced, and this penalty diminishes remarkably. Thus, as M increases, all capacities of the various policies converge to the capacity of an array of M independent AWGN channels (8.54). However, it is not possible in practice to completely eliminate the effects of fading through space diversity since the number of diversity branches is limited. This is especially true for the down-link (base station to mobile), since mobile receivers are generally constrained in size and power.

Since channel inversion is the least complex technique, there is a tradeoff of complexity and capacity for the various adaptation methods and diversity-combining techniques. The diversity gain for all policies is quite important, especially for total channel inversion. For example, in Fig. 8.11 we see that the capacity with total channel inversion and two-branch MRC exceeds that of a single branch system with optimal adaptation. Note that this figure also illustrates the typical diminishing returns obtained as the number of branches increases. In addition, for $M = 1$ total channel inversion suffers a large capacity penalty relative to truncated channel inversion. However,

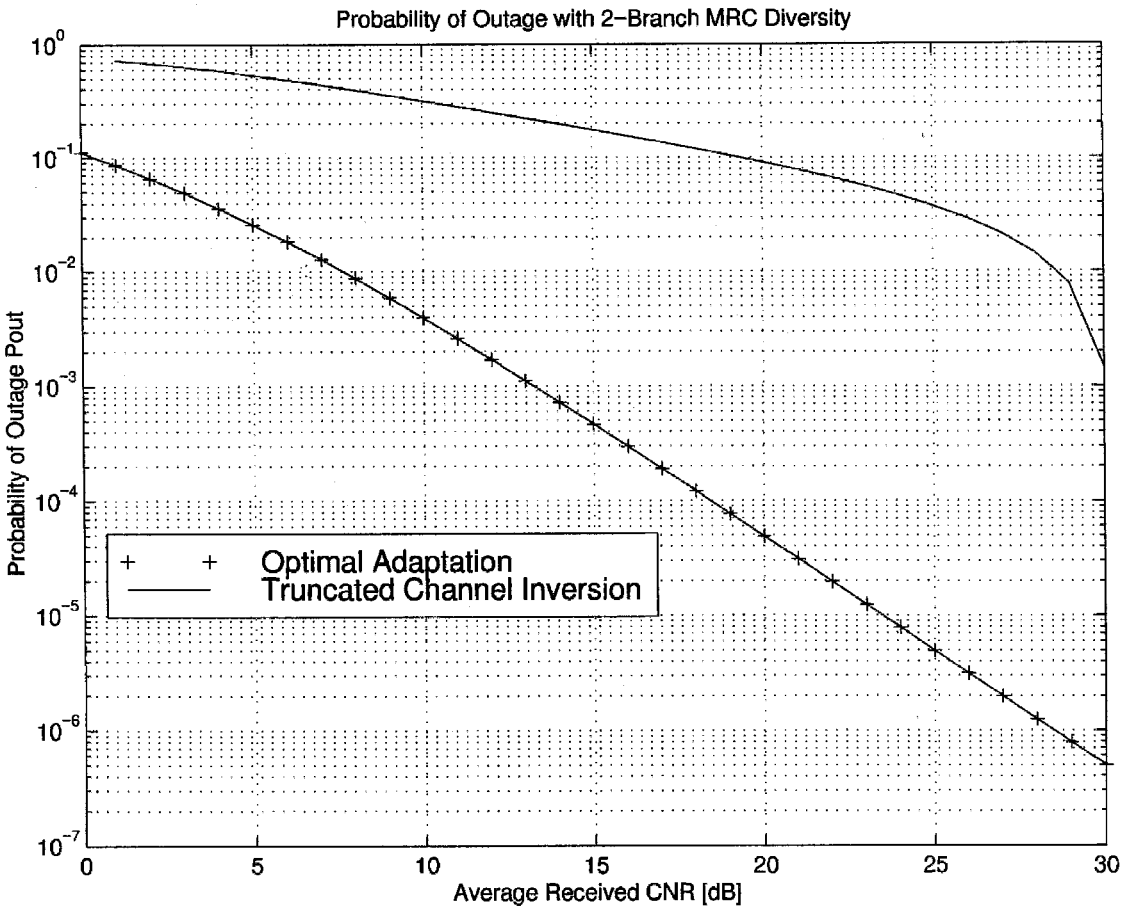

Figure 8.12: Outage probability of the optimal adaptation and truncated channel inversion with MRC diversity.

as the number of combining branches M increases, the effect of fading is progressively reduced, and this penalty diminishes remarkably. In particular, as M increases, we see that truncated channel inversion yields a small increase in capacity over total channel inversion, and this small increase in capacity diminishes as the average CNR $\overline{\gamma}$ and/or the number of combined branches M increase. The corresponding outage probability (8.23) for the optimal adaptation and truncated channel inversion (with optimal cutoff γ_o^*) policies with MRC are shown in Fig. 8.12.

Fig. 8.13 shows the channel capacity per unit bandwidth as a function of $\overline{\gamma}$ for the different adaptation policies with SC diversity. As expected, SC provides less diversity gain than MRC, with rapidly diminishing returns as M increases. However, the diversity impact on channel inversion is still important for SC diversity, since the capacity with this policy and with two-branch combining exceeds that of a single branch system with optimal adaptation for all $\overline{\gamma} > 8$ dB.

Fig. 8.14 compares the channel capacity per unit bandwidth as function of $\overline{\gamma}$ for the different adaptation policies with (a) 4-branch MRC diversity and (b) 4-branch SC diversity. These curves illustrate the extra diversity gain provided by MRC over SC. We see from this figure that MRC

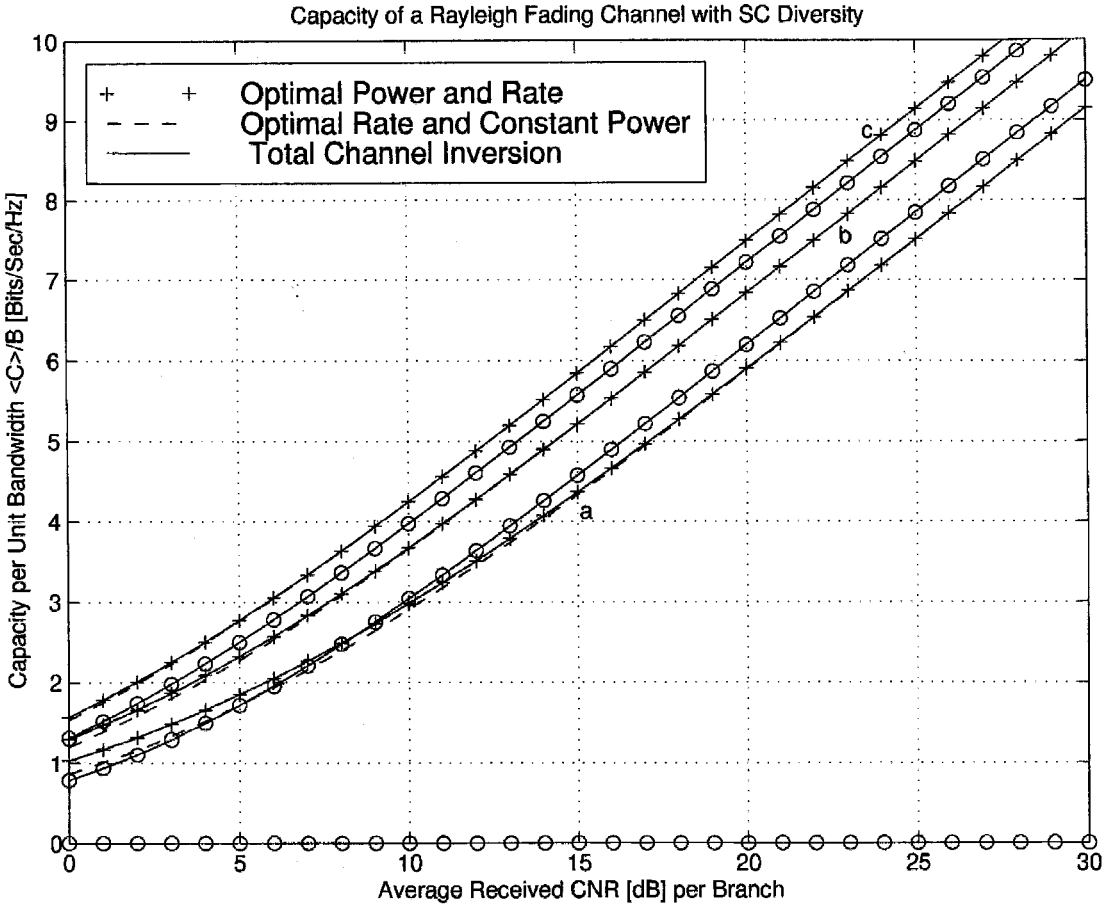

Figure 8.13: Channel capacity per unit bandwidth for a Raleigh fading channel versus average carrier-to-noise ratio $\overline{\gamma}$ for different adaptation policies with SC diversity ((a) $M = 1$, (b) $M = 2$, and (c) $M = 4$).

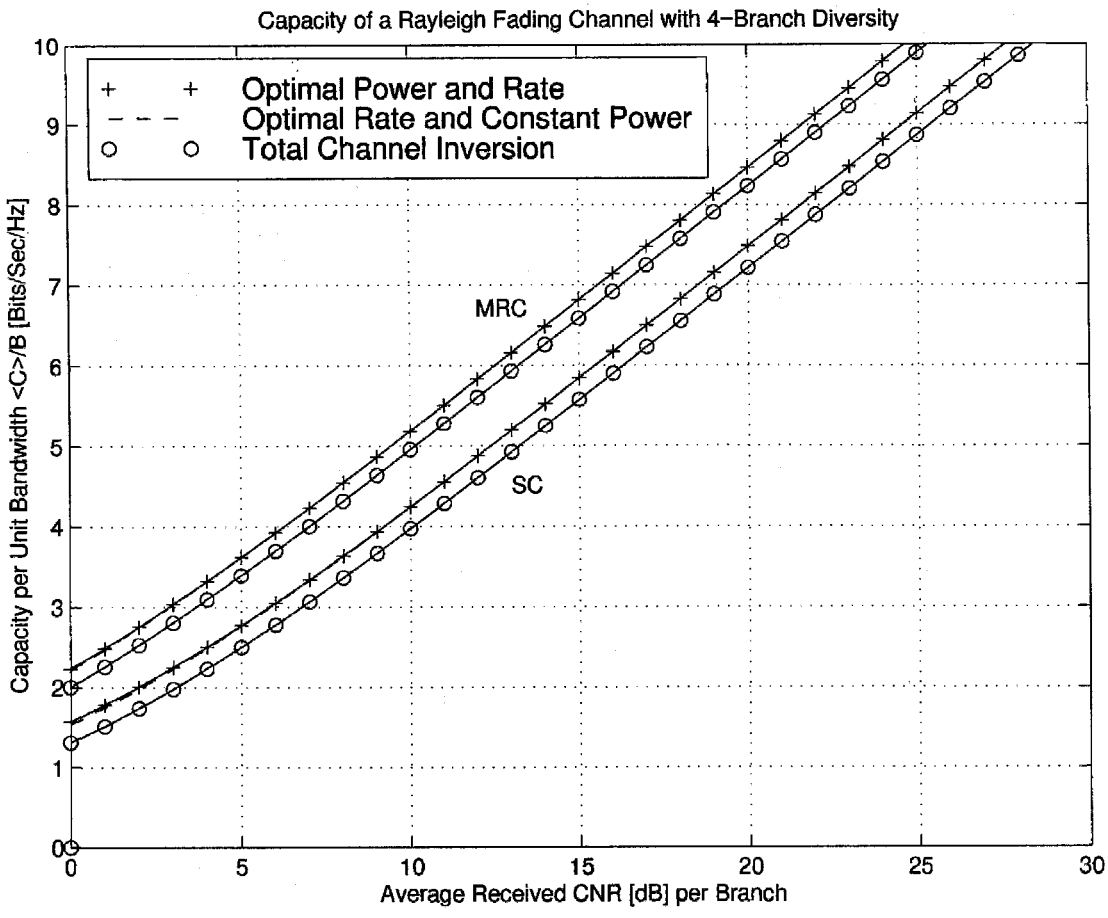

Figure 8.14: Channel capacity per unit bandwidth for a Raleigh fading channel versus average carrier-to-noise ratio $\overline{\gamma}$ for different adaptation policies with (a) 4-branch MRC diversity combining and (b) 4-branch SC diversity combining ((a) $M = 1$, (b) $M = 2$, and (c) $M = 4$).

provides about 1 Bit/Sec/Hz improvement over SC at any $\overline{\gamma}$ and for any of the considered adaptive transmission policies.

8.7 Conclusion

We have examined the Shannon capacity or, equivalently, the upper-bound on spectral efficiency of three adaptive transmission techniques over Rayleigh fading channels. In particular, we obtained closed-form expressions for the capacity when these adaptive schemes are used in conjunction with diversity combining.

We first compared the capacity of an AWGN channel with the capacity of a Rayleigh channel with optimal rate adaptation and constant transmit power. When expressed in terms of the average CNR per branch, the capacity of an array of M independent Rayleigh channels is bigger than the capacity of a single branch AWGN channel, but is always smaller than the capacity of an array of M

independent AWGN channels, and converges to it as M tends to infinity. On the other hand, when expressed in terms of the average combined CNR, the capacity of a Rayleigh channel with diversity cannot "beat" the capacity of a single branch AWGN channel, but comes close to it as the number of diversity branches approaches infinity.

We also compared the channel capacities of the various adaptation policies both with and without diversity combining. Optimal power and rate adaptation yields a small increase in capacity over just optimal rate adaptation, and this small increase in capacity diminishes as the average received CNR and/or the number of diversity branches increases. In addition, channel inversion suffers the largest capacity penalty relative to the two other policies. However, this capacity penalty diminishes and all capacities approach the capacity of the AWGN channel with increasing diversity.

Diversity yields large capacity gains for all the techniques with diminishing returns on the number of branches. The diversity gain is most pronounced for channel inversion. In addition, selective-combining provides less diversity gain than maximal-ratio combining for all the adaptive policies, as expected.

Although the results derived herein are Shannon bounds, similar analysis has been applied to adaptive M-QAM modulation without diversity [130]. Thus, we expect that the same general trends will be observed on any adaptive modulation method, although the spectral efficiency will be smaller.

Appendix A

Evaluation of $\mathcal{J}_n(\mu)$ (8.14)

We evaluate the integral $\mathcal{J}_n(\mu)$ defined in (8.14) using partial integration, namely:

$$\int_1^{+\infty} u\, dv = \lim_{t\to+\infty}(u\, v) - \lim_{t\to 1}(u\, v) - \int_1^{+\infty} v\, du. \tag{8.58}$$

First, let

$$u = \ln t. \tag{8.59}$$

Thus

$$du = \frac{dt}{t}. \tag{8.60}$$

Then, let

$$dv = t^{n-1}\, e^{-\mu\, t}\, dt. \tag{8.61}$$

Performing $n-1$ successive integration by parts yields [53, (2.321.2), p. 112]

$$v = -\, e^{-\mu\, t} \sum_{k=1}^{n} \frac{(n-1)!}{(n-k)!}\, \frac{t^{n-k}}{\mu^k}. \tag{8.62}$$

Substituting (8.59), (8.62), and (8.60) in (8.58), we see that the first two terms go to zero. Hence,

$$\mathcal{J}_n(\mu) = \sum_{k=1}^{n} \frac{(n-1)!}{\mu^k (n-k)!} \int_1^{+\infty} t^{n-k-1}\, e^{-\mu\, t}\, dt. \tag{8.63}$$

The integral in (8.63) can be written in a closed-form with the help of [53, (3.381.3), p. 364], giving

$$\mathcal{J}_n(\mu) = \frac{(n-1)!}{\mu^n} \sum_{k=0}^{n-1} \frac{\Gamma(k,\mu)}{k!}, \tag{8.64}$$

where $\Gamma(.,.)$ is the complementary incomplete gamma function (or Prym's function as it is sometimes called) defined by [53, (8.350.2), p. 949]

$$\Gamma(\alpha, x) = \int_x^{+\infty} t^{\alpha-1}\, e^{-t}\, dt. \tag{8.65}$$

For k positive integers,

$$\Gamma(k,\mu) = (k-1)!\, \mathcal{P}_k(\mu); \qquad k \geq 2, \tag{8.66}$$

where $\mathcal{P}_k(.)$ denotes the Poisson distribution defined as

$$\mathcal{P}_k(\mu) = e^{-\mu} \sum_{j=0}^{k-1} \frac{\mu^j}{j!}. \tag{8.67}$$

For $k = 0$ [53, (8.359.1) p. 951]

$$\Gamma(0, \mu) = E_1(\mu), \tag{8.68}$$

where $E_1(.)$ is the exponential-integral of first order function defined as

$$E_1(x) = \int_1^{+\infty} \frac{e^{-x\ t}}{t}\ dt. \tag{8.69}$$

Thus, for n positive integers, (8.64) can be written as

$$\mathcal{J}_n(\mu) = \frac{(n-1)!}{\mu^n} \left(E_1(\mu) + \sum_{k=1}^{n-1} \frac{\mathcal{P}_k(\mu)}{k} \right). \tag{8.70}$$

In particular when $n = 1$, (8.70) reduces to

$$\mathcal{J}_1(\mu) = \frac{E_1(\mu)}{\mu}. \tag{8.71}$$

Appendix B

Evaluation of $\mathcal{I}_n(\mu)$ (8.32)

We evaluate the integral $\mathcal{I}_n(\mu)$ defined in (8.32) using partial integration, namely:

$$\int_0^{+\infty} u\ dv = \lim_{t \to +\infty} (u\ v) - \lim_{t \to 0} (u\ v) - \int_0^{+\infty} v\ du. \tag{8.72}$$

First, let

$$u = \ln(1 + t). \tag{8.73}$$

Thus

$$du = \frac{dt}{1+t}. \tag{8.74}$$

Then, let

$$dv = t^{n-1}\ e^{-\mu\ t}\ dt. \tag{8.75}$$

Performing $n - 1$ successive integration by parts yields [53, (2.321.2), p. 112]

$$v = -\ e^{-\mu\ t} \sum_{k=1}^{n} \frac{(n-1)!}{(n-k)!} \frac{t^{n-k}}{\mu^k}. \tag{8.76}$$

Substituting (8.73), (8.76), and (8.74) in (8.72), we see that the first two terms go to zero. Hence,

$$\mathcal{I}_n(\mu) = \sum_{k=1}^{n} \frac{(n-1)!}{\mu^k (n-k)!} \int_0^{+\infty} \frac{t^{n-k}\, e^{-\mu\, t}}{1+t}\, dt. \tag{8.77}$$

The integral in (8.77) can be written in a closed-form with the help of [53, (3.383.10), p. 366], giving

$$\mathcal{I}_n(\mu) = (n-1)!\, e^{\mu} \sum_{k=1}^{n} \frac{\Gamma(-n+k, \mu)}{\mu^k}, \tag{8.78}$$

where $\Gamma(.,.)$ is the complementary incomplete gamma function defined in (8.65). Note that when $n = 1$, (8.78) reduces to

$$\mathcal{I}_1(\mu) = e^{\mu}\, \frac{\Gamma(0, \mu)}{\mu}, \tag{8.79}$$

which can be written as

$$\mathcal{I}_1(\mu) = e^{\mu}\, \frac{E_1(\mu)}{\mu}, \tag{8.80}$$

where $E_1(.)$ is the exponential-integral of first order defined by (8.69).

Chapter 9 Adaptive Modulation over Nakagami-m Fading Channels

9.1 Introduction

In this chapter we first investigate the theoretical spectral efficiency limits of adaptive transmission in Nakagami-m multipath fading (NMF) channels [13]. We then propose and study adaptive multi-level quadrature amplitude modulation (M-QAM) schemes which improve link spectral efficiency (R/W [Bits/Sec/Hz]), defined as the average transmitted data rate per unit bandwidth for a specified average transmit power and bit-error-rate (BER). We also evaluate the performance of these schemes relative to the theoretical spectral efficiency limit. More specifically we use the analyses developed in Chapter 8 to obtain closed-form expressions for the capacity of NMF channels under different adaptive transmission schemes. We consider the same adaptive policies as in the previous chapter: optimal simultaneous power and rate adaptation, constant power with optimal rate adaptation, and channel inversion with fixed rate. We then present numerical results confirming that rate adaptation is the key to achieving high link spectral efficiency. Rate adaptation can be achieved through a variation of the symbol time duration [121] or constellation size [124]. The former method requires complicated hardware and results in a variable-bandwidth system, whereas the latter technique is better suited for hardware implementation, since it results in a variable-throughput system with a fixed bandwidth. Based on these advantages we analyze the performance of constant-power variable-rate M-QAM schemes for spectrally efficient data transmission over NMF channels. Similar analysis has been presented in [130] for a variable-power variable-rate M-QAM in Rayleigh fading and log-normal shadowing, and in [142] for constant-power variable-rate M-QAM in Rayleigh fading. We extend the results of [130, 142] to constant-power variable-rate M-QAM by analyzing the resulting spectral efficiency and BER for the more general NMF distribution. We also analyze the impact of time delay on the performance of adaptive M-QAM.

The remainder of this chapter is organized as follows. In Section 9.2 we outline the channel and communication system models. In Section 9.3 we derive the capacity of NMF channels for the optimal adaptive policy, constant power policy, and channel inversion policy, and we present some numerical examples comparing (i) the NMF channel capacity with the capacity of an additive white Gaussian noise (AWGN) channel, and (ii) the NMF channel capacity for the various adaptive policies. In Section 9.4 we propose and evaluate the performance of an adaptive constant-power

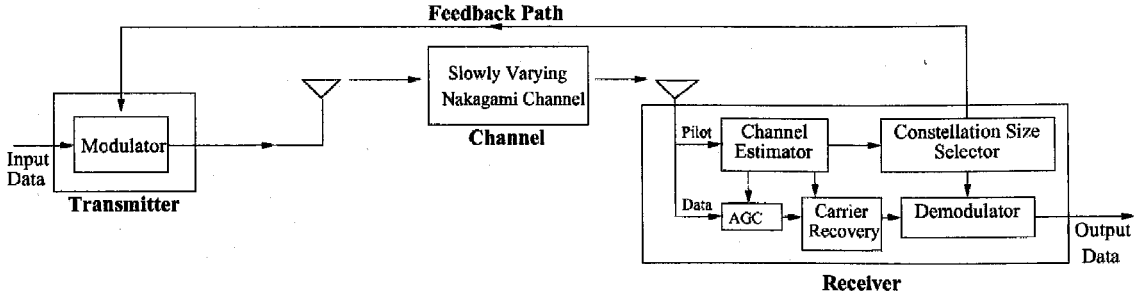

Figure 9.1: Adaptive communication system model.

variable-rate M-QAM system assuming perfect channel estimation and negligible time delay. The BER degradation due to time delay is analyzed in Section 9.5. A summary of our results is presented in Section 9.6.

9.2 System and Channel Models

9.2.1 Adaptive Communication System Model

A block diagram of the adaptive communication system is shown in Fig. 9.1. A pilot tone continually sends a known "channel sounding" sequence so that the channel-induced envelope fluctuation α and phase shift ϕ can be extracted at the channel estimation stage. Based on this channel gain estimate $\hat{\alpha}$, a decision device selects the rate and power to be transmitted, configures the demodulator accordingly, and informs the transmitter about that decision via the feedback path. The constellation size assignment for the proposed constant-power variable-rate M-QAM scheme will be discussed in more detail in Section 9.4.1. The transmission system keeps its configuration unchanged (i.e., no re-adaptation) for a duration $1/\tau_t$ [s]. Meanwhile, the phase estimate $\hat{\phi}$ is used at the receiver for full compensation of the phase variation (i.e., ideal coherent phase detection), whereas the channel gain estimate $\hat{\alpha}$ is used on a continuous basis by the automatic gain controller (AGC)/demodulator for symbol-by-symbol maximum-likelihood detection.

For satisfactory operation the modulator and demodulator must be configurated at any instant for the same constellation size. Efficient error control schemes are therefore required to insure an error-free feedback path. However, such schemes inevitably introduce a certain time delay τ_{fb} [s], which may include decoding/ARQ delay, and propagation time via the feedback path. Hence, even if perfect channel estimates are available at the receiver, the system will not be able to adapt to the actual channel fading but rather to at best a τ_{fb} delayed version of it. In practice, the choice of the power and/or constellation is based on a channel estimate at time t, but the data are sent over the

channel at time $t+\tau$ such that $\tau_{fb} \leq \tau \leq \tau_t$, where τ_t is the rate at which we change the constellation size and power. The goal is to operate with the smallest possible τ_{fb} to minimize the impact of feedback delay, and with the largest possible τ_t to minimize the rate of system reconfiguration. This issue will be further discussed in Section 9.5.

9.2.2 Channel Model and Fading Statistics

We consider a slowly-varying flat-fading channel changing at a rate much slower than the symbol data rate, so the channel remains roughly constant over hundreds of symbols. For NMF channels the probability distribution function (PDF) of the channel gain α is given by (2.14) and the received CNR, γ, is then gamma distributed according to the PDF, $p_\gamma(\gamma)$, given by (2.15)

$$p_\gamma(\gamma) = \left(\frac{m}{\overline{\gamma}}\right)^m \frac{\gamma^{m-1}}{\Gamma(m)} \exp\left(-m\,\frac{\gamma}{\overline{\gamma}}\right), \qquad \gamma \geq 0, \tag{9.1}$$

where $\overline{\gamma}$ is the average received CNR.

9.3 Capacity of Nakagami Fading Channels

9.3.1 Optimal Adaptation

Following the same steps as in Section 8.3.2, it can be shown that the channel capacity of NMF fading channel with optimal power and rate adaptation ($<C>_{\text{opra}}$ [Bit/Sec]) is given by

$$\frac{<C>_{\text{opra}}}{W} = \log_2(e) \sum_{k=0}^{m-1} \frac{\Gamma\left(k, m\,\frac{\gamma_o}{\overline{\gamma}}\right)}{k!}, \tag{9.2}$$

where $\Gamma(.,.)$ is the complementary incomplete gamma function (or Prym's function) and γ_o is the optimal cutoff CNR level below which data transmission is suspended, and which must satisfy

$$\frac{\Gamma\left(m, m\,\frac{\gamma_o}{\overline{\gamma}}\right)}{\frac{\gamma_o}{\overline{\gamma}}} - m\,\Gamma\left(m-1, m\,\frac{\gamma_o}{\overline{\gamma}}\right) = \overline{\gamma}\,\Gamma(m). \tag{9.3}$$

For the special case of the Rayleigh fading channel ($m = 1$), (9.2) reduces to (8.16)

$$\frac{<C>_{\text{opra}}}{B} = \log_2(e)\; E_1\left(\frac{\gamma_o}{\overline{\gamma}}\right). \tag{9.4}$$

As for the Rayleigh fading case, it can be shown that there is a unique γ_o which satisfies (9.3), that γ_o increases as $\overline{\gamma}$ increases, and that γ_o always lies in the interval [0,1]. Note that equation (9.2) can

also be written as

$$\frac{<C>_{\text{opra}}}{W} = \log_2(e)\left(E_1(m\gamma_o/\overline{\gamma}) + \sum_{k=1}^{m-1}\frac{\mathcal{P}_k(m\gamma_o/\overline{\gamma})}{k}\right), \tag{9.5}$$

where $\mathcal{P}_k(.)$ denotes the Poisson distribution defined by (8.67),

$$\mathcal{P}_k(\mu) = e^{-\mu}\sum_{j=0}^{k-1}\frac{\mu^j}{j!}. \tag{9.6}$$

Since no data is sent when $\gamma < \gamma_o$, the optimal policy suffers a probability of outage P_{out}, equal to the probability of no transmission, given for NMF channels by

$$P_{\text{out}} = 1 - \frac{\Gamma(m, m\gamma_o/\overline{\gamma})}{\Gamma(m)} = 1 - \mathcal{P}_m(m\ \gamma_o/\overline{\gamma}). \tag{9.7}$$

9.3.2 Constant Transmit Power

Following the same steps as in Section 8.4.2, it can be shown that with optimal rate adaptation to channel fading and with a constant transmit power, the NMF channel capacity $<C>_{\text{ora}}$ [Bits/Sec] is given by

$$\frac{<C>_{\text{ora}}}{W} = \log_2(e)\ e^{m/\overline{\gamma}}\sum_{k=0}^{m-1}\left(\frac{m}{\overline{\gamma}}\right)^k\Gamma\left(-k, \frac{m}{\overline{\gamma}}\right). \tag{9.8}$$

One may also express (9.8) in terms of the Poisson distribution as

$$\frac{<C>_{\text{ora}}}{W} = \log_2(e)\left(\mathcal{P}_m(-m/\overline{\gamma})\ E_1(m/\overline{\gamma}) + \sum_{k=1}^{m-1}\frac{\mathcal{P}_k(m/\overline{\gamma})\ \mathcal{P}_{m-k}(-m/\overline{\gamma})}{k}\right). \tag{9.9}$$

Note that Yao and Sheikh [143] provided a closed-form expression for the capacity of NMF channels in terms of the complementary incomplete gamma function. However, their derivation is different than ours and their resulting expression [143, Eqn. (7)] contains mth order derivatives. For the special case of the Rayleigh fading channel ($m = 1$), (9.8) reduces to (8.34)

$$\frac{<C>_{\text{ora}}}{W} = \log_2(e)\ e^{1/\overline{\gamma}}\ E_1(1/\overline{\gamma}). \tag{9.10}$$

9.3.3 Channel Inversion with Fixed Rate

Following the same steps as in Section 8.5.2, it can be shown that the channel capacity when the transmitter inverts the channel fading is given for all $m \geq 1$ by

$$\frac{<C>_{\text{cifr}}}{W} = \log_2\left(1 + \frac{m-1}{m}\ \overline{\gamma}\right). \tag{9.11}$$

Thus the capacity of a Rayleigh fading channel ($m = 1$) is zero as found in Section 8.5.1. Note that the capacity of this policy for an NMF channel is the same as the capacity of an AWGN channels with equivalent CNR=$\frac{m-1}{m}\overline{\gamma}$.

The capacity of NMF channels with truncated channel inversion and fixed rate policy ($<C>_{\text{tifr}}$ [Bits/Sec]) can be found as

$$\frac{<C>_{\text{tifr}}}{W} = \log_2\left(1 + \frac{\overline{\gamma}\,\Gamma(m)}{m\,\Gamma(m-1, m\gamma_o/\overline{\gamma})}\right)\frac{\Gamma(m, m\gamma_o/\overline{\gamma})}{\Gamma(m)}, \quad \forall m \geq 1. \tag{9.12}$$

For the special case of the Rayleigh fading channel ($m = 1$), the capacity per unit bandwidth with truncated channel inversion reduces to (8.48)

$$\frac{<C>_{\text{tifr}}}{W} = \log_2\left(1 + \frac{\overline{\gamma}}{E_1(\gamma_o/\overline{\gamma})}\right) e^{-\gamma_o/\overline{\gamma}}. \tag{9.13}$$

9.3.4 Numerical Results

Figures 9.2, 9.3, and 9.4 show the capacity per unit bandwidth as a function of $\overline{\gamma}$ for an NMF channel under the three different adaptive policies for $m = 1$ (Rayleigh channel), $m = 2$, and $m = 4$, respectively. We see from these figures that the capacity of NMF channels is always smaller than the capacity of an AWGN channel for $\overline{\gamma} \geq 0$ dB but converges to it as the m parameter increases or, equivalently, as the amount of fading decreases. We also see that optimal power and rate adaptation yields a small increase in capacity over just optimal rate adaptation, and this small increase in capacity diminishes as the average received CNR and/or fading parameter m increases. Note finally that fixed rate transmission with channel inversion suffers the largest capacity penalty. However, this penalty diminishes as the amount of fading decreases.

9.4 Adaptive M-QAM Modulation

9.4.1 Proposed Adaptive Schemes

The BER of coherent M-QAM with two-dimensional Gray coding over an additive white Gaussian noise (AWGN) channel assuming perfect clock and carrier recovery can be well approximated by [130]

$$\text{BER}(M, \gamma) \simeq 0.2\ \exp\left(-\frac{3\,\gamma}{2\,(M-1)}\right). \tag{9.14}$$

Exact expressions for the BER of "square" M-QAM (when the number of bits per symbol n is even) are known [115, Chapter 5], and are plotted by the solid lines in Fig. 9.5. On the other hand, tight upper-bounds on the BER of "non-square" M-QAM (when the number of bits per symbol n is odd) are also available [1, p. 283], and are plotted by the cross/solid lines in Fig. 9.5. For comparison,

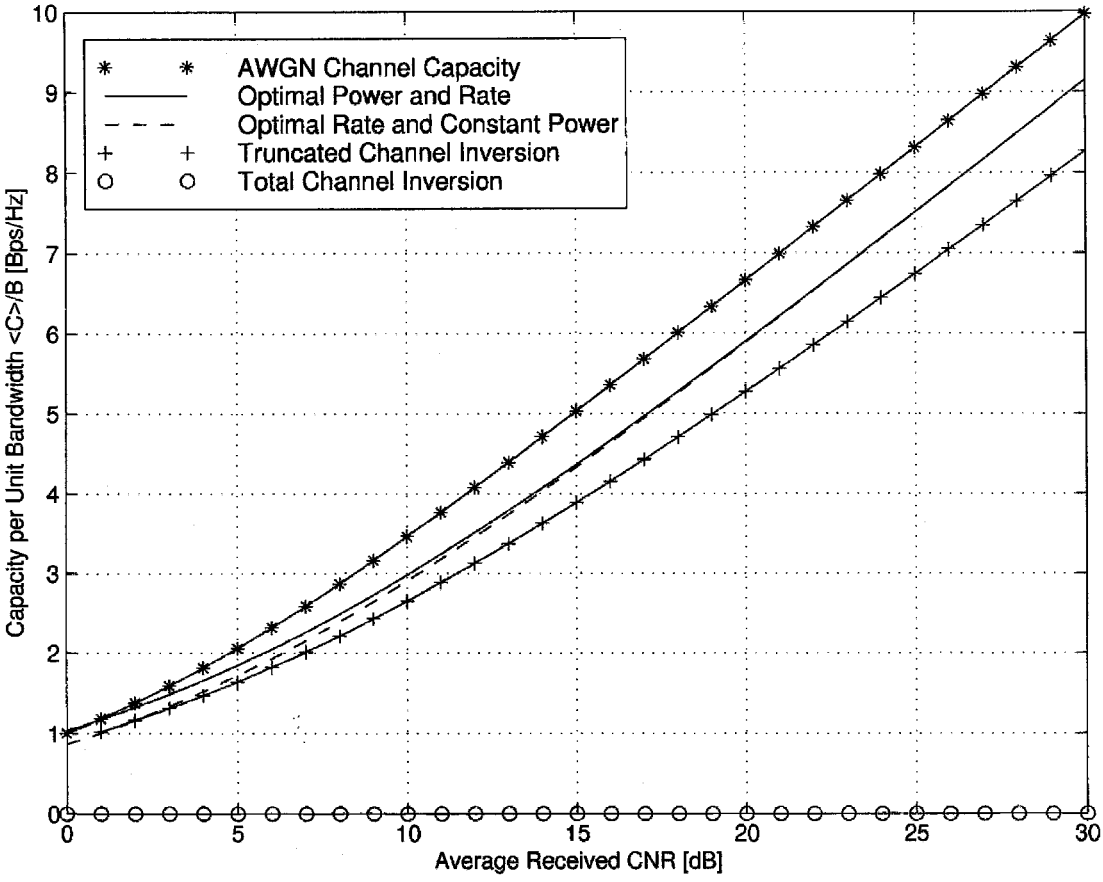

Figure 9.2: Capacity per unit bandwidth for a Rayleigh fading channel (m=1) under different adaption policies.

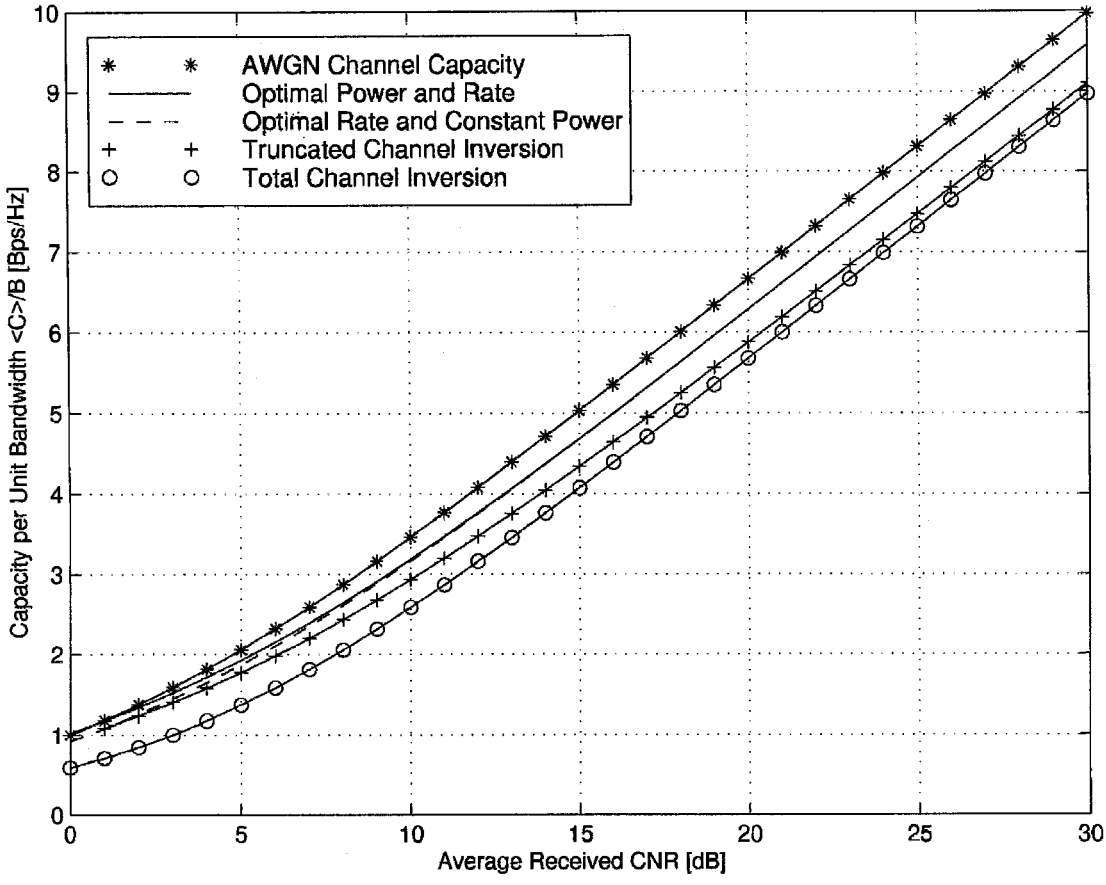

Figure 9.3: Capacity per unit bandwidth for a Nakagami fading channel with m=2, and for different adaption policies.

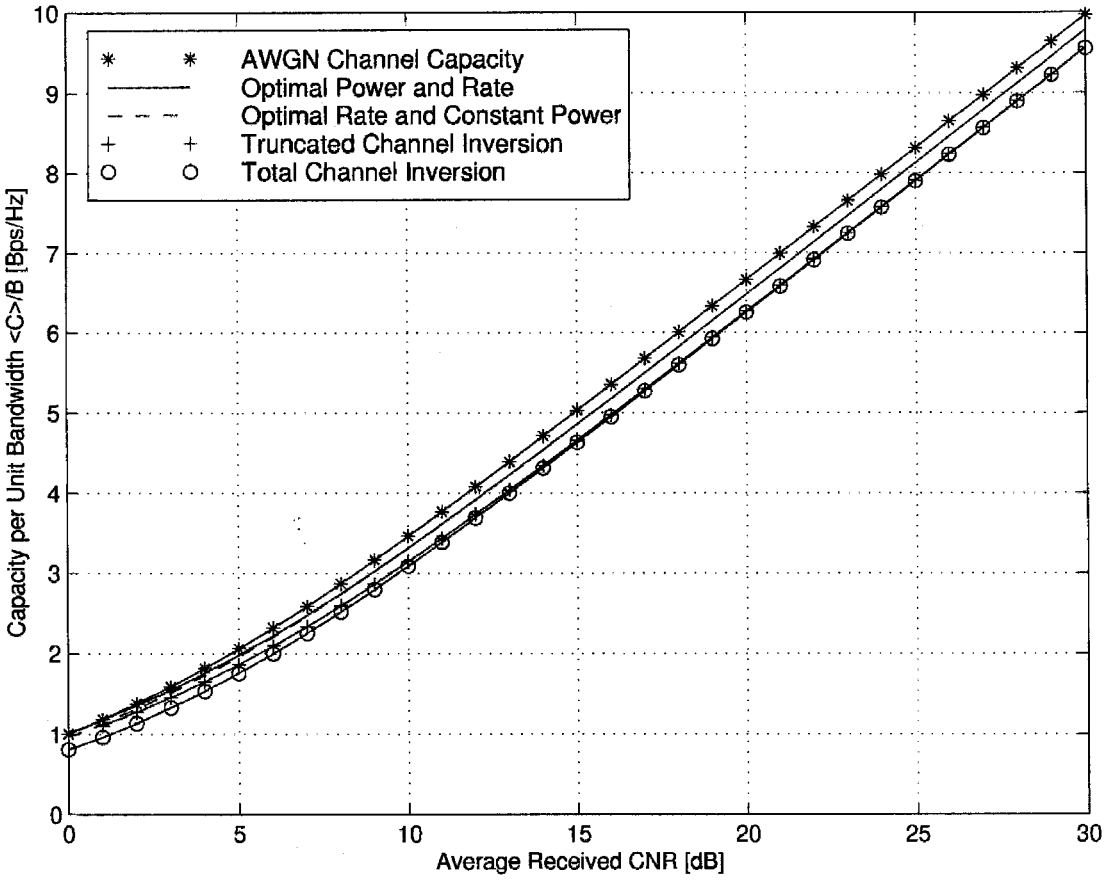

Figure 9.4: Capacity per unit bandwidth for a Nakagami fading channel with m=4, and for different adaption policies.

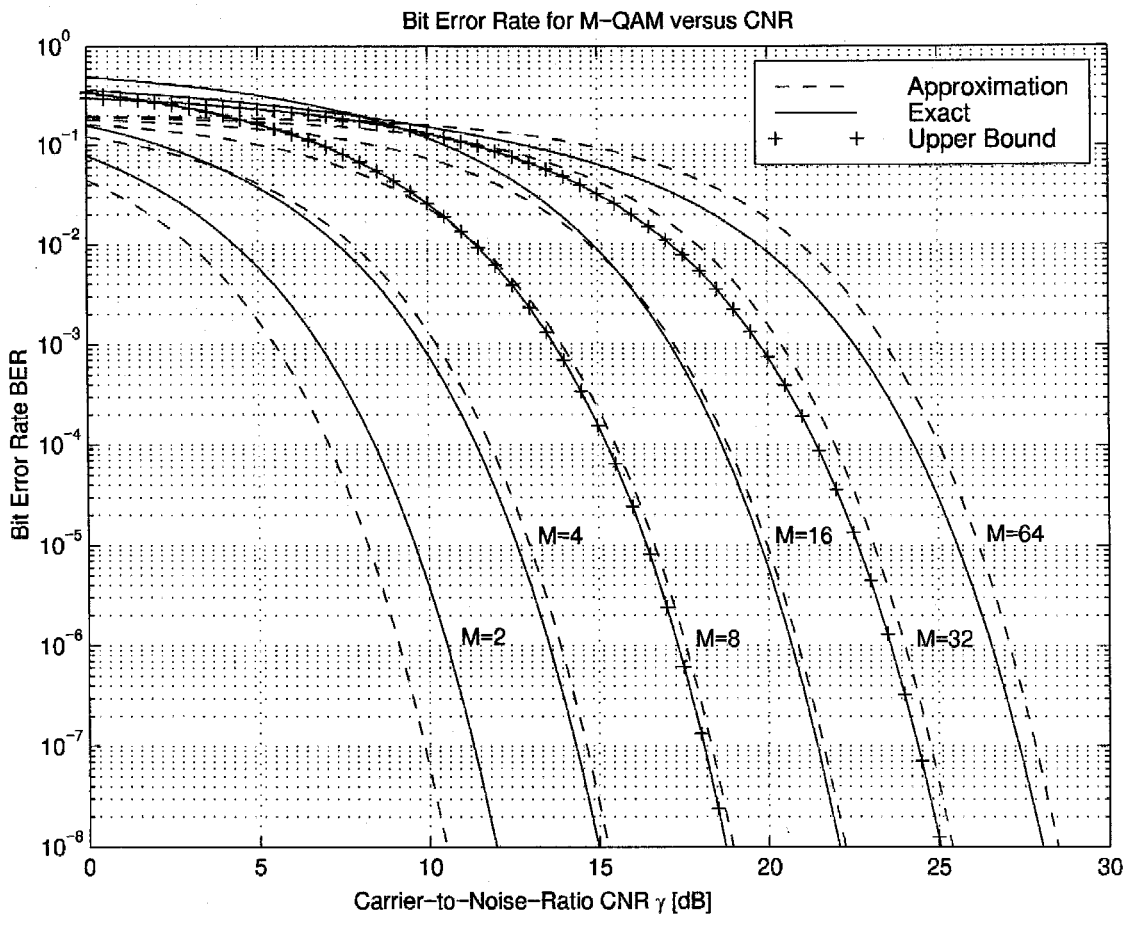

Figure 9.5: BER for M-QAM versus CNR.

the dashed lines in this figure show the BER approximation (9.14) for different values of M. Note that the approximate BER expression upper bounds the exact BER for $M \geq 4$ and for BER $\leq 10^{-2}$, which is the BER range of interest. We will use this approximation when needed in our analysis since it is "invertible" in the sense that it provides a simple closed-form expression for the link spectral efficiency of M-QAM as a function of the CNR and the BER. In addition, (9.14) and its inverse are very simple functions which lead, as shown below, to closed-form analytical expressions and insights that are unattainable with more complicated BER expressions.

Assuming ideal Nyquist pulses and given a fixed CNR (γ) and BER (BER_0), the spectral efficiency of continuous-rate M-QAM can be approximated by inverting (9.14), giving

$$\frac{R}{W} = \log_2(M) = \log_2\left(1 + \frac{3\,\gamma}{2\,K_0}\right), \tag{9.15}$$

where $K_0 = -\ln(5\ \text{BER}_0)$. The adaptive continuous rate (ACR) M-QAM scheme responds to the instantaneous channel CNR fluctuation by varying the number of bits per symbol according to

(9.15). In the context of this chapter, continuous-rate means that the number of bits per symbol is not restricted to integer values. While continuous-rate M-QAM is possible [144], it is more practical to study the performance of adaptive discrete rate (ADR) M-QAM, where the constellation size M_n is restricted to 2^n for n a positive integer. In this case the scheme responds to the instantaneous channel CNR fluctuation by varying its constellation size as follows. The CNR range is divided into $N+1$ *fading regions*, and the constellation size M_n is assigned to the nth region ($n = 0, 1, \cdots, N$). When the received CNR is estimated to be in the nth region, the constellation size M_n is transmitted.

Suppose we set a target BER equal to BER_0. The region boundaries (or switching thresholds) $\{\gamma_n\}$ are then set to the CNR required to achieve the target BER_0 using M_n-QAM over an AWGN channel. Specifically

$$\begin{aligned} \gamma_1 &= [\text{erfc}^{-1}(2\ \text{BER}_0)]^2, \\ \gamma_n &= \frac{2}{3} K_0\ (2^n - 1); \qquad n = 0, 2, 3, \cdots, N, \\ \gamma_{N+1} &= +\infty, \end{aligned} \tag{9.16}$$

where $\text{erfc}^{-1}(.)$ denotes the inverse complementary error function. Then, region n corresponds to values of γ between γ_n and γ_{n+1}. When the switching thresholds are chosen according to (9.16), the system will operate with a BER below the target BER, as will be confirmed in Section 9.4.4. Note in particular that all the γ_ns (except γ_1 which corresponds to M=2) are chosen according to (9.14). Since (9.14) is an upper-bound of the BER only for $M \geq 4$, γ_1 is chosen according to the exact BER performance of 2-QAM (BPSK). The thick line in Fig. 9.6 shows the number of bits per symbol as a function of the received CNR for ADR M-QAM with 8-regions, along with the corresponding switching thresholds. For comparison the thin line in this figure shows the bits per symbol of ACR M-QAM.

9.4.2 Outage Probability

Since no data is sent when the received CNR falls below γ_1, the ADR M-QAM scheme suffers an outage probability, P_{out}, of

$$P_{\text{out}} = \int_0^{\gamma_1} p_\gamma(\gamma)\ d\gamma = 1 - \frac{\Gamma\left(m, \frac{m\gamma_1}{\bar{\gamma}}\right)}{\Gamma(m)}. \tag{9.17}$$

Figs. 9.7 shows the outage probability for various values of the Nakagami fading parameter and for target BERs of 10^{-3} and 10^{-6}, respectively.

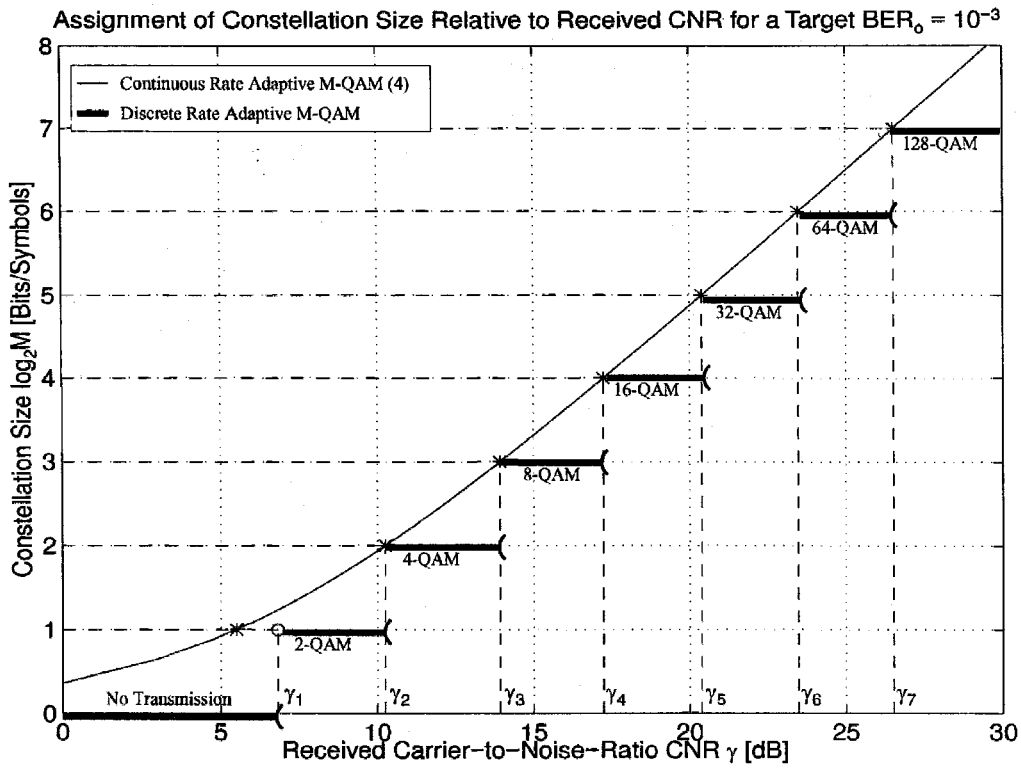

Figure 9.6: Number of bits per symbol versus CNR.

9.4.3 Achievable Spectral Efficiency

Integrating (9.15) over (9.1) and following the same steps of Section 9.3.2 which obtained (9.8), we find the average link spectral efficiency, $<R>_{\text{acr}}/W$, of the ACR M-QAM over NMF channels as

$$\frac{<R>_{\text{acr}}}{W} = \frac{e^{\frac{2mK_0}{3\overline{\gamma}}}}{\ln(2)} \sum_{k=0}^{m-1} \left(\frac{2mK_0}{3\overline{\gamma}}\right)^k \Gamma\left(-k, \frac{2mK_0}{3\overline{\gamma}}\right). \tag{9.18}$$

The average link spectral efficiency, $<R>_{\text{adr}}/W$, of the ADR M-QAM over NMF channels is just the sum of the data rates ($\log_2[M_n] = n$) associated with the individual $N+1$ regions, weighted by the probability $a_n = \int_{\gamma_n}^{\gamma_{n+1}} p_\gamma(\gamma)\, d\gamma$ that the CNR γ falls in the nth region:

$$\frac{<R>_{\text{adr}}}{W} = \sum_{n=1}^{N} n\, a_n, \tag{9.19}$$

where the a_ns can be expressed as

$$a_n = \frac{\Gamma\left(m, \frac{m\,\gamma_n}{\overline{\gamma}}\right) - \Gamma\left(m, \frac{m\,\gamma_{n+1}}{\overline{\gamma}}\right)}{\Gamma(m)}. \tag{9.20}$$

Figs. 9.8, 9.9, and 9.10 show the average link spectral efficiency of ACR M-QAM (9.18) and

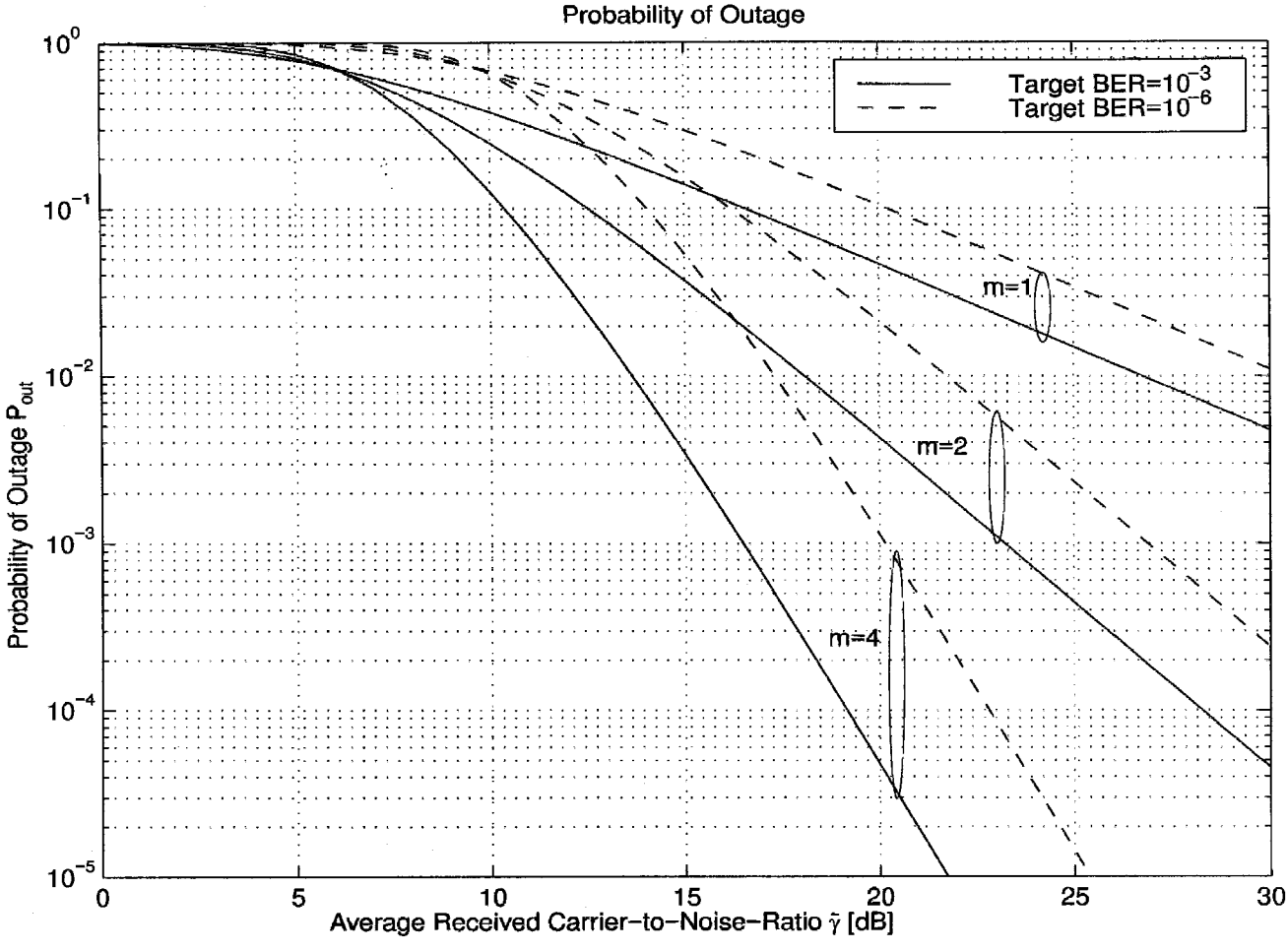

Figure 9.7: Outage probability in Nakagami fading.

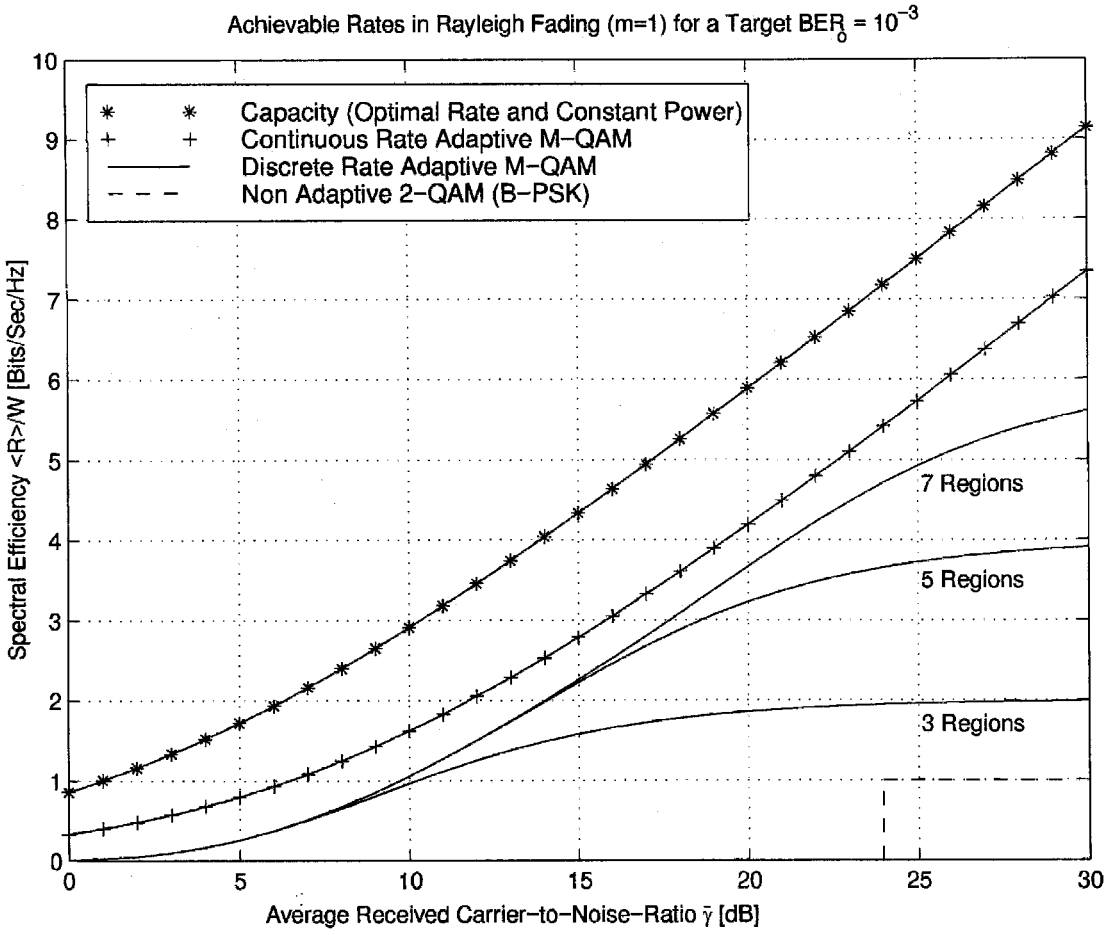

Figure 9.8: Achievable spectral efficiency for a target BER of 10^{-3} and $m = 1$ (Rayleigh fading).

ADR M-QAM (9.19) for a target $\text{BER}_0 = 10^{-3}$ and for m=1, $m = 2$, and $m = 4$, respectively. The Shannon capacity using constant-power and variable-rate (9.8) is also shown for comparison, along with the spectral efficiency of nonadaptive 2-QAM (BPSK). This latter efficiency is found by determining the value of the average received CNR for which the average BER of nonadaptive BPSK over Nakagami fading channel, as given by (9.24), equals the target BER. Note that the achievable spectral efficiency of ACR M-QAM comes within 5 dB of the Shannon capacity limit. ADR M-QAM suffers a minimum additional 1.2 dB penalty, whereas nonadaptive BPSK suffers a large spectral efficiency penalty.

9.4.4 Average Bit Error Rate

ACR M-QAM always operates at the target BER. However, since the choice of M_n in ADR M-QAM is done in a conservative fashion, this discrete technique operates at an average BER, $<\text{BER}>_{\text{adr}}$, smaller than the target BER. This BER can be computed exactly as the ratio of the average number

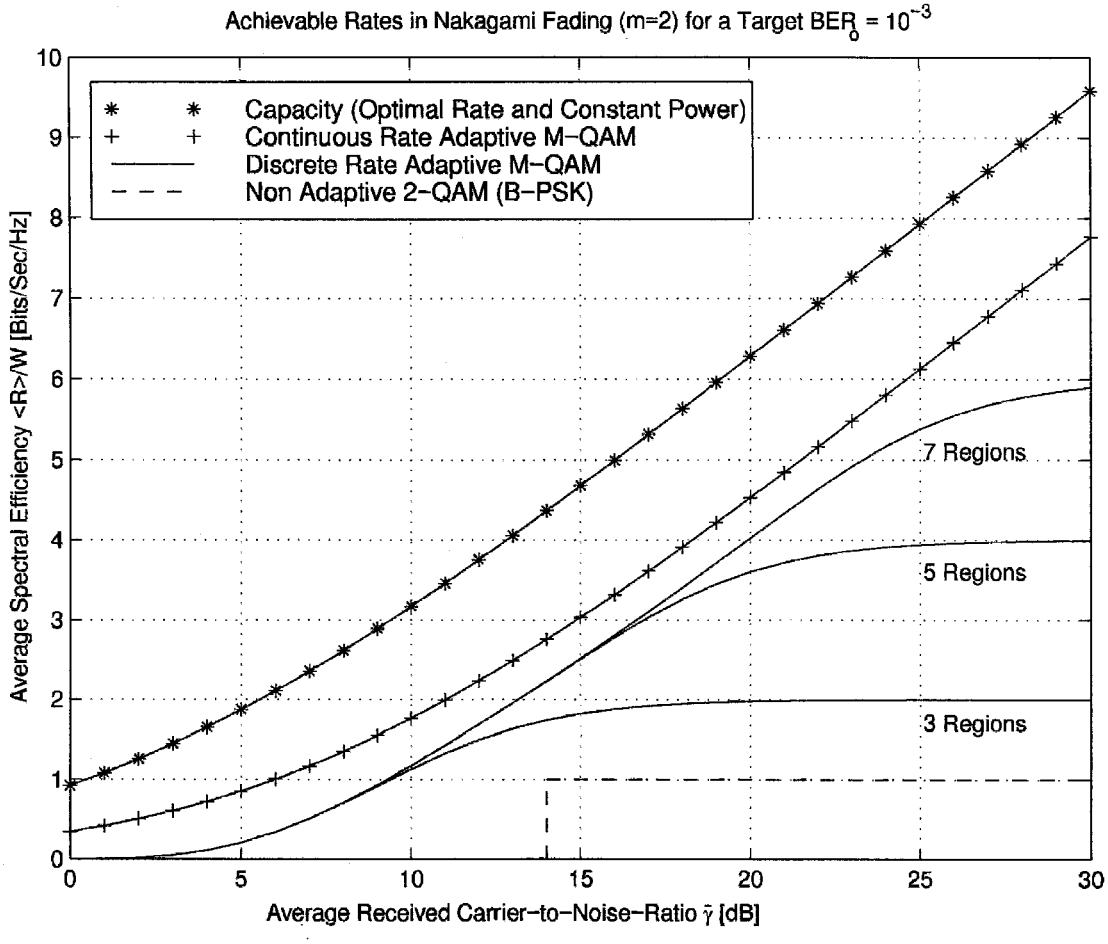

Figure 9.9: Achievable spectral efficiency for a target BER of 10^{-3} and $m = 2$.

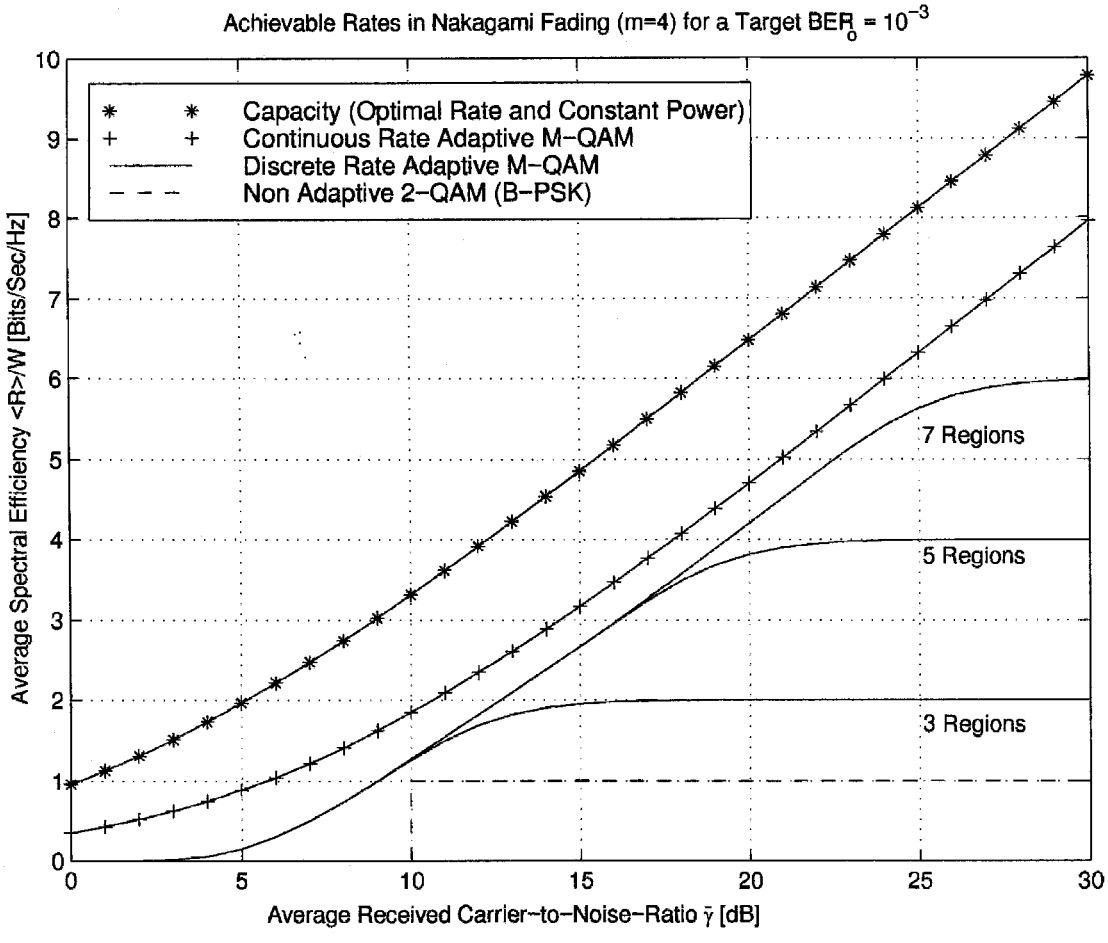

Figure 9.10: Achievable spectral efficiency for a target BER of 10^{-3} and $m = 4$.

of bits in error over the total average number of transmitted bits:

$$<\text{BER}>_{\text{adr}} = \frac{\sum_{n=1}^{N} n\ \overline{\text{BER}}_n}{\sum_{n=1}^{N} n\ a_n}, \tag{9.21}$$

where

$$\overline{\text{BER}}_n = \int_{\gamma_n}^{\gamma_{n+1}} \text{BER}(M_n, \gamma)\ p_\gamma(\gamma)\ d\gamma. \tag{9.22}$$

Using (9.1) and the approximation (9.14) in (9.22) $\overline{\text{BER}}_n$ can be expressed in closed-form as

$$\overline{\text{BER}}_n = \frac{0.2}{\Gamma(m)} \left(\frac{m}{\overline{\gamma}}\right)^m \frac{\Gamma(m, b_n\gamma_n) - \Gamma(m, b_n\gamma_{n+1})}{(b_n)^m}, \tag{9.23}$$

where

$$b_n = \frac{m}{\overline{\gamma}} + \frac{3}{2\ (2^n - 1)}; \qquad n = 1, 2, \cdots, N.$$

$\overline{\text{BER}}_n$ can also be computed exactly by using the exact expressions for the $\text{BER}(M_n, \gamma)$ as given in [115, Chapter 5] and [142].

Figs. 9.11, 9.12, and 9.13 show the average BER for ADR M-QAM for a target BER of 10^{-3} and for $m = 1$, $m = 2$, and $m = 4$, respectively. The BER calculations based on the approximation (9.23) are plotted as solid lines whereas the exact average BERs are plotted as star/solid lines. The average BER of nonadaptive BPSK over Nakagami fading channel is given by

$$<\text{BER}>_{\text{bpsk}} = \frac{1}{2}\sqrt{\frac{\overline{\gamma}}{\pi}}\ \frac{m^m}{(m+\overline{\gamma})^{m+1/2}}\ \frac{\Gamma(m+1/2)}{\Gamma(m+1)}\ {}_2F_1\left(1, m+1/2; m+1; \frac{m}{m+\overline{\gamma}}\right), \tag{9.24}$$

where ${}_2F_1(.,.;.;.)$ denotes the Gauss' hypergeometric function [53]. We plot (9.24) in Figs. 9.11, 9.12, and 9.13 in dashed lines for comparison with (9.21).

In these figures we observe similar trends in the average BER for various values of the m parameter. For instance, we see that the average BER of ADR M-QAM is always below the 10^{-3} target BER. Recall that the approximation (9.14) lower bounds the exact BER for M=2 and that ADR M-QAM often uses the 2-QAM constellation (B-PSK) at low average CNRs. This explains why the average BER based on the approximation (9.23) lower bounds the exact average BER for $\overline{\gamma} \leq 10$ dB. Conversely, because of the fact that the approximation (9.14) upper bounds the exact BER for $M > 2$ and because ADR M-QAM often uses the high constellation sizes at high average CNRs the closed-form approximate average BER for ADR M-QAM tightly upper-bounds the exact average BER for $\overline{\gamma} \geq 10$ dB. Since ADR M-QAM uses the largest available constellation often when the average CNR is large, the average BER prediction as $\overline{\gamma}$ increases becomes dominated by the BER performance of that constellation.

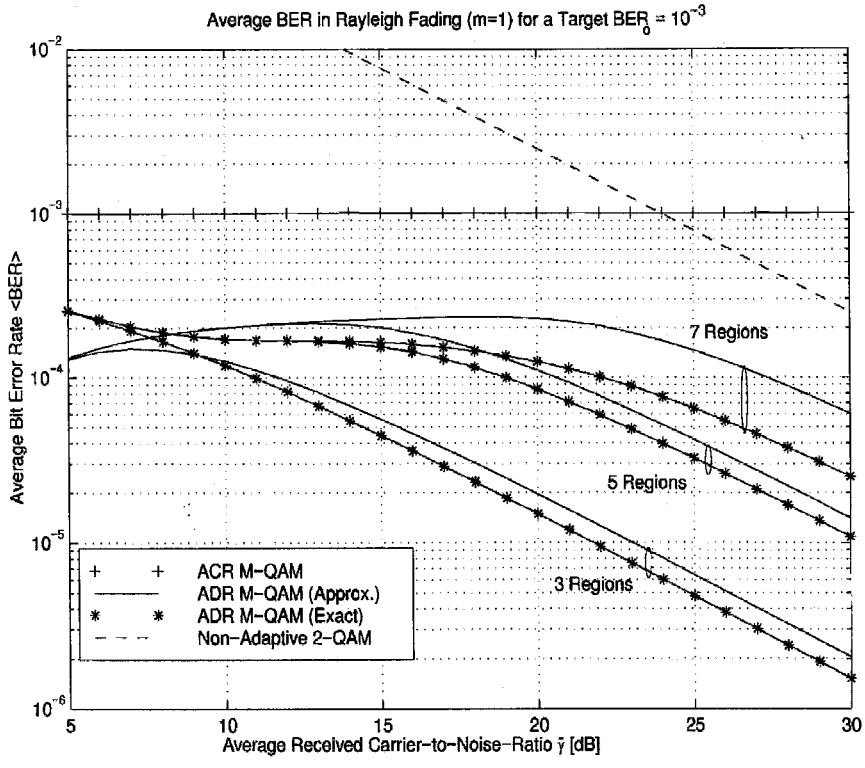

Figure 9.11: Average BER for a target BER of 10^{-3} and $m = 1$ (Rayleigh).

9.5 Impact of Time Delay

Recall from Section 9.2.1 that the choice of the constellation size is based on a channel estimate at time t, whereas the data are sent over the channel at time $t+\tau$ such that $\tau_{fb} \leq \tau \leq \tau_t$. If a delay of τ_{fb} degrades BER significantly, then this adaptive technique will not work, since τ_{fb} is an inherent and unavoidable parameter of the system. However, if a delay of $\tau \geq \tau_{fb}$ has a small impact on the BER then we should choose τ_t as large as possible so that we meet the BER requirement while minimizing the rate of system reconfiguration. In this section we analyze the impact of time delay on the performance of adaptive M-QAM over NMF channels, assuming perfect channel estimates.

9.5.1 Fading Correlation

Investigating the impact of time delay requires the second-order statistics for the channel variation, which are known for Nakagami fading. Let α and α_τ denote the channel gains at a time t and $t+\tau$, respectively. For a slowly-varying channel we can assume that the *average* received power remains constant over the time delay τ (i.e., $\Omega = E(\alpha^2) = E(\alpha_\tau^2)$). Under these conditions the joint PDF

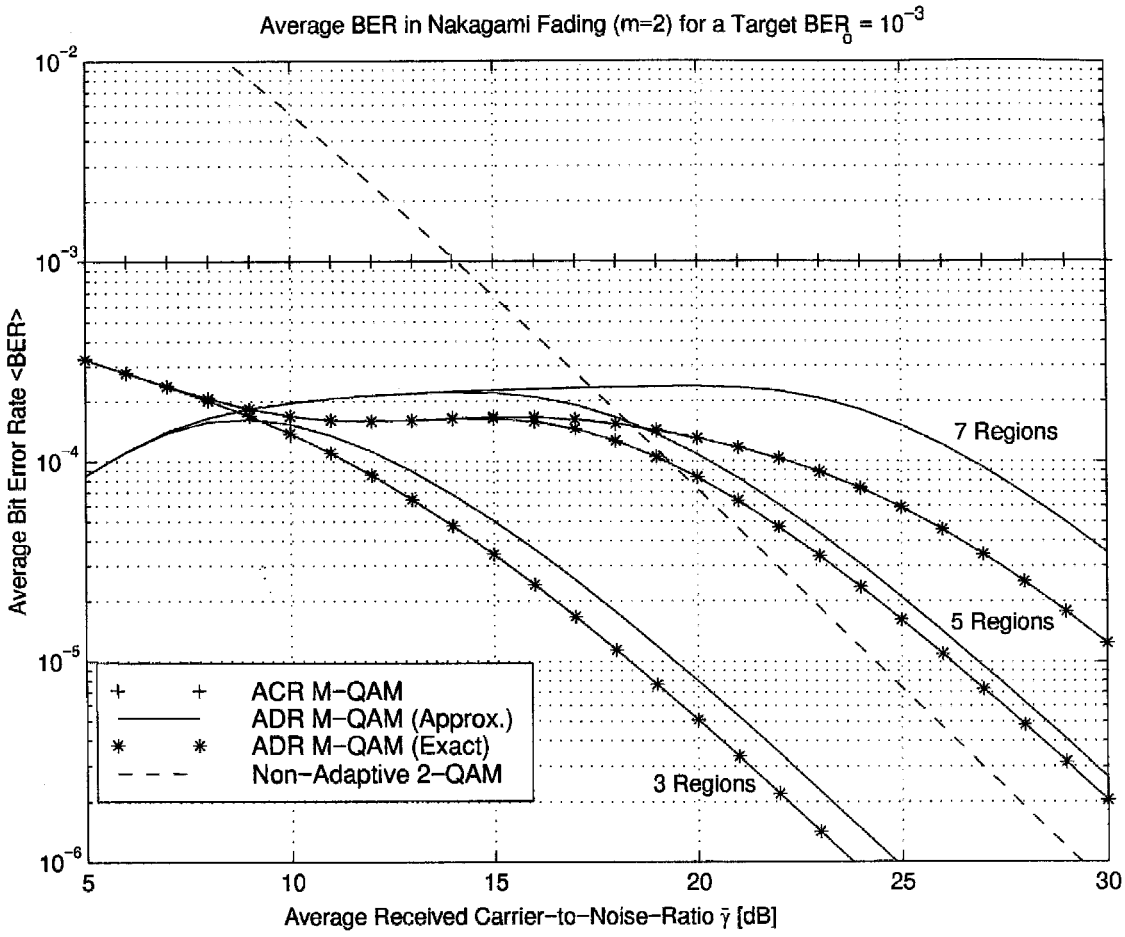

Figure 9.12: Average BER for a target BER of 10^{-3} and $m = 2$.

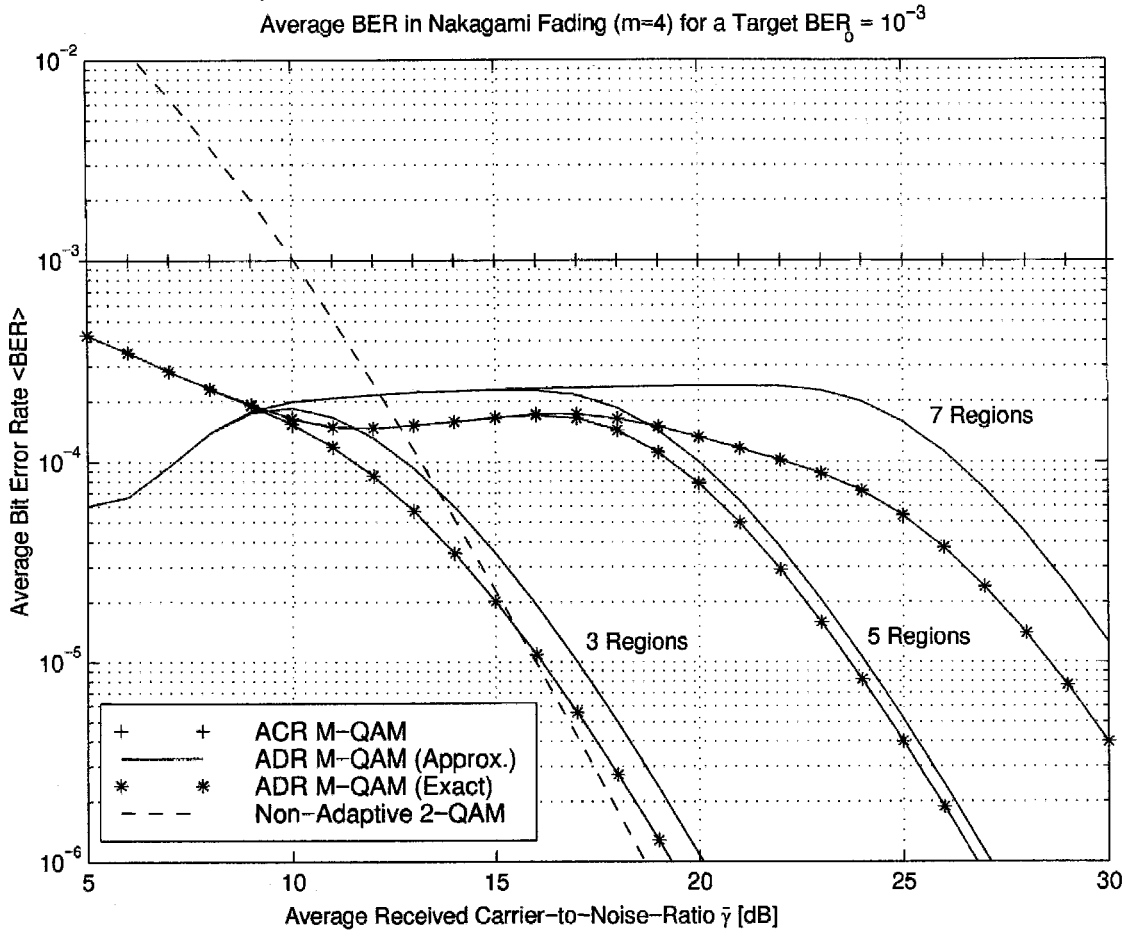

Figure 9.13: Average BER for a target BER of 10^{-3} and $m = 4$.

$p_{\alpha,\alpha_\tau}(\alpha,\alpha_\tau)$ of these two correlated Nakagami-m distributed channel gains is given by [13, (126)]

$$p_{\alpha,\alpha_\tau}(\alpha,\alpha_\tau) = \frac{4\ (\alpha\ \alpha_\tau)^m}{(1-\rho)\ \Gamma(m)\ \rho^{(m-1)/2}} \left(\frac{m}{\Omega}\right)^{m+1} I_{m-1}\left(\frac{2m\sqrt{\rho}\ \alpha\alpha_\tau}{(1-\rho)\Omega}\right) \exp\left(-\frac{m\ (\alpha^2+\alpha_\tau^2)}{(1-\rho)\ \Omega}\right), \tag{9.25}$$

where $I_{m-1}(.)$ is the $(m-1)th$-order modified Bessel function of the first kind [53], and ρ is the correlation factor between α and α_τ. Since Nakagami fading assumes isotropic scattering of the multipath components, ρ can be expressed in terms of the time delay τ, the mobile speed, v [m/s], and the wavelength of the carrier frequency λ_c [m] as $\rho = J_0^2(2\pi f_D \tau)$, where $J_0(.)$ is the zero-order Bessel function of the first kind [53], and $f_D = v/\lambda_c$ [Hz] is the maximum Doppler frequency shift [108, p. 31].

The PDF of α_τ conditioned on α, $p_{\alpha_\tau/\alpha}(\alpha_\tau/\alpha)$, is given by

$$p_{\alpha_\tau/\alpha}(\alpha_\tau/\alpha) = \frac{p_{\alpha_\tau,\alpha}(\alpha_\tau,\alpha)}{p_\alpha(\alpha)}. \tag{9.26}$$

Inserting (11.3) and (9.25) in (9.26) and expressing the result in terms of the CNRs γ and γ_τ yields

$$p_{\gamma_\tau/\gamma}(\gamma_\tau/\gamma) = \frac{m}{(1-\rho)\overline{\gamma}} \left(\frac{\gamma_\tau}{\rho\ \gamma}\right)^{(m-1)/2} I_{m-1}\left(\frac{2m\sqrt{\rho\gamma\gamma_\tau}}{(1-\rho)\ \overline{\gamma}}\right) \exp\left(-\frac{m(\rho\gamma+\gamma_\tau)}{(1-\rho)\ \overline{\gamma}}\right). \tag{9.27}$$

9.5.2 Analysis

Adaptive Continuous Rate M-QAM

For all delays τ let the communication system be configured according to γ (CNR at $\tau = 0$) such that $M(\gamma)$ is given by

$$M(\gamma) = 1 + \frac{3\ \gamma}{2\ K_0}. \tag{9.28}$$

The constellation size $M(\gamma)$ is based on the value γ at time t, but that constellation is transmitted over the channel at time $t+\tau$, when γ has changed to γ_τ. Since M does not depend on γ_τ (CNR at time τ), time delay does not affect the link spectral efficiency $<\log_2 M>$, as calculated in Section IV-C. However, delay affects the instantaneous BER, which becomes a function of the "mismatch" between γ_τ and γ:

$$\mathrm{BER}(\gamma_\tau/\gamma) = \mathrm{BER}(M(\gamma),\gamma_\tau) = 0.2\ (5\ \mathrm{BER_o})^{\gamma_\tau/\gamma}. \tag{9.29}$$

Integrating (9.29) over the conditional PDF (9.27) yields the average BER conditioned on γ, $\mathrm{BER}(\gamma)$, as

$$\mathrm{BER}(\gamma) = \int_0^{+\infty} \mathrm{BER}(\gamma_\tau/\gamma)\ p_{\gamma_\tau/\gamma}(\gamma_\tau/\gamma)\ d\gamma_\tau. \tag{9.30}$$

Inserting (9.27) and (9.29) in (9.30), $\mathrm{BER}(\gamma)$ can be written in closed-form with the help of the

generalized Marcum Q-function of order m, $Q_m(.,.)$ [145, p. 299, (11.63)]

$$\mathrm{BER}(\gamma)=0.2\left(\frac{m\,\gamma}{m\,\gamma+\overline{\gamma}\,(1-\rho)\,K_0}\right)^m \exp\left(-\frac{\rho\,K_0\,m\,\gamma}{m\,\gamma+\overline{\gamma}\,(1-\rho)\,K_0}\right) Q_m\left(\frac{\rho\,m^2\,\gamma^2}{\overline{\gamma}(1-\rho)(m\gamma+\overline{\gamma}(1-\rho)K_0)},0\right). \tag{9.31}$$

Using the recurrence relation [145, p. 299, (11.64)]

$$Q_{m+1}(x,y)=Q_m(x,y)+\left(\frac{y}{x}\right)^{m/2} I_m(2\sqrt{xy})\,e^{-x}, \tag{9.32}$$

we get that for all x, $Q_m(x,0)=Q_1(x,0)$, which can be shown to equal 1. Therefore, $\mathrm{BER}(\gamma)$ reduces to:

$$\mathrm{BER}(\gamma)=0.2\left(\frac{m\,\gamma}{m\,\gamma+\overline{\gamma}\,(1-\rho)\,K_0}\right)^m \exp\left(-\frac{\rho\,K_0\,m\,\gamma}{m\,\gamma+\overline{\gamma}\,(1-\rho)\,K_0}\right). \tag{9.33}$$

Although this formula was derived for integer m it is also valid for all non-integer values of $m \geq 1/2$. Averaging (9.33) over the PDF of γ (9.1) yields the average BER of ACR M-QAM, $<\mathrm{BER}>_{\mathrm{acr}}$, as

$$<\mathrm{BER}>_{\mathrm{acr}}=\int_{\gamma_1}^{+\infty} \mathrm{BER}(\gamma)\,p_\gamma(\gamma)\,d\gamma. \tag{9.34}$$

Finally, using (9.33) in (9.34) and making the substitution $u=\frac{m\,\gamma}{m\,\gamma+(1-\rho)K_0\overline{\gamma}}$ yields

$$<\mathrm{BER}>_{\mathrm{acr}}=\frac{0.2\,(1-\rho)^m\,K_0^m}{\Gamma(m)}\int_{u_1}^{1}\frac{u^{2m-1}}{(1-u)^{m+1}}\exp\left(-\frac{K_0u(1-\rho u)}{1-u}\right)du, \tag{9.35}$$

where

$$u_1=\frac{m\,\gamma_1}{m\,\gamma_1+(1-\rho)K_0\overline{\gamma}}.$$

Since this analysis assumes continuous rate adaptation and since $M_n(\gamma) \leq M(\gamma)$ for all γ, (9.35) represents an upper-bound on the average BER degradation for ADR M-QAM, as will be confirmed in the following sections.

Adaptive Discrete Rate M-QAM

Suppose now that the constellation size M_n is chosen based on the value of γ according to the ADR M-QAM scheme described in Section 9.4.1. This constellation is transmitted over the channel when γ has changed to γ_τ. As in the continuous rate M-QAM case, we can easily see that the link spectral efficiency of ADR M-QAM is unaffected by time delay. However, delay affects $<\mathrm{BER}>_{\mathrm{adr}}$, which is computed from (9.21) with $\overline{\mathrm{BER}}_n$ replaced by $\overline{\mathrm{BER}}_n'$, where

$$\overline{\mathrm{BER}}_n'=\int_{\gamma_n}^{\gamma_{n+1}}\int_0^{\infty}\mathrm{BER}(M_n,\gamma_\tau)\,p_{\gamma_\tau/\gamma}(\gamma_\tau/\gamma)\,d\gamma_\tau\,p_\gamma(\gamma)\,d\gamma.$$

Using again the generalized Marcum Q-functions, it can be shown that

$$\overline{\mathrm{BER}}_n' = \frac{0.2}{\Gamma(m)} \left(\frac{m}{\overline{\gamma}}\right)^m \frac{\Gamma(m, b_n'\gamma_n) - \Gamma(m, b_n'\gamma_{n+1})}{(b_n)^m}, \tag{9.36}$$

where

$$b_n' = \frac{m}{\overline{\gamma}} + \frac{3\,\rho\,m}{3(1-\rho)\overline{\gamma} + 2m(2^n - 1)}; \qquad n = 1, 2, \cdots, N.$$

Note that as $\rho \to 1$ (i.e., $\tau \to 0$), $b_n' \to b_n$, and $\overline{\mathrm{BER}}_n'$ (9.36) reduces to $\overline{\mathrm{BER}}_n$ (9.23), as expected.

9.5.3 Numerical Results

Figs. 9.14 and 9.15 show $<\mathrm{BER}>_{\mathrm{acr}}$ and $<\mathrm{BER}>_{\mathrm{adr}}$ as a function of the normalized time delay $f_D\tau$ for different values of the Nakagami m parameter, for a target BER of 10^{-3} and 10^{-6}, respectively. It can be seen from Figs. 9.14 and 9.15 that a normalized time delay up to about 10^{-2} can be tolerated without a noticeable degradation in the average BER. For example, for a 900 MHz carrier frequency and a target BER of 10^{-3}, a time delay up to 3.33 ms can be tolerated for pedestrians with a speed of 1 m/s (3.6 km/hr), and a time delay up to 0.133 ms can be tolerated for mobile vehicles with a speed of 25 m/s (90 km/hr). Comparing Figs. 9.14 and 9.15, we see that systems with the lower BER requirements of 10^{-6} are more sensitive to time delay, as they will suffer a higher "rate of increase" in BER. For example, in Rayleigh fading, systems with a 10^{-3} BER requirement suffer about one order of magnitude degradation for $f_D\tau$ between 10^{-2} and 10^{-1}, whereas systems with a 10^{-6} BER requirement suffer about four orders of magnitude degradation for the same range of $f_D\tau$. However, in both cases these systems will be able to operate satisfactorily if the normalized delay is below the critical value of 10^{-2}.

9.6 Conclusion

We have studied the capacity of NMF channels with an average power constraint for three power and rate adaptation policies. We obtained closed-form solutions for NMF channel capacity for each power and rate adaptation strategy. Our results show that optimal power and rate adaptation yields a small increase in capacity over just optimal rate adaptation with constant power, and this small increase in capacity diminishes as the average received carrier-to-noise ratio, and/or the m parameter increases. Fixed rate transmission with channel inversion suffers the largest capacity penalty. However, this penalty diminishes as the amount of fading decreases. Based on these results we conclude that rate rather than power adaptation is the key to increasing link spectral efficiency. We therefore proposed and studied the performance of constant-power variable-rate M-QAM schemes over NMF channels assuming perfect channel estimation and negligible time delay.

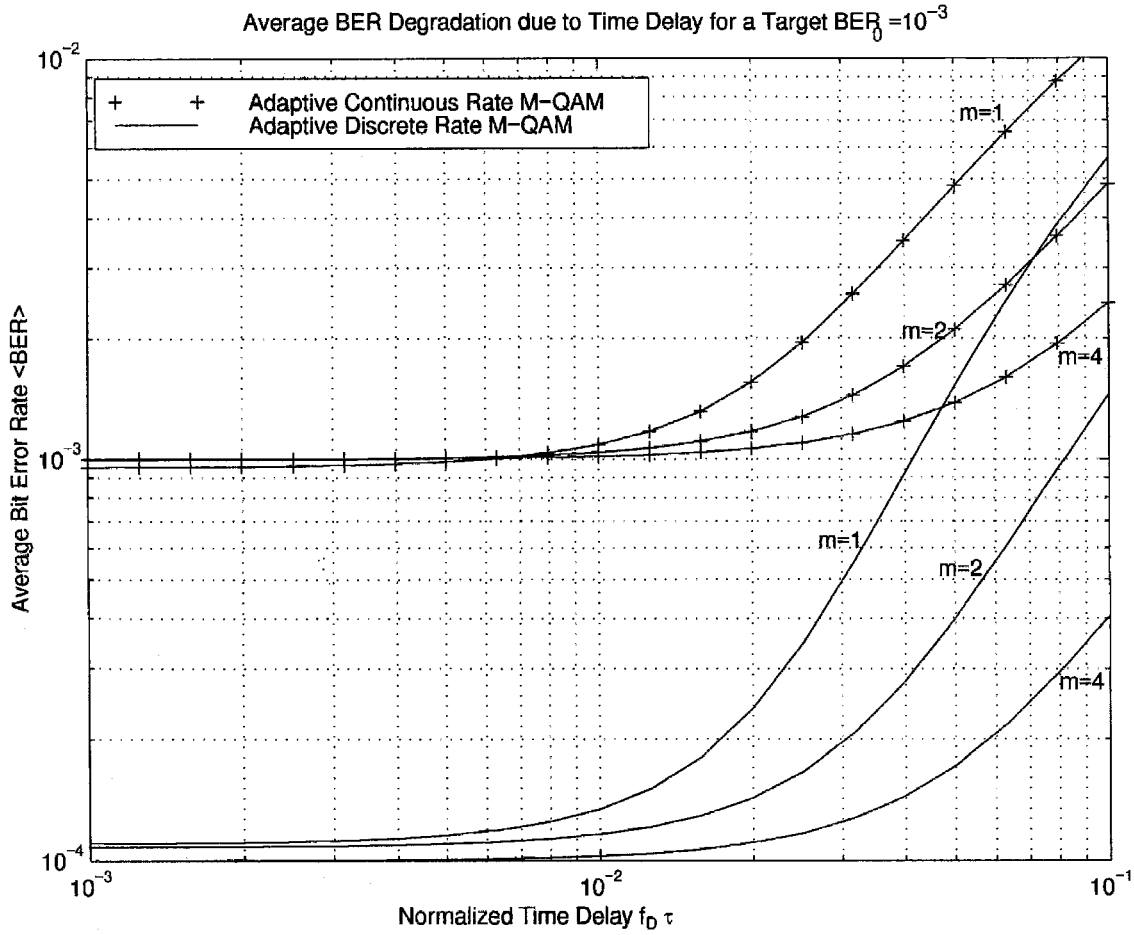

Figure 9.14: Average BER vs. normalized time delay for a BER_0 of 10^{-3}, $\overline{\gamma}$=20 dB, and 5 fading regions.

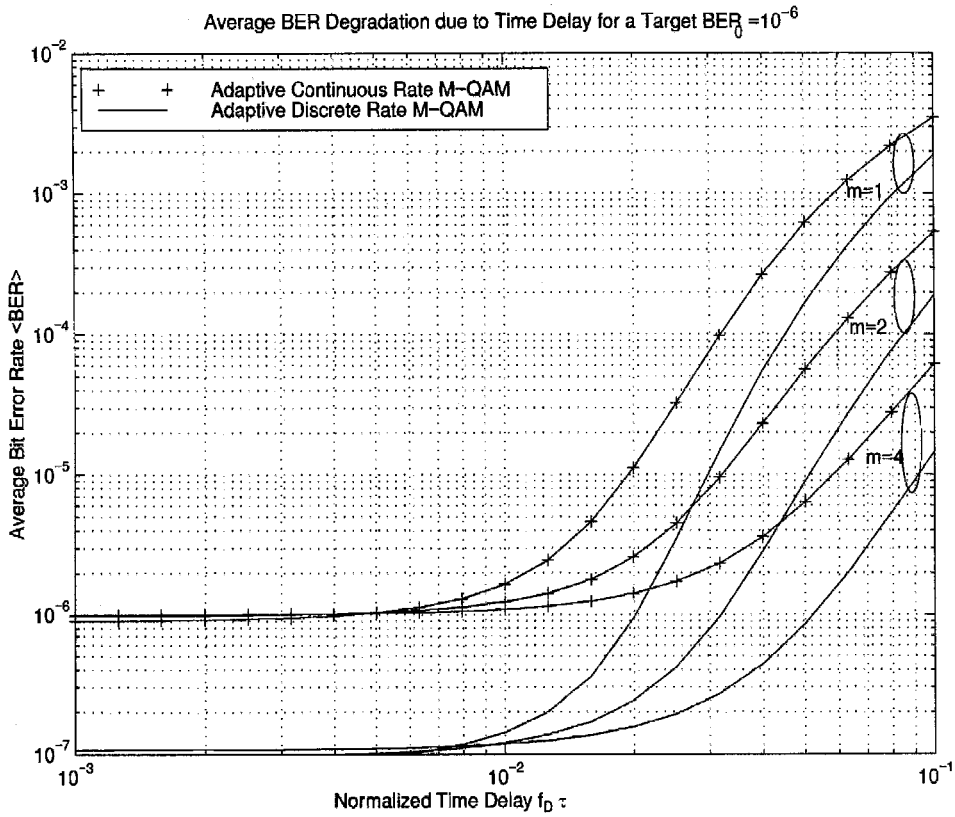

Figure 9.15: Average BER vs. normalized time delay for a BER_0 of 10^{-6}, $\overline{\gamma}$=20 dB, and 5 fading regions.

We determined their spectral efficiency and compared this to the theoretical maximum. Our results show that for a target BER of 10^{-3}, the spectral efficiency of adaptive continuous rate M-QAM comes within 5 dB of the Shannon capacity limit and adaptive discrete rate M-QAM comes within 6.2 dB of this limit. We also analyzed the impact of time delay on the BER of adaptive M-QAM. Results show that systems with low BER requirements will be more sensitive to time delay but will still be able to operate satisfactorily if the normalized time delay is below the critical value of 10^{-2}.

Chapter 10 Simultaneous Voice and Data Transmission over Fading Channels

10.1 Introduction

Future wireless communication systems will have to support not only voice services but also data services including facsimile, file transfer, e-mail, and Internet access. The need for spectrally-efficient communication has recently led to the development of adaptive transmission techniques as described in the previous chapter. In general, voice transmission has low data rate requirements with real-time delay constraints, while data transmission demands higher rates with less stringent delay requirements. This suggests that fixed-rate transmission combined with power adaptation, where the transmitter adjusts its power to maintain a constant CNR at the receiver, is well-suited to voice, while bursty variable-rate transmission which maximizes average spectral efficiency is best suited to data communication. In addition, voice and data typically have very different bit-error-rate (BER) requirements which must be incorporated into their respective transmission schemes.

Several Media Access Control (MAC) proposals have been presented in recent years to allow the integration of voice and data for wireless systems [146, 147, 148, 149, 150, 151]. Other techniques have been developed for simultaneous voice and data transmission over the general switched telephone network [152]. In this paper we propose a new hybrid adaptive scheme which supports simultaneous voice and data transmission over fading channels[1]. The originality of the proposed scheme is that it offers a link layer solution to the voice and data integration problem by designing the modulation to support their respective requirements.

The remainder of this chapter is organized as follow. The next section describes the channel model. Section 10.3 presents the details of the proposed scheme. The performance of this scheme assuming perfect channel estimation and negligible time delay is analyzed in Section 10.4. In particular closed-form expressions for the outage probability, average allocated power, achievable spectral efficiency, and average BER for both voice and data transmission are derived. Numerical and simulation results that allow discussion of the behavior of the proposed scheme are also presented. Our conclusion are given in Section 10.5.

[1]More generally the proposed scheme is capable of handling two independent information streams which are inherently different: i.e., they may be generated by different sources and may also differ in their delay and BER requirements.

10.2 Channel Model

We consider a slowly-varying flat-fading channel changing at a rate much slower than the symbol data rate, so the channel remains roughly constant over hundreds of symbols. We assume that the multipath fading environment is characterized by the Nakagami-m probability density function (PDF). Hence the channel fading amplitude α is given by (2.14)

$$p_\alpha(\alpha) = 2\left(\frac{m}{\Omega}\right)^m \frac{\alpha^{2m-1}}{\Gamma(m)} \exp\left(-m\frac{\alpha^2}{\Omega}\right), \quad \alpha \geq 0, \tag{10.1}$$

where $\Omega = E(\alpha^2)$ is the average received power, m is the Nakagami *fading parameter* ($m \geq 1/2$), and $\Gamma(.)$ is the *gamma function* defined by [53, p. 942, (8.310.1)]:

$$\Gamma(z) = \int_0^{+\infty} t^{z-1}\, e^{-t}\, dt; \quad z \geq 0. \tag{10.2}$$

Given the channel fading amplitude α, a signal power P [W], a signal bandwidth of W [Hz], and a noise power density of N_0 [W/Hz], let us define the CNR $\gamma = \frac{\alpha^2 P}{N_0 W}$. By using a standard transformation of random variables, it can be shown that the CNR, γ, is distributed according to a gamma distribution, $p_\gamma(\gamma)$, given by (9.1)

$$p_\gamma(\gamma) = \left(\frac{m}{\overline{\gamma}}\right)^m \frac{\gamma^{m-1}}{\Gamma(m)} \exp\left(-m\,\frac{\gamma}{\overline{\gamma}}\right), \quad \gamma \geq 0, \tag{10.3}$$

where $\overline{\gamma}$ is the average CNR.

As discussed in Section 2.3.1 we use the Nakagami-m distribution since it can represent a range of multipath channels via the m parameter. Another feature of the Nakagami-m model is that the fading parameter m, when restricted to integer values, can be interpreted as the order of diversity available for a Rayleigh channel with maximal-ratio combining (MRC). Hence all the expressions derived herein can be used to obtain the performance over a Rayleigh fading channel with m-fold MRC diversity, assuming that m is an integer.

10.3 Proposed Modulation Scheme

The proposed modulation scheme is a generalized and adaptive version of the Unbalanced Quadrature Phase Shift Keying (UQPSK) [153], [51, p. 622], which also offers the capability of handling two different types of data. For instance, UQPSK was used by the space shuttle and the Tracking and Data Relay Satellite System (TDRSS) to communicate scientific data on the inphase (I) channel and operational/telemetry data on the quadrature (Q) channel. In our case we propose to devote the I channel to data communications while transmitting voice over the Q channel. In contrast to

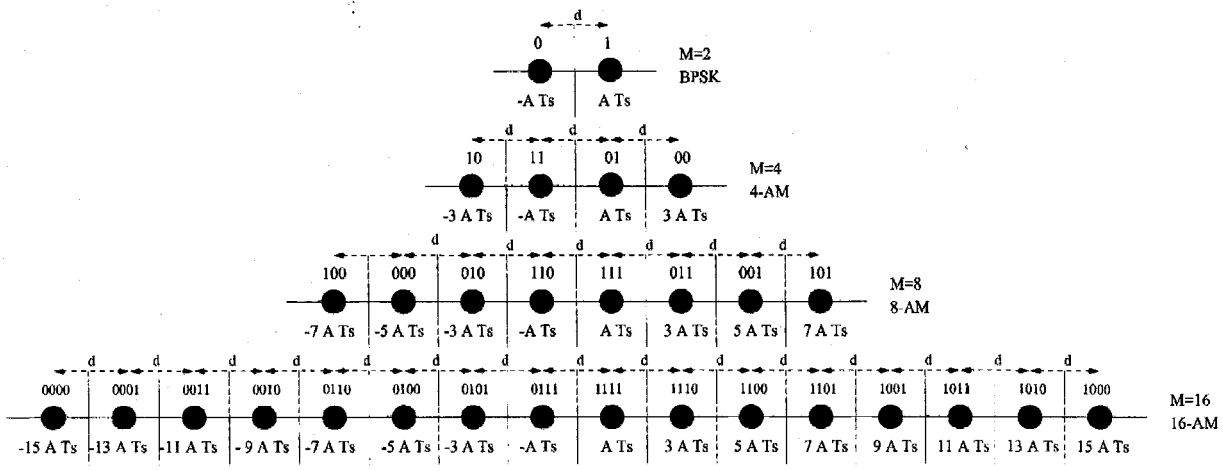

Figure 10.1: Gray mapping for the M-AM constellations.

UQPSK, where binary phase shift keying (BPSK) modulation is used on both channels, our scheme uses BPSK on the Q channel for voice and M-ary amplitude modulation (M-AM) [51, p. 219], [1, p. 272] (also known as M-ary amplitude shift keying (M-ASK)) [2] on the I channel for data. In this section we first introduce the hybrid BPSK/M-AM modulation scheme. We then present the details of the proposed adaptive scheme.

10.3.1 Hybrid BPSK/M-AM Modulation Scheme

A block diagram of the proposed hybrid BPSK/M-AM modulation scheme is shown in Fig. 10.2. Following the form of the UQPSK modulation [51, p. 622], the hybrid BPSK/M-AM transmitted signal can be written as

$$s(t) = \sqrt{2}\ \left[\sqrt{P_d}\ d(t)\ \cos(\omega_c t) - \sqrt{P_v}\ v(t)\ \sin(\omega_c t)\right], \tag{10.4}$$

where w_c is the radian carrier frequency, and P_d and P_v are the powers of the I (data) and Q (voice) components of $s(t)$, respectively. In (10.4) $d(t)$ and $v(t)$ correspond to the data and voice symbol streams, respectively, that is,

$$\begin{aligned} d(t) &= \sum_{i=-\infty}^{\infty} \tilde{d}_i\ p(t - iT_s) \\ v(t) &= \sum_{i=-\infty}^{\infty} v_i\ p(t - iT_s), \end{aligned} \tag{10.5}$$

where $p(t)$ is a unit power shaping pulse of duration T_s (the signal bandwidth is hence $W \simeq 1/T_s$). In (10.5) $\{\tilde{d}_i\}$ ($\tilde{d}_i = \pm 1, \pm 3, \cdots, \pm M - 1$) are the Gray-mapped data symbols of the data bits $\{d_i\}$

[2] We use here a symmetric M-AM constellation in which the signal points are symmetrically located about the origin as shown in Fig. 10.1.

(as depicted in Fig. 10.1) and $\{v_i\}$ are the voice bits.

The channel introduces a multiplicative fading gain α, a phase shift θ and additive white Gaussian noise (AWGN) term $n(t)$ with power spectral density $N_0/2$ [W/Hz]. Hence the received signal can be written as

$$r(t) = \sqrt{2}\ \alpha \left[\sqrt{P_d}\ d(t)\ \cos(\omega_c t + \theta) - \sqrt{P_v}\ v(t)\ \sin(\omega_c t + \theta)\right] + n(t). \tag{10.6}$$

Assuming perfect channel estimation ($\hat{\alpha} = \alpha$ and $\hat{\theta} = \theta$), the received signal is first coherently demodulated, then the I (data) signal is passed through an adaptive gain controller (AGC). Both I and Q signals are passed through matched filters, then sampled (at times $t = (i+1)T_s$) to form the decision variables $V_{d,i}$ and $V_{v,i}$ given by

$$\begin{aligned} V_{d,i} &= \alpha\ \sqrt{P_d}\ \tilde{d}_i + N_I, \\ V_{v,i} &= \alpha\ \sqrt{P_v}\ v_i + N_Q, \end{aligned} \tag{10.7}$$

where N_I and N_Q are independent zero-mean Gaussian noise samples with the same variance $N_0 T_s/2$. For uncoded data and voice streams and independent hard decisions on the I and Q channels (see Fig. 10.2), the conditional (conditioned on α) symbol error rate (SER), $\mathrm{SER}_d(M, \gamma_d)$, for data and BER, $\mathrm{BER}_v(\gamma_v)$, for voice are given by [51, p.631]

$$\mathrm{SER}_d(M, \gamma_d) = \frac{M-1}{M}\ \mathrm{erfc}\left(\sqrt{\frac{3\ \gamma_d}{M^2-1}}\right), \tag{10.8}$$

$$\mathrm{BER}_v(\gamma_v) = \frac{1}{2}\ \mathrm{erfc}\left(\sqrt{\gamma_v}\right), \tag{10.9}$$

where $\gamma_d = \frac{\alpha^2\ P_d}{N_0\ W}$, and $\gamma_v = \frac{\alpha^2\ P_v}{N_0\ W}$ are the "data" and "voice" instantaneous CNR, respectively, and $\mathrm{erfc}(\cdot)$ is the *complementary error function* defined by

$$\mathrm{erfc}(z) = \frac{2}{\sqrt{\pi}} \int_z^\infty e^{-t^2}\ dt. \tag{10.10}$$

The data symbol estimates $\hat{\tilde{d}}_i$ are then passed through an M-ary Gray de-mapper to obtain an estimate of the source data bits $\hat{d}_i$. Using the same procedure described in [154], [115, Chapter 5] to obtain the exact BER of square M-ary quadrature amplitude modulation (M-QAM) with two-dimensional Gray coding, we derived exact BER expressions for the M-AM modulation with Gray coding as shown in Fig. 10.1. The procedure as well as the exact BER expressions are given in the Appendix. These exact BER expressions are plotted by the solid lines in Fig. 10.3 and are in excellent agreement with Monte-Carlo simulated BER values which are plotted by 'o' on the same Fig. 10.3. For large CNR, where the probability of symbol error is dominated by the probability

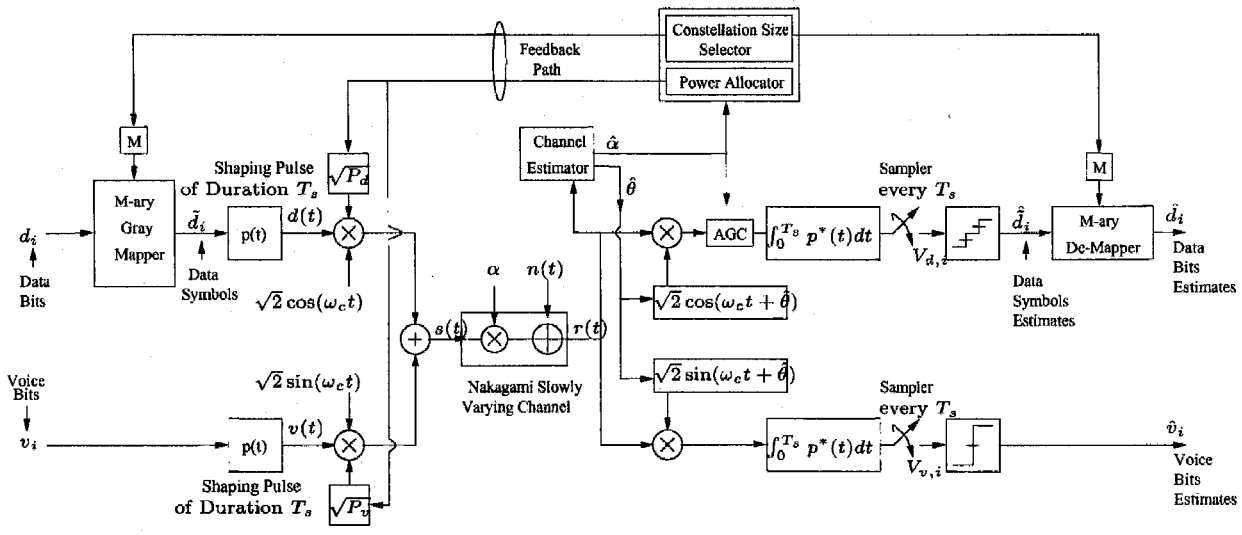

Figure 10.2: Block diagram of the proposed adaptive system.

of adjacent symbol error, the BER with Gray encoding can be approximated by [51, p. 210], [1, p. 265]

$$\mathrm{BER}_d(M, \gamma_d) \simeq \frac{\mathrm{SER}_d(M, \gamma_d)}{\log_2 M}. \tag{10.11}$$

For comparison, the dash lines in Fig. 10.3 show the BER approximation (10.11) for different values of M. Note that (10.11) lower bounds the exact BER expressions (as given in the Appendix) for all values of M and the bound is tighter for low M and high CNR. Using the Chernoff-bound on the erfc(·) function in (10.11), it can be shown that (10.11) is upper-bounded for large CNR by

$$\mathrm{BER}_d(M, \gamma_d) \simeq \frac{\mathrm{SER}_d(M, \gamma_d)}{\log_2 M} \leq 0.1 \exp\left(-\frac{3\,\gamma_d}{2\,(M^2-1)}\right). \tag{10.12}$$

For comparison, the BER upper-bound (10.12) is plotted in Fig. 10.3 by star/solid lines for different values of M. Note that (10.12) tightly upper bounds the exact BER expressions (as given in the Appendix) for all values of M and for BER $\leq 10^{-4}$, which is the BER range of interest for data transmission. Hence we will use this upper-bound (10.12) to derive closed-form expressions which upper-bound the average data BER. In addition, (10.12) has the advantage of being "invertible" in the sense that it provides simple expressions for the data "switching thresholds," as shown below.

10.3.2 Proposed Adaptive Scheme

We now describe the details of our proposed system shown in Fig. 10.2. A pilot tone continually sends a known "channel sounding" sequence so that the channel-induced envelope fluctuation α can

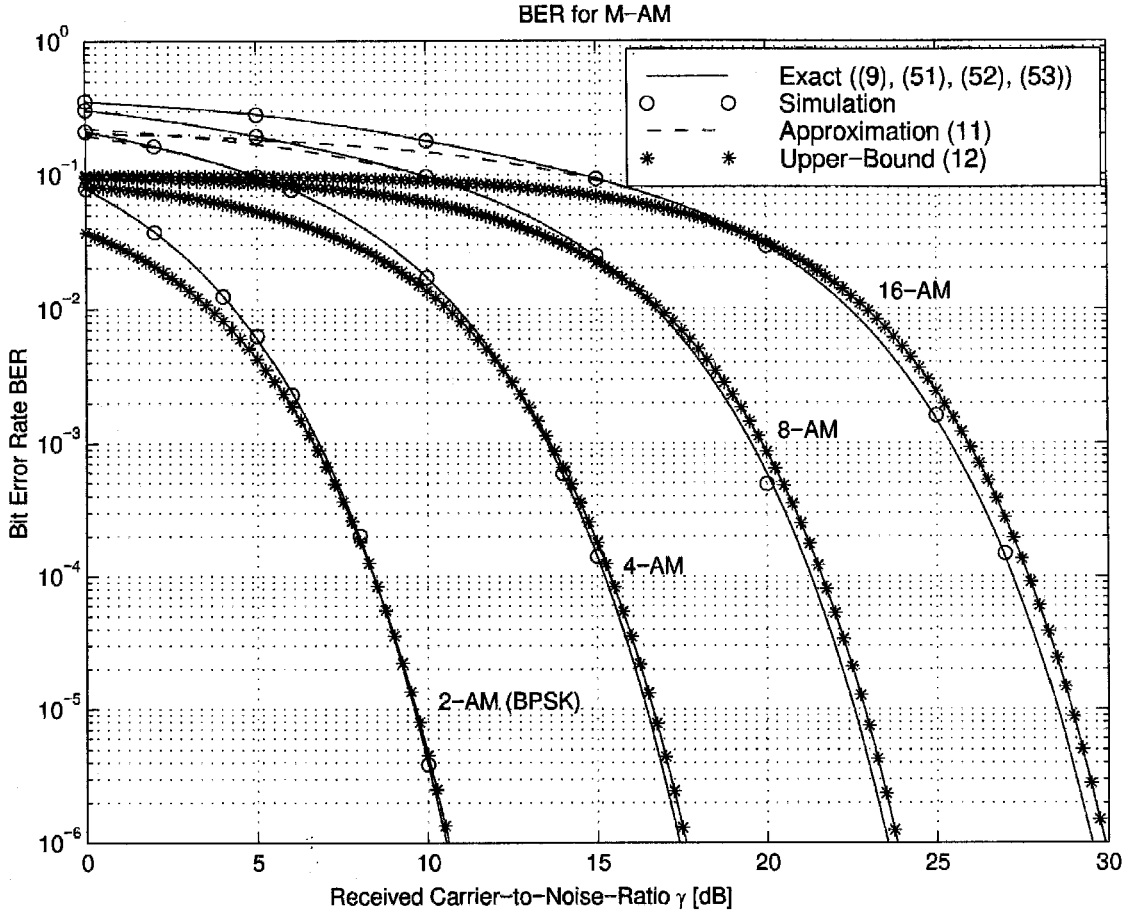

Figure 10.3: Bit-error-rate vs. received CNR for M-AM.

be extracted at the channel estimation stage. Assuming a perfect channel fading amplitude estimate $\hat{\alpha} = \alpha$ (equivalently, a perfect channel CNR estimation $\hat{\gamma} = \gamma$) and a peak power constraint of P [W], variable-power $P_v(\gamma) \leq P$ [W] is used on the BPSK of the Q channel to insure continuous fixed-rate voice transmission at the target voice BER, BER_{v_0}, i.e., the power allocated to voice $P_v(\gamma)$ is set to just meet the voice BER requirement, BER_{v_0}. The remaining available power $P_d(\gamma) = P - P_v(\gamma)$ [W] is dynamically assigned on the I channel to support the (adaptive) M-AM below the target data BER, BER_{d_0}. Specifically, based on the channel CNR estimate and on the available power $P_d(\gamma)$, the decision device at the receiver selects the signal constellation size M to be transmitted on the I channel, configures the demodulator accordingly, and informs the transmitter about that decision via the feedback path. We now describe the power allocation for voice and data as well as the constellation size assignment for data transmission in more detail.

Our proposed modulation scheme uses the channel state information at the transmitter to minimize its average power consumption subject to the peak power constraints. Specifically, voice transmission is not attempted when the power $P_v(\gamma)$ required to meet the target voice BER exceeds the peak power constraint P, and in this case a voice outage is declared. Furthermore, since the voice has to operate at the target BER_{v_0}, we see from (10.9) that the power allocated to voice transmission must be set to

$$P_v(\gamma) = \begin{cases} \frac{\gamma_{v_1}}{\gamma} P & P_v(\gamma) \leq P \text{ (or } \textit{equivalentely}, \gamma \geq \gamma_{v_1}) \\ 0 & \text{otherwise} \end{cases} \tag{10.13}$$

where $\gamma_{v_1} = \left[\text{erfc}^{-1}(2\ \text{BER}_{v_0})\right]^2$ and $\text{erfc}^{-1}(\cdot)$ denotes the *inverse complementary error function.* For data the scheme responds to the instantaneous channel CNR fluctuation by varying its constellation size as follows. The data CNR range is divided into $N+1$ *fading regions*, and the constellation size $M_n = 2^n$ (where n is the number of bits per M_n-AM symbol) is assigned to the nth region ($n = 0, 1, \cdots, N$). When the received data CNR is estimated to be in the nth region, the constellation size M_n is transmitted. The region boundaries (or switching thresholds) $\{\gamma_{d_n}\}_{n=0}^{N+1}$ are set to the CNR required to achieve the target BER_{d_0} using M_n-AM over an AWGN channel. Specifically from (10.12) we have

$$\begin{aligned} \gamma_{d_n} &= \frac{1 - 2^{2n}}{3} \ln(10\ \text{BER}_{d_0}); \qquad n = 0, 1, 2, \cdots, N, \\ \gamma_{d_{N+1}} &= +\infty. \end{aligned} \tag{10.14}$$

If during voice transmission the remaining available power $P_d(\gamma) = P - P_v(\gamma)$ is not able to support BPSK on the I channel then no data is transmitted, and a data outage is declared. Hence the power

allocated to data transmission can be written as

$$P_d(\gamma) = \begin{cases} \left(1 - \frac{\gamma_{v_1}}{\gamma}\right) P & \gamma_d \geq \gamma_{d_1} \ (equivalently\ \gamma \geq (\gamma_{v_1} + \gamma_{d_1})) \\ 0 & \text{otherwise.} \end{cases} \tag{10.15}$$

10.4 Performance Analysis

In this section we analyze the performance of the proposed scheme and we present both numerical and simulation results which are in perfect agreement, as can be seen in Figs. 10.4-10.11. All our numerical and simulation results are plotted as a function of the average CNR $\overline{\gamma}$ for different values of the Nakagami fading parameter m and for different maximum constellation sizes ("levels"). Note that all these numerical and simulation results assume a target uncoded voice BER, BER_{v_0}, of 10^{-2}, and a target uncoded data BER, BER_{d_0}, of 10^{-4}. We used these values to speed-up our simulations, however our analytic derivations apply to any set of BER requirements.

We use the MATLAB Communication Toolbox for our computer simulations. The powers allocated for voice and data as well as the constellation size for data transmission are determined at each symbol time according to the fading level, as explained in Section 10.3.2. We assume perfect channel estimation, coherent phase detection at the receiver, and Gray coding for bit mapping on the M-AM constellations, as shown in Fig. 10.1. All our simulations use a "4 level" modem which is able to support up to 16-AM modulation for data transmission.

10.4.1 Outage Probability

Since no voice is sent when the required power $P_v(\gamma)$ exceeds P, the voice transmission suffers an outage probability, P_{out}^v, of

$$P_{\text{out}}^v = \int_0^{\gamma_{v_1}} p_\gamma(\gamma)\, d\gamma = 1 - \frac{\Gamma\left(m, m\frac{\gamma_{v_1}}{\overline{\gamma}}\right)}{\Gamma(m)}, \tag{10.16}$$

where $\Gamma(.,.)$ is the *complementary incomplete gamma function* (or *Prym's function*) defined by [53, (8.350.2), p. 949]

$$\Gamma(z, \mu) = \int_\mu^{+\infty} t^{z-1}\, e^{-t}\, dt. \tag{10.17}$$

For $z = k$ positive integers [53, (8.352.2) p. 949],

$$\Gamma(k, \mu) = (k-1)!\, e^{-\mu}\, \mathcal{P}_k(\mu); \qquad k \geq 1, \tag{10.18}$$

where $\mathcal{P}_k(.)$ denotes the $k-1$ degree polynomial defined by

$$\mathcal{P}_k(\mu) = \sum_{j=0}^{k-1} \frac{\mu^j}{j!}. \tag{10.19}$$

Thus if we restrict ourselves to integer values of m, (10.16) can be expressed as

$$P_{\text{out}}^v = 1 - e^{-m\frac{\gamma_{v_1}}{\overline{\gamma}}}\ \mathcal{P}_m\left(m\ \frac{\gamma_{v_1}}{\overline{\gamma}}\right). \tag{10.20}$$

For the special case of the Rayleigh fading channel ($m = 1$), (10.20) reduces to

$$P_{\text{out}}^v = 1 - e^{-\frac{\gamma_{v_1}}{\overline{\gamma}}}. \tag{10.21}$$

Since no data is sent when the available power P_d is insufficient to support BPSK on the I channel, data transmission suffers an outage probability P_{out}^d of

$$P_{\text{out}}^d = \int_0^{\gamma_{v_1}+\gamma_{d_1}} p_\gamma(\gamma)\ d\gamma = 1 - \frac{\Gamma\left(m, m\frac{\gamma_{v_1}+\gamma_{d_1}}{\overline{\gamma}}\right)}{\Gamma(m)}, \tag{10.22}$$

where γ_{d_1} is the first data switching threshold. If we restrict ourselves to integer values of m (10.22) can be expressed as

$$P_{\text{out}}^d = 1 - e^{-m\frac{\gamma_{v_1}+\gamma_{d_1}}{\overline{\gamma}}}\ \mathcal{P}_m\left(m\frac{\gamma_{v_1}+\gamma_{d_1}}{\overline{\gamma}}\right). \tag{10.23}$$

Hence for the special case of the Rayleigh fading channel ($m = 1$), (10.23) reduces to

$$P_{\text{out}}^d = 1 - e^{-\frac{\gamma_{v_1}+\gamma_{d_1}}{\overline{\gamma}}}. \tag{10.24}$$

Fig. 10.4 shows the outage probability P_{out}^v and P_{out}^d for voice and data transmission, respectively. In the high average CNR region (i.e., higher than 4 dB for voice and higher than 9 dB for data), the higher the average CNR, the lower the outage probability, as expected. Furthermore, for a fixed m data suffers a higher outage probability than voice at all average CNRs. Although these outage curves appear simple and intuitive, they will in fact be crucial to explain many of our subsequent performance results.

10.4.2 Average Power Allocation

The normalized average power allocated for voice transmission $<P_v>/P$ is given by

$$\frac{<P_v>}{P} = \int_0^\infty \frac{P_v(\gamma)}{P}\ p_\gamma(\gamma)\ d\gamma = \frac{m\gamma_{v_1}}{\overline{\gamma}}\frac{\Gamma\left(m-1, m\frac{\gamma_{v_1}}{\overline{\gamma}}\right)}{\Gamma(m)}. \tag{10.25}$$

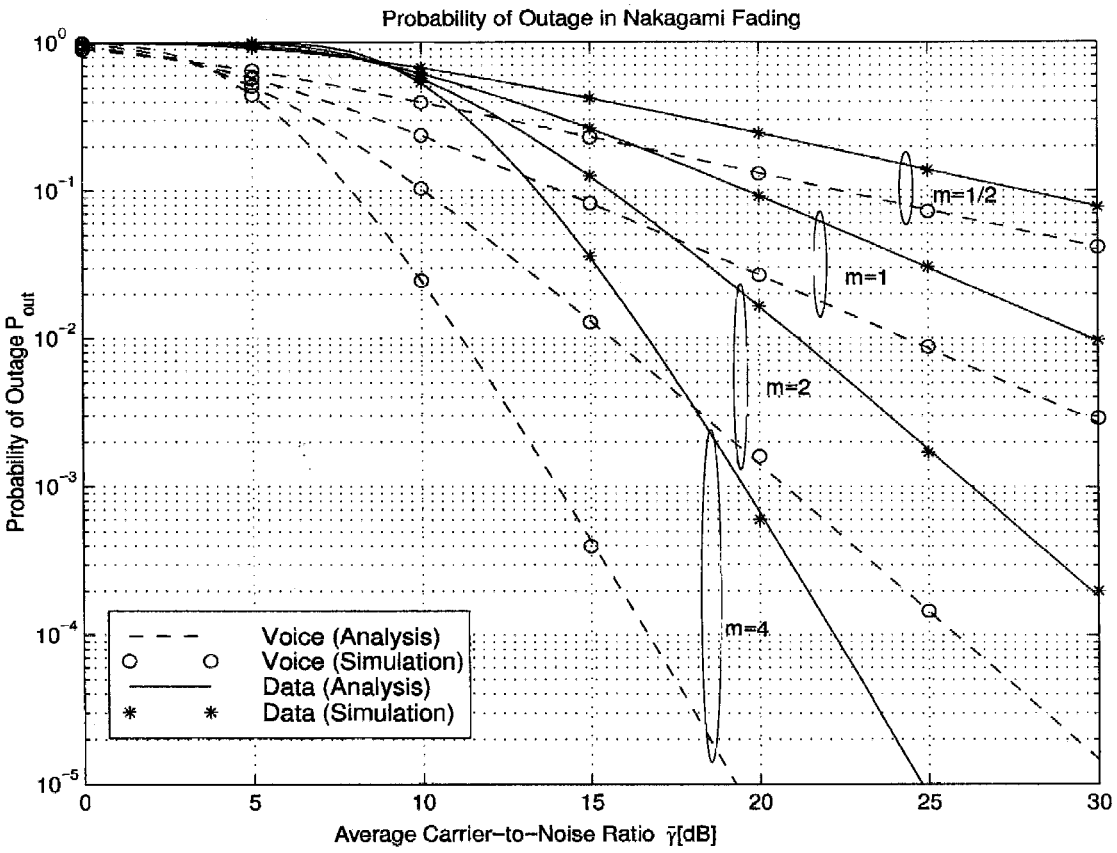

Figure 10.4: Outage probability for voice P_{out}^{v} and data P_{out}^{d} vs. the average CNR $\bar{\gamma}$.

If we restrict ourselves to integer values of $m \geq 2$, (10.25) can be expressed as

$$\frac{<P_v>}{P} = \frac{m}{m-1} \frac{\gamma_{v_1}}{\overline{\gamma}} e^{-m\frac{\gamma_{v_1}}{\overline{\gamma}}} \mathcal{P}_{m-1}\left(m \frac{\gamma_{v_1}}{\overline{\gamma}}\right). \tag{10.26}$$

For $z = 0$ we have [53, (8.359.1) p. 951]

$$\Gamma(0, \mu) = \mathrm{E}_1(\mu), \tag{10.27}$$

where $\mathrm{E}_1(.)$ is the *exponential-integral of first order function* defined by

$$\mathrm{E}_1(x) = \int_1^{+\infty} \frac{e^{-x\ t}}{t}\ dt. \tag{10.28}$$

Thus for the special case of the Rayleigh fading channel ($m = 1$), using (10.27) in (10.25) we obtain

$$\frac{<P_v>}{P} = \frac{\gamma_{v_1}}{\overline{\gamma}} \mathrm{E}_1\left(\frac{\gamma_{v_1}}{\overline{\gamma}}\right). \tag{10.29}$$

The normalized average power allocated for data transmission $<P_d>/P$ is given by

$$\frac{<P_d>}{P} = \int_0^{\infty} \frac{P_d(\gamma)}{P}\ p_\gamma(\gamma)\ d\gamma = \frac{\Gamma\left(m, m\frac{\gamma_{v_1}+\gamma_{d_1}}{\overline{\gamma}}\right)}{\Gamma(m)} - \frac{m\gamma_{v_1}}{\overline{\gamma}} \frac{\Gamma\left(m-1, m\frac{\gamma_{v_1}+\gamma_{d_1}}{\overline{\gamma}}\right)}{\Gamma(m)}. \tag{10.30}$$

If we restrict ourselves to integer values of $m \geq 2$, (10.30) can be expressed as

$$\frac{<P_d>}{P} = e^{-m\frac{\gamma_{v_1}+\gamma_{d_1}}{\overline{\gamma}}} \left[\mathcal{P}_m\left(m\frac{\gamma_{v_1}+\gamma_{d_1}}{\overline{\gamma}}\right) - \frac{m}{m-1} \frac{\gamma_{v_1}}{\overline{\gamma}} \mathcal{P}_{m-1}\left(m\frac{\gamma_{v_1}+\gamma_{d_1}}{\overline{\gamma}}\right)\right]. \tag{10.31}$$

For the particular case of the Rayleigh fading channel ($m = 1$), using (10.27) in (10.30) we get

$$\frac{<P_d>}{P} = e^{-\frac{\gamma_{v_1}+\gamma_{d_1}}{\overline{\gamma}}} - \frac{\gamma_{v_1}}{\overline{\gamma}} \mathrm{E}_1\left(\frac{\gamma_{v_1}+\gamma_{d_1}}{\overline{\gamma}}\right). \tag{10.32}$$

Fig. 10.5 shows in dash lines the normalized average power allocated for voice transmission, $<P_v>/P$. This figure also displays in solid lines the normalized average power allocated for data transmission, $<P_d>/P$. The overall normalized average power $<P>/P = <P_v>/P + <P_d>/P$ is shown in Fig. 10.6. The behavior of the curves in Fig. 10.5, which varies in the different regions of average CNR, can be explained by the outage curves in Fig. 10.4. In particular, we see in Fig. 10.4 that at low $\overline{\gamma}$s both voice and data suffer a large outage probability. Hence, since there is no transmission during outage, the corresponding power consumptions in Figs. 10.5 and 10.6 are low. Consider now the region of extremely low average CNR (i.e., $\overline{\gamma} \leq 2.5$ dB). Observe that for a fixed $\overline{\gamma}$ in this region, as m increases (i.e., the amount of fading decreases) the power consumption for voice decreases. This can be explained by the following argument. At these extremely low values

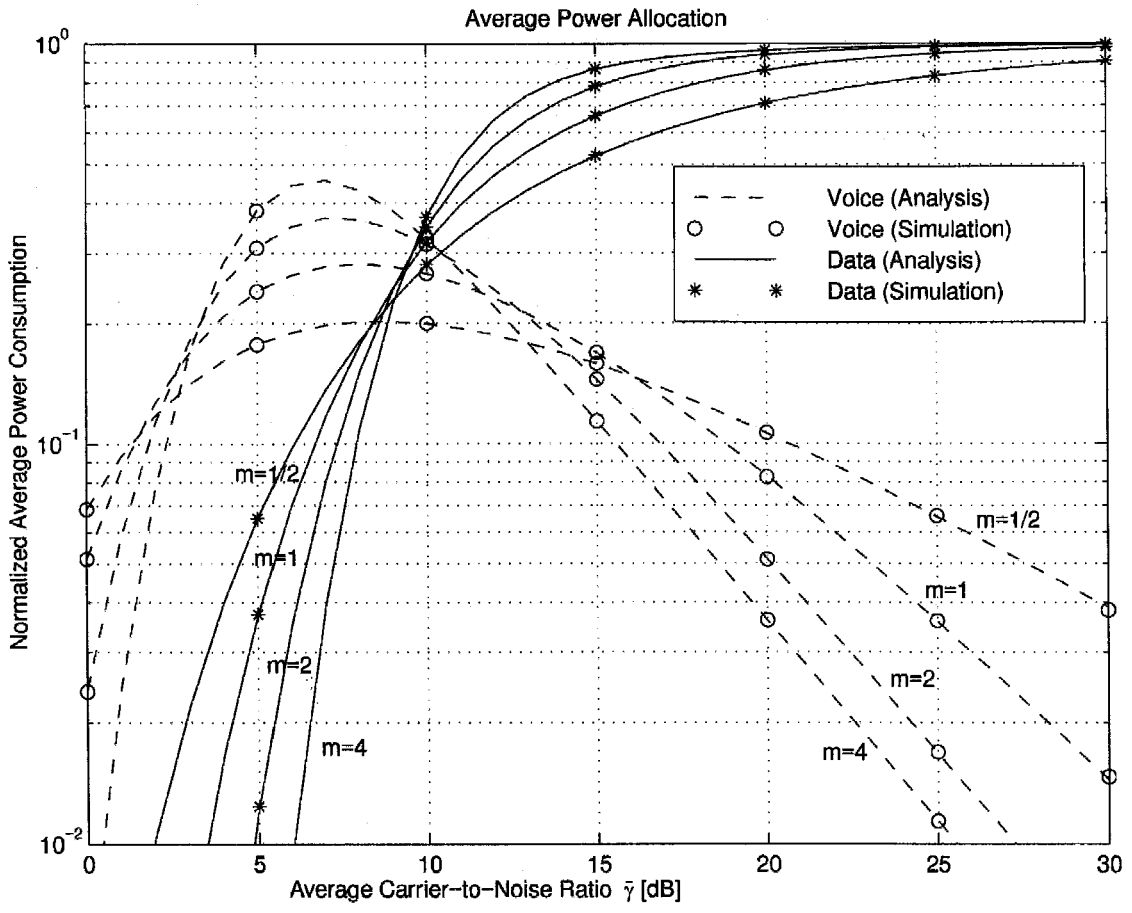

Figure 10.5: Average power allocation for voice $< P_v > / P$ and data $< P_d > / P$ vs. the average CNR $\overline{\gamma}$.

of $\overline{\gamma}$ note from Fig. 10.4 that the outage probability for voice is essentially the same for all ms. However, whenever voice transmission is possible more power will be needed to "invert" channels with a higher amount of fading. Thus, in this region power consumption for voice increases relative to the amount of fading. In the medium CNR region (i.e., 2.5 dB $\leq \overline{\gamma} \leq$ 12.5 dB), we see that a larger value of m corresponds to a larger power consumption for voice and a smaller one for data. This can be explained by observing that in Fig. 10.4 the data outage probability in this region is essentially independent of m but the voice outage probability decreases as m increases. Thus, as m increases, we are transmitting voice more often and therefore we must allocate a larger percentage of our power to voice. In the region of high average CNR (i.e., 12.5 dB $\geq \overline{\gamma}$), voice outage probability is small, and since the channel is quite good, a small fraction of the total power is needed for the voice transmission. Thus most of the power is allocated to data transmission. In this favorable region a large m (i.e., a small amount of fading) implies that less power is needed for voice transmission and therefore more power can be allocated to high rate M-ary data transmission.

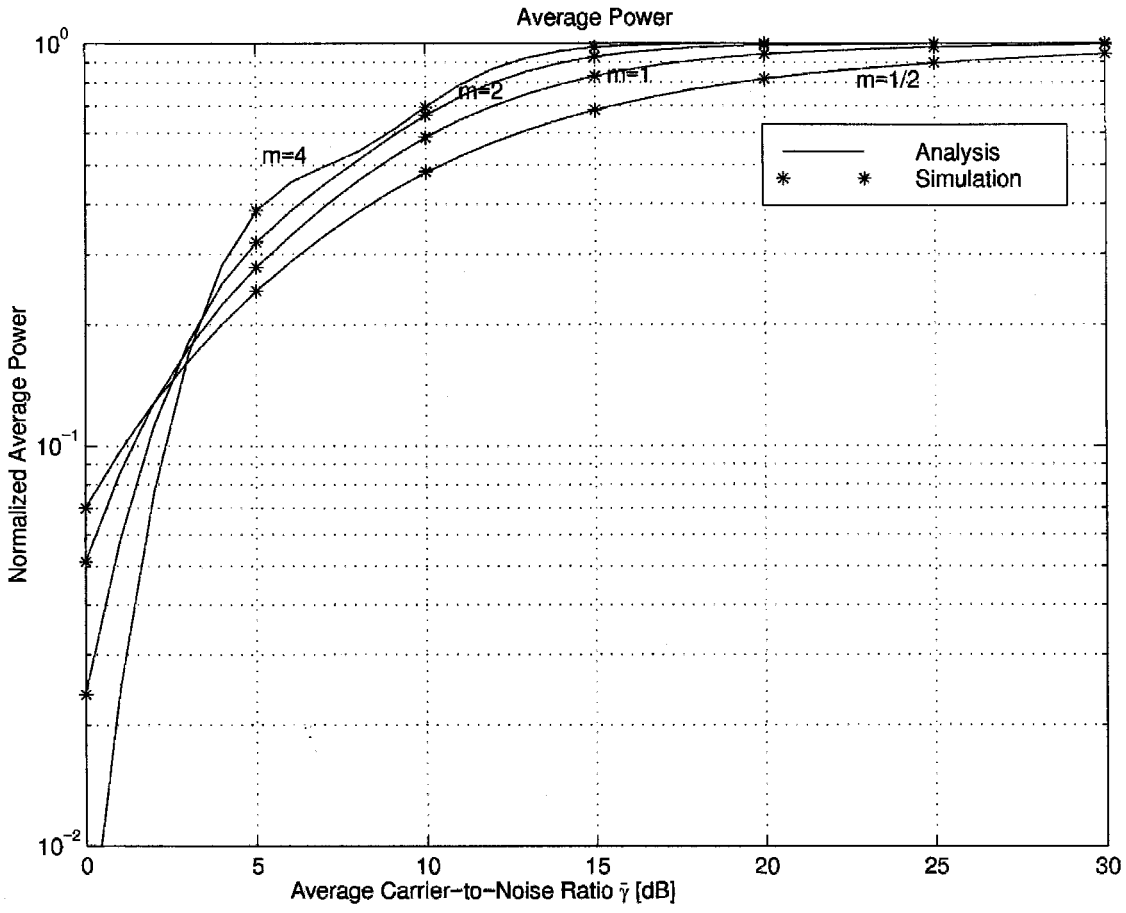

Figure 10.6: Overall normalized average power $< P > / P$ allocated to both voice and data vs. the average CNR $\overline{\gamma}$.

10.4.3 Achievable Spectral Efficiency

The average link spectral efficiency for voice transmission $< R_v > /W$ is given by

$$\frac{< R_v >}{W} = 1 - P_{\text{out}}^{v} = \frac{\Gamma\left(m, m\frac{\gamma_{v_1}}{\overline{\gamma}}\right)}{\Gamma(m)}. \tag{10.33}$$

When m is restricted to integer values (10.33) may be written as

$$\frac{< R_v >}{W} = e^{-m\frac{\gamma_{v_1}}{\overline{\gamma}}} \mathcal{P}_m\left(m\,\frac{\gamma_{v_1}}{\overline{\gamma}}\right), \tag{10.34}$$

which reduces to

$$\frac{< R_v >}{W} = e^{-\frac{\gamma_{v_1}}{\overline{\gamma}}} \tag{10.35}$$

for the special Rayleigh fading case ($m = 1$). The average link spectral efficiency for data transmission, $< R_d > /W$, is just the sum of the data rates ($\log_2[M_n] = n$) associated with the individual $N + 1$ regions, weighted by the probability $a_n = \int_{\gamma_{v_1}+\gamma_{d_n}}^{\gamma_{v_1}+\gamma_{d_{n+1}}} p_\gamma(\gamma)\, d\gamma$ that the data CNR γ_d falls in the nth fading region:

$$\frac{< R_d >}{W} = \sum_{n=1}^{N} n\, a_n, \tag{10.36}$$

where the a_ns can be expressed as

$$a_n = \frac{\Gamma\left(m, m\frac{\gamma_{v_1}+\gamma_{d_n}}{\overline{\gamma}}\right) - \Gamma\left(m, m\frac{\gamma_{v_1}+\gamma_{d_{n+1}}}{\overline{\gamma}}\right)}{\Gamma(m)} \tag{10.37}$$

in the most general case and may be written as

$$a_n = e^{-m\frac{\gamma_{v_1}}{\overline{\gamma}}} \left[e^{-m\frac{\gamma_{d_n}}{\overline{\gamma}}} \mathcal{P}_m\left(m\frac{\gamma_{v_1}+\gamma_{d_n}}{\overline{\gamma}}\right) - e^{-m\frac{\gamma_{d_{n+1}}}{\overline{\gamma}}} \mathcal{P}_m\left(m\frac{\gamma_{v_1}+\gamma_{d_{n+1}}}{\overline{\gamma}}\right)\right] \tag{10.38}$$

when m is restricted to integer values. For the Rayleigh fading case (10.38) reduces to

$$a_n = e^{-\frac{\gamma_{v_1}}{\overline{\gamma}}} \left[e^{-\frac{\gamma_{d_n}}{\overline{\gamma}}} - e^{-\frac{\gamma_{d_n+1}}{\overline{\gamma}}}\right]. \tag{10.39}$$

The dashed lines in Fig. 10.7 show the average spectral efficiency for voice transmission, $< R_v > /W$. This figure also shows the average spectral efficiency for data transmission, $< R_d > /W$, for different maximum constellation sizes. The overall average spectral efficiency $< R > /W = < R_v > /W + < R_d > /W$, is shown in Fig. 10.8. At high average CNR a large m corresponds to a large overall average spectral efficiency for voice and data. However, at low average CNR (i.e., less than 4 dB for voice and less than 10 dB for data) a large m corresponds to a low overall average spectral efficiency. This may seem surprising at first but can be explained by the following argument.

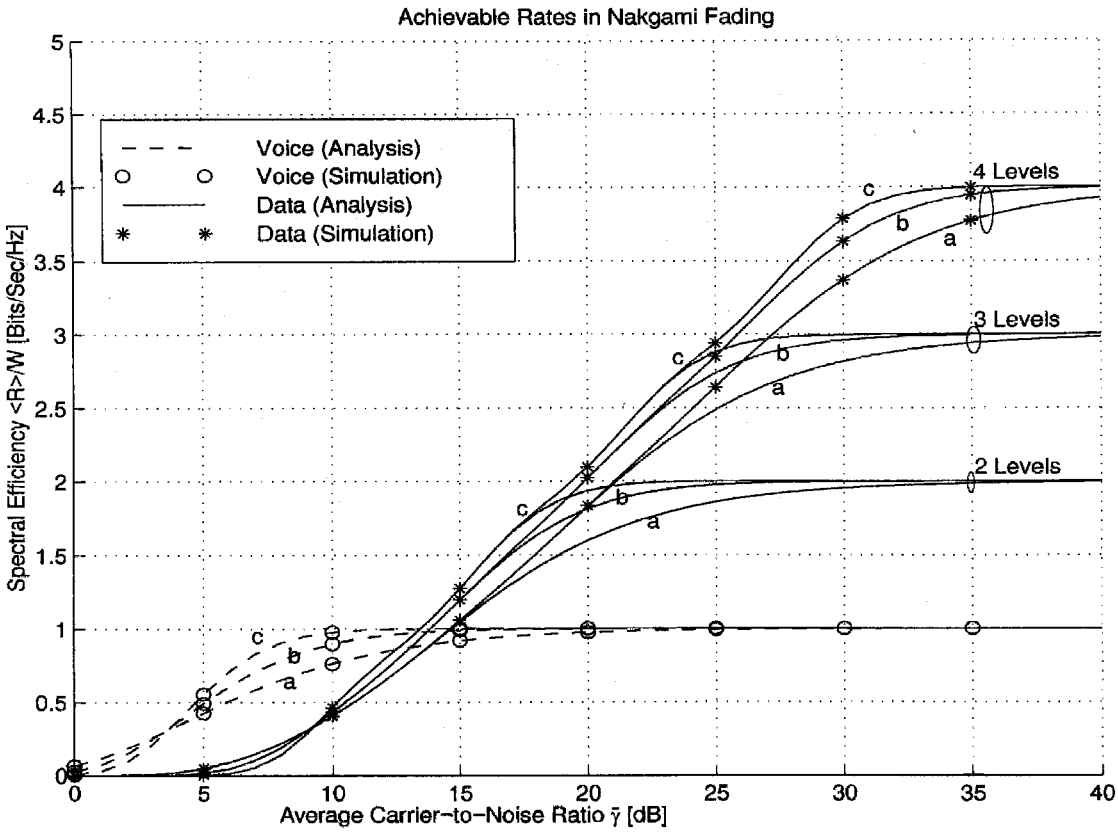

Figure 10.7: Achievable spectral efficiency for voice $< R_v > /W$ and data $< R_d > /W$ vs. the average CNR $\overline{\gamma}$: (a) m =1, (b) m =2, and (c) m =4.

Channels with a small m exhibit significant fading and a corresponding wide range of CNR values. Channels with a large m will have most of their CNR concentrated around the average CNR which is small in the low average CNR region. Hence channels with a smaller fading parameter m will have a slightly higher spectral efficiency since the larger CNR fluctuation results in a lower probability of outage in this low average CNR region (as can be seen in Fig. 10.4).

10.4.4 Average Bit Error Rate

Voice transmission is always operating at the target BER, BER_{v_0}. On the other hand, since the choice of the constellation size for data transmission is done in a conservative fashion, data is transmitted at an average BER, $< \text{BER}_d >$, smaller than BER_{d_0}. This average BER can be computed exactly as the ratio of the average number of bits in error over the total average number of transmitted bits

$$< \text{BER}_d > = \frac{\sum_{n=1}^{N} n \, \overline{\text{BER}_n}}{\sum_{n=1}^{N} n \, a_n}, \tag{10.40}$$

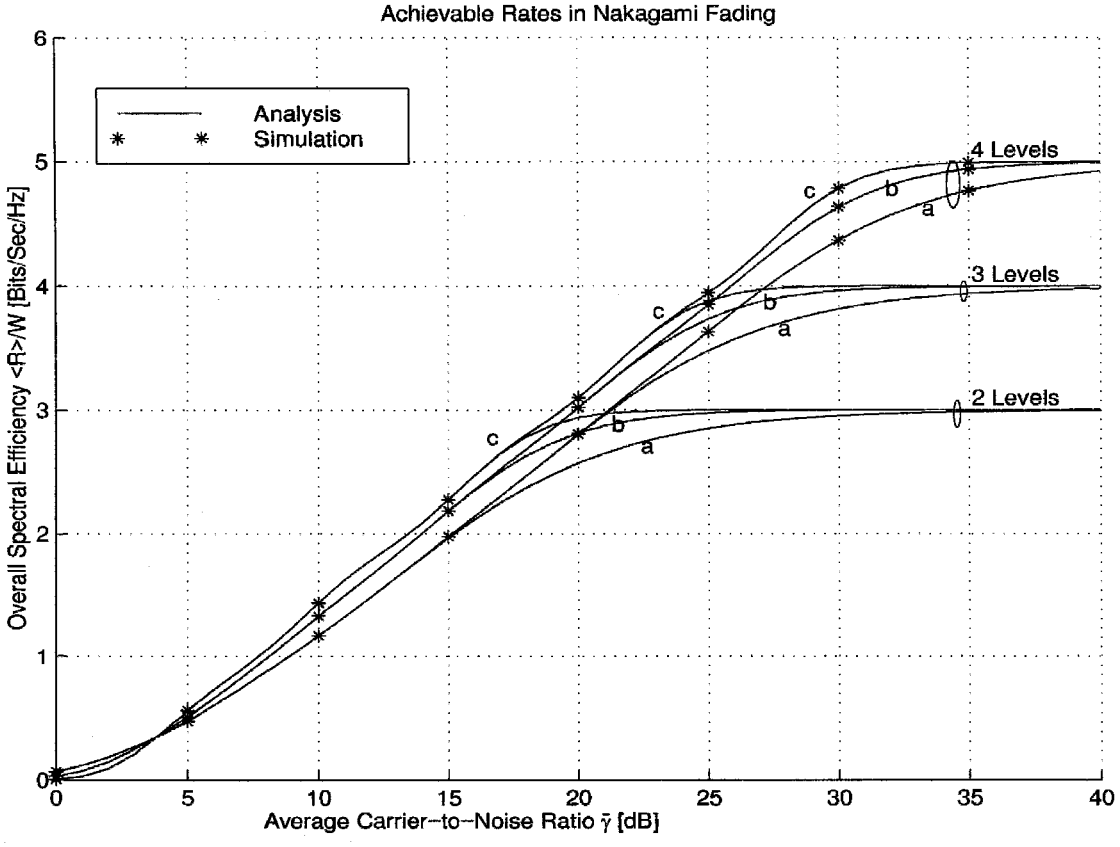

Figure 10.8: Overall spectral efficiency $< R > /W$ vs. the average CNR $\overline{\gamma}$: (a) m =1, (b) m =2, and (c) m =4.

where

$$\overline{\mathrm{BER}}_n = \int_{\gamma_{v_1}+\gamma_{d_n}}^{\gamma_{v_1}+\gamma_{d_{n+1}}} \mathrm{BER}(M_n, \gamma-\gamma_{v_1})\; p_\gamma(\gamma)\; d\gamma. \tag{10.41}$$

It can be shown using (9.1) and (10.12) in (10.41) that $\overline{\mathrm{BER}}_n$ is upper-bounded by

$$\begin{aligned}
\overline{\mathrm{BER}}_n &\leq \frac{0.1}{\Gamma(m)} \exp\left(\frac{3\gamma_{v_1}}{2^{2n}-1}\right) \\
&\quad \times \frac{\Gamma\left(m, m\,\frac{b_n(\gamma_{v_1}+\gamma_{d_n})}{\overline{\gamma}}\right) - \Gamma\left(m, m\,\frac{b_n(\gamma_{v_1}+\gamma_{d_{n+1}})}{\overline{\gamma}}\right)}{(b_n)^m}; n = 1, 2, \cdots, N-1, \\
\overline{\mathrm{BER}}_N &\leq \frac{0.1}{\Gamma(m)} \exp\left(\frac{3\gamma_{v_1}}{2^{2N}-1}\right) \frac{\Gamma(m, m\, b_N \frac{\gamma_{v_1}+\gamma_{d_N}}{\overline{\gamma}})}{(b_N)^m},
\end{aligned} \tag{10.42}$$

where

$$b_n = 1 + \frac{3\overline{\gamma}}{m(2^{2n}-1)}; \qquad n = 1, 2, \cdots, N.$$

When m is restricted to integer values these bounds become

$$\begin{aligned}
\overline{\mathrm{BER}}_n &\leq \frac{0.1\; e^{-m\frac{\gamma_{v_1}}{\overline{\gamma}}}}{(b_n)^m} \\
&\quad \left[e^{-m\frac{b_n\,\gamma_{d_n}}{\overline{\gamma}}} \mathcal{P}_m\left(m\frac{b_n(\gamma_{v_1}+\gamma_{d_n})}{\overline{\gamma}}\right) - e^{-m\frac{b_n\,\gamma_{d_{n+1}}}{\overline{\gamma}}} \mathcal{P}_m\left(m\frac{b_n(\gamma_{v_1}+\gamma_{d_{n+1}})}{\overline{\gamma}}\right)\right]; n = 1, \cdots, N-1, \\
\overline{\mathrm{BER}}_N &\leq \frac{0.1\; e^{-m\frac{(\gamma_{v_1}+b_N\,\gamma_{d_N})}{\overline{\gamma}}}}{(b_N)^m} \mathcal{P}_m\left(m\frac{b_n(\gamma_{v_1}+\gamma_{d_N})}{\overline{\gamma}}\right),
\end{aligned} \tag{10.43}$$

which reduces in the Rayleigh case ($m = 1$) to

$$\begin{aligned}
\overline{\mathrm{BER}}_n &\leq \frac{0.1\; e^{-\frac{\gamma_{v_1}}{\overline{\gamma}}}}{b_n} \left[e^{-\frac{b_n\,\gamma_{d_n}}{\overline{\gamma}}} - e^{-\frac{b_n\,\gamma_{d_{n+1}}}{\overline{\gamma}}}\right]; \; n = 1, 2, \cdots, N-1, \\
\overline{\mathrm{BER}}_N &\leq \frac{0.1\; e^{-\frac{(\gamma_{v_1}+b_N\,\gamma_{d_N})}{\overline{\gamma}}}}{b_N}.
\end{aligned} \tag{10.44}$$

Fig. 10.9 shows the average BER for both voice and data, for different maximum constellation sizes or levels. Note that voice transmission is always operating at the target BER, BER_{v_0}. On the other hand, data is transmitted at an average BER, $<\mathrm{BER}_d>$, smaller than the target BER_{d_0}, as expected from our conservative choice of constellation size. Since data transmission uses the largest constellation often when the average CNR is high, the average BER prediction as $\overline{\gamma}$ increases becomes dominated by the BER performance of that constellation. In addition, at high average CNR as m increases the average BER for data decreases, as one might expect. However, at low average CNR (i. e. $\overline{\gamma} \leq 10$ dB) the average BER for data actually increases as m increases. This behavior may seem surprising at first, but can be explained by the fact that for $\overline{\gamma} \leq 10$ dB a large m implies that only a small amount of power is allocated to data transmission, as can be seen in

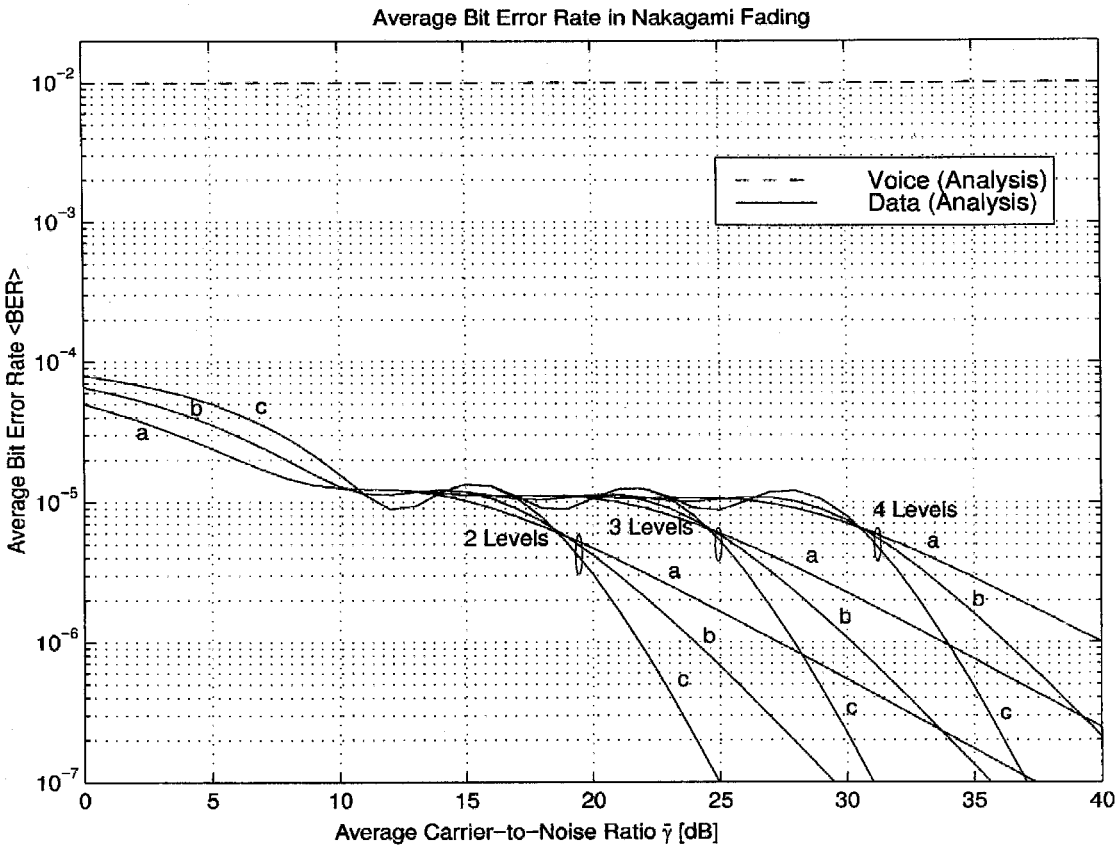

Figure 10.9: Average BER for voice $<\mathrm{BER}_v>$ and data $<\mathrm{BER}_d>$ vs. the average CNR $\overline{\gamma}$: (a) m =1, (b) m =2, and (c) m =4.

Fig. 10.5. Hence since data can only use a small fraction of the power, its BER increases.

We show the simulated BER for Rayleigh fading ($m = 1$) and for Nakagami fading with $m = 2$ in Figs. 10.10 and 10.11, respectively. The BER simulation results for voice transmission in these figures are in perfect agreement with the analytical calculations. However, the simulated BERs for data transmission are slightly lower than the analytical calculations since the latter are based on the upper-bound (10.12) of the BER performance of M-AM with Gray coding. The fact that this bound is tighter (10.12) for lower M (see Fig. 10.3) combined with the fact that the scheme often uses the smallest available constellation at low average CNRs explains why the overall average BER upper-bound for data transmission is tighter at low average CNRs.

10.5 Conclusion

We have proposed an adaptive modulation scheme which offers a simple and energy-efficient solution to voice and data integration over fading channels. The proposed design is intended to provide the user with a high average spectral efficiency for data communications while meeting the stringent delay

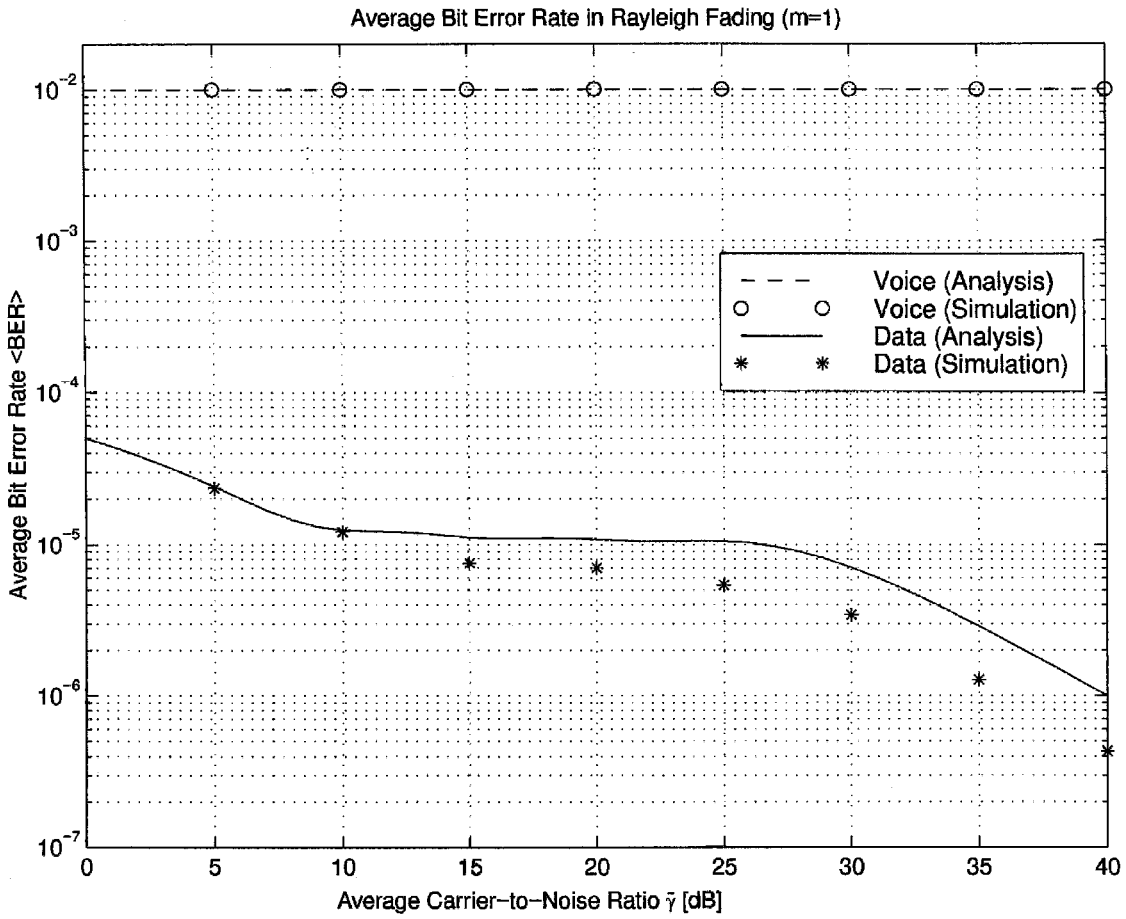

Figure 10.10: Average BER for voice $< \mathrm{BER}_v >$ and data $< \mathrm{BER}_d >$ vs. the average CNR $\overline{\gamma}$ for Rayleigh fading (m=1).

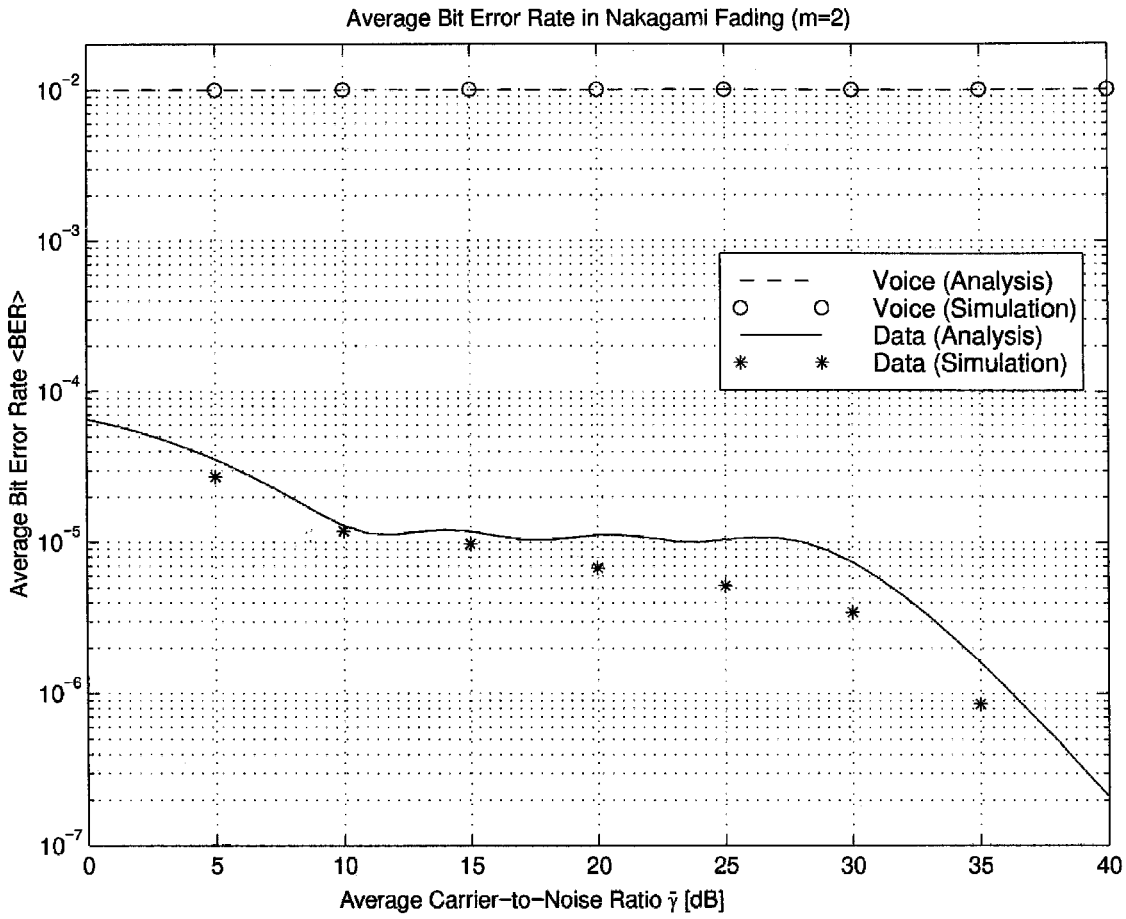

Figure 10.11: Average BER for voice $< \mathrm{BER}_v >$ and data $< \mathrm{BER}_d >$ vs. the average CNR $\overline{\gamma}$ for Nakagami fading (m=2).

requirements imposed by voice. For favorable channel conditions most of the power is allocated to high rate data transmission by using M-AM with a large constellation size. As the channel degrades the modem reduces its data throughput and reallocates most of its available power to insure a continuous and satisfactory voice transmission. We evaluated the performance of our proposed scheme in terms of outage probability, average allocated power, achievable spectral efficiency, and average BER for both voice and data transmission.

There are several possible improvements to our adaptive scheme. One possibility is to further increase the spectral efficiency by using a speech activity detector (SAD). A SAD can be used to segment a conversation speech into talkspurts and silences [155]. Hence a SAD can be used in conjunction with an adaptive multimode modem to send adaptive M-QAM for data transmission during the silences when voice is not transmitted on the Q channel, and our proposed scheme for simultaneous voice and data transmission during the talkspurts. Another area of study is how to superimpose coding on the proposed modulation scheme.

Appendix

Exact BER Expressions for M-AM over an AWGN Channel

In this appendix we derive the exact BER expression for 4-AM with Gray coding over an AWGN channel, and give the exact BER expressions for 8-AM and 16-AM.

For 4-AM the 4 symbols are symmetrically distributed about zero with equal distance between two adjacent symbols as shown in Fig. 10.1. In Fig. 10.1 A is the amplitude level, T_s is the symbol duration, $d = 2\ A\ T_s$ is the distance between two adjacent symbols, and the dashed vertical lines represent the decision boundaries. Since we consider an AWGN channel with a noise power spectral density of N_0, the noise is normally distributed with zero mean and variance $\sigma^2 = \frac{N_0\ T_s}{2}$.

Consider first the left bit of each 4-AM symbol, as shown in Fig. 10.1. A bit error occurs when the bit 1, corrupted by noise, falls into the boundaries of bit 0 or vice versa. For example, the left bit of the symbol 10, i.e., 1, will be interpreted 0 when the noise is larger than $\frac{3d}{2}$. Hence its probability of error P_{1l} is given by

$$P_{1l} = Q\left(\frac{3d}{2\sigma}\right) \tag{10.45}$$

where $Q(.)$ is the *Gaussian Q-function* which is related to the error complementary function as defined in (10.10) by

$$Q(z) = \frac{1}{2}\ \text{erfc}\left(\frac{z}{\sqrt{2}}\right) \tag{10.46}$$

Similarly, $P_{2l} = P_{3l} = Q\left(\frac{d}{2\sigma}\right)$, and $P_{4l} = P_{1l} = Q\left(\frac{3d}{2\sigma}\right)$. Assuming each of the 4 symbols has equal probability, the error probability of the left bit P_{el} is

$$\begin{aligned} P_{el} &= \frac{1}{4}(P_{1l} + P_{2l} + P_{3l} + P_{4l}) \\ &= \frac{1}{2}\left[Q\left(\frac{d}{2\sigma}\right) + Q\left(\frac{3d}{2\sigma}\right)\right]. \end{aligned} \tag{10.47}$$

Consider now the right bit of each 4-AM symbol as shown in Fig. 10.1. Following the same procedure it can be shown that its probability of error P_{er} is given by

$$P_{er} \quad = \quad Q\left(\frac{d}{2\sigma}\right) + \frac{1}{2}Q\left(\frac{3d}{2\sigma}\right) - \frac{1}{2}Q\left(\frac{5d}{2\sigma}\right). \tag{10.48}$$

Hence the average BER for 4-AM is given by

$$\text{BER}_{4-\text{AM}} = \frac{1}{2}\left(P_{er} + P_{el}\right) = \frac{3}{4}Q\left(\frac{d}{2\sigma}\right) + \frac{1}{2}Q\left(\frac{3d}{2\sigma}\right) - \frac{1}{4}Q\left(\frac{5d}{2\sigma}\right). \tag{10.49}$$

On the other hand the average power per symbol is P_{av}:

$$P_{\text{av}} = \frac{1}{4}(9+1+1+9)A^2 = 5A^2. \tag{10.50}$$

Thus

$$\frac{d}{\sigma} = \frac{2\,A\,T_s}{\sqrt{\frac{N_0\,T_s}{2}}} = \sqrt{\frac{8\,Pav}{5\,N_0\,W}},$$

where $W \simeq \frac{1}{T_s}$ is the signal bandwidth. The exact BER of 4-AM can hence be rewritten in terms of average CNR, $\gamma_{\text{av}} \triangleq \gamma = \frac{P_{\text{av}}}{N_o\,B}$, as

$$\text{BER}_{4-\text{AM}} = \frac{3}{4}Q\left(\sqrt{\frac{2}{5}\gamma}\right) + \frac{1}{2}Q\left(3\sqrt{\frac{2}{5}\gamma}\right) - \frac{1}{4}Q\left(5\sqrt{\frac{2}{5}\gamma}\right). \tag{10.51}$$

The exact BER expressions for 8-AM and 16-AM can be calculated in a similar way and are given by

$$\begin{aligned}\text{BER}_{8-\text{AM}} = \; & \frac{7}{12}Q\left(\sqrt{\frac{2}{21}\gamma}\right) + \frac{1}{2}Q\left(3\sqrt{\frac{2}{21}\gamma}\right) - \frac{1}{12}Q\left(5\sqrt{\frac{2}{21}\gamma}\right) \\ & + \frac{1}{12}Q\left(9\sqrt{\frac{2}{21}\gamma}\right) - \frac{1}{12}Q\left(13\sqrt{\frac{2}{21}\gamma}\right).\end{aligned} \tag{10.52}$$

$$\begin{aligned}\text{BER}_{16-\text{AM}} = \; & \frac{15}{32}Q\left(\sqrt{\frac{2}{85}\gamma}\right) + \frac{14}{32}Q\left(3\sqrt{\frac{2}{85}\gamma}\right) + \frac{5}{32}Q\left(5\sqrt{\frac{2}{85}\gamma}\right) - \frac{6}{32}Q\left(7\sqrt{\frac{2}{85}\gamma}\right) \\ & - \frac{7}{32}Q\left(9\sqrt{\frac{2}{85}\gamma}\right) + \frac{6}{32}Q\left(11\sqrt{\frac{2}{85}\gamma}\right) + \frac{9}{32}Q\left(13\sqrt{\frac{2}{85}\gamma}\right) + \frac{8}{32}Q\left(15\sqrt{\frac{2}{85}\gamma}\right) \\ & - \frac{7}{32}Q\left(17\sqrt{\frac{2}{85}\gamma}\right) - \frac{6}{32}Q\left(19\sqrt{\frac{2}{85}\gamma}\right) - \frac{1}{32}Q\left(21\sqrt{\frac{2}{85}\gamma}\right) + \frac{2}{32}Q\left(23\sqrt{\frac{2}{85}\gamma}\right) \\ & + \frac{3}{32}Q\left(25\sqrt{\frac{2}{85}\gamma}\right) - \frac{2}{32}Q\left(27\sqrt{\frac{2}{85}\gamma}\right) - \frac{1}{32}Q\left(29\sqrt{\frac{2}{85}\gamma}\right).\end{aligned} \tag{10.53}$$

Chapter 11 Area Spectral Efficiency of Cellular Systems

11.1 Introduction

Spectral efficiency is achieved by cellular systems which exploit the power falloff with distance of signal propagation to reuse the same frequency channel at spatially separated locations [156]. However, while frequency-reuse provides more efficient use of the limited available spectrum, it also introduces unavoidable co-channel interference [157, 158, 159, 160, 161, 162], which ultimately determines the bit-error-rates (BERs) available to each user. Thus, there is a tradeoff between the *system* spectral efficiency, measured in [bits/sec]/[Hz · m^2] or Erlangs/[Hz · m^2], and the communication link quality, measured in terms of the BER provided to the users [159, 162].

Another technique to increase spectral efficiency is to use multilevel modulation, such as M-QAM, which increase *link* spectral efficiency, measured in [bits/sec]/Hz, by sending multiple bits per symbol [115]. However, wireless channels are subject to severe propagation impairments which results in a serious degradation in the link carrier-to-noise ratio (CNR), and even if efficient fading compensations techniques are used, multilevel schemes will still require higher power levels than binary modulations for a specified BER. Therefore, to keep the co-channel interference at an acceptable level it is necessary to increase the frequency-reuse distance (or equivalently the cluster size) which in turn leads to a lower *system* efficiency. This problem has been recently addressed by Haas and Belfiore [163], who showed that there is a tradeoff between the system and link spectral efficiencies. This was also confirmed by Morinaga *et al.* [164], who claimed that 4-QAM is the optimum multilevel modulation for high capacity cellular systems, and that opting for higher modulation levels will just reduce the system spectral efficiency. This is essentially due to the fact that fixed modulation systems are designed relative to the worst-case interference and fading conditions. However, adapting certain parameters of the transmitted signal relative to the CNR leads to better link and system spectral efficiencies.

Previous studies of the system spectral efficiency for cellular systems assumed that the data rate is constant and equal for all users, regardless of interference conditions and channel quality [158, 159, 162, 163, 165, 166, 167]. In these papers spectral efficiency was based on a criterion introduced by Hatfield [165] and defined as the ratio of the carried traffic per cell (in Erlangs) to the product of the total system bandwidth and area supported by a base station. This criterion is not suitable for

data systems since Erlangs are just a measure of traffic loading rather than throughput intensity. A more pertinent measure of spectral efficiency in cellular data systems is the total throughput, i.e., number of [bits/sec]/[Hz · m^2] associated with each base station (BS).

In this chapter we investigate the theoretical limits of this spectral efficiency for cellular data systems where mobile users continuously adapt their rate relative to their fading and interference conditions. This efficiency, called the *area spectral efficiency* (ASE), is defined as the sum of the maximum average data rates per unit bandwidth per unit area for a specified BER. The ASE definition captures the tradeoffs between a cellular system's spectral efficiency, the users' link spectral efficiency, and the communication link quality provided to these users. We take into account the effect of the random user locations in their respective cells as well as the impact of shadowing and multipath fading superimposed on path loss, with propagation parameters for both macrocells and microcells. Although both shadowing and fading will typically be superimposed on path loss, we first consider these two phenomena separately to assess their respective impact. We then study their combined effect on the ASE. For our analyses and simulations, we analyze only the uplink (mobile to BS) of systems using frequency-division multiple access (FDMA) or time-division multiple access (TDMA). We first consider fully-loaded cellular systems. We then generalize our analysis to partially-loaded systems, and determine the effect of traffic loading on the ASE.

The remainder of this chapter is organized as follows. The next section describes in more detail our propagation, co-channel interference, adaptive transmission system, and user's random location models. Section 11.3 introduces the concept of ASE for fully-loaded cellular systems. Section 11.4 presents analyses, computer simulations, and numerical results for the ASE when only path loss is considered. The impact of shadowing and multipath fading on the ASE are studied in Section 11.5 and 11.6, respectively. Section 11.7 considers the combined effect of shadowing and multipath fading on the ASE. Section 11.8 deals with the ASE of partially-loaded systems. Finally, the paper concludes with a review of the main results.

11.2 Channel and System Models

In this section we first outline the models for the different propagation impairments affecting cellular systems. We then present our assumptions for the co-channel interference and the adaptive communication system under consideration. We finally describe the random location model for the users' positions.

11.2.1 Propagation Models

As described in Chapter 2, signal propagation in a radio mobile environment is affected by three independent phenomena: (i) deterministic path loss variation with distance, (ii) random slow shad-

owing, and (iii) random fast multipath fading.

Path loss is due to the decay of the intensity of a propagating radio-wave. In both our analyses and simulations we use the *two-slope* path loss model [168] to obtain the average received power as function of distance. According to this model the average received signal power, $\overline{S}$ [W], is given by

$$\overline{S} = \frac{K}{r^a\,(1+r/g)^b}\,S_t, \tag{11.1}$$

where K is a constant, r [m] is the distance between the mobile and the BS, a is the basic path loss exponent (approximately 2), b is the additional path loss exponent (ranges from 2 to 6), and S_t [W] is the transmitted signal power. The parameter g [m] is called the *break point* of the path loss curve and is given by $g = (4\ h_B\ h_m)/\lambda_c$, where h_B [m] is the BS antenna height, h_m [m] is the mobile antenna height, and λ_c [m] is the wavelength of the carrier frequency. We use the following typical values in our analyses and simulations [169]: $h_m = 2$ m, $h_B = 10$ m for microcells, and $h_B = 50$ m for macrocells. The resultant break points for 900 MHz systems are $g \simeq 240.3$ m for microcells and $g \simeq 1212$ m for macrocells. For 2 GHz systems the break points increase to $g \simeq 533$ m for microcells and $g \simeq 2667$ m for macrocells.

In urban microcells systems the link quality is also affected by the shadowing of the line-of-sight path from terrain, buildings, and trees. The shadowing is generally modeled as log-normal distributed [2, Sec. 2.4]. The probability density function (PDF) of the slowly-varying received signal power is thus given by the standard log-normal expression

$$p_S(s) = \frac{\xi}{\sqrt{2\,\pi}\,\sigma\,s}\,\exp\left(-\frac{(\xi\ln(s)-\mu)^2}{2\,\sigma^2}\right); \qquad s \geq 0, \tag{11.2}$$

where $\xi = 10/\ln 10 = 4.3429$, $\mu = \xi\ln(\overline{S})$ is the area (logarithmic) mean power which is related to path loss and which is expressed in decibels (dB), and σ is the shadow (logarithmic) standard deviation in dB.

Mobile radio systems are also subject to fast (relative to the shadowing effect) multipath fading due to the combination of randomly-delayed reflected, scattered, and diffracted signal components. We consider slowly-varying flat-fading multipath channels. The slowly-varying condition holds when the channel fading changes at a rate much slower than the data rate, so the channel remains constant over hundreds of symbols. Flat-fading occurs when the symbol time duration is much greater than the delay spread so the signal is just affected by a degradation in its strength without a distortion in its shape. We assume that the multipath fading environment is characterized by a Nakagami-m distribution such that the PDF of the amplitude of the received signal, A, is given by [13, (11)]

$$p_A(a) = 2\,\left(\frac{m}{\Omega}\right)^m\,\frac{a^{2m-1}}{\Gamma(m)}\,\exp\left(-m\frac{a^2}{\Omega}\right); \qquad a \geq 0, \tag{11.3}$$

where $\Omega = E_S[S] = E_A[A^2]$ is the local mean received power which is related to path loss and shadowing, m is the Nakagami *fading parameter* ($m \geq 1/2$), and $\Gamma(.)$ is the *gamma function* defined by [53, p. 942, (8.310.1)]:

$$\Gamma(z) = \int_0^{+\infty} t^{z-1}\, e^{-t}\, dt; \qquad z \geq 0. \tag{11.4}$$

Thus, the PDF of the received signal power $S = A^2$ is a gamma distribution given by

$$p_S(s) = \left(\frac{m}{\Omega}\right)^m \frac{s^{m-1}}{\Gamma(m)} \exp\left(-m\,\frac{s}{\Omega}\right); \qquad s \geq 0. \tag{11.5}$$

Although path loss, shadowing, and multipath fading simultaneously affect a radio mobile communication link, we first analyze their effects separately to quantify their respective impact on the ASE. We then study their combined effect on the ASE. This separation is valuable since in many cases log-normal or Nakagami distributions give the best fit for the overall fading process. For instance Suzuki [22] concludes that the distribution of the path strengths within a site tends to follow a log-normal or a Nakagami distribution. In addition Abbes and Sheikh [170] recently showed that both log-normal and Nakagami distributions fit the overall fading data for LOS microcells, and argued that the segregation of slow and fast fading components (e.g., log-normal and Nakagami) is therefore unnecessary.

11.2.2 Interference and Adaptive System Models

To simplify the analyses the following assumptions have been made in the co-channel interference model. First, we consider interference-limited systems in which the thermal noise power is negligible relative to the co-channel interference power [166]. Thus, the ratio of carrier power to noise plus interference power reduces to the carrier-to-interference power ratio (CIR). We also neglect co-channel interferers outside the first dominant tier of interfering cells and all inter-channel interference [166]. Therefore, the desired user CIR, γ_d, can be written as

$$\gamma_d(n_I) = \frac{S_d}{S_I} = \frac{S_d(r)}{\sum_{i=1}^{n_I} S_i(r_i)}; \qquad n_I = 1, .., N_I, \tag{11.6}$$

where S_d [W] is the received power level from the desired mobile at a distance r from its BS, S_I [W] is the total interference power, and S_i [W] is the received power level from the ith interfering mobile at a distance r_i from the desired mobiles' BS. We assume throughout our study that the co-channel interfering signals add up incoherently since this leads to a more realistic assessment of the co-channel interference in cellular systems [159]. In (11.6) n_I is the number of active co-channel interferers in the first tier, and N_I is the maximum number for n_I. For example $N_I = 6$ for non-sectorized cellular systems, whereas $N_I = 2$ for 120^0 cell sectorized systems or linear highway cellular systems. The interference model for the uplink of a fully-loaded non-sectorized ($N_I = 6$) cellular

system is shown in Fig. 11.1.

Since the signal powers of both the desired and interfering mobiles experience fluctuations due to multipath fading, shadowing, and the random location of users in their respective cells, γ_d is also a random variable which depends on the distribution of the S_d and S_is. Accurate techniques for "real-time" estimation of these variations in the CIR are available [171], and we assume throughout this paper that the fluctuations in the CIR γ_d are tracked perfectly by the BS receiver. We also assume that this information is sent back to the transmitting mobiles via an error-free feedback path. The time delay in this feedback path is also assumed to be negligible compared to the rate of the channel and interference variations. All these assumptions, which are reasonable for slowly-varying channels, allow the mobiles to adapt their transmission rate relative to the actual CIR state. A block diagram of the adaptive transmission system model is shown in Fig. 11.2.

11.2.3 Users' Random Location Model

For analytical convenience we assume that the cell shape is approximated by a circle of radius R. All the mobiles (desired and interfering users) are assumed to be mutually independent and uniformly distributed in their respective cells. Thus, the PDF of the mobiles polar coordinates (r, θ) relative to their BSs are

$$p_r(r) = \frac{2\,(r - R_o)}{(R - R_o)^2}; \quad R_o \leq r \leq R, \tag{11.7}$$

$$p_\theta(\theta) = \frac{1}{2\,\pi}; \quad 0 \leq \theta \leq 2\pi. \tag{11.8}$$

R_o corresponds to the closest distance the mobile can be from the BS antenna, and is approximately equal to 20 m for microcellular systems and 80 m for macrocellular systems. Note that we do not use mobility correlation statistics in this model because they do not affect the adaptive model (instantaneous adaptation) and its corresponding ASE.

11.3 Area Spectral Efficiency

In this section we introduce the concept of area spectral efficiency for fully-loaded systems in which the cell's resource (serviced channels) are fully-used and the number of interferers is constant and equal to N_I. We generalize the ASE to partially-loaded systems in Section 11.8.

Define the *reuse distance* D [m] to be the distance between two BSs using the same set of frequencies. The ASE of a cell is defined as the sum of the maximum bit rates/Hz/unit area supported by a cell's BS. Since frequencies are reused at a distance D, the area covered by one of these partitions is roughly $\pi\,(D/2)^2$ [m^2]. The ASE, A_e [bits/sec/Hz/m^2], is therefore approximated

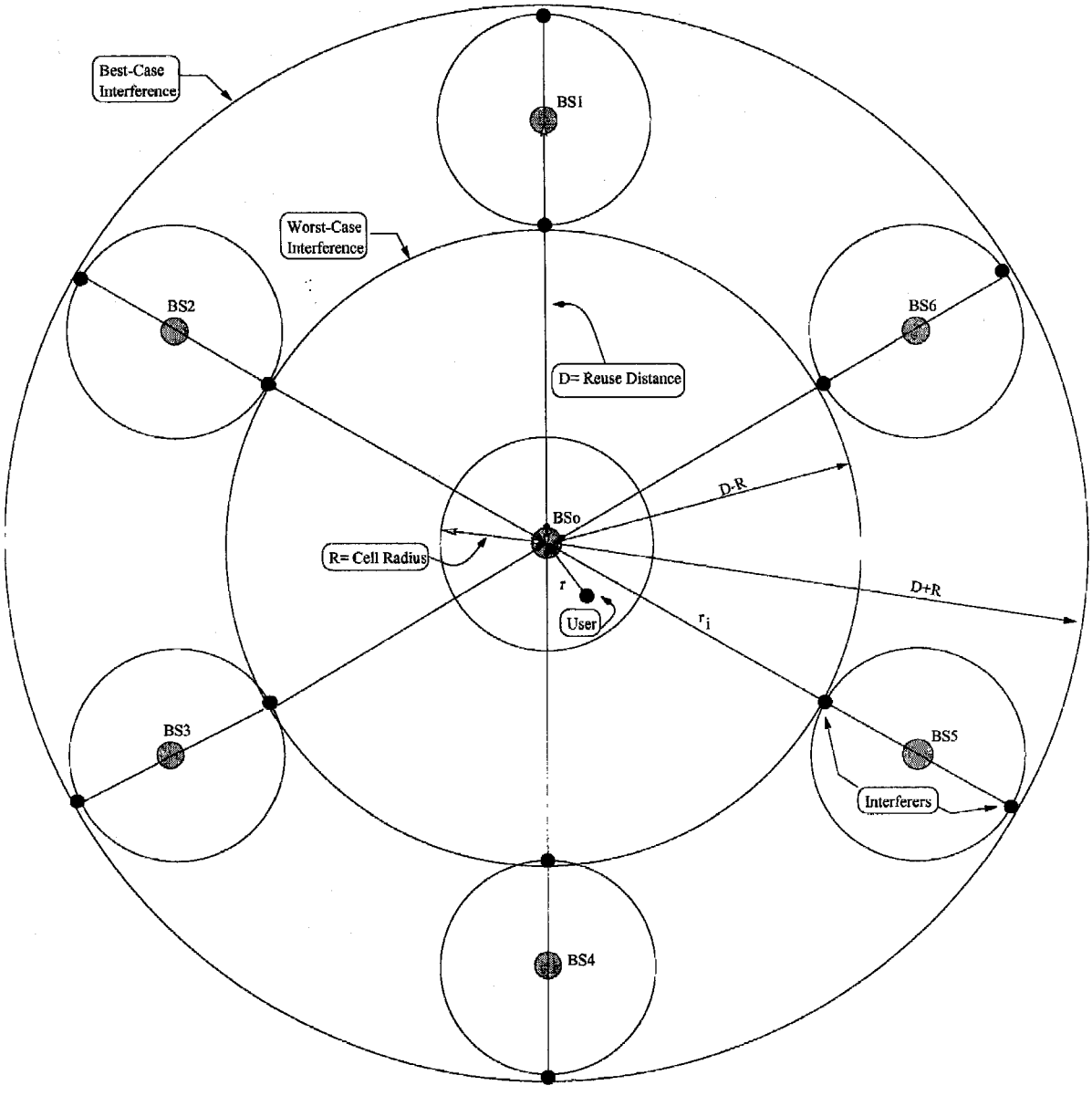

Figure 11.1: Co-channel interference on the up link at a desired BS. In fully-loaded cellular systems there are 6 primary co-channel interfering mobiles.

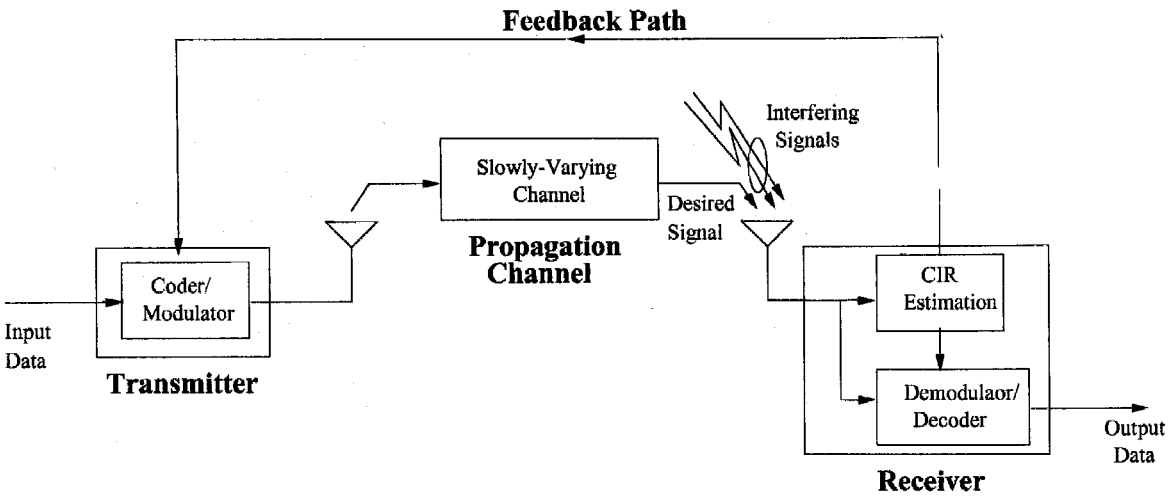

Figure 11.2: Adaptive communication system model (CIR: Carrier-to-interference power ratio).

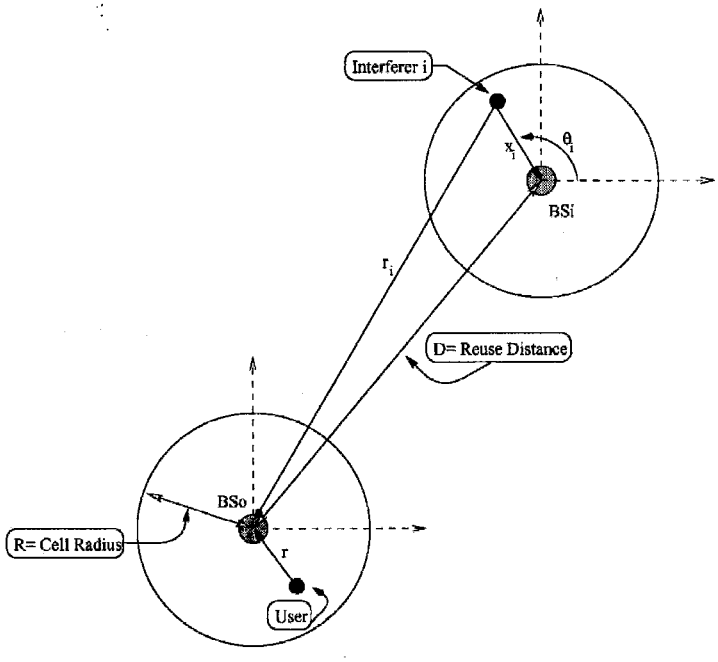

Figure 11.3: Geometry of the problem.

by

$$A_e = \frac{\sum_{k=1}^{N_s} C_k}{\pi\, W\, (D/2)^2}, \tag{11.9}$$

where N_s is the total number of active serviced channels per cell, C_k [bits/sec] is the maximum data rate of the kth user, and W [Hz] is the total allocated bandwidth per cell. We define the maximum rate C_k to be the Shannon capacity of the kth user in the cell, which depends on γ_k, the received CIR of that user, and W_k, the bandwidth allocated to that user. The Shannon capacity formula assumes that the interference has Gaussian characteristics. With FDMA or TDMA, there are usually only a few dominant interferers coming from the first ring of interfering cells, so the central limit theorem does not apply and the Gaussian assumption for the interference signal may not be valid. However, for capacity calculations, Gaussian interference is a **worst-case** noise assumption [172, 173], and under this assumption the capacity-achieving transmit spectrum for all users (i.e., desired and interfering users) is Gaussian [174]. Our ASE (11.9) is not parameterized by BER Since Shannon's capacity formula indicates an arbitrarily small BER. The ASE thus quantifies the tradeoff between the increased system efficiency induced by a small frequency reuse and the decreased capacity of each user resulting from the corresponding increase in co-channel interference. In particular, if we shrink the reuse distance, then the denominator of (11.9) is reduced. However, decreasing the reuse distance increases intercell interference, thereby reducing the CIR of each user, and its corresponding channel capacity. Therefore, there should be an optimal reuse distance which maximizes (11.9).

For γ_k constant, C_k is given by Shannon's formula: $C_k = W_k \log(1+\gamma_k)$. However, γ_k is not constant in our system since both the interference and signal power of the kth user will vary with mobiles locations and propagation conditions. When γ_k varies with time, C_k equals the average channel capacity of the kth user [135, 137], given by

$$\overline{C}_k = W_k \int_0^{+\infty} \log_2(1+\gamma_k)\; p_{\gamma_k}(\gamma_k)\; d\gamma_k, \tag{11.10}$$

where $p_{\gamma_k}(\gamma_k)$ is the PDF of the kth user's CIR. The average capacity intrinsicly assumes that the users' rate are continuously adapted relative to their CIR (i.e., interference conditions) in such a manner that the BER goes to zero asymptotically. We therefore define the *average area spectral efficiency*, $\overline{A}_e$ [bits/sec/Hz/m^2], as the sum of the maximum average data rates/Hz/unit area for the system, given by (11.9), with C_k replaced by $\overline{C}_k$. If all users are assigned the same bandwidth then $\overline{C}_k (= \overline{C})$ becomes the same for all users, and $\overline{A}_e$ can therefore be written as

$$\overline{A}_e = \frac{4\, N_s\, \overline{C}}{\pi\, W\, R_u^2\, R^2}, \tag{11.11}$$

where R_u is the *normalized reuse distance*, $R_u = D/R$.

Consider first FDMA systems, where all users are allocated the same bandwidth $W_k = W_o =$

W/N_s. Substituting in (11.11) yields

$$\overline{A}_e^{\text{FDMA}} = \frac{4}{\pi\ R_u^2\ R^2} \int_0^{+\infty} \log_2(1+\gamma)\ p_\gamma(\gamma)\ d\gamma. \tag{11.12}$$

In TDMA systems the total bandwidth is allocated to only one active user per time slot ($N = 1$ and $W_k = W$). Substituting this in (11.11) we see that TDMA systems have the same ASE as FDMA systems, so

$$\overline{A}_e^{\text{FDMA}} = \overline{A}_e^{\text{TDMA}} = \overline{A}_e. \tag{11.13}$$

11.4 Effect of Path Loss

In this section we study the ASE of fully-loaded systems, ignoring the effects of shadowing and multipath fading. We obtain the reuse distance which maximizes the ASE and also determine the impact of the cell size, carrier frequency, propagation parameters, and cell sectorization.

11.4.1 Analyses

Recall that due to the random location of users in their respective cells, γ_d is a random variable depending on the random positions of the $(N_I + 1)$ desired and interfering mobiles. To simplify our analysis, we reduce the problem from $(N_I + 1)$ dimensions to 1 dimension by computing γ_d and the corresponding ASE for the worst-case (-) and best-case (+) interference configurations. Without power control to compensate for path loss the worst-case interference configuration corresponds to the case where all the N_I co-channel interferers are on the near boundary of their respective cells, at a distance $r_I^- = D - R$ [m] from the desired mobile's BS. On the other hand, the best-case interference configuration corresponds to the case where all the N_I co-channel interferers are on the far boundary of their cells, at a distance $r_I^+ = D + R$ [m] from this BS. The worst-case and the best-case interference configurations are illustrated in Fig. 11.1. Assuming that the transmitted power of all users is the same and substituting (11.1) into (11.6) yields

$$\overline{\gamma}_d^{\pm}(N_I, r) = \frac{S_d}{(\sum_{i=1}^{N_I} S_i)^{\pm}} = \frac{1}{N_I} \left[\frac{R\ (R_u \pm 1)}{r}\right]^a \left[\frac{g + (R_u \pm 1)R}{g + r}\right]^b. \tag{11.14}$$

Note that γ_d is function of r, so the desired user capacity is

$$\overline{C}^{\pm}(N_I, r) = W_o\ \log_2(1 + \overline{\gamma}_d^{\pm}(N_I, r)) \tag{11.15}$$

for γ_d given by (11.14). Substituting (11.15) in (11.11) yields the ASE conditioned on the desired mobile position r, for a fully-loaded system. Integrating (11.15) over the desired user's position PDF

(11.7) yields the average ASE for the two extreme interference configurations as

$$<\overline{A}_e(N_I)>^{\pm}=\frac{4}{\pi R_u^2 R^2}\int_{R_o}^{R}\log_2\left(1+\overline{\gamma}_d^{\pm}(N_I,r)\right)\ p_r(r)\ dr. \tag{11.16}$$

In (11.16) and in what follows the brackets denotes the operation of averaging over the desired user's position PDF (11.7). In practice, when each interferer i is uniformly distributed at a distance r_i between r_I^- and r_I^+, the average ASE will be between these bounding values, as we will confirm by Monte-Carlo simulations.

11.4.2 Monte-Carlo Simulations

The exact analytical value of $<\overline{A}_e>$, averaged over the random positions of the desired and interfering users, requires a numerical (N_I+1)-fold integration, which is not only computationally burdensome but also subject to roundoff and stability problems. Rather than computing this integral, we instead opted for a Monte Carlo simulation to estimate it. The simulation algorithm is composed of the following steps:

1. The position of the desired user is randomly picked according to (11.7) as follows:
   - generate a pseudo-random number u uniformly distributed in [0,1].
   - deduce the user's position r according to (11.7) using the percentile transformation method [76, p. 226]:
   $$r = R_o + (R - R_o)\ \sqrt{u}. \tag{11.17}$$
2. The polar coordinates (x_i, θ_i) of the N_I co-channel interferers are randomly picked according to (11.7) and (11.8) as follows:
   - generate N_I pseudo-random, pseudo-independent numbers u_i and v_i uniformly distributed in [0,1].
   - deduce the N_I polar coordinates (x_i, θ_i) as:
   $$x_i = R_o + (R - R_o)\ \sqrt{u_i}, \tag{11.18}$$
   $$\theta_i = 2\pi\ v_i. \tag{11.19}$$
3. The distance r_i from each co-channel interferer to the considered BS is calculated as (see Fig. 11.3):
   $$r_i = \sqrt{D^2 + x_i^2 + 2\ D\ x_i\ \sin(\theta_i)}. \tag{11.20}$$

4. The $N_I + 1$ average received signal powers of the desired user and interfering mobiles ($\overline{S}_d$ and $\overline{S}_i$s) are calculated using the two-slope path model (11.1).

5. The CIR of the desired user, γ_d, is then obtained according to (11.6).

6. The ASE A_e is calculated as

$$\overline{A}_e = \frac{4}{\pi R_u^2 R^2} \log_2(1 + \gamma_d). \tag{11.21}$$

Repeating the above process (step 1 to step 6) 10,000 times, we can estimate the value of $<\overline{A_e}>$ by taking the average of all the observations of the ASE as given by (11.21). After 10,000 computations, $<\overline{A_e}>$ converges to within 3-digit accuracy.

11.4.3 Numerical and Simulation Results

In this section we compute the effects of propagation parameters, the cell size, and the carrier frequency on the ASE of fully-loaded cellular systems. The ASE for the worst-case ($< A_e >^-$) and the best-case ($< A_e >^+$) interference configurations are numerically computed for specific system parameters. The value of $< A_e >$ for average interference conditions is also computed using the Monte Carlo simulation described in Section 11.4.2 for the same system parameters of interest.

Fig. 11.4 depicts the effect of path loss propagation parameters on the ASE. Our computer simulations confirm our analysis, since the simulated values always lie between the predicted theoretical bounds corresponding to the two extreme interference configurations. As expected the spectral efficiency improves as the additional path loss exponent b increases, since the interfering signals are more attenuated.

Fig. 11.5 shows plots of the ASE versus the normalized reuse distance for typical microcellular systems ((a) $R = 200$ m and (b) $R = 800$ m) and macrocellular systems ((c) $R = 5$ km). We see from this figure that the spectral efficiency is increased by decreasing the cell size. This observation is further investigated in Fig. 11.6, where we plot the ASE as a function of the cell radius. The 'o' points in Fig. 11.6 correspond to simulation results, whereas the curves correspond to the best fit in the mean-square-error sense of these simulated values. We found that the ASE decreases as an exponential of a 4th order polynomial relative to the cell size. Thus we have exactly quantified how spectral efficiency of cellular systems increases as cell size decreases.

Figs. 11.4-11.5 both indicate that, based on the worst-case interference configuration curves, the optimal reuse distance to maximize the ASE is 4. In fact, the actual optimum occurs for a reuse distance of about 3. However, our statement is based on the fact that R_u is constrained, by definition, to be an even number. On the other hand, the best-case interference configuration and the average interference configuration (simulation) curves do not show an ASE maximum. This implies

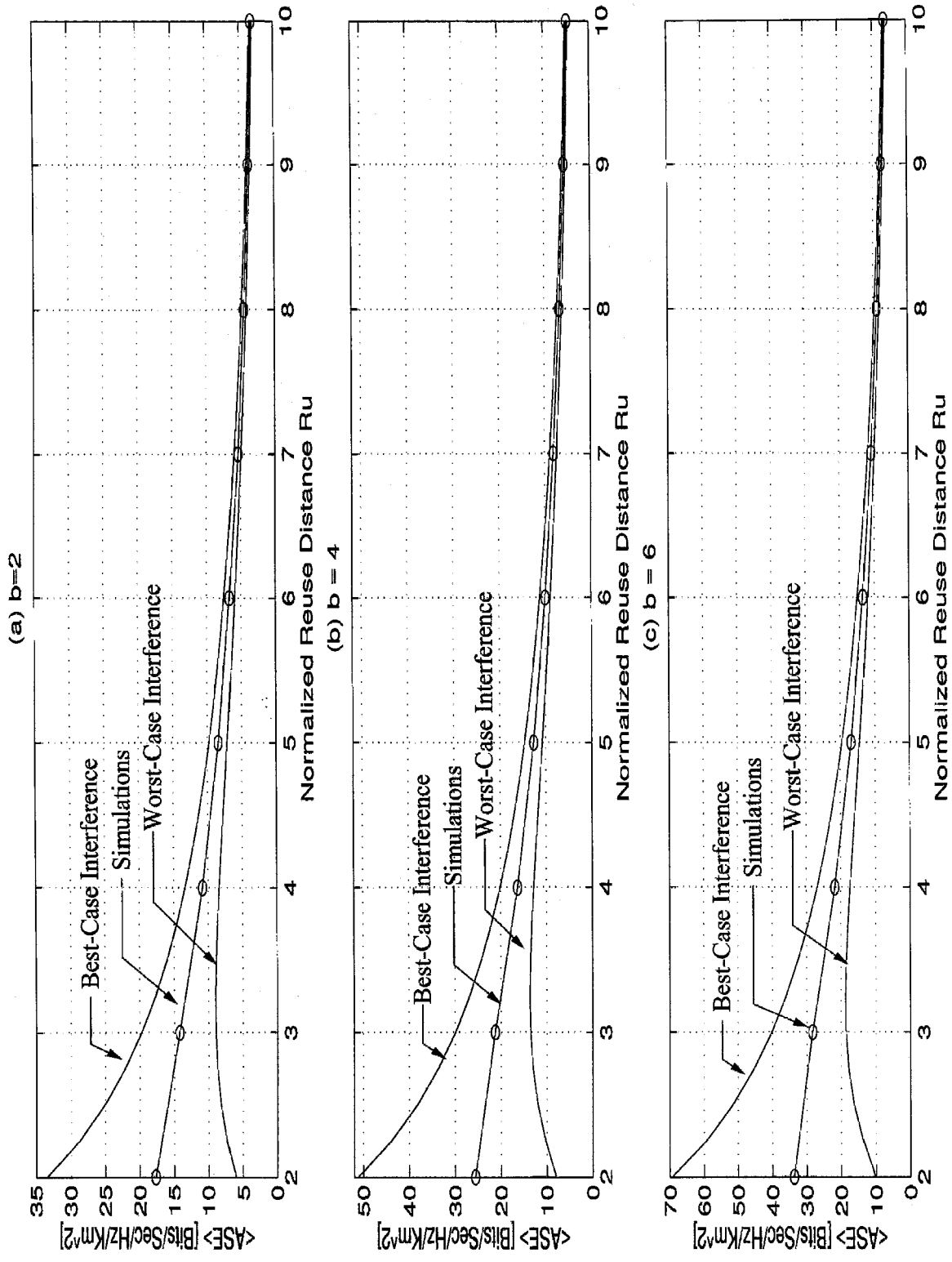

Figure 11.4: Comparison of the average up link spectral efficiency versus the normalized reuse distance for different values of the additional path exponent b. (Fully-loaded system with $N_I = 6$; Cell Radius R= 200m; $R_o = 20$ m; Antenna heights: 10 m BS, 2 m mobile; Carrier frequency: 900 MHz; Basic path exponent: $a = 2$).

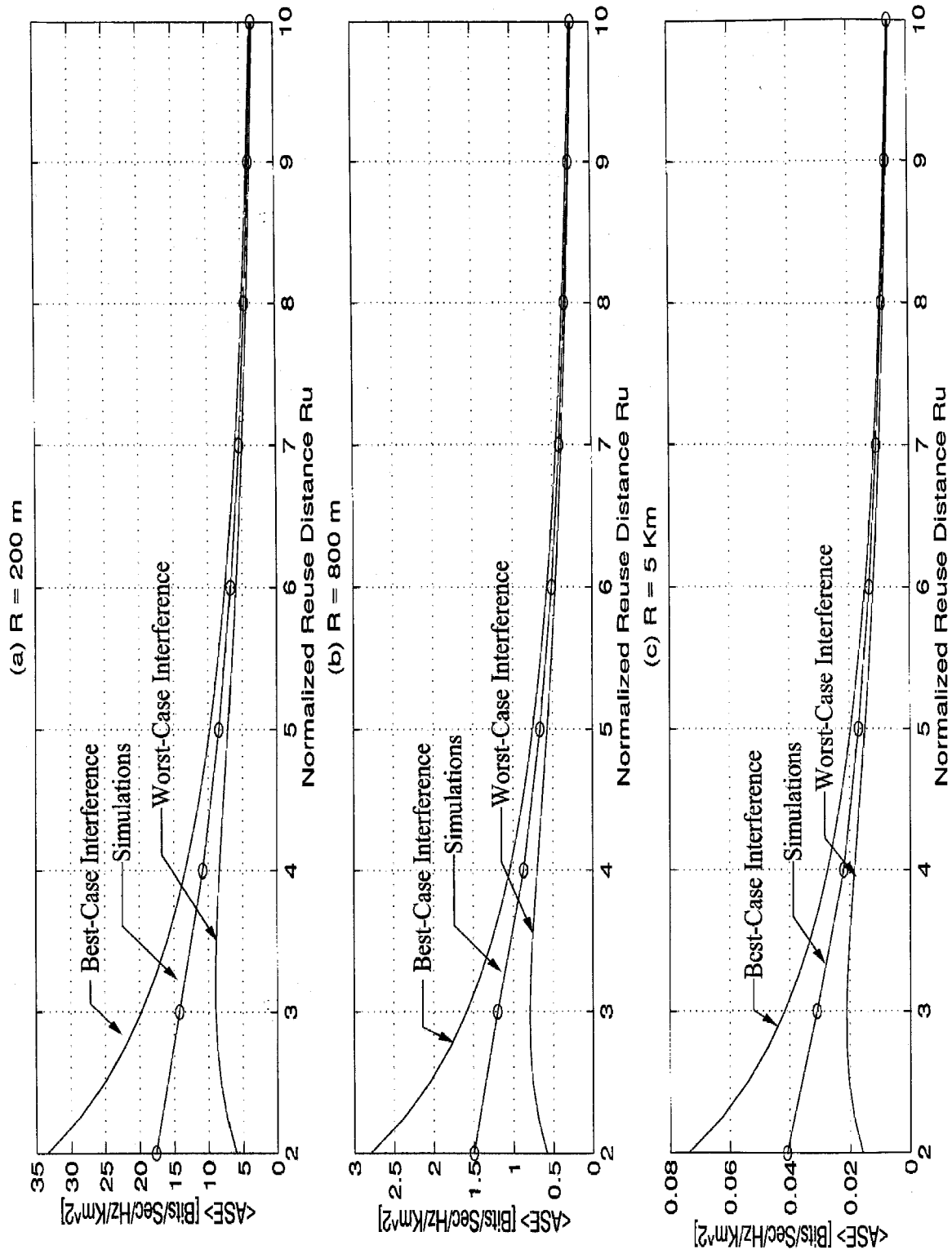

Figure 11.5: Comparison of the average up link spectral efficiency versus the normalized reuse distance for different cell sizes. (Fully-loaded system with $N_I = 6$; Carrier frequency: 900 MHz; Propagation parameters: $a = b = 2$).

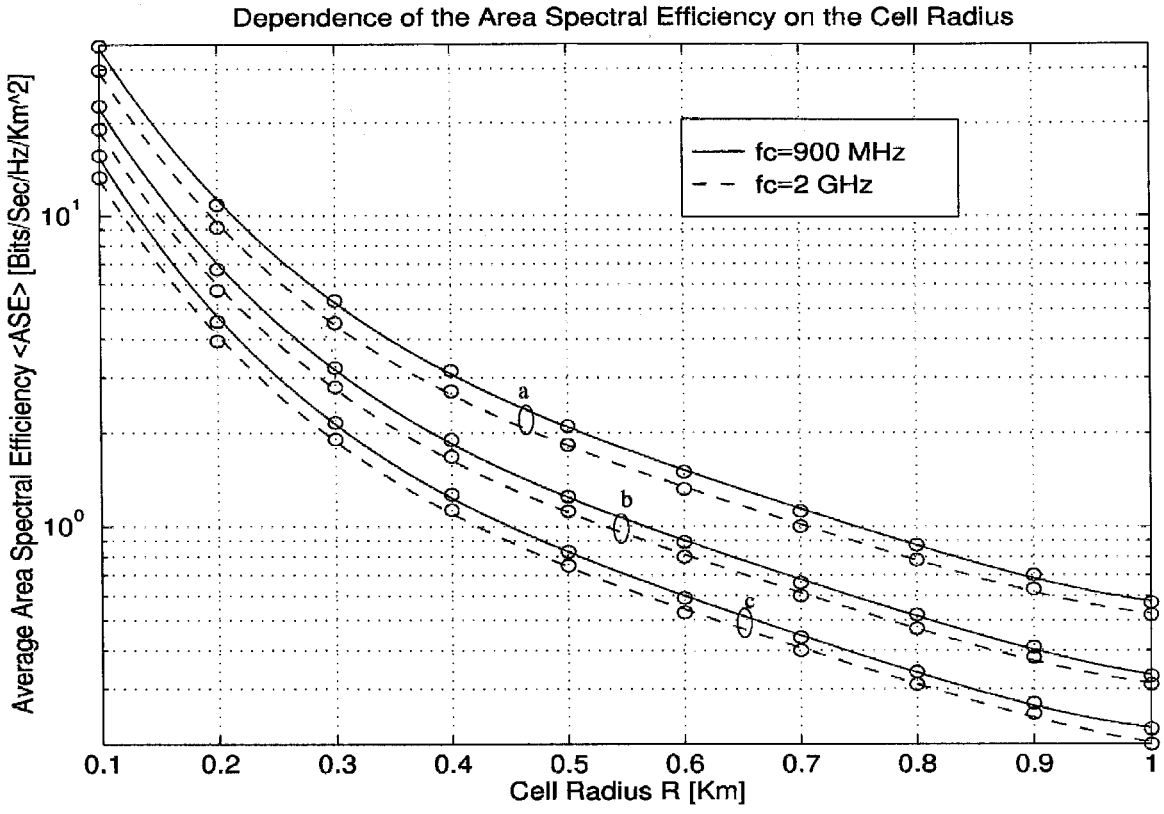

Figure 11.6: Average up link spectral efficiency versus cell radius for different reuse distances ((a) $R_u = 4$, (b) $R_u = 6$, and (c) $R_u = 8$) and carrier frequencies ((-) $f_c = 900$ MHz and (- -) $f_c = 2$ GHz.). (Fully-loaded system with $N_I = 6$; $R_o = 20m$; Antenna heights: 10 m BS, 2 m mobile; Propagation parameters: $a = b = 2$.)

that, for typical interference conditions, the spectral efficiency is maximized by a reuse distance of 2 (i.e., frequencies are reused every cell), and is monotonically decreasing for $R_u \geq 2$. Note that because our ASE is defined in terms of Shannon capacity, this increase in spectral efficiency is not obtained at the expense of a higher BER. In fact, smaller frequency reuse results in a higher BER only if the data rate of the system is not adapted to compensate for the resulting higher level of co-channel interference [158, 159, 162]. We will see in the following sections that all these results still hold when shadowing and fading are taken into account.

The ASE is increased if interference can be reduced while maintaining the same number of users per cell and the same reuse distance. Cell sectorization [175] is commonly employed to accomplish this, whereby directional antennas are used at the BS. In fully-loaded systems, 3-sector antennas (or 120^o cell sectorization) reduce the number of primary co-channel interferers from $N_I = 6$ to $N_I = 2$. Fig. 11.7 shows the improvement in ASE when a 120^o cell sectorization is employed for a $R = 200$ m microcellular system. Note the ASE increase in both the upper and lower dashed curves compared to the omni-directional case (solid curves). Further improvement in the ASE can be obtained with 60^o cell sectorization (6-sector antennas) since the number of primary co-channel interferers is reduced in that case to $N_I = 1$.

11.5 Effect of Shadowing

In this section we consider the ASE of a fully-loaded cellular system when both the desired and interfering users are affected by log-normal shadowing superimposed on path loss.

11.5.1 Analyses

The desired user's signal is assumed to be log-normally shadowed according to (11.2) with area mean power μ_d and standard deviation σ_d. There are N_I mutually independent log-normally shadowed interferers, each with mean μ_i and standard deviation σ_i. The interferers are assumed to be statistically identical so that

$$\mu_i = \mu_I; \quad i = 1, 2, \ldots, N_I, \tag{11.22}$$

$$\sigma_i = \sigma_I; \quad i = 1, 2, \ldots, N_I. \tag{11.23}$$

We will refer to all these assumptions as the independent identically distributed (i.i.d.) hypothesis on the S_is. Assumptions (11.22) and (11.23) hold when all the N_I interferers are constrained to be on a circle of radius r_I from the considered BS. Note that these assumptions are not essential in our derivation of the ASE. Our analyses can be easily generalized for interferers which are not i.i.d., but this assumption makes our analyses more tractable.

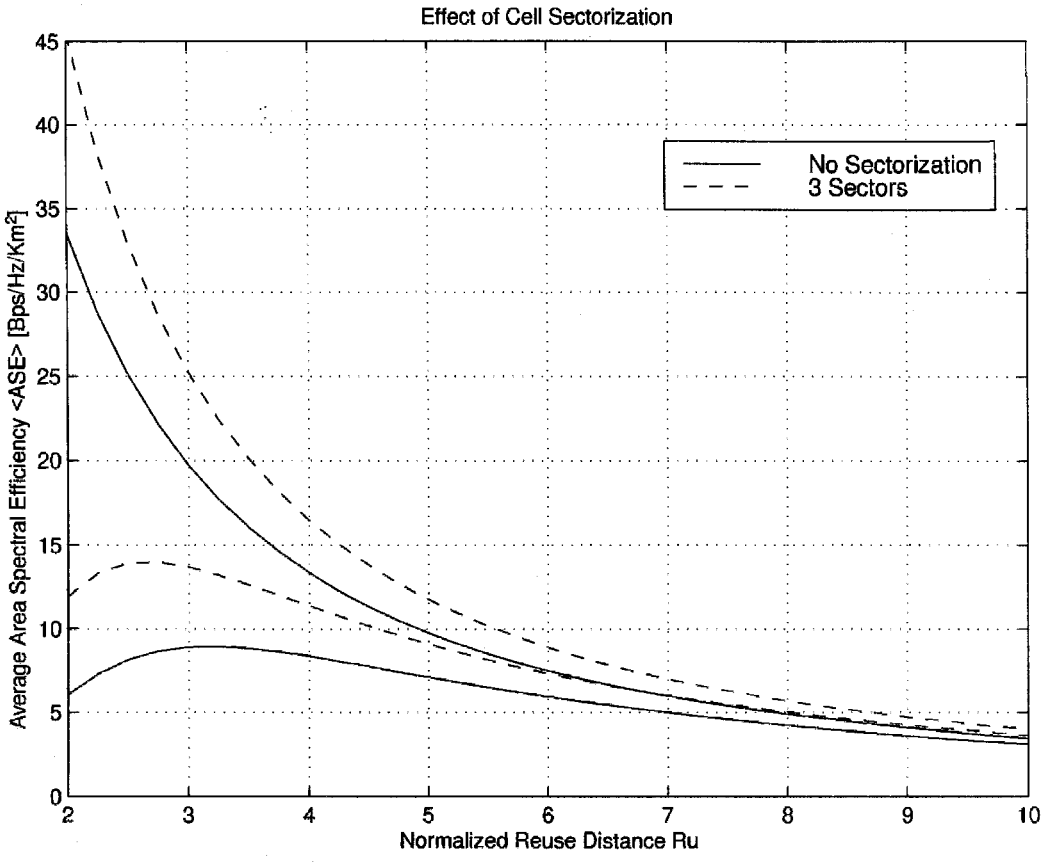

Figure 11.7: Average up link spectral efficiency versus normalized reuse distance with 120^o cell sectorization. (Fully-loaded system with $N_I = 6$; Cell Radius R= 200m; R_o = 20 m; Antenna heights: 10 m BS, 2 m mobile; Carrier frequency $f_c = 900$ MHz; Propagation parameters: $a = b = 2$).

PDF of the Desired User CIR

The total interference power S_I is the sum of N_I i.i.d. log-normally distributed RVs. Although no exact closed-form expression for the PDF of the sum of log-normally distributed RVs is known, it is widely accepted that such a sum can be accurately approximated by another log-normal distribution [2, Sec. 3.1]. Several methods have been proposed to find the mean and variance of the resulting log-normal PDF [176, 177]. A very thorough description and comparison of these methods is available in [2, Sec. 3.1]. Here we use the Fenton-Wilkinson method [176] for its relative simplicity. According to this method, the logarithmic mean μ_{S_I} and the logarithmic variance σ_{S_I} of S_I can be found by matching the first and second order moments, which yields

$$\mu_{S_I} = \mu_I + \xi \ln(N_I) + \frac{\sigma_I^2}{2\,\xi} - \frac{\xi}{2} \ln\left(\frac{N_I - 1 + e^{\sigma_I^2/\xi^2}}{N_I}\right), \tag{11.24}$$

$$\sigma_{S_I}^2 = \xi^2 \ln\left(\frac{N_I - 1 + e^{\sigma_I^2/\xi^2}}{N_I}\right). \tag{11.25}$$

Since the ratio of two log-normal RVs is also a log-normal RV, the desired user CIR, γ_d, is also log-normally distributed with the following logarithmic mean μ_{γ_d} and logarithmic variance $\sigma_{\gamma_d}^2$:

$$\mu_{\gamma_d} = \mu_d - \mu_{S_I}, \tag{11.26}$$

$$\sigma_{\gamma_d}^2 = \sigma_d^2 + \sigma_{S_I}^2. \tag{11.27}$$

The PDF of γ_d can therefore be written as

$$p_{\gamma_d}(\gamma) = \frac{\xi}{\sqrt{2\pi}\,\sigma_{\gamma_d}\,\gamma} \exp\left(-\frac{(\xi \ln(\gamma) - \mu_{\gamma_d})^2}{2\,{\sigma_{\gamma_d}}^2}\right); \quad \gamma \geq 0. \tag{11.28}$$

Desired User Average Capacity

Inserting (11.28) in (11.10), the average capacity of the desired user can be written as

$$\overline{C} = \frac{W_o \log_2(e)\,\xi}{\sqrt{2\pi}\,\sigma_{\gamma_d}} \int_0^{+\infty} \frac{\ln(1+\gamma)}{\gamma} \exp\left(-\frac{(\xi \ln(\gamma) - \mu_{\gamma_d})^2}{2\,{\sigma_{\gamma_d}}^2}\right) d\gamma_d. \tag{11.29}$$

Using the following inequality in (11.29):

$$\ln(1+\gamma) \leq \ln(\gamma) + \frac{1}{\gamma}; \quad \gamma \geq 0, \tag{11.30}$$

we obtain an upper bound on the desired user average capacity $\overline{C}_{\text{up}}$ given by

$$\overline{C} \leq \overline{C}_{\text{up}} = W_o \log_e(e) \left[\frac{\mu_{\gamma_d}}{\xi} + \exp\left(-\frac{\mu_{\gamma_d}}{\xi} + \frac{\sigma_{\gamma_d}^2}{2\,\xi^2}\right)\right]. \tag{11.31}$$

On the other hand, using the following inequalities in (11.29):

$$\begin{aligned} \ln(1+\gamma) &\geq \ln(\gamma) + \frac{1}{1+\gamma} \\ &\geq \ln(\gamma) + (1-\gamma)P_{[0,1]}(\gamma); \quad \gamma \geq 0, \end{aligned} \tag{11.32}$$

where $P_{[0,1]}(\gamma) = 1$ when $\gamma \in [0,1]$ and 0 otherwise, we obtain a lower bound on the desired user average capacity $\overline{C}_{\text{low}}$ given by

$$\overline{C} \geq \overline{C}_{\text{low}} = W_o \ \log_e(e) \ \left[\frac{\mu_{\gamma_d}}{\xi} + Q\left(\frac{\mu_{\gamma_d}}{\sigma_{\gamma_d}}\right) - \exp\left(\frac{\mu_{\gamma_d}}{\xi} + \frac{\sigma^2_{\gamma_d}}{2\,\xi^2}\right) \ Q\left(\frac{\mu_{\gamma_d}}{\sigma_{\gamma_d}} + \frac{\sigma_{\gamma_d}}{\xi}\right)\right], \tag{11.33}$$

where $Q(.)$ is the *Gaussian integral function* defined as

$$Q(z) = \frac{1}{\sqrt{2\pi}} \int_z^{+\infty} e^{-t^2/2}\, dt. \tag{11.34}$$

ASE for the Two Extreme Interference Configurations

Substituting (11.29) in (11.11) yields the ASE for the two extreme interference configurations in a shadowing environment as

$$\overline{A}_e^{\pm}(r) = \frac{4\ \overline{C}^{\pm}(r)}{\pi\ W_o\ R_u^2\ R^2}. \tag{11.35}$$

Similarly, substituting (11.31) and (11.33) in (11.11) yields an upper and a lower bound on the ASE as given by (11.35) for the two extreme interference configurations:

$$\frac{4\ \overline{C}^{\pm}_{\text{low}}(r)}{\pi\ W_o\ \ R_u^2\ R^2} \leq \overline{A}_e^{\pm}(r) \leq \frac{4\ \overline{C}^{\pm}_{\text{up}}(r)}{\pi\ \ W_o\ R_u^2\ R^2}. \tag{11.36}$$

Note that $\overline{C}^{\pm}(r)$, $\overline{C}^{\pm}_{\text{up}}(r)$, and $\overline{C}^{\pm}_{\text{low}}(r)$ are computed using

$$\begin{aligned} \mu^{\pm}_{\gamma_d} &= \mu_d - \mu^{\pm}_{S_I} \\ &= \xi\ \ln\left[\left[\frac{R\ (R_u \pm 1)}{r}\right]^a \left[\frac{g + (R_u \pm 1)R}{g + r}\right]^b\right] - \xi\ \ln(N_I) + \frac{\sigma^2_{S_I} - \sigma^2_I}{2\,\xi}, \end{aligned} \tag{11.37}$$

and $\sigma^2_{\gamma_d}$ given by (11.27). Since the expressions in (11.35) and (11.36) are conditioned on the desired mobile position, they are averaged over the user's position PDF (11.7) to obtain the overall average ASE $<\overline{A_e}>^{\pm}$ for the two extreme interference configurations.

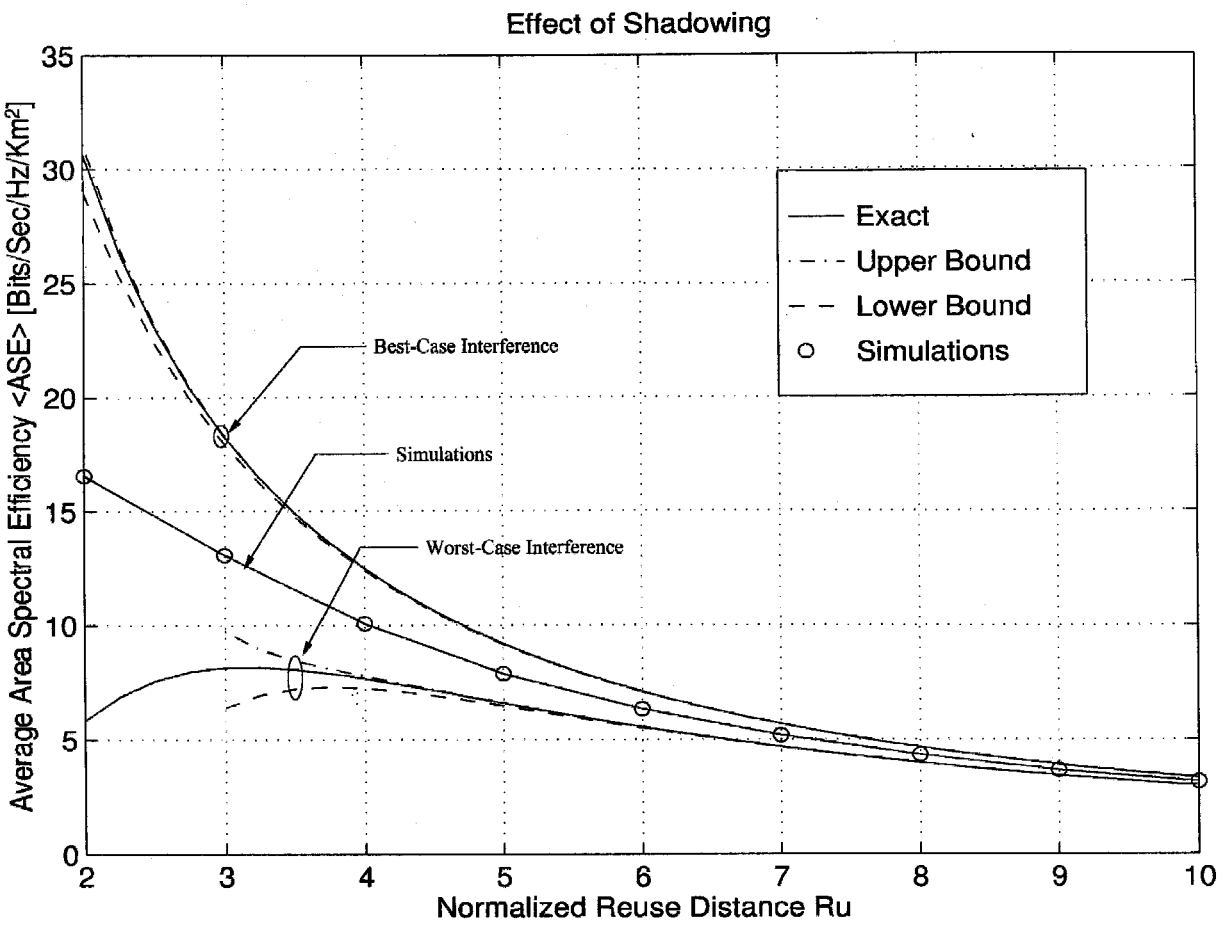

Figure 11.8: Comparison of the bounds and the exact values for the average up link spectral efficiency with shadowed users (- -) with $\sigma_d = \sigma_I = 4$ dB. (Fully-loaded system with $N_I = 6$; Cell Radius R= 200m; $R_o = 20$ m; Antenna heights: 10 m BS, 2 m mobile; Carrier frequency $f_c = 900$ MHz; Propagation parameters: $a = b = 2$).

11.5.2 Numerical and Simulation Results

Fig. 11.8 compares the closed-form upper and lower bounds (11.36) averaged over (11.7) with the exact value $<\overline{A_c}>^{\pm}$ found by averaging (11.35) over (11.7) with $\sigma_d = \sigma_I = 4$ dB for the two extreme interference configurations. The bounds are very tight for the best-case interference configuration. As R_u increases the bounds become tighter. On the other hand the bounds are quite loose for the worst interference configuration when $R_u < 3$. This is because the inequalities (11.30) and (11.32) are not tight when γ is small. However, the bounds improve as R_u increases and become very tight for $R_u \geq 4$. The 'o' points in Fig. 11.9 correspond to simulation results obtained using an algorithm similar to the one described in Section 11.4 except for step 4 which is changed to incorporate the effects of shadowing. The changes in the simulation algorithm are described in detail in Appendix A-1. Note again that the simulated values corresponding to average interference configurations always lie between the predicted theoretical values for the two extreme interference conditions.

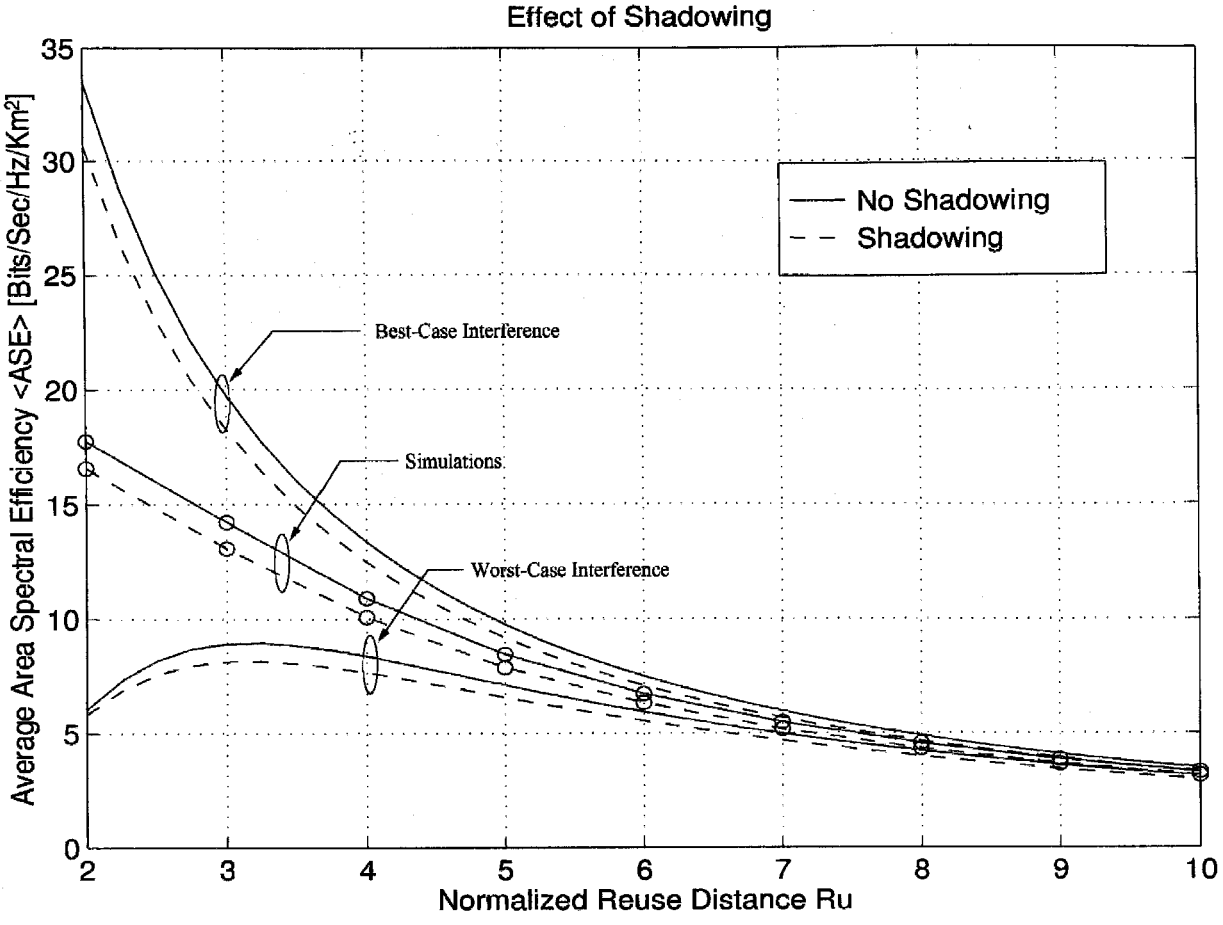

Figure 11.9: Comparison of the average up link spectral efficiency versus normalized reuse distance with non shadowed users (-) and shadowed users (- -) with $\sigma_d = \sigma_I = 4$ dB. (Fully-loaded system with $N_I = 6$; Cell Radius R= 200m; $R_o = 20$ m; Antenna heights: 10 m BS, 2 m mobile; Carrier frequency $f_c = 900$ MHz; Propagation parameters: $a = b = 2$).

Fig. 11.9 compares the ASE with and without shadowing. We see in all cases that the ASE curves for different interference configurations have the same relative shape. However, the ASE with shadowing is always smaller. We will see in the next section that multipath fading also reduces the ASE.

11.6 Effect of Multipath Fading

In this section we consider the ASE of fully-loaded cellular systems with Nakagami fading superimposed on path loss. Specifically, we study how the ASE is affected by different amounts of fading on the desired and interfering users. This is of particular interest for microcellular environments in which the desired signal typically experiences less severe fading then the co-channel interfering signals.

11.6.1 Analyses

The fading of the desired user's signal has a Nakagami parameter m_d and a local mean power $\overline{S}_d$. There are N_I interferers, each with mutually independent fading and with Nakagami fading parameter m_i and mean power $\overline{S}_i$. The interferers are assumed to be statistically identical so that the S_is are i.i.d.:

$$\overline{S}_i = \overline{S}_I, \quad i = 1, 2, \ldots, N_I, \tag{11.38}$$

$$m_i = m_I; \quad i = 1, 2, \ldots, N_I. \tag{11.39}$$

Assumption (11.38) holds when all the N_I interferers are constrained to be on a circle of radius r_I from the considered BS. This assumption is convenient for deriving the ASE in the worst-case and best-case interference configurations.

PDF of the Desired User CIR

Let $\Phi_{S_i}(.)$ denote the characteristic function (CF) of the received power of the i-th interferer. As a CF of a gamma RV, $\Phi_{S_i}(.)$ is given by

$$\Phi_{S_i}(\omega) = E(e^{j\omega S_i}) = \frac{1}{(1 - j\omega\overline{S}_I/m_I)^{m_I}}. \tag{11.40}$$

Since we assume that the S_i are i.i.d., the CF of S_I is just $\Phi_{S_i}(.)$ raised to the power N_I:

$$\Phi_{S_I}(\omega) = \frac{1}{(1 - j\omega\overline{S}_I/m_I)^{m_I N_I}}. \tag{11.41}$$

Thus N_I Nakagami interferers are equivalent to a single Nakagami interferer with parameter m_I N_I and with local mean power N_I $\overline{S}_I$. Therefore, S_I is gamma distributed with a PDF given by

$$p_{S_I}(s) = \left(\frac{m_I}{\overline{S}_I}\right)^{m_I N_I} \frac{s^{m_I N_I - 1}}{\Gamma(m_I\ N_I)} \exp\left(-m_I \frac{s}{\overline{S}_I}\right); \quad s \geq 0. \tag{11.42}$$

Since S_d and S_I are independent, the PDF of γ_d is given by [76, p.138, (6-43)]

$$p_{\gamma_d}(\gamma) = \int_0^{+\infty} S_I \ p_{S_d}(\gamma\ S_I)\ p_{S_I}(S_I)\ dS_I; \quad \gamma \geq 0. \tag{11.43}$$

Substituting (11.5) and (11.42) in (11.43), the PDF of γ_d is found using [53, p.364, (3.381.4)]:

$$p_{\gamma_d}(\gamma) = \left(\frac{m_d}{\overline{S}_d}\right)^{m_d} \left(\frac{m_I}{\overline{S}_I}\right)^{m_I N_I} \frac{\gamma^{m_d - 1}}{B(m_d, m_I N_I)\ \left(\frac{m_d}{\overline{S}_d}\gamma + \frac{m_I}{\overline{S}_I}\right)^{m_d + m_I N_I}}, \tag{11.44}$$

where $B(.,.)$ is the *beta function* defined by [53, p.957, (3.380.1)] as

$$B(p,q) = \int_0^1 t^{p-1}\,(1-t)^{q-1}\,dt; \qquad p>0,\ q>0, \tag{11.45}$$

and related to the *gamma function* by

$$B(p,q) = \frac{\Gamma(p)\,\Gamma(q)}{\Gamma(p+q)}. \tag{11.46}$$

Defining the parameters $\rho = m_d + m_I N_I$ and $y = \frac{m_I\,\overline{S}_d}{m_d\,\overline{S}_I}$, we can rewrite (11.44) in a more compact form as

$$p_{\gamma_d}(\gamma) = \frac{y^{\rho-m_d}\,\gamma^{m_d-1}\,(\gamma+y)^{-\rho}}{B(m_d,\rho-m_d)}. \tag{11.47}$$

Note that for the special case where m_d and m_I are restricted to be positive integers, $p_{\gamma_d}(\gamma)$ reduces to

$$p_{\gamma_d}(\gamma) = \frac{(\rho-1)!}{(\rho-m_d-1)!}\,y^{\rho-m_d}\,\gamma^{m_d-1}\,(\gamma+y)^{-\rho}. \tag{11.48}$$

Desired User Average Capacity

Inserting (11.48) in (11.10), the average capacity of the desired user can be written as

$$\overline{C} = \frac{W_o\,\log_2(e)\,y^{\rho-m_d}}{B(m_d,\rho-m_d)}\int_0^{+\infty}\frac{\gamma^{m_d-1}\,\ln(1+\gamma)}{(\gamma+y)^{\rho}}\,d\gamma. \tag{11.49}$$

The integral in (11.49) can be viewed as the *ρth order generalized Stieltjes transform* (GST) [178, p. 213], $\mathcal{G}_\rho\{f_{m_d}(.);y\}$, of the function $f_{m_d}(\gamma) = \gamma^{m_d-1}\,\ln(1+\gamma)$. Thus $\overline{C}$ can be written as

$$\overline{C} = \frac{W_o\,\log_2(e)\,y^{\rho-m_d}}{B(m_d,\rho-m_d)}\,\mathcal{G}_\rho\{f_{m_d}(\gamma);y\}. \tag{11.50}$$

The GST as well as some of its properties that will be useful in our analyses are reviewed in Appendix B. We restrict ourselves in this section to integer values of m_d but we do not put any constraint on m_I. The evaluation of $\mathcal{G}_\rho\{f_{m_d}(\gamma);y\}$ is derived in Appendix C and is given in (11.82). Using that result, we can rewrite $\overline{C}$ as

$$\overline{C} = \frac{W_o\,\log_2(e)\,y}{B(m_d,\rho-m_d)}\left|\sum_{j=0}^{m_d-1}\frac{(-1)^j\,\binom{m_d-1}{j}}{(\rho-j-1)^2}\,F(1,1;\rho-j;1-y)\right|, \tag{11.51}$$

where $F(.,.;.;.)$ is the *Gauss' hypergeometric function* defined as [53, p. 1065, (9.100)]

$$F(\alpha,\beta;\gamma;z) = \frac{\Gamma(\gamma)}{\Gamma(\alpha)\,\Gamma(\beta)}\sum_{j=0}^{+\infty}\frac{\Gamma(\alpha+j)\,\Gamma(\beta+j)}{\Gamma(\gamma+j)}\cdot\frac{z^j}{j!}, \tag{11.52}$$

and $\binom{n}{k}$ denotes the binomial coefficient.

For the special case of $y = 1$ (i.e., $\frac{\overline{S}_d}{m_d} = \frac{\overline{S}_I}{m_I}$), using [53, p. 589, (4.293.14)] $\overline{C}$ reduces to

$$\overline{C} = W_o \ \log_2(e) \left(\psi(\rho) - \psi(\rho - m_d)\right), \tag{11.53}$$

where $\psi(.)$ is the *Euler's psi function* defined by [53, p. 952, (8.360)]

$$\psi(z) = \frac{d}{dz} \ln[\Gamma(z)]. \tag{11.54}$$

Note that in this special $y = 1$ case, (11.53) applies even if m_d is not restricted to be an integer (contrary to (11.51)). If m_d is restricted to be an integer, we can applies [53, p. 954, (8.365.7)] to (11.53) to get a very simple expression for $\overline{C}$ as

$$\overline{C} = W_o \ \log_2(e) \ \sum_{j=0}^{m_d-1} \frac{1}{j + m_I \ N_I}. \tag{11.55}$$

ASE for the Two Extreme Interference Configurations

Substituting (11.51) in (11.11), we get the ASE averaged over the multipath fading and conditioned on the desired mobile position r as

$$\overline{A}_e^{\pm}(r) = \frac{4 \ \log_2(e) \ y^{\pm}}{\pi B(m_d, m_I N_I) R_u^2 R^2} \left| \sum_{j=0}^{m_d-1} \frac{(-1)^j \ \binom{m_d-1}{j}}{(m_d + m_I N_I - j - 1)^2} F(1, 1; m_d + m_I N_I - j; 1 - y^{\pm}) \right|, \tag{11.56}$$

where

$$y^{\pm} = \frac{m_I}{m_d} \left[\frac{R \ (R_u \pm 1)}{r}\right]^a \left[\frac{g + (R_u \pm 1)R}{g + r}\right]^b. \tag{11.57}$$

Integrating (11.56) over the user's position PDF (11.7) yields the overall average ASE $<\overline{A}_e>^{\pm}$ for the two extreme interference configurations.

11.6.2 Numerical and Simulation Results

Figures 11.10 and 11.11 show the ASE for the two extreme interference configuration computed numerically for different values of the Nakagami m fading parameter. These figures also show the exact value of $<\overline{A}_e>$ based on a Monte Carlo simulation algorithm using the same system and fading parameters. The simulation algorithm is similar to the one described in Section 11.4.2 except for step 4 which is changed to incorporate the effects of Nakagami fading. The changes in the simulation algorithm are described in detail in Appendix A-2.

First, note again that our computer simulations confirm our analyses, since the simulated values

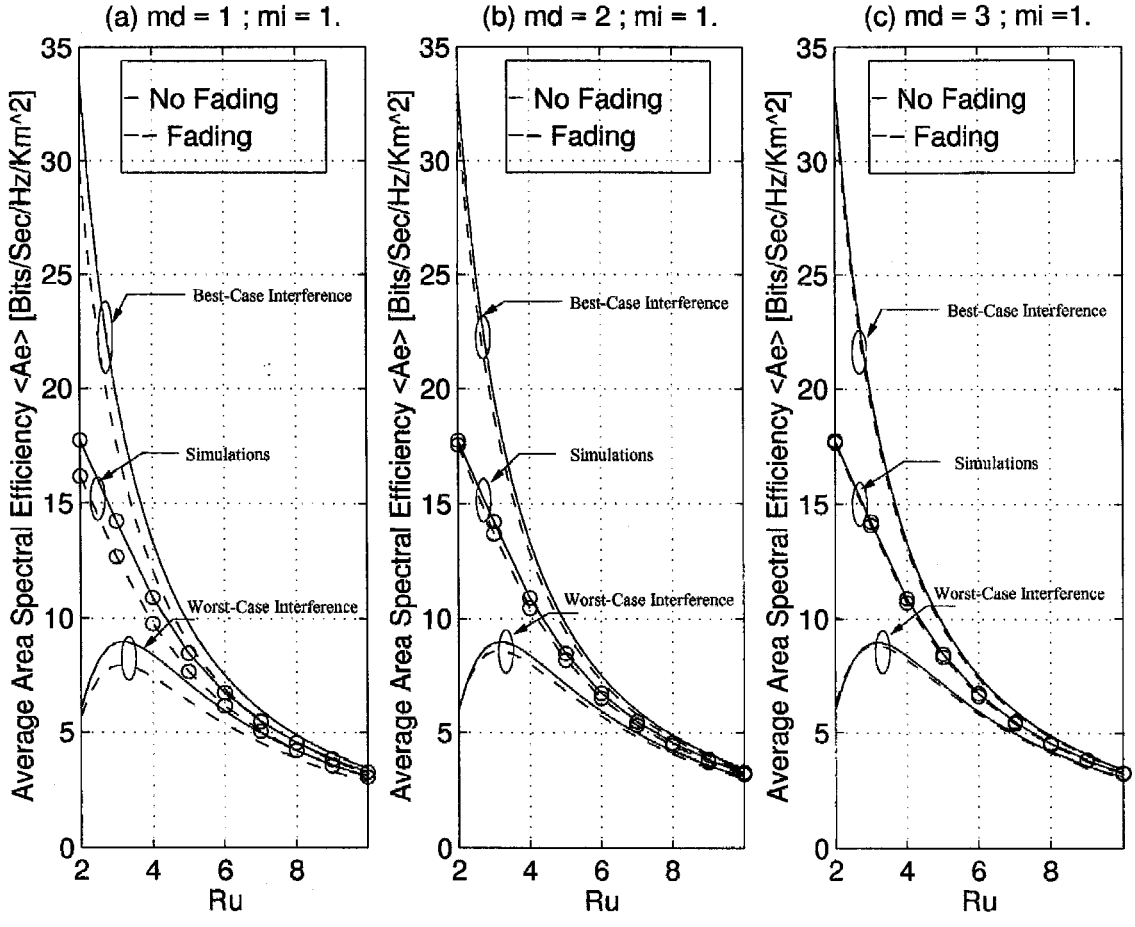

Figure 11.10: Effect of the desired users' amount of fading on the average up link spectral efficiency. (Fully-loaded system with $N_I = 6$; Cell Radius R= 200m; $R_o = 20$ m; Antenna heights: 10 m BS, 2 m mobile; Carrier frequency $f_c = 900$ MHz; Propagation parameters: $a = b = 2$).

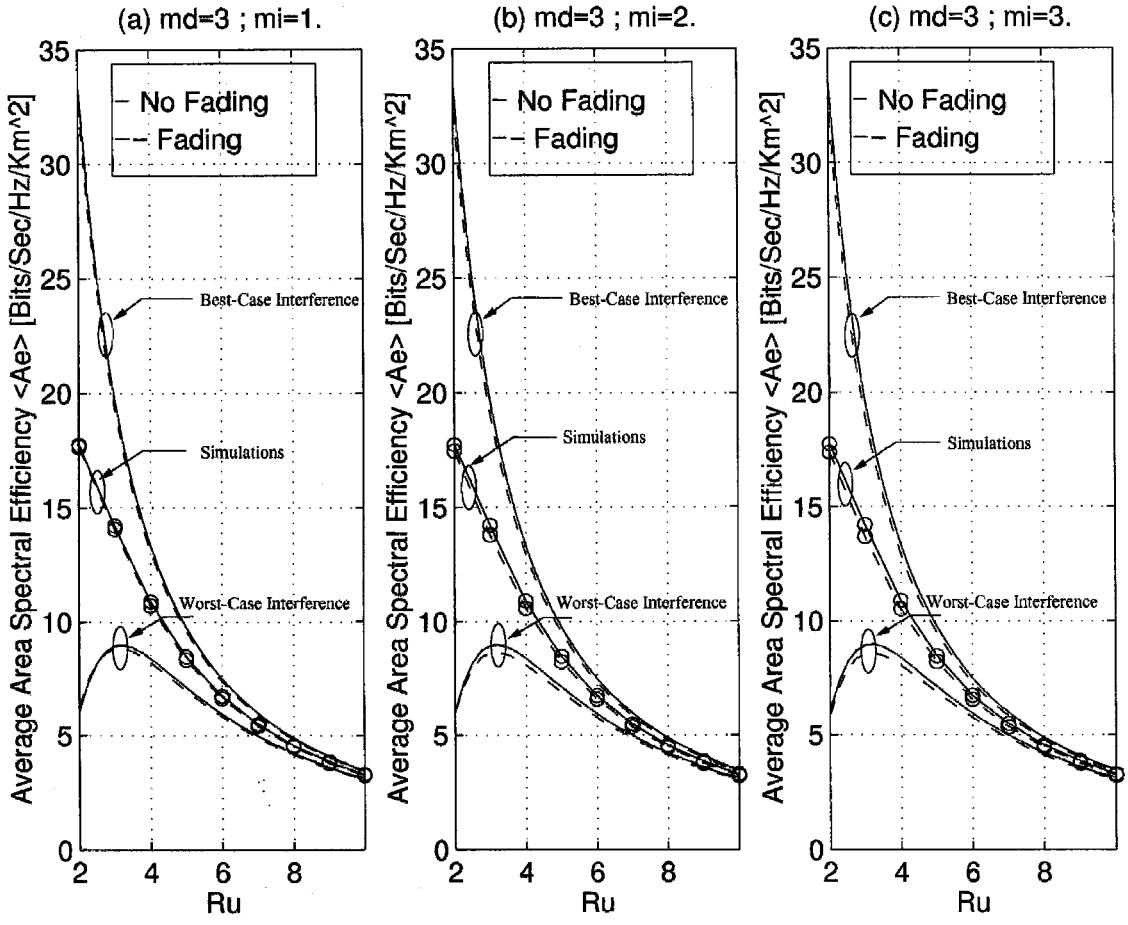

Figure 11.11: Effect of the co-channel interferers' amount of fading on the average up link spectral efficiency. (Fully-loaded system with $N_I = 6$; Cell Radius R= 200m; $R_o = 20$ m; Antenna heights: 10 m BS, 2 m mobile; Carrier frequency $f_c = 900$ MHz; Propagation parameters: $a = b = 2$).

always lie between the predicted theoretical bounds. Comparing these ASE results with our ASE results without fading we see that both sets of ASE curves have the same relative shape, although the ASE with fading is always smaller. Recall that the same behavior was observed for shadowing.

Fig. 11.10 shows how the desired user's $AF_d = 1/m_d$ affects ASE by fixing $m_I = 1$ (Rayleigh fading) and setting m_d to 1 (Fig. 11.10-a), 2 (Fig. 11.10-b), or 3 (Fig. 11.10-c). We see that the ASE curves with fading (dashed lines) approach the ASE curves without fading (solid lines) as m_d increases. Hence as the channel quality between the user and its BS improves (i.e., severity of fading decreases), the system average ASE increases.

Fig. 11.11 shows how the interferers $AF_I = 1/m_I$ affects the ASE by fixing m_d to be 3 and setting m_I to 1 (Fig. 11.11-a), 2 (Fig. 11.11-b), or 3 (Fig. 11.11-c). The interferers' AF seems to have little impact, since the average ASE is about the same (in fact, slightly decreasing with AF_I) for all cases in Fig. 11.11. Hence, the ASE is predominantly affected by the channel quality of the desired users, rather than by the fading parameters of the interferers.

11.7 Combined Effect of Shadowing and Multipath Fading

In this section we consider the ASE of fully-loaded cellular systems in a shadowed/Nakagami fading environment, consisting of Nakagami multipath fading superimposed on log-normal shadowing and two-slope path loss. This is typically the scenario in congested downtown areas with a high number of slow moving pedestrians and vehicles. Under these conditions the system does not average out the envelope fading due to multipath but rather adapts to the instantaneous composite shadowed/faded signal power.

11.7.1 Analyses

The desired user's signal is assumed to follow a Nakagami distribution with parameter m_d and a slowly-varying local mean power $\overline{S}_d$, which is itself log-normally distributed with area logarithmic mean μ_d and logarithmic standard deviation σ_d. There are N_I i.i.d Nakagami faded interferers, each with parameter m_I and a log-normally distributed local mean power $\overline{S}_I$ with area logarithmic mean μ_i and logarithmic variance σ_I.

Combining (11.2) and (11.5) we see that the composite shadowed/faded received signal power for all users follows a *gamma/log-normal* PDF given by [2, p. 92, (2.187)]

$$p_S(s) = \int_0^{+\infty} \left(\frac{m}{\overline{S}}\right)^m \frac{s^{m-1}}{\Gamma(m)} \exp\left(-m\,\frac{s}{\overline{S}}\right) \frac{\xi}{\sqrt{2\,\pi}\,\sigma\,\overline{S}} \exp\left(-\frac{(\xi \ln \overline{S} - \mu)^2}{2\,\sigma^2}\right) d\overline{S}. \qquad (11.58)$$

This integral form of the PDF requires numerical techniques for solution and becomes computationally burdensome when further analysis is required. Fortunately, Ho and Stüber [2, p. 92] showed that

the composite gamma/log-normal PDF can be accurately approximated by another log-normal PDF with logarithmic mean $\tilde{\mu}$ and logarithmic variance $\tilde{\sigma}^2$. These parameters are obtained by matching the first two moments of (11.58) with the first two moments of a log-normal approximation giving [2, p. 106]

$$\tilde{\mu} = \xi\,(\psi(m) - \ln(m)) + \mu, \tag{11.59}$$

$$\tilde{\sigma}^2 = \xi^2\,\zeta(2,m) + \sigma^2, \tag{11.60}$$

where $\psi(.)$ is the *Euler's psi function* defined in (11.54), and $\zeta(.,.)$ is the *generalized Reimann's zeta function* defined by [53, p. 1101, (9.521.1)]

$$\zeta(z,n) = \sum_{j=0}^{+\infty} \frac{1}{(n+j)^z}; \qquad z > 1; n \neq 0, -1, -2, \cdots. \tag{11.61}$$

Therefore, all the analyses of Section V applies in this case, with the substitution in all the expressions of the μ's by $\tilde{\mu}$'s and the σ^2's by $\tilde{\sigma}^2$'s, for the desired user as well as for the co-channel interferers.

11.7.2 Numerical and Simulation Results

The combined effect of shadowing and Nakagami fading on the ASE for the two extreme/average interference configurations is shown in Fig. 11.12 and Fig. 11.13 with different sets of shadowing and fading parameters. The ASE for the average interference configuration is determined using a simulation algorithm similar to the one used previously except for the generation of the desired (S_d) and interfering (S_i) signal powers, which are obtained as described in Appendix A-3.

Comparing these results with Figs. 11.10 and 11.11, we see that the ASE curves still conserve the same relative shape. However, simulations show clearly that for the same amount of multipath fading on the desired and interfering mobiles, shadowing further reduces the system ASE. It is reported in [159, 167, 177] that the Fenton-Wilkinson method loses its accuracy for $\sigma > 4$ dB and leads to optimistic results for the co-channel interference calculations in that case. This, combined with the fact that the Ho and Stüber approximation increases the shadow standard deviation to incorporate the effect of Nakagami fading (11.60), explains the slightly high theoretical predictions of the ASE under the combined impact of shadowing and fading. More accurate ASE predictions can be obtained for high shadow standard deviation if the Schwartz and Yeh's method [177] as reviewed by Prasad and Arnbak [167] is used. This remark also applies to the analytical results in Section 11.5 when $\sigma > 4$ dB. Specifically, a more accurate ASE for $\sigma > 4$ dB is obtained by using the same analysis in Sections 11.5 and 11.7 with (11.24) and (11.25) recomputed according to the Schwartz and Yeh's recursive technique [167, 177].

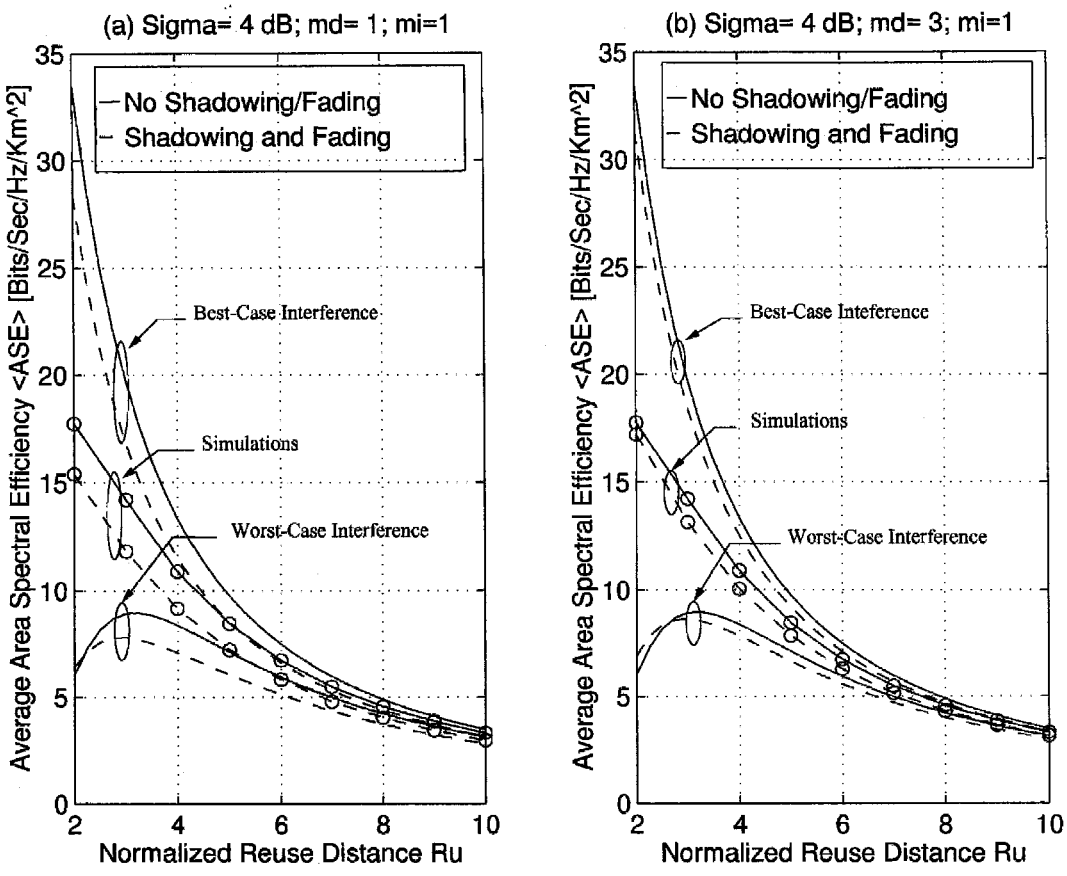

Figure 11.12: Combined effect of shadowing ($\sigma_d = \sigma_I = 4$ dB) and Nakagami fading on the average up link spectral efficiency. (Fully-loaded system with $N_I = 6$; Cell Radius R= 200m; R_o = 20 m; Antenna heights: 10 m BS, 2 m mobile; Carrier frequency f_c = 900 MHz; Propagation parameters: $a = b = 2$).

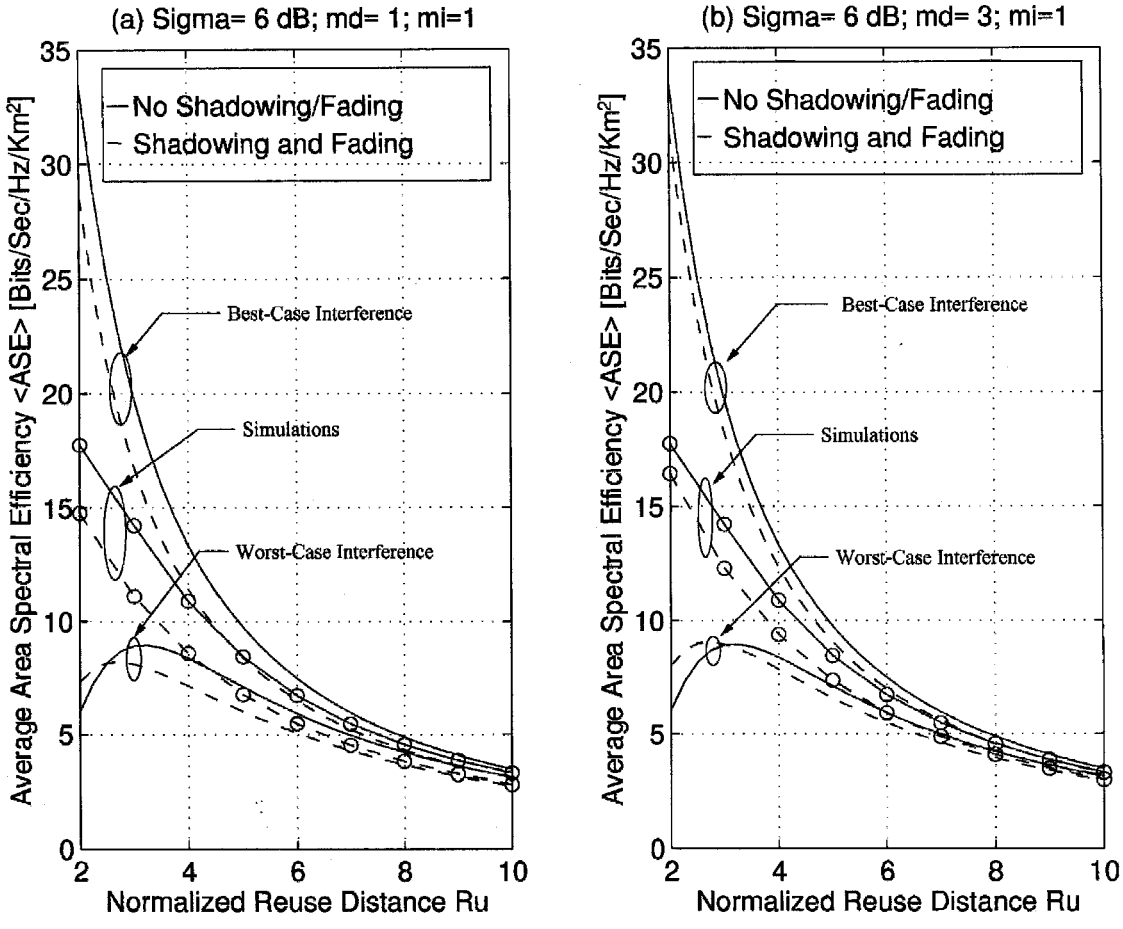

Figure 11.13: Combined effect of shadowing ($\sigma_d = \sigma_I = 6$ dB) and Nakagami fading on the average up link spectral efficiency. (Fully-loaded system with $N_I = 6$; Cell Radius R= 200m; R_o = 20 m; Antenna heights: 10 m BS, 2 m mobile; Carrier frequency f_c = 900 MHz; Propagation parameters: $a = b = 2$).

11.8 Partially-Loaded Systems

In Section 11.3 we introduced the ASE for fully-loaded cellular systems in which (i) the cell's serviced channels N_s are all used, and (ii) the number of interferers is constant and equal to N_I. In this section we consider partially-loaded systems in which the cell's serviced channels and the number of interferers are random variables depending on the traffic loading. In what follows, we first briefly describe a fixed channel assignment scheme. We then study the effect of traffic loading on the ASE when this fixed channel assignment scheme is employed.

11.8.1 Channel Assignment Scheme

Each cell has a dedicated and constant number of channels, N_s, with the same bandwidth $W_o = W/N_s$ [Hz]. In this scheme, if free channels are available in the cell, the BS allocates randomly one of its free channels to a new connection request or handoff attempt. On the other hand, if all serviced channels are busy, any new/handoff connection is blocked or dropped. We assume that the calls are not dynamically ordered/rearranged in order to minimize the number of co-channel interference channels. We also assume that queuing is not provided for connection requests which have been initially blocked or dropped. This channel allocation scheme is obviously quite simple. Besides making our analyses tractable, this scheme offers the advantage of being "instantaneous" (no delay in calls rearrangement), fully distributed, and of very low complexity.

The serviced channels are considered to be independent and active with the same probability p_a. Hence the blocking/dropping probability B is given by $B = (p_a)^{N_s}$. Equivalently, we have $p_a = B^{1/N_s}$. Thus, the probability that n_s serviced channels are active has a binomial distribution, $P_{n_s}(n_s)$ given by

$$\begin{aligned} P_{n_s}(n_s) &= \binom{N_s}{n_s} (p_a)^{n_s} (1-p_a)^{N_s-n_s}, \\ &= \binom{N_s}{n_s} B^{n_s/N_s} (1-B^{1/N_s})^{N_s-n_s}, \quad n_s = 0,1,2,\ldots,N_s, \end{aligned} \tag{11.62}$$

where $\binom{N_s}{n_s}$ denotes the binomial coefficient.

For a cell with n_s active users, let the number of active co-channel interferers of the kth desired user be denoted by $n_I^{(k)}$, and let $\mathbf{n_I}$ be the vector $[n_I^{(1)}, n_I^{(2)}, ..., n_I^{(n_s)}]$. We assume that the $\{n_I^{(k)}\}$ are mutually independent. Hence the joint distribution of the $\{n_I^{(k)}\}$, $P_{\mathbf{n_I}}(\mathbf{n_I})$, is given by

$$P_{\mathbf{n_I}}(\mathbf{n_I}) = \prod_{k=1}^{n_s} P_{n_I^{(k)}}(n_I^{(k)}). \tag{11.63}$$

In addition, the $\{n_I^{(k)}\}$ are assumed to be independent from n_s, and the traffic loading conditions are considered to be uniform so that the blocking/dropping probability B is the same for all the cells

(desired cell and co-channel interfering cells). Hence the $\{n_I^{(k)}\}$ are identically distributed according to a binomial distribution $P_{n_I}(n_I)$ given by [157]

$$P_{n_I}(n_I) = \binom{N_I}{n_I} B^{n_I/N_s} (1 - B^{1/N_s})^{N_I - n_I}, \quad n_I = 0, 1, 2, \ldots, N_I. \tag{11.64}$$

11.8.2 Analyses

Recall that in partially-loaded systems the number of active users, n_s, and the number of active co-channel interferers $\{n_I^{(k)}\}$ are random variables. Let $\overline{A}_e(n_s, \mathbf{n_I})$ [bits/sec/Hz/m^2] denote the ASE conditioned on n_s and $\mathbf{n_I}$ and given by

$$\overline{A}_e(n_s, \mathbf{n_I}) = \frac{4}{\pi\ W\ R_u^2\ R^2} \sum_{k=1}^{n_s} \overline{C}_k(n_I^{(k)}). \tag{11.65}$$

Averaging (11.65) over the joint distribution of the $\{n_I^{(k)}\}$, $P_{\mathbf{n_I}}(\mathbf{n_I})$, yields

$$\overline{A}_e(n_s) = \frac{4}{\pi\ W\ R_u^2\ R^2} \sum_{\mathbf{n_I}} \sum_{k=1}^{n_s} \overline{C}_k(n_I^{(k)})\ P_{\mathbf{n_I}}(\mathbf{n_I}). \tag{11.66}$$

Substituting (11.63) in (11.66) yields

$$\overline{A}_e(n_s) = \frac{4}{\pi\ W\ R_u^2\ R^2} \sum_{k=1}^{n_s} \sum_{n_I^{(k)}=0}^{N_I} \overline{C}_k(n_I^{(k)})\ P_{n_I^{(k)}}(n_I^{(k)}). \tag{11.67}$$

Using the fact that all users are assigned the same bandwidth, and that the $\{n_I^{(k)}\}$ are independent from n_s and are identically distributed according to $P_{n_I}(n_I)$, (11.67) simplifies to

$$\overline{A}_e(n_s) = \frac{4\ n_s}{\pi\ W\ R_u^2\ R^2} \sum_{n_I=0}^{N_I} \overline{C}(n_I)\ P_{n_I}(n_I). \tag{11.68}$$

Averaging (11.68) over the binomial distribution of n_s (11.62) yields the average ASE for a partially-loaded system as a function of N_s, N_I, and B as

$$\overline{A}_e(N_s, N_I, B) = \frac{4\ N_s\ B^{1/N_s}}{\pi\ W\ R_u^2\ R^2} \sum_{n_I=0}^{N_I} \overline{C}(n_I)\ P_{n_I}(n_I). \tag{11.69}$$

Integrating (11.69) over the user's position PDF (11.7) yields the overall average ASE, $<\overline{A}_e(N_I, N_s, B)>^{\pm}$, for a partially-loaded system, and for the two extreme configurations. Recall that the traffic loading is directly proportional to the blocking probability B. In the limit of heavy-loaded traffic conditions, $B \to 1$, so that $P_{n_I}(n_I) \to \delta(n_I - N_I)$, where $\delta(k)$ denotes the *Krönecker delta function* which is equal to 1 for k=0 and 0 otherwise. As expected the ASE in this case $<\overline{A}_e(N_s, N_I, B)>^{\pm} \overset{B \to 1}{\longrightarrow} <$

$\overline{A}_e(N_I)>^{\pm}$, corresponding to the ASE of a fully-loaded system.

11.8.3 Numerical and Simulation Results

The effect of system loading (as parameterized by B) on the ASE for the two extreme and the average interference configurations is shown in Fig. 11.14 for a microcellular radio system with a cell radius $R = 200$ m. Since the effect of shadowing and fading has been thoroughly studied in previous sections, only path loss has been taken into account in computing the desired user average capacity $\overline{C}(n_I)$ in (11.69). These results can be easily generalized to include the effects of shadowing and fading by recomputing $\overline{C}(n_I)$ in (11.69) according to (11.29) and (11.51), respectively. The 'o' points in Fig. 11.14 correspond to simulation results obtained using an algorithm similar the one described in Section 11.4.2 except that the number of co-channel interferers n_I is randomly picked following (11.64). Partially-loaded systems have a lower spectral efficiency than fully-loaded systems since the ASE increases as the blocking probability increases. Therefore, although the desired users in a partially loaded system have less interference and can achieve higher rates this effect is more than offset by the fact that there are fewer active desired users, and thus only a fraction of the cell allocated bandwidth is used.

11.9 Conclusion

We have presented a general analytical framework to quantify the overall spectral efficiency of cellular systems in which mobile users continuously adapt their rate relative to the variation in their respective carrier-to-interference power ratio. This overall spectral efficiency, named the area spectral efficiency (ASE) is defined as the sum of the maximum average data rates/unit bandwidth/unit area supported by a cell's base station. The ASE captures the tradeoff between a cellular system' spectral efficiency, the link spectral efficiency, and the communication link quality provided to the users. We have calculated this efficiency for FDMA and TDMA systems as a function of the reuse distance for the worst-case and best-case interference configurations. We have also developed Monte Carlo simulations to estimate the value of this efficiency for average interference conditions. Our theoretical analyses are in good agreement with the corresponding simulated values.

We haven take into account the effect of the users random location in their respective cells and have presented numerical results showing the impact of propagation parameters, cell size, carrier frequency, and cell sectorization on the spectral efficiency. Results indicate that, based on the worst-case interference configuration, the optimal reuse distance is approximately four. However, this optimal reuse distance is two for the best-case and the average interference configurations (i.e., frequencies should be reused every cell). Moreover, simulations show that area efficiency decreases as an exponential of a 4th order polynomial relative to the cell size.

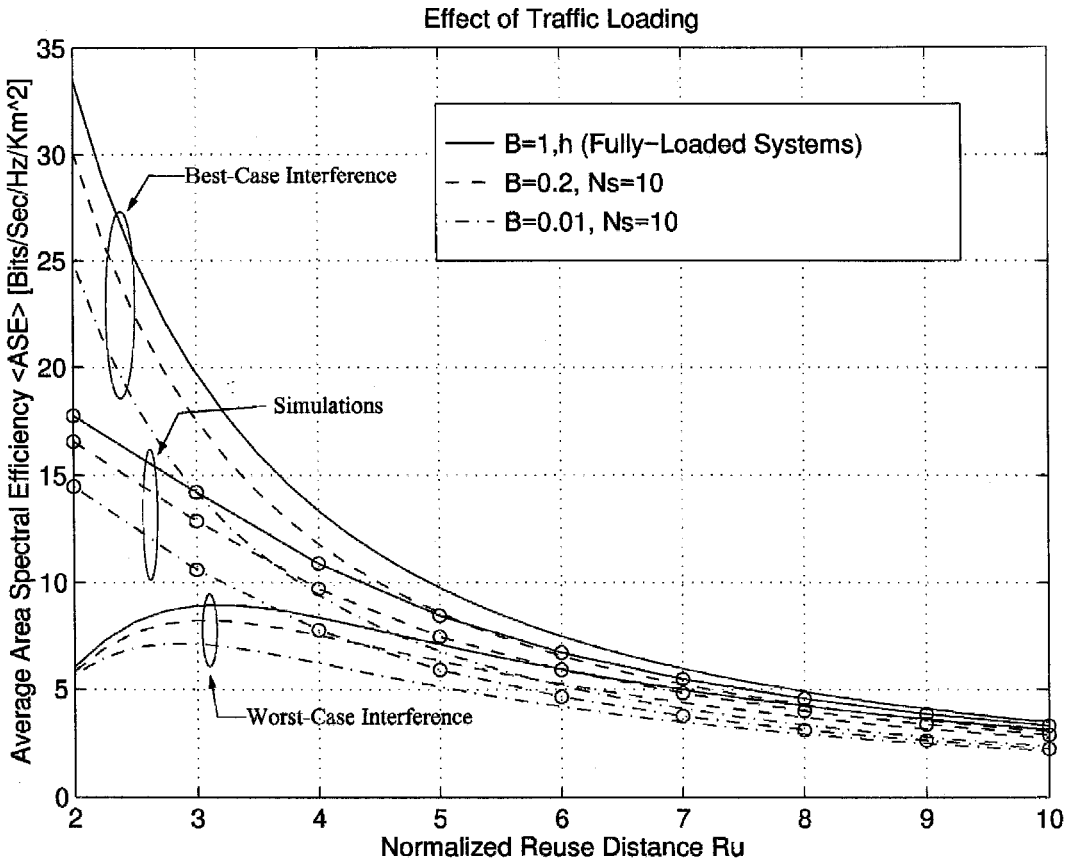

Figure 11.14: Comparison of the average up link spectral efficiency versus the normalized reuse distance for different traffic loading conditions. (Interferers $N_I = 6$; Cell Radius R= 200m; $R_o = 20$ m; Antenna heights: 10 m BS, 2 m mobile; Carrier frequency: 900 MHz; Propagation parameters: $a = b = 2$).

We have also studied the area spectral efficiency under the influence Nakagami multipath fading, log-normal shadowing, and combined shadowing and fading when superimposed on path loss. Results show that both shadowing and fading reduce the area spectral efficiency but do not affect its general behavior relative to the reuse distance. In addition, the spectral efficiency is predominantly affected by the fading parameters of the desired users, rather than by the fading parameters of the interferers.

This chapter also presented initial steps toward the determination of the area spectral efficiency of partially-loaded systems. Results reveal that heavier traffic loading (i.e., higher blocking probability) leads to a higher area spectral efficiency with a simple fixed channel allocation scheme is used. A study with more sophisticated channel allocation schemes should be conducted to better assess the impact of partial loading on the area spectral efficiency.

Our results are useful for the prediction of the spectral efficiency of cellular systems with variable-rate transmission under various "realistic" conditions. Furthermore, they provide system engineers with valuable input information for the efficient design, planning, and dimensioning of such systems. In particular, these results give guidelines for optimizing reuse distance and cell size.

Appendix A

Monte Carlo Simulations

A-1 Shadowing

The step 4 of the algorithm described in Section 11.4.2 is changed as follows to incorporate the effect of shadowing:

- The $N_I + 1$ area mean powers (μ_d and μ_is) at the considered BS are calculated using the two-slope path model (11.1).
- The instantaneous received power from the desired and interfering mobiles (S_d and S_is) are randomly generated according to a log-normal distribution (11.2) with area means μ_d and $\mu_i s$ respectively, and standard deviations σ_d and σ_I, respectively.

Since we need to average out the additional effect of shadowing, a higher number of iterations is required (typically 100.000) than in section IV-B for the same degree of accuracy in the estimation of $<\overline{A_e}>$.

A-2 Multipath Fading

The step 4 of the algorithm described in section IV-B is changed as follows to incorporate the effect of Nakagami multipath fading:

- The $N_I + 1$ local mean powers ($\overline{S}_d$ and $\overline{S}_i$s) at the considered BS are calculated using the two-slope path model (11.1).
- The instantaneous received powers from the desired and interfering mobiles (S_d and S_is) are randomly generated according to a gamma distribution (11.5) with fading parameters m_d and m_I respectively, and local mean powers $\overline{S}_d$ and $\overline{S}_i$s respectively.

The same number of iterations as in the shadowing case is typically required to average out the additional effect of multipath and to estimate $<\overline{A_e}>$ within a 3-digit accuracy.

A-3 Combined Effect of Shadowing and Multipath Fading

The step 4 of the algorithm described in Section IV-B is changed as follows to incorporate the combined effect of shadowing and Nakagami multipath fading:

- The $N_I + 1$ area mean powers (μ_d and μ_is) at the considered BS are calculated using the two-slope path model (11.1).

- The slowly-varying local mean powers from the desired and interfering mobiles ($\overline{S}_d$ and $\overline{S}_i$s) are randomly generated according to a log-normal distribution (11.2) with area means μ_d and $\mu_i s$ respectively, and standard deviations σ_d and σ_I respectively.

- The instantaneous received power from the desired and interfering mobiles (S_d and $S_i s$) are randomly generated according to a gamma distribution (11.5) with fading parameters m_d and m_I respectively, and local mean powers $\overline{S}_d$ and $\overline{S}_i$s respectively.

Since we need to average out the effect of both shadowing and Nakagami fading, a higher number of iterations is required (typically 300.000 iterations) than in the previous cases for the same degree of accuracy in the estimation of $<\overline{A_e}>$.

Appendix B

Some Properties of the Generalized Stieltjes Transform (GST)

In this appendix, we review some basic properties of the GST. We restrict our review to the properties that are useful in our derivation of the ASE in Nakagami fading environment. A more detailed summary of the GST and its properties can be found in [178, Chapter XIV].

The GST of order ρ of the function $f(x)$ is defined by

$$\mathcal{G}_\rho\{f(x);y\} = g(y;\rho) = \int_0^{+\infty} f(x)\ (x+y)^{-\rho}\ dx, \tag{11.70}$$

where y and ρ can be complex variables. The relationship between $g(.;.)$ and $f(.)$ can also be expressed symbolically by a GST transform pair as

$$f(x) \overset{GST}{\longleftrightarrow} g(y;\rho). \tag{11.71}$$

Theorem 1 (Differentiation property) *[178, p. 233, (5)]*

Assuming (11.71) then

$$\frac{d}{dx}f(x) \overset{GST}{\longleftrightarrow} \rho\ g(y;\rho+1) - y^{-\rho}\ f(0). \tag{11.72}$$

Theorem 2 (Multiplication by x property) *[178, p. 233, (2)]*

Assuming (11.71) then

$$x\ f(x) \overset{GST}{\longleftrightarrow} g(y;\rho-1) - y\ g(y;\rho). \tag{11.73}$$

Theorem 3 (A useful GST pair) *[178, p. 233, (9)]*

For $\rho > n-1$ and assuming (11.71) then

$$If\ f(x) = \frac{x^{n-1}}{1+x},\ then\ g(y;\rho) = \frac{\Gamma(n)\ \Gamma(1-n+\rho)\ y^{n-\rho}}{\Gamma(1+\rho)}\ F(1,n;1+\rho;1-y), \tag{11.74}$$

where $F(.,.;.;.)$ is Gauss' hypergeometric function defined in (11.52).

Appendix C

Evaluation of $\mathcal{G}_\rho\{f_n(x); y\} = g_n(y; \rho)$

In this appendix, we evaluate the GST of $f_n(x) = x^{n-1}\ \ln(1+x)$. To simplify our notations, let us denote $\mathcal{G}_\rho\{f_n(x); y\}$ by $g_n(y; \rho)$. First of all, note that

$$f_1(x) = \ln(1+x), \tag{11.75}$$

so that

$$\frac{d}{dx} f_1(x) = \frac{1}{1+x}. \tag{11.76}$$

Using the differentiation property of the GST (11.72), note that the second term vanishes so that

$$\mathcal{G}_\rho\{\frac{d}{dx} f_1(x); y\} = \rho\ g_1(y; \rho+1). \tag{11.77}$$

Using the GST transform pair (11.74) applied (for $n = 1$) to (11.76), then substituting the result in the left-hand side of (11.77), yields

$$g_1(y; \rho) = \frac{y^{2-\rho}}{(\rho-1)^2}\ F(1, 1; \rho; 1-y), \tag{11.78}$$

where $F(.,.;.;.)$ is defined in (11.52). Note that since $\rho = m_d + N_I\ m_I$ and $n = m_d$, we have $\rho - n = N_I m_I > -1$ and therefore (11.74) always applies with no singularities.

As a second step of our derivation, we apply the property (11.73) to $f_{n-1}(x)$. This provides a difference equation given by

$$g_n(y; \rho) = g_{n-1}(y; \rho-1) - y\ g_{n-1}(y; \rho). \tag{11.79}$$

Then it can be show by induction that for n positive integer,

$$g_n(y; \rho) = \left| \sum_{j=0}^{n-1} (-1)^j \binom{n-1}{j}\ g_1(y; \rho-j)\ y^{n-j-1} \right| \tag{11.80}$$

is solution for the difference equation (11.79) where $\binom{n-1}{j}$ denotes the binomial coefficient given by

$$\binom{n-1}{j} = \frac{(n-1)!}{j!\ (n-j-1)!}. \tag{11.81}$$

Finally, inserting (11.78) in (11.80), we find $g_n(y;\rho)$ as

$$g_n(y;\rho) = \left| \sum_{j=0}^{n-1} (-1)^j \binom{n-1}{j} \frac{y^{n-\rho+1}}{(\rho-j-1)^2} F(1,1;\rho-j;1-y) \right| . \tag{11.82}$$

Chapter 12 Summary of Contributions and Further Work

12.1 Introduction

This final chapter summarizes the main contributions of this thesis and discusses further work to extend these results. A summary of these results is presented in the next section whereas interesting and important future research directions are suggested in Section 12.3.

12.2 Summary of Contributions

Collectively, the main contributions of this work are twofold. First it presents a new approach for the performance evaluation of digital communications over fading channels. Second it discusses various methods of adapting to random channel variation in order to increase spectral efficiency of wireless systems, and evaluate their performance.

12.2.1 Performance of Diversity Techniques

The first half of the thesis presents a new unified approach to the performance analysis of digital communications, with and without diversity combining, over generalized fading channels. In particular in Chapter 3 we derive a generic form for the average bit-error-rate of coherent, differentially coherent, and noncoherent binary signals over fading channels. The generic form relies on an alternate representation of the incomplete gamma function. For all the channel fading models under consideration we obtain an expression for the average bit-error-rate which involves a single finite-range integral of tabulated functions which can easily be computed numerically.

In Chapter 4 we present a unified analytical framework to determine the exact average symbol-error-rate of linearly-modulated signals over generalized fading channels. The results, which are based on an alternate representation of the Gaussian Q-function, are applicable to systems employing coherent demodulation with optimal maximal-ratio combining multichannel reception. The analyses assume independent fading paths which are not necessarily identically distributed nor even distributed according to the same family of distributions. In all cases the proposed approach leads to an expression of the average symbol-error rate involving a single finite-range integral which can be easily computed numerically. In addition, as special cases, expressions for single channel recep-

tion are obtained. These expressions reduce to well-known solutions, give alternate (often simpler) expressions for previous results, or provide new formulas which are either closed-form expressions or simple to compute numerically.

Since optimal diversity-combining requires more hardware complexity and more sensitivity to channel estimation errors, in Chapter 5 we study ideal coherent detection of various modulations with suboptimal diversity combining techniques. These suboptimal schemes are less complex (hence more practical for actual implementation) and more robust to imperfect channel estimation. In particular, we develop a generic expression for the probability of error of coherent equal gain combining over Nakagami-m fading channels. The final form of this expression is a single integral with finite limits and an integrand composed of tabulated functions. In addition a performance analysis of the generalized selective combining scheme over Rayleigh and Nakagami-m fading channels with a flat power delay profile is presented. Our numerical results show that the performance degradation of equal gain combining or generalized selective combining relative to maximal-ratio combining is independent of the average signal-to-noise ratio regardless of the severity of the fading. In addition the performance of equal gain combining approaches that of maximal ratio combining for channels with low amounts of fading, whereas the performance of higher order selective combining approaches that of maximal-ratio combining for channels with high amounts of fading.

In many applications the phase of the received signal cannot be tracked accurately in which case differentially coherent or noncoherent modulation must be used. In Chapter 6 we present a unified approach to determine the exact bit-error-rate of these modulations with single and multichannel reception over generalized fading channels. The multichannel reception results assume independent fading in the channels and are applicable to systems that employ postdetection equal gain combining. Our approach relies on an alternate form of the Marcum Q-function and leads to expressions of the bit-error-rate involving a single finite-range integral which can be readily evaluated numerically. As in the case of Chapter 4, the new approach provides simple BER expressions for general modulations and channel models which previously defied a simple solution as well as unifying past known results. In particular we obtain simple BER expressions for multichannel reception where the fading on each channel need not be identically distributed nor even distributed according to the same family of distributions.

In order to obtain significant diversity gain, independent fading in the channels should be achieved. However, this is not always realized in practice because, for example, of insufficient antenna spacing in small-size terminals equipped with space antenna diversity and as a result, the maximum theoretical diversity gain cannot be achieved. In Chapter 7 we assess the impact of correlation on the outage probability and average error probability of dual selective combining, coherent maximal-ratio combining, and noncoherent equal-gain combining diversity receivers. For dual selective combining we use a simple finite integral representation for the cumulative distribution function

and the probability density function of the output of the combiner to express the outage probability and error probability performances of this system in the presence of slow correlated Rayleigh fading either in closed form or in terms of a single integral with finite limits and an integrand composed of elementary functions. For coherent maximal-ratio combining and noncoherent equal-gain combining we obtain generic easy-to-compute expressions for the average error rate of multichannel reception of digital signals over equicorrelated and exponentially correlated slowly varying Nakagami-m fading channels. In all cases, because of their simple forms, these results offer a useful analytical tool for the accurate characterization of the impact of correlation on the performance of various systems of practical interest.

12.2.2 Adaptive Techniques

The second half of the thesis proposes several adaptive transmission schemes for flat fading fading channels and studies their performance. The Shannon capacity of adaptive modulation with diversity combining is derived in Chapter 8. This capacity provides an upper bound on spectral efficiency using these techniques. We obtained closed-form solutions for the Rayleigh fading channel capacity under three adaptive policies: optimal power and rate adaptation, constant power with optimal rate adaptation, and channel inversion with fixed rate. Our numerical results show that optimal power and rate adaptation yields a small increase in capacity over just rate adaptation, and this increase diminishes as the average received carrier-to-noise ratio or the number of diversity branches increases. Channel inversion suffers the largest capacity penalty relative to the optimal technique; however, the penalty diminishes with increased diversity. Although diversity yields large capacity gains for all the techniques, the gain is most pronounced with channel inversion. For example, the capacity using channel inversion with two-branch diversity exceeds that of a single-branch system using optimal rate and power adaptation. Since channel inversion is the least complex scheme to implement, there is a tradeoff between complexity and capacity for the various adaptation methods and diversity-combining techniques.

In Chapter 9 we extend the capacity results to Nakagami-m fading channels for the three power and rate adaptation policies discussed above. As for the Rayleigh channel, numerical results show that most of the spectral efficiency increase comes from rate adaptation alone. We therefore analyzed the performance of constant-power variable-rate M-QAM schemes over Nakagami-m channels. We obtain closed-form expressions for the outage probability, spectral efficiency, and average bit-error-rate of these schemes assuming perfect channel estimation and negligible time delay. We also analyze the impact of time delay on the BER of adaptive M-QAM, and show that adaptive systems can operate satisfactorily if the time delay is below a critical value, regardless of the severity of fading.

The basic premise behind adaptive modulation is to take advantage of good channel realizations, at the expense of some delay and complexity. We use this concept in a new adaptive modulation

technique for simultaneous voice and data transmission over fading channels in Chapter 10, and study its performance. The proposed scheme takes advantage of the time-varying nature of fading to dynamically allocate the transmitted power between the inphase (I) and quadrature (Q) channels. It uses fixed-rate binary phase shift keying modulation on the Q channel for voice, and variable-rate M-ary amplitude modulation on the I channel for data. For favorable channel conditions most of the power is allocated to high rate data transmission on the I channel. The remaining power is used to support the variable-power voice transmission on the Q channel. As the channel degrades the modulation gradually reduces its data throughput and reallocates most of its available power to insure a continuous and satisfactory voice transmission. The scheme is intended to provide a high average spectral efficiency for data communications while meeting the stringent delay requirements imposed by voice. We present closed-form expressions as well as numerical and simulation results for the outage probability, average allocated power, achievable spectral efficiency, and average bit-error-rate for both voice and data transmission over Nakagami-m fading channels. We also discuss the features and advantages of the proposed scheme.

Finally Chapter 11 introduces a general analytical framework quantifying the spectral efficiency of cellular systems with variable-rate transmission. This efficiency, the area spectral efficiency, defines the sum of the maximum average data rates per unit bandwidth per unit area supported by a cell's base station. Analytical expressions for this efficiency as a function of the reuse distance for the worst-case and best-case interference configurations were derived. Moreover, Monte Carlo simulations were developed to estimate the value of this efficiency for average interference conditions. Both fully-loaded and partially-loaded cellular systems were investigated. The effect of random user location was taken into account and the impact of log-normal shadowing and Nakagami-m multipath fading was also studied.

12.3 Future Research Directions

We conclude with some brief remarks on future extensions of the work presented in this thesis. These extensions fall into two categories. In the next section we present some of the potential applications where our unified approach can be applied to obtain accurate performance results. We then discuss the potential of adaptive schemes for multimedia transmission over fading channels.

12.3.1 Applications of the Unified Approach to Performance Analysis of Diversity Systems

One of the main contributions of this thesis was to develop a unified approach for the performance evaluation of digital communications with diversity reception over fading channels. Since various communications applications use the diversity concept in one form or another, we believe that many

of the performance analyses of these applications can benefit from our approach. For example, our results can be extended to include the performance of direct sequence code division multiple access (DS-CDMA) systems with RAKE reception, thereby generalizing the results obtained by Eng and Milstein [96], Prasad *et al.* [179], and Efthymoglou *et al.* [97]. This particular interesting subject will be reported in a forthcoming paper [180], as a part of a general analytical framework for the performance evaluation of coherent, noncoherent, differentially coherent single carrier and multi-carrier DS-CDMA systems. Another interesting application of our generic results is Beamfomer Bi-dimensional RAKE receivers. These structures, also called smart antennas, exploit both the temporal and spatial dimension for diversity and use adaptive beamforming techniques to reduce co-channel interference. Since cellular systems are mainly limited by fading and interference, smart antennas are currently receiving a great deal of attention as very promising techniques to improve the performance of DS-CDMA cellular systems. As another example the performance evaluation of wireless packet communications which use a certain form of diversity can also benefit from our approach. Although this thesis has offered many performance analyses of communication systems over fading channels, several related problems remain open. In particular all our performance analyses assumed receiver diversity. A generic approach for the accurate performance evaluation of transmit diversity (also know as simulcast transmission) over fading channels is also an interesting future research topic.

12.3.2 Adaptive Schemes for Multimedia Transmission over Fading Channels

This thesis proposed a new hybrid adaptive scheme which supports simultaneous voice and data transmission over fading channels. The originality of the proposed scheme is that it offers a simple link layer solution to the voice and data integration problem by designing the modulation to support their respective requirements. Similarly, support of multimedia services over wireless channels will require the development of communication schemes capable of handling various information streams which are inherently different not only in their nature but also in their quality of service requirements (e.g., priority, delay, rate, and BER). Therefore, the design of elaborate adaptive techniques which incorporate into their respective transmission schemes these very different information streams' requirements will also be another interesting future research direction.

Bibliography

[1] J. G. Proakis, *Digital Communications.* New York, NY: McGraw-Hill, second ed., 1989.

[2] G. L. Stüber, *Principles of Mobile Communications.* Norwell, MA: Kluwer Academic Publishers, 1996.

[3] U. Charash, *A study of multipath reception with unknown delays.* PhD thesis, University of California, Berkley, January 1974.

[4] U. Charash, "Reception through Nakagami fading multipath channels with random delays," *IEEE Trans. Commun.*, vol. COM-27, pp. 657–670, April 1979.

[5] M. K. Simon and M. -S. Alouini, "Digital communications over generalized fading channels: A unified approach to performance analysis." New York, NY: John Wiley & Sons, to be published.

[6] H. B. James and P. I. Wells, "Some tropospheric scatter propagation measurements near the radio-horizon," *Proc. IRE*, pp. 1336–1340, October 1955.

[7] G. R. Sugar, "Some fading characteristics of regular VHF ionospheric propagation," *Proc. IRE*, pp. 1432–1436, October 1955.

[8] S. Basu, E. M. MacKenzie, S. Basu, E. Costa, P. F. Fougere, H. C. Carlson, and H. E. Whitney, "250 MHz/GHz scintillation parameters in the equatorial, polar, and aural environments," *IEEE J. Select. Areas Commun.*, vol. SAC-5, pp. 102–115, Febuary 1987.

[9] T. L. Staley, R. C. North, W. H. Ku, and J. R. Zeidler, "Performance of coherent MPSK on frequency selective slowly fading channels," in *Proc. IEEE Veh. Technol. Conf. VTC'96, Atlanta, GA*, pp. 784–788, April 1996. Full paper submitted to *IEEE Trans. Veh. Technol.*

[10] T. L. Staley, R. C. North, W. H. Ju, and J. R. Zeidler, "Channel estimate-based error probability performance prediction for multichannel reception of linearly modulated coherent systems on fading channels," in *Proc. IEEE Mil. Commun. Conf. MILCOM'96, McLean, VA*, October 1996. Full paper submitted to *IEEE Trans. Commun.*

[11] T. L. Staley, R. C. North, W. H. Ku, and J. R. Zeidler, "Probability of error evaluation for multichannel reception of coherent MPSK over Ricean fading channels," in *Proc. IEEE Int. Conf. on Commun. ICC'97, Montreal, Canada*, pp. 30–35, June 1997. Full paper submitted to *IEEE Trans. Veh. Technol.*

[12] R. S. Hoyt, "Probability functions for the modulus and angle of the normal complex variate," *Bell Syst. Tech. J.*, vol. 26, pp. 318–359, April 1947.

[13] M. Nakagami, "The m-distribution- A general formula of intensity distribution of rapid fading," in *Statistical Methods in Radio Wave Propagation*, pp. 3–36, Pergamon Press, Oxford, U. K., 1960.

[14] B. Chytil, "The distribution of amplitude scintillation and the conversion of scintillation indices," *J. Atmos. Terr. Phys.*, vol. 29, pp. 1175–1177, September 1967.

[15] K. Bischoff and B. Chytil, "A note on scintillaton indices," *Planet. Space Sci.*, vol. 17, pp. 1059–1066, 1969.

[16] S. O. Rice, "Statistical properties of a sine wave plus random noise," *Bell Syst. Tech. J.*, vol. 27, pp. 109–157, January 1948.

[17] K. A. Stewart, G. P. Labedz, and K. Sohrabi, "Wideband channel measurements at 900 MHz," in *Proc. IEEE Veh. Technol. Conf. VTC'95, Chicago, IL*, pp. 236–240, July 1995.

[18] R. J. C. Bultitude, S. A. Mahmoud, and W. A. Sullivan, "A comparison of indoor radio propagation characteristics at 910 MHz and 1.75 GHz," *IEEE J. Select. Areas Commun.*, vol. SAC-7, pp. 20–30, January 1989.

[19] T. S. Rappaport and C. D. McGillem, "UHF fading in factories," *IEEE J. Select. Areas Commun.*, vol. SAC-7, pp. 40–48, January 1989.

[20] G. H. Munro, "Scintillation of radio signals from satellites," *J. Geophys. Res.*, vol. 68, April 1963.

[21] P. D. Shaft, "On the relationship between scintillation index and Rician fading," *IEEE Trans. Commun.*, vol. COM-22, pp. 731–732, May 1974.

[22] H. Suzuki, "A statistical model for urban multipath propagation," *IEEE Trans. on Commun.*, vol. COM-25, pp. 673–680, July 1977.

[23] T. Aulin, "Characteristics of a digital mobile radio channel," *IEEE Trans. Veh. Technol.*, vol. VT-30, pp. 45–53, May 1981.

[24] W. R. Braun and U. Dersch, "A physical mobile radio channel model," *IEEE Trans. Veh. Technol.*, vol. VT-40, pp. 472–482, May 1991.

[25] A. U. Sheikh, M. Handforth, and M. Abdi, "Indoor mobile radio channel at 946 MHz: Measurements and modeling," in *Proc. IEEE Veh. Technol. Conf. VTC'93, Secaucus, NJ*, pp. 73–76, May 1993.

[26] E. J. Fremouw and H. F. Bates, "Worldwide behavior of average VHF-UHF scintillation," *Radio Sci.*, vol. 6, pp. 863–869, October 1971.

[27] H. E. Whitney, J. Aarons, R. S. Allen, and D. R. Seeman, "Estimation of the cumulative probability distribution function of ionospheric scintillations," *Radio Sci.*, vol. 7, pp. 1095–1104, December 1972.

[28] E. J. Fremouw, R. C. Livingston, and D. A. Miller, "On the statistics of scintillating signals," *J. Atmos. Terr. Phys.*, vol. 42, pp. 717–731, August 1980.

[29] P. K. Banerjee, R. S. Dabas, and B. M. Reddy, "C-band and L-band transionospheric scintillation experiment - Some results for applications to satellite radio systems," *Radio Sci.*, vol. 27, pp. 955–969, June 1992.

[30] G. L. Turin, F. D. Clapp, T. L. Johnston, S. B. Fine, and D. Lavry, "A statistical model of urban multipath propagation," *IEEE Trans. Veh. Technol.*, vol. VT-21, pp. 1–9, February 1972.

[31] H. Hashemi, "Simulation of the urban radio propagation channel," *IEEE Trans. Veh. Technol.*, vol. VT-28, pp. 213–225, August 1979.

[32] T. S. Rappaport, S. Y. Seidel, and K. Takamizawa, "Statistical channel impulse response models for factory and open plan building radio communication system design," *IEEE Trans. Commun.*, vol. COM-39, pp. 794–807, May 1991.

[33] P. Yegani and C. McGlilem, "A statistical model for the factory radio channel," *IEEE Trans. Commun.*, vol. COM-39, pp. 1445–1454, October 1991.

[34] H. Hashemi, "Impulse response modeling of indoor radio propagation channels," *IEEE J. Select. Areas Commun.*, vol. SAC-11, pp. 967–978, September 1993.

[35] F. Hansen and F. I. Meno, "Mobile fading- Rayleigh and lognormal superimposed," *IEEE Trans. Veh. Technol.*, vol. VT-26, pp. 332–335, November 1977.

[36] M. J. Ho and G. L. Stüber, "Co-channel interference of microcellular systems on shadowed Nakagami fading channels," in *Proc. IEEE Veh. Technol. Conf. VTC'93, Secaucus, NJ*, pp. 568–571, May 1993.

[37] C. Loo, "A statistical model for a land-mobile satellite link," *IEEE Trans. Veh. Technol.*, vol. VT-34, pp. 122–127, August 1985.

[38] G. Corazza and F. Vatalaro, "A statistical model for land mobile satellite channels and its application to nongeostationary orbit systems," *IEEE Trans. Veh. Technol.*, vol. VT-43, pp. 738–742, August 1994.

[39] S. -H Hwang, K. -J. Kim, J. -Y. Ahn, and K. -C. Wang, "A channel model for nongeostationnary orbiting satellite system," in *Proc. IEEE Veh. Technol. Conf. VTC'97, Phoenix, AZ*, pp. 41–45, May 1997.

[40] E. Lutz, D. Cygan, M. Dippold, F. Dolainsky, and W. Papke, "The land mobile satellite communication channel - Recording, statistics, and channel model," *IEEE Trans. Veh. Technol.*, vol. VT-40, pp. 375–386, May 1991.

[41] M. Rice and B. Humpherys, "Statistical models for the ACTS K-band land mobile satellite channel," in *Proc. IEEE Veh. Technol. Conf. VTC'97, Phoenix, AZ*, pp. 46–50, May 1997.

[42] R. M. Barts and W. L. Stutzman, "Modeling and simulation of mobile satellite propagation," *IEEE Trans. Antennas Propagat.*, vol. AP-40, pp. 375–382, April 1992.

[43] S. A. Abbas and A. U. Sheikh, "A geometric theory of Nakagami fading multipath mobile radio channel with physical interpretations," in *Proc. IEEE Veh. Technol. Conf. VTC'96, Atlanta, GA*, pp. 637–641, April 1996.

[44] D. Molkdar, "Review on radio propagation into and within buildings," *IEE Proc. H*, vol. 138, pp. 61–73, February 1991.

[45] COST 207 TD(86)51-REV 3 (WG1), "Proposal on channel transfer functions to be used in GSM test late 1986," tech. rep., Office Official Publications European Communities, September 1986.

[46] T. Eng and L. B. Milstein, "Coherent DS-CDMA performance in Nakagami multipath fading," *IEEE Trans. Commun.*, vol. COM-43, pp. 1134–1143, February/March/April 1995.

[47] B. Glance and L. J. Greenstein, "Frequency-selective fading effects in digital mobile radio with diversity combining," *IEEE Trans. Commun.*, vol. COM-31, pp. 1085–1094, September 1983.

[48] P. F. M. Smulders and A. G. Wagemans, "Millimetre-wave biconical horn antennas for near uniform coverage in indoor picocells," *Electron. Lett.*, vol. 28, pp. 679–681, March 1992.

[49] S. Ichitsubo, T. Furuno, and R. Kawasaki, "A statistical model for microcellular multipath propagation environment," in *Proc. IEEE Veh. Technol. Conf. VTC'97, Phoenix, AZ*, pp. 61–66, May 1997.

[50] M. Wittmann, J. Marti, and T. Kürner, "Impact of the power delay profile shape on the bit error rate in mobile radio systems," *IEEE Trans. Veh. Technol.*, vol. VT-46, pp. 329–339, May 1997.

[51] M. K. Simon, S. M. Hinedi, and W. C. Lindsey, *Digital Communication Techniques- Signal Design and Detection.* Englewood Cliffs, NJ: PTR Prentice Hall, 1995.

[52] A. H. Wojnar, "Unkown bounds on performance in Nakagami channels," *IEEE Trans. Commun.*, vol. COM-34, pp. 22–24, January 1986.

[53] I. S. Gradshteyn and I. M. Ryzhik, *Table of Integrals, Series, and Products.* San Diego, CA: Academic Press, fifth ed., 1994.

[54] A. Erdelyi, W. Magnus, F. Oberhettinger, and F. Tricomi, *Table of Integral Transforms*, vol. 1. New York, NY: McGraw-Hill, 1954.

[55] J. G. Proakis, "Probabilities of error for adaptive reception of M-phase signals," *IEEE Trans. Commun. Technol.*, vol. COM-16, pp. 71–81, Febuary 1968.

[56] Y. Miyagaki, N. Morinaga, and T. Namekawa, "Error probability characteristics for CPSK signal through m-distributed fading channel," *IEEE Trans. Commun.*, vol. COM-26, pp. 88–100, January 1978.

[57] C. K. Pauw and D. L. Schilling, "Probability of error M-ary PSK and DPSK on a Rayleigh fading channel," *IEEE Trans. Commun.*, vol. COM-36, pp. 755–758, June 1988.

[58] N. Ekanayake, "Performance of M-ary PSK signals in slow Rayleigh fading channels," *Electron. Lett.*, vol. 26, pp. 618–619, May 1990.

[59] G. Efthymoglou and V. Aalo, "Performance of RAKE receivers in Nakagami fading channel with arbitary fading parameters," *Electron. Lett.*, vol. 31, pp. 1610–1612, August 1995.

[60] S. Chennakeshu and J. B. Anderson, "Error rates for Rayleigh fading multichannel reception of MPSK signals," *IEEE Trans. Commun.*, vol. COM-43, pp. 338–346, February/March/April 1995.

[61] M. G. Shayesteh and A. Aghamohammadi, "On the error probability of linearly modulated signals on frequency-flat Ricean, Rayleigh, and AWGN channels," *IEEE Trans. Commun.*, vol. COM-43, pp. 1454–1466, February/March/April 1995.

[62] V. Aalo and S. Pattaramalai, "Average error rate for coherent MPSK signals in Nakagami fading channels," *Electron. Lett.*, vol. 32, pp. 1538–1539, August 1996.

[63] C. Tellambura, A. J. Mueller, and V. K. Bhargava, "Analysis of M-ary phase-shift keying with diversity reception for land-mobile satellite channels," *IEEE Trans. Veh. Technol.*, vol. VT-46, pp. 910–922, November 1997.

[64] D. Brennan, "Linear diversity combining techniques," *Proc. IRE*, vol. 47, pp. 1075–1102, June 1959.

[65] R. F. Pawula, S. O. Rice, and J. H. Roberts, "Distribution of the phase angle between two vectors perturbed by Gaussian noise," *IEEE Trans. Commun.*, vol. COM-30, pp. 1828–1841, August 1982.

[66] J. W. Craig, "A new, simple, and exact result for calculating the probability of error for two-dimensional signal constellations," in *Proc. IEEE Milit. Commun. Conf. MILCOM'91, McLean, VA*, pp. 571–575, October 1991.

[67] M. K. Simon and D. Divsalar, "Some new twists to problems involving the Gaussian probability integral," *IEEE Trans. Commun.*, vol. COM-46, pp. 200–210, February 1998.

[68] E. K. Hall and S. G. Wilson, "Design and analysis of turbo codes on Rayleigh fading channels," *IEEE J. Select. Areas Commun.*, vol. SAC-16, February 1998.

[69] F. S. Weinstein, "Simplified relationships for the probability distribution of the phase of a sine wave in narrow-band normal noise," *IEEE Trans. on Inform. Theory*, vol. IT-, pp. 658–661, September 1974.

[70] M. Abramowitz and I. A. Stegun, *Handbook of Mathematical Functions with Formulas, Graphs, and Mathematical Tables.* New York, NY: Dover Publications, ninth ed., 1970.

[71] J. Lu, T. T. Tjhung, and C. C. Chai, "Error probability performance of l-branch diversity reception of MQAM in Rayleigh fading," *IEEE Trans. Commun.*, vol. 46, pp. 179–181, February 1998.

[72] M. K. Simon and M. -S. Alouini, "A unified performance analysis of digital communications with dual selective combining diversity over correlated Rayleigh and Nakagami-m fading channels." To appear in *IEEE Trans. Commun.*

[73] T. Eng, N. Kong, and L. B. Milstein, "Comparison of diversity combining techniques for Rayleigh-fading channels," *IEEE Trans. on Commun.*, vol. COM-44, pp. 1117–1129, September 1996.

[74] N. C. Beaulieu and A. A. Abu-Dayya, "Analysis of equal gain diversity on Nakagami fading channels," *IEEE Trans. Commun.*, vol. COM-39, pp. 225–234, February 1991.

[75] Q. T. Zhang, "Probability of error for equal-gain combiners over Rayleigh channels: Some closed-form solutions," *IEEE Trans. on Commun.*, vol. COM-45, pp. 270–273, March 1997.

[76] A. Papoulis, *Probability, Random Variables, and Stochastic Processes.* McGraw-Hill, third ed., 1991.

[77] N. Kong, T. Eng, and L. B. Milstein, "A selection combining scheme for RAKE receivers," in *Proc. IEEE Int. Conf. Univ. Personal Comm. ICUPC'95, Tokyo, Japan*, pp. 426–429, November 1995.

[78] N. Kong and L. B. Milstein, "Combined average SNR of a generalized diveristy selection combining scheme," in *Proc. IEEE Int. Conf. on Commun. ICC'98, Atlanta, GA*, pp. 1556–1560, June 1998.

[79] E. K. Al-Hussaini and A. M. Al-Bassiouni, "Performance of MRC diversity systems for the detection of signals with Nakagami fading," *IEEE Trans. Commun.*, vol. COM-33, pp. 1315–1319, December 1985.

[80] J. A. Edwards, *A Treatise on the Integral Calculus*, vol. II. London, England: Macmillan, 1922.

[81] M. -S. Alouini and A. Goldsmith, "A unified approach for calculating the error rates of linearly modulated signals over generalized fading channels." Submitted to *IEEE Trans. Commun.*

[82] J. G. Proakis, "On the probability of error for multichannel reception of binary signals," *IEEE Trans. Commun. Technol.*, vol. COM-16, pp. 68–71, Febuary 1968.

[83] W. C. Lindsey, "Error probabilities for Ricean fading multichannel reception of binary and N-ary signals," *IEEE Trans. on Inform. Theory*, vol. IT-10, pp. 339–350, October 1964.

[84] J. F. Weng and S. H. Leung, "Analysis of DPSK with equal gain combining in Nakagami fading channels," *Electron. Lett.*, vol. 33, pp. 654–656, April 1997.

[85] F. Patenaude, J. H. Lodge, and J. -Y. Chouinard, "Error probability expressions for non-coherent diversity in Nakagami fading channels," in *Proc. IEEE Veh. Technol. Conf. VTC'97, Phoenix, AZ*, pp. 1484–1487, May 1997.

[86] T. T. Tjhung, C. Loo, and N. P. Secord, "BER performance of DQPK in slow Rician fading," *Electron. Lett.*, vol. 28, pp. 1763–1765, August 1992.

[87] M. Tanda, "Bit error rate of DQPSK signals in slow Nakagami fading," *Electron. Lett.*, vol. 29, pp. 431–432, March 1993.

[88] C. Tellambura and V. K. Bhargava, "Unified error analysis of DQPSK in fading channels," *Electron. Lett.*, vol. 30, pp. 2110–2111, December 1994.

[89] C. W. Helstrom, *Elements of Signal Detection and Estimation.* Englewood Cliffs, NJ: PTR Prentice-Hall, 1995.

[90] M. K. Simon, "A new twist on the Marcum Q-function and its applications," *IEEE Commun. Letters*, vol. 2, pp. 39–41, February 1998.

[91] G. M. Dillard, "Recursive computation of the generalized Q-function," *IEEE Trans. Aerosp. Electron. Syst.*, vol. AES-9, pp. 614–615, July 1973.

[92] R. F. Pawula, "Relations between Rice I_e-function and Marcum Q-function with applications to error rate calculations," *Electron. Lett.*, vol. 31, pp. 1717–1719, September 1995.

[93] B. B. Barrow, "Error probabilities for data transmission over fading radio paths," Tech. Rep. TM-26, SHAPE Air Defense Technical Center, 1962.

[94] P. J. Crepeau, "Uncoded and coded performance of MFSK and DPSK in Nakagami fading channels," *IEEE Trans. Commun.*, vol. COM-40, pp. 487–493, March 1992.

[95] S. Stein, "Unified analysis of certain coherent and noncoherent binary communication systems," *IEEE Trans. Inform. Theory*, vol. IT-10, pp. 43–51, January 1964.

[96] T. Eng and L. B. Milstein, "Comparison of hybrid FDMA/CDMA systems in frequency selective Rayleigh fading," *IEEE J. Select. Areas Commun.*, vol. SAC-12, pp. 938–951, June 1994.

[97] G. P. Efthymoglou, V. A. Aalo, and H. Helmken, "Performance analysis of noncoherent binary DS/CDMA systems in a Nakagami multipath channel with arbitrary parameters," in *Proc. IEEE Global Commun. Conf. GLOBECOM'96, London, U. K.*, pp. 1296–1300, November 1996. Full paper published in the *IEE Proc. Commun.*, vol. 144, pp. 166-172, June 1997.

[98] J. N. Pierce and S. Stein, "Multiple diversity with nonindependent fading," *Proc. IRE*, vol. 48, pp. 89–104, January 1960.

[99] V. A. Aalo, "Performance of maximal-ratio diversity systems in a correlated Nakagami-fading environment," *IEEE Trans. Commun.*, vol. COM-43, pp. 2360–2369, August 1995.

[100] M. Schwartz, W. R. Bennett, and S. Stein, *Communication Systems and Techniques.* New York, NY: McGraw-Hill, 1966.

[101] M. A. Blanco, "Diversity receiver performance in Nakagami fading," in *Proc. IEEE Southeastern Conf., Orlando, FL*, pp. 529–532, April 1983.

[102] F. Adachi, K. Ohno, and M. Ikura, "Postdetection selection diversity reception with correlated, unequal average power Rayleigh fading signals for $\pi/4$-shift QDPSK mobile radio," *IEEE Trans. Veh. Technol.*, vol. VT-41, pp. 199–210, May 1992.

[103] S. Okui, "Probability of co-channel interference for selection diversity reception in the Nakagami m-fading channel," *IEE. Proc I*, vol. 139, pp. 91–94, February 1992.

[104] W. C. Wan and J. C. Chen, "Fading distribution of diversity techniques with correlated channels," in *Proc. IEEE International Symp. Personal, Indoor, and Mobile Commun. PIMRC'95, Toronto, Ontario, Canada*, pp. 1202–1206, September 1995.

[105] G. Fedele, I. Izzo, and M. Tanda, "Dual diversity reception of m-ary DPSK signals over Nakagami fading channels," in *Proc. IEEE International Symp. Personal, Indoor, and Mobile Commun. PIMRC'95, Toronto, Ontario, Canada*, pp. 1195–1201, September 1995.

[106] C. C. Tan and N. C. Beaulieu, "Infinite series representation of the bivariate Rayleigh and Nakagami-m distributions," *IEEE Trans. Commun.*, vol. COM-45, pp. 1159–1161, October 1997.

[107] M. K. Simon and M. -S. Alouini, "A simple single integral representation of the bivariate Rayleigh distribution," *IEEE Commun. Letters*, vol. 2, pp. 128–130, May 1998.

[108] W. C. Jakes, *Microwave Mobile Communication.* Piscataway, NJ: IEEE Press, second ed., 1994.

[109] H. Staras, "Diversity reception with correlated signals," *J. Appl. Phys.*, vol. 27, pp. 93–94, January 1956.

[110] K. S. Packard, "Effect of correlation on combiner diversity," *Proc. IRE*, vol. 46, pp. 362–363, January 1958.

[111] J. Gurland, "Distribution of the maximum of the arithmetic mean of correlated random variables," *Annals of Math. Statistics*, vol. 26, pp. 294–300, 1955.

[112] J. A. Lawson and G. E. Uhlenbeck, *Threshold Signals.* New York, NY: McGraw-Hill Book Co., 1952.

[113] S. Kotz and J. Adams, "Distribution of sum of identically distributed exponentially correlated gamma variables," *Annals of Math. Statistics*, vol. 35, pp. 227–283, June 1964.

[114] K. Pahlavan and A. H. Levesque, "Wireless data communications," *Proc. IEEE*, vol. 82, pp. 1398–1430, September 1994.

[115] W. T. Webb and L. Hanzo, *Modern Quadrature Amplitude Modulation.* New York, NY: IEEE Press, 1994.

[116] S. Sampei and T. Sunaga, "Rayleigh fading compensation for QAM in land mobile radio communications," *IEEE Trans. Veh. Technol.*, vol. VT-42, pp. 137–147, May 1993.

[117] T. Sunaga and S. Sampei, "Performance of multi-level QAM with post-detection maximal ratio combining space diversity for digital land-mobile radio communications," *IEEE Trans. Veh. Technol.*, vol. VT-42, pp. 294–301, August 1993.

[118] S. Sampei, Y. Kamio, and H. Sasaoka, "Field experiments on pilot symbol aided 16 QAM modems for land mobile communications," *Electronics Letters*, vol. 28, pp. 2198–2199, December 1992.

[119] S. Sampei, E. Moriyama, H. Sasaoka, N. Kinoshita, K. Hiramatsu, K. Inogai, and K. Honma, "Field experiments on a 16 QAM/TDMA system for land mobile communications," *Electronics Letters*, vol. 30, pp. 185–186, February 1994.

[120] J. F. Hayes, "Adaptive feedback communications," *IEEE Trans. Commun. Technol.*, vol. COM-16, pp. 29–34, February 1968.

[121] J. K. Cavers, "Variable-rate transmission for Rayleigh fading channels," *IEEE Trans. Commun.*, vol. COM-20, pp. 15–22, February 1972.

[122] V. O. Hentinen, "Error performance for adaptive transmission on fading channels," *IEEE Trans. Commun.*, vol. COM-22, pp. 1331–1337, September 1974.

[123] S. Otsuki, S. Sampei, and N. Morinaga, "Square-QAM adaptive modulation/TDMA/TDD systems using modulation level estimation with Walsh function," *Electron. Lett.*, vol. 31, pp. 169–171, February 1995.

[124] W. T. Webb and R. Steele, "Variable rate QAM for mobile radio," *IEEE Trans. on Commun.*, vol. COM-43, pp. 2223–2230, July 1995.

[125] Y. Kamio, S. Sampei, H. Sasaoka, and N. Morinaga, "Performance of modulation-level-controlled adaptive-modulation under limited transmission delay time for land mobile communications," in *Proc. IEEE Veh. Technol. Conf. VTC'95, Chicago, IL*, pp. 221–225, July 1995.

[126] B. Vucetic, "An adaptive coding scheme for time-varying channels," *IEEE Trans. Commun.*, vol. COM-39, pp. 653–663, May 1991.

[127] A. Goldsmith and P. Varaiya, "Increasing spectral efficiency through power control," in *Proc. IEEE Int. Conf. on Commun. ICC'93, Geneva, Switzerland*, pp. 600–604, June 1993.

[128] S. M. Alamouti and S. Kallel, "Adaptive trellis-coded multiple-phased-shift keying for Rayleigh fading channels," *IEEE Trans. Commun.*, vol. COM-42, pp. 2305–2314, June 1994.

[129] T. Ue, S. Sampei, and N. Morinaga, "Symbol rate and modulation level controlled adaptive modulation/TDMA/TDD for personal communication systems," in *Proc. IEEE Veh. Technol. Conf. VTC'95, Chicago, IL*, pp. 306–310, July 1995. Full paper published in the *IEICE Trans. Commun.*, vol. E78-B, pp. 1117-1124, August 1995.

[130] A. J. Goldsmith and S. G. Chua, "Variable-rate variable-power M-QAM for fading channels," *IEEE Trans. Commun.*, vol. COM-45, pp. 1218–1230, October 1997.

[131] H. Matsuoka, S. Sampei, N. Morinaga, and Y. Kamio, "Adaptive modulation system with variable coding rate concatenated code for high quality multi-media communication systems," in *Proc. IEEE Veh. Technol. Conf. VTC'96, Atlanta, GA*, pp. 487–491, April 1996. Full paper published in the *IEICE Trans. Commun.*, vol. E79-B, pp. 328-334, March 1996.

[132] A. Goldsmith and S. G. Chua, "Adaptive coded modulation for fading channels," *IEEE Trans. Commun.*, vol. COM-46, pp. 595–602, May 1998.

[133] S. Sampei, N. Morinaga, and Y. Kamio, "Adaptive modulation/TDMA with a BDDFE for 2 Mbit/s multi-media wireless communication systems," in *Proc. IEEE Veh. Technol. Conf. VTC'95, Chicago, IL*, pp. 311–315, July 1995.

[134] A. Goldsmith and P. Varaiya, "Capacity of fading channels with channel side information," *IEEE Trans. on Information Theory*, vol. IT-43, pp. 1896–1992, November 1997.

[135] W. C. Y. Lee, "Estimate of channel capacity in Rayleigh fading environment," *IEEE Trans. Veh. Technol.*, vol. VT-39, pp. 187–190, August 1990.

[136] L. Ozarow, S. Shamai, and A. Wyner, "Information theoretic considerations for cellular mobile radio," *IEEE Trans. on Veh. Technol.*, vol. VT-43, pp. 359–378, May 1994.

[137] C. G. Günther, "Comment on "Estimate of channel capacity in Rayleigh fading environment"," *IEEE Trans. Veh. Technol.*, vol. VT-45, pp. 401–403, May 1996.

[138] J. Wolfowitz, *Coding Theorems of Information Theory.* New York, NY: Springer-Verlag, second ed., 1964. Theorem 4.6.1.

[139] T. Ericson, "A Gaussian channel with slow fading," *IEEE Trans. Inform. Theory*, vol. IT-16, pp. 353–355, May 1970.

[140] R. J. McEliece and W. E. Stark, "Channels with block interference," *IEEE Trans. on Information Theory*, vol. IT-30, pp. 44–53, January 1984.

[141] K. M. Cheung and V. Vilnrotter, "Channel capacity of an array system for Gaussian channels with applications to combining and noise cancellation," in *JPL / Telecommunications and Data Acquisition Progress Report*, no. 42-124, pp. 53–62, February 1996.

[142] J. M. Torrance and L. Hanzo, "Upper bound performance of adaptive modulation in a slow Rayleigh fading channel," *Electron. Lett.*, vol. 32, pp. 718–719, April 1996.

[143] Y. -D. Yao and A. U. H. Sheikh, "Evaluation of channel capacity in a generalized fading channel," in *Proc. IEEE Veh. Technol. Conf. VTC'93, Secaucus, NJ*, pp. 134–137, May 1993.

[144] G. D. Forney Jr., R. G. Gallager, G. R. Lang, F. M. Longstaff, and S. U. Qureshi, "Efficient modulation for band-limited channels," *IEEE J. Select. Areas Commun.*, vol. SAC-2, pp. 632–646, September 1984.

[145] N. M. Temme, *Special Functions- An Introduction to the Classical Functions of Mathematical Physics.* New York, NY: John Wiley & Sons, 1996.

[146] D. J. Goodman, R. A. Valenzuela, K. T. Gayliard, and B. Ramamurthi, "Packet reservation multiple access for local wireless communications," *IEEE Trans. on Commun.*, vol. COM-37, pp. 885–890, August 1989.

[147] K. Zhang and K. Pahlavan, "An integrated voice/data system for mobile indoor radio networks," *IEEE Trans. Veh. Technol.*, vol. VT-39, pp. 75–82, February 1990.

[148] S. Nanda, "Analysis of packet reservation multiple access: Voice data integration for wireless networks," in *Proc. IEEE Global Commun. Conf. GLOBECOM'90, San Diego, CA*, pp. 1984–1988, November 1990.

[149] N. Wilson, R. Ganesh, K. Joseph, and D. Raychaudhuri, "Packet CDMA versus dynamic TDMA for multiple access in an integrated voice/data PCN," *IEEE J. Sel. Areas Commun.*, vol. SAC-11, pp. 870–884, August 1993.

[150] G. Wu, K. Mukumoto, and A. Fukud, "Analysis of an integrated voice and data transmission system using packet reservation multiple access," *IEEE Trans. Veh. Technol.*, vol. VT-43, pp. 289–297, May 1994.

[151] B. C. Kim and C. K. Un, "An efficient wireless voice/data integrated access algorithm in noisy channel environments," *IEICE Trans. Commun.*, vol. E79-B, pp. 1394–1403, September 1996.

[152] G. Bremer and K. D. Ko, "Simultaneous voice and data on the general switched telephone network using framed QADM," *IEEE Commun. Mag.*, vol. 34, pp. 58–63, December 1996.

[153] M. K. Simon, "Error probability performance of unbalanced QPSK receivers," *IEEE Trans. on Commun.*, vol. COM-26, pp. 1390–1397, September 1978.

[154] P. M. Fortune, L. Hanzo, and R. Steele, "On the computation of 16-QAM performance in Rayleigh-fading channels," *IEICE Trans. Commun.*, vol. E75-B, pp. 466–475, June 1992.

[155] P. T. Brady, "A model for generating on-off speech patterns in two-way conversation," *Bell Syst. Tech. J.*, vol. 48, pp. 2445–2472, September 1969.

[156] V. H. MacDonald, "The cellular concept," *Bell System Tech. J.*, vol. 58, pp. 15–41, January 1979.

[157] R. Muammar and S. C. Gupta, "Cochannel interference in high-capacity mobile radio systems," *IEEE Trans. Commun.*, vol. COM-30, pp. 1973–1978, August 1982.

[158] Y. Nagata and Y. Akaiwa, "Analysis for spectrum efficiency in single cell trunked and cellular mobile radio," *IEEE Trans. Veh. Technol.*, vol. VT-35, pp. 100–113, August 1987.

[159] R. Prasad and A. Kegel, "Improved assessement of interference limits in cellular radio performance," *IEEE Trans. Veh. Technol.*, vol. VT-40, pp. 412–419, May 1991.

[160] A. A. Abu-Dayya and N. C. Beaulieu, "Outage probabilities of cellular mobile radio systems with multiple Nakagami interferers," *IEEE Trans. Veh. Technol.*, vol. VT-40, pp. 757–768, November 1991.

[161] Y. -D Yao and A. U. H. Sheikh, "Investigations in cochannel interference in microcellular mobile radio systems," *IEEE Trans. Veh. Technol.*, vol. VT-41, pp. 114–123, May 1992.

[162] R. Prasad and A. Kegel, "Effects of Rician faded and log-normal shadowed signals on spectrum efficiency in microcellular radio," *IEEE Trans. Veh. Technol.*, vol. VT-42, pp. 274–280, August 1993.

[163] R. Haas and J. Belfiore, "Spectrum efficiency limits in mobile cellular systems," *IEEE Trans. Veh. Technol.*, vol. VT-45, pp. 33–40, February 1996.

[164] N. Morinaga, M. Yokoyama, and S. Sampei, "Intelligent radio communications techniques for advanced wireless communication systems," *IEICE Trans. Commun.*, vol. E79-B, pp. 214–221, March 1996.

[165] D. N. Hatfield, "Measure of spectral efficiency in land mobile radio," *IEEE Trans. Electromagnet. Compat.*, vol. EMC-19, pp. 266–268, August 1977.

[166] W. C. Y. Lee, "Spectrum efficiency in cellular," *IEEE Trans. Veh. Technol.*, vol. VT-38, pp. 69–75, May 1989.

[167] R. Prasad and J. C. Arnbak, "Comments on "Analysis for spectrum efficiency in single cell trunked and cellular mobile radio"," *IEEE Trans. Veh. Technol.*, vol. VT-37, pp. 220–222, November 1988.

[168] P. Harley, "Short distance attenuation measurements at 900 MHz and 1.8 GHz using low antenna heights for microcells," *IEEE J. Select. Areas Commun.*, vol. SAC-7, pp. 5–11, January 1989.

[169] M. V. Clark, V. Erceg, and L. J. Greenstein, "Reuse efficiency in urban microcellular networks," in *Proc. IEEE Veh. Technol. Conf. VTC'96, Atlanta, GA*, pp. 421–425, April 1996.

[170] S. A. Abbas and A. U. Sheikh, "On understanding the nature of slow fading in LOS microcellular channels," in *Proc. IEEE Veh. Technol. Conf. VTC'97, Phoenix, AZ*, pp. 662–666, May 1997.

[171] Y. Karasawa and M. Yasunaga, "Interference evaluation method for mobile-satellite systems under Nakagami-Rice fading conditions," *IEICE Trans. Commun.*, vol. E75-B, pp. 42–49, January 1992.

[172] S. Ihara, "On the capacity of channels with additive non-Gaussian noise," *Inform. and Control*, vol. 37, pp. 34–39, 1978.

[173] S. Shamai and A. D. Wyner, "Information-theoretic consideration for symmetric cellular, multiple-access fading channels - Part I," *IEEE Trans. Inform. Theory*, vol. IT-43, pp. 1877–1894, November 1997.

[174] A. Lapidoth, "Nearest neighbor decoding for additive non-Gaussian noise channels," *IEEE Trans. Inform. Theory*, vol. IT-42, pp. 1520–1529, September 1996.

[175] G. K. Chan, "Effects of sectorization on the spectrum efficiency of cellular radio systems," *IEEE Trans. Veh. Technol.*, vol. VT-41, pp. 217–225, August 1992.

[176] L. F. Fenton, "The sum of log-normal probability distributions in scatter transmission systems," *IRE Trans. Commun.*, vol. COM-8, pp. 57–67, March 1960.

[177] S. Schwratz and Y. S. Yeh, "On the distribution function and moments of power sums with log-normal components," *Bell System Tech. J.*, vol. 61, pp. 1441–1462, September 1982.

[178] A. Erdelyi, W. Magnus, F. Oberhettinger, and F. Tricomi, *Table of Integral Transforms*, vol. 2. New York, NY: McGraw-Hill, 1954.

[179] R. Prasad, H. S. Misser, and A. Kegel, "Performance evaluation of direct-sequence spread spectrum multiple-access for indoor wireless communication in a Rician fading channel," *IEEE Trans. Commun.*, vol. COM-43, pp. 581–592, February/March/April 1995.

[180] M. -S. Alouini, M. K. Simon, and A. Goldsmith, "A unified performance analysis of DS-CDMA systems over generalized frequency-selective fading channels," in *Proc. IEEE Int. Symposium Inform. Theory ISIT'98, Cambridge, MA*, August 1998. Full paper in preparation for submission to the *IEEE J. Select. Areas Commun. Special Issue on Spread Spectrum for Global Communications.*